# Genetic and Physiological Studies in Friedreich's Ataxia

*Alexander F. Brown*

A dissertation submitted in partial fulfilment

Of the requirements for the degree of

**Doctor of Philosophy**

Of

**University College London**

Department of Molecular Neuroscience

University College London

6th July 2018

# Declaration

I, Alexander F Brown, confirm that the work presented in this thesis is my own. Where information has been derived from other sources, I confirm that this has been indicated in the work.

# Abstract

This thesis combines genetic and physiological studies of Friedreich's ataxia (FRDA), an autosomal recessive disorder caused by a GAA triplet expansion mutation leading to a deficiency of the protein frataxin. This gives rise to a complex pathophysiology that affects not only the nervous system but also cardiac function, with the majority of FRDA patients dying from heart-related complications. In the genetic study, a sample of 2000 clinically undiagnosed ataxia cases referred to the National Hospital for Neurology and Neurosurgery (NHNN) over a 20-year period and who had not been previously screened for FRDA, were screened for the presence of any of the known FRDA mutations. Only 3 FRDA-positive cases were found, all conforming to the regular FRDA genotype of homozygous GAA triplet repeat expansion. These findings indicated the reliability of current FRDA diagnostic method and increased understanding of the FRDA genotype-phenotype correlation among atypical FRDA cases, such as late-onset FRDA. In the physiological study, I studied the unexplored role of $Ca^{2+}$ dysregulation in FRDA heart pathology. Frataxin was knocked-down in neonatal and adult FRDA-like cardiomyocyte models and $Ca^{2+}$ homeostasis investigated. Both revealed a decreased $Ca^{2+}$ sarcoplasmic reticulum (SR) content, combined with increased cellular and mitochondrial ROS levels. These data were confirmed in primary heart cells from well-established FRDA mouse models, such as the YG8R model. This was linked to increased leakage from the ryanodine receptors (RyR), causing $Ca^{2+}$ to exit the SR, indicating a possible RyR potentiation in FRDA model heart cells due to frataxin deficiency. Together, these studies may lead to a better understanding of the impact of genetics on the FRDA clinical phenotype, and also widen our knowledge of the underlying mechanisms of the disease, with particular focus on the impact on $Ca^{2+}$ signaling in heart cells affected by reduced frataxin.

# Acknowledgements

*In memory of my grandfather, Dr. Franco Bernardi, 1926-2019, whose 'durante la guerra' stories are real, and not metaphorical like mine.*

I would firstly like to give thanks to the UCL Grand Challenges scheme, who provided funding for my PhD, and Ataxia UK for supporting the project. I would also like to thank Dr Paola Giunti, my supervisor, for her help and guidance during my PhD, her specific advice regarding the FRDA screening study, and for allowing me to form part of her research group. I would like to thank my secondary supervisor, Prof. Sandip Patel, for his expert guidance at key stages of the study.

I would like to thank Dr Rosella Abeti, who was my first port of call for advice on my work in $Ca^{2+}$ signaling and kept me focused on surmounting the various challenges a PhD can bring. I must thank her for allowing me to grow as a person, as well as a scientist.

I would like to thank all current and past members of the UCL Ataxia group, with whom I have greatly enjoyed working. I am very grateful to Dr Michael Parkinson, Ms Heather Ging, Dr Suran Nethisinghe, Dr Gilbert Thomas-Black and Dr Aurelien Bayot for their valuable feedback and advice over the course of the PhD. I am also very grateful to Ms Ese Mudanohwo and Dr Robyn Labrum for their help with the genetics-based section of my study, and to Prof. Andrey Abramov for his advice on $Ca^{2+}$ signaling and microscopy. Prof. John Hardy also provided much valuable feedback during my final year of experimentation.

Finally, I must list those certain people or creatures who, whether in the long-term or in certain moments, even unforeseen ones, have given me

crucial support and motivation. Mention must be made of Rupert Brown, Francesca Brown, Marina Bernardi, Franco Bernardi, Nella Maria Ferrari, Luigi Bernardi, Sydney (the family cat), Nejc Haberman, Ari (the dog), Raf Ferrari, Léa R'Bibo, Aarti Singh, Phillip Smethurst, Demis Kia, Daniel Kay, Tom Gayford, Robin McGhee, Max Whittaker, Iacopo Cordaro, Alessandro Acerno, Simone Peronaci, Alessandro de Rosa, Mirco Belli, Lorenzo Tomasoni, Nicolò Maffei, Magali Vagirault, Amelia Webb, Hamud Mbarak, Petra Kokol, Sophie Parrock, Mehaa Bajaj, Ellie Knuckey, Kate Pereira, Anya James, Grace Willatt, David Zhang and Melissa Gassman. I must perhaps single out my mother, Mrs Cristiana Bernardi, and Ms Fathia Mbarak, without whose particular help and loving support in key moments this PhD work and thesis may not have been completed. Therefore, this thesis is officially dedicated to these two people.

*Per me si va ne la città dolente,*
*per me si va ne l'etterno dolore,*
*per me si va tra la perduta gente.*

# Abbreviations

$\Delta\psi_m$: Mitochondrial Membrane Potential

$[Ca^{2+}]_c$: Cytosolic $[Ca^{2+}]$

AM: Acetoxymethyl

BAC: Bacterial Artificial Chromosome

BSA: Bovine Serum Albumin

CCD: Charge-Coupled Device

CICR: $Ca^{2+}$-Induced $Ca^{2+}$-Release

CLSM: Confocal Laser-Scanning Microscope

CoQ10: Coenzyme Q10

DMSO: Dimethyl sulphoxide

DRG: Dorsal Root Ganglia

ECG: Electrocardiogram

EDQ: Exon Dosage Quotient

EFACTS: European Friedreich's Ataxia Consortium for Translational Studies

ETC: Electron Transport Chain

FBS: Foetal Bovine Serum

FCCP: Carbonyl cyanide-4-(trifluoromethoxy)phenylhydrazone

FRDA: Friedreich's Ataxia

FxnKD: Frataxin Knock-Down

H/R: Hypoxia/Reoxygenation

HBSS: HEPES-buffered salt solution

Het: Dihydroethidium

HRP: Horseradish Peroxidase

IMM: Inner Mitochondrial Membrane

iPSC: Induced Pluripotent Stem Cell

IRE: Iron-Responsive Element

IRP1: Iron-Responsive element binding Protein

ISC: Iron-Sulphur Cluster

kD: Kilodalton

MCU: Mitochondrial $Ca^{2+}$ Uniporter

MPP: Mitochondrial Processing Peptidase

NCX: $Na^{+}$-$Ca^{2+}$ Exchanger

NHNN: National Hospital for Neurology and Neurosurgery

OCT: Optical Coherence Tomography

PBS: Phosphate Buffered Saline

PFA: Paraformaldehyde

PGC1α: peroxisome proliferator-activated receptor gamma coactivator 1-alpha

PMT: Photomultiplier Tubes

PPARγ: Peroxisome Proliferator-Activated Receptor Gamma

RIPA: Radioimmunoprecipitation Assay

RNAi: RNA interference

ROS: Reactive Oxygen Species

RYR2: Ryanodine Receptor 2

Scr: 'Scrambled' (Negative Control siRNA)

SERCA: Sarcoplasmic/Endoplasmic Reticulum $Ca^{2+}$ ATPase

siRNA: Small Interfering RNA

SR: Sarcoplasmic Reticulum

TBS: Tris-Buffered Saline

TMRM: Tetramethyl Rhodamine, Methyl Ester

TUNEL: Terminal deoxynucleotidyl transferase dUTP nick-end labelling

YAC: Yeast Artificial Chromosome

YFP: Yellow Fluorescent Protein

# Table of Contents

*Declaration* ..... *2*
*Abstract* ..... *3*
*Acknowledgements* ..... *4*
*Abbreviations* ..... *6*
*Table of Contents* ..... *8*
*Table of Figures* ..... *10*
*Table of Tables* ..... *12*
*Publications and Presentations during PhD* ..... *13*
*Chapter 1 : Introduction* ..... *15*
*1.1 Introduction* ..... *15*
*1.2 Background* ..... *16*
*1.3 Genetics of Friedreich's Ataxia* ..... *17*
*1.4 Pathophysiology of Friedreich's Ataxia* ..... *23*
**1.4.1 Role of Frataxin** ..... **23**
**1.4.2 Iron Accumulation and Oxidative Stress in Friedreich's Ataxia** ..... **29**
**1.4.3 $Ca^{2+}$ Signalling and Oxidative Stress in Cardiomyocytes** ..... **34**
**1.4.4 Cellular and Animal Models of FRDA** ..... **38**
*1.5 Clinical Features* ..... *44*
**1.5.1 Early Onset Friedreich's Ataxia** ..... **45**
**1.5.2 Classical Friedreich's Ataxia** ..... **45**
Neurological Features ..... 45
Non-Neurological Features ..... 50
**1.5.3 Late-Onset FRDA** ..... **54**
*1.6 FRDA Compound Heterozygotes* ..... *57*
**1.6.1 Compound Heterozygotes with Point Mutations** ..... **57**
**1.6.2 Compound Heterozygotes with Large Deletions** ..... **61**
*1.7 Justification for Current Study* ..... *64*
*Chapter 2 : Methods* ..... *66*
*2.1 Genetic Screening Study of Ataxia Patients* ..... *66*
**2.1.1 Case Ascertainment** ..... **66**
**2.1.2 Triplet-Primed Polymerase Chain Reaction** ..... **67**
**2.1.3 Long Range PCR** ..... **71**
**2.1.4 Point Mutation Screening and Large Deletion Screening** ..... **74**

**2.1.5 Large Deletion Screening ..... 75**

***2.2 Physiology of $Ca^{2+}$ in Cardiomyocytes in Friedreich's Ataxia 80***

**2.2.1 Cell Culture ..... 80**

Preparation of Complete Claycomb Medium ..... 80
Passaging of HL-1/H9c2 Cells ..... 81
Isolation of Neonatal Cardiomyocytes ..... 83

**2.2.2 Transfection of HL-1/H9c2 Cardiomyocytes ..... 85**

**2.2.3 Fluorescence Imaging ..... 89**

Basics of Fluorescence ..... 89
CCD Microscopy ..... 90
Confocal Microscopy ..... 90
$Ca^{2+}$ Imaging ..... 91
Measurements of ROS production ..... 96
Measurement of NAD(P)H Autofluorescence ..... 97
Measurement of Mitochondrial Membrane Potential ($\Delta\psi_m$) ..... 97
Immunofluorescence ..... 98

**2.2.4 DNA Analysis of YG8R/Y47R/WT mice ..... 100**

**2.2.5 Statistical Analysis ..... 102**

***Chapter 3 : Genetic Screening Study of Ataxia Patients for Friedreich's Ataxia ..... 103***

***3.1 Introduction ..... 103***

***3.2 Results ..... 105***

**3.2.1 Genetic Analysis ..... 105**

**3.2.2 MLPA Testing ..... 110**

**3.2.3 Clinical Features ..... 114**

Very Late-onset Patient 1: Intrafamilial Variability ..... 114
Patient 2: Borderline LOFA case ..... 115
Very Late-onset Patient 3: A Clinical Conundrum ..... 116

**3.2.4 Comparison of Clinical Data ..... 116**

**3.2.5 FRDA Carrier Clinical Details ..... 118**

**3.2.6 Comparison to FRDA-referred Cohort Study* ..... 122**

**3.2.7 Results Summary ..... 140**

***3.3 Discussion ..... 142***

***Chapter 4 : Reduced $Ca^{2+}$ Levels in Cardiomyocytes in Friedreich's Ataxia Models ..... 151***

***4.1 Introduction ..... 151***

***4.2 Results ..... 154***

**4.2.1 Fxn-siRNA-induced Knockdown ..... 154**

**4.2.2 Increased ROS in Fxn KD HL-1 and H9c2 cells ..... 156**

**4.2.3 Decreased NADH Redox Index in Fxn KD HL-1 and H9c2 cells .. 160**

**4.2.4 Mitochondrial Energy Imbalance in FRDA Pathophysiology (from Abeti et al., 2018) ..... 162**

**4.2.6 Caffeine-Induced $Ca^{2+}$ Response Decrease in Fxn KD Cells ..... 163**

**4.2.7 Thapsigargin Experiments ..... 166**
Thapsigargin Response Indicates Reduced SR $Ca^{2+}$ Levels in Fxn KD HL-1 and H9c2 cells ..... 166
Dantrolene Increases Amplitude of Thapsigargin-Induced $Ca^{2+}$ Response in both Control and Fxn KD HL-1 and H9c2 cells ..... 168
**4.2.8 Primary Cell Data ..... 171**
Caffeine-Induced $Ca^{2+}$ Response Decreased in YG8R Mouse Model Cells ..... 171
**4.2.9 Results Summary ..... 172**
***4.3 Discussion ..... 174***
***Chapter 5 : Final Discussion ..... 184***
***References ..... 191***

# Table of Figures

## Chapter One: Introduction

Figure 1. FXN gene, chromosome 9q21.11. ..... 18
Figure 2. Schematic representation of GAA expansion in FXN intron 1 causing decreased frataxin production. ..... 19
Figure 3. Mature frataxin protein. α-helices shown as ribbons, β-strands as arrows and C-terminal tail in red. Image in public domain, based on PyMOL rendering. ..... 23
Figure 4: Potential pathway for FRDA pathophysiology. ..... 33
Figure 5. Ca2+ Signalling in Cardiomyocytes. ..... 36

## Chapter Two: Methods

Figure 6: TP-PCR results visualized by capillary electrophoresis, showing that TP-PCR does not distinguish between FRDA carriers and FRDA positives. ..... 70
Figure 7: Transfection Efficiency in HL-1 Cells. ..... 89
Figure 8: Confocal Microscope. Image in public domain. ..... 91

## Chapter Three: Genetic Screening Study of Ataxia Patients for Friedreich's Ataxia

Figure 9: Long-range FXN PCR Example Photo..... 107
Figure 10. Long Range PCR: FRDA Positive and Carrier Data. ..... 110
Figure 11: Peak height comparison chart for patient 8..... 113
Figure 12: Peak ratios (EDQ) for patient 8. ..... 113
Figure 13: Flowchart summary of genetic results in 2000-patient two-stage PCR study..... 118
Figure 14: Flowchart summary of genetic results in M.H. Parkinson study. ..... 125
Figure 15: Flowchart summary of genetic results in both 2000-patient two-stage PCR study and M. H. Parkinson study combined..... 125
Figure 16: Proportion of FRDA positives, carriers, no result and negatives among screened cohorts of A) ataxia patients not referred for FRDA, and B) ataxia patients referred for FRDA (M.H. Parkinson). ..... 126

## Chapter Four: Reduced $Ca^{2+}$ Levels in Cardiomyocytes in Friedreich's Ataxia Models

Figure 17: Immunofluorescence Experiments on HL-1 and H9c2 cells: knock-down of endogenous frataxin in cardiac cell lines using siRNA... 156
Figure 18: Increased rate of generation of cytosolic reactive oxygen species (cROS) over time in frataxin-deficient cells from two FRDA cell models. ..... 158
Figure 19: Increased rate of generation of mitochondrial reactive oxygen species (mROS) over time in HL-1 cells with lower frataxin levels..... 159
Figure 20: Representative NADH level traces in HL-1 cells following FCCP and NaCN addition, showing decreased redox index in Fxn-siRNA cells. ..... 161
Figure 21: NADH Levels: Decrease in cells with lower frataxin levels. .. 162
Figure 22: Comparison of TMRM levels during caffeine response in HL-1 and H9c2 cells: abnormal bioenergetics response to caffeine in both cell lines (from Abeti et al, 2018). ..... 163
Figure 23: Caffeine-Induced Ca2+ Transient Amplitude: decrease in cells with lower frataxin levels. ..... 165

Figure 24: Phase II of the caffeine-induced $Ca^{2+}$ signalling response in HL-1 cells (from Abeti et al, 2018). ..... 166
Figure 25: Thapsigargin-Induced Ca2+ Transient Amplitude: decrease in cells with lower frataxin levels in both FRDA cell models. ..... 167
Figure 26: Thapsigargin-Induced $Ca^{2+}$ Transient Amplitude Following Pre-Incubation with Dantrolene: decrease in cells with reduced frataxin levels in the HL-1 FRDA cell model. ..... 169
Figure 27: Thapsigargin-Induced $Ca^{2+}$ Transient Amplitude: increase in average amplitude in dantrolene-treated frataxin-deficient HL-1 cells. .. 170
Figure 28: Thapsigargin-Induced Ca2+ Transient Amplitude: decrease in YG8R primary cells with lower frataxin levels. ..... 172
Figure 29. Summary of Key Findings in FRDA Ca2+ Pathophysiology. 176

# Table of Tables

## Chapter Two: Methods

Table 1: Probes in MRC-Holland SALSA MLPA P316-B2 Recessive Ataxias Probemix. ..... 76
Table 2: QDX2 control fragments in MRC-Holland SALSA MLPA P316-B2 Recessive Ataxias probemix. ..... 77
Table 3: Thermocycler Program for MLPA Reaction. ..... 79
Table 4: Isolation Buffer ..... 83
Table 5: Digestion Buffer ..... 84
Table 6: $Ca^{2+}$-free Medium ..... 95
Table 7: PCR Mastermix for DNA Analysis of YG8R/Y47R Mice. ..... 100
Table 8: PCR Cycles for DNA Analysis of YG8R/Y47R Mice. ..... 101

## Chapter Three: Genetic Screening Study of Ataxia Patients for Friedreich's Ataxia

Table 9: FXN Exon Dosage Quotients (EDQ) for 12 GAA+/- samples and controls. ..... 112

Table 10: General summary of FRDA-positive cases from ataxic patient screening study. ..... 114
Table 11: Clinical features of FRDA-positive cases from ataxic patient screening study, Part 1. ..... 121
Table 12: Clinical features of FRDA-positive cases from ataxic patient screening study, Part 2. ..... 121
Table 13: Clinical features of EFACTS FRDA patients from M.H. Parkinson study, Part 1. ..... 127
Table 14: Clinical Features of EFACTS FRDA Patients from M. H. Parkinson Study, Part 2. ..... 131
Table 15: Clinical features of non-EFACTS FRDA patients from M.H. Parkinson study, Part 1. ..... 136
Table 16: Clinical features of non-EFACTS FRDA patients from M.H. Parkinson study, Part 2. ..... 137
Table 17: Clinical Features in FRDA Patients, M. H. Parkinson Study. . 140

# Publications and Presentations during PhD

## *Publications*

Abeti, R., Brown, A. F., Maiolino, M., Giunti, P. (2018). Calcium deregulation: novel insights to understand Friedreich's ataxia pathophysiology. *Frontiers in Neuroscience*, *12,* 264. https://doi.org/10.3389/fncel.2018.00264

## *Abstracts from Presentations*

**FRDA Screening Study of SCA-Negative Ataxia Patients**; Brown A. F., Parkinson M. H., Sweeney M., Labrum R., Mudanohwo E., Giunti P.; *International Ataxia Research Conference* abstract, Windsor, UK (2015); *Ataxia UK Annual Conference* abstract, Stansted airport, UK (2015).

**Exploring $Ca^{2+}$ Signalling in Friedreich's Ataxia Model Cardiomyocytes;** Brown A. F., Abeti R., Giunti P.; *International Meeting on Spastic Paraparesis and Ataxias* abstract, Paris, France (2016); *Ataxia UK Annual Conference* abstract, East Midlands airport, UK (2016).

# Chapter 1 : Introduction

## 1.1 Introduction

Friedreich's ataxia (FRDA) is an autosomal recessive condition that results in selective neuronal atrophy, affecting the dorsal root ganglia (DRG; Dyck et al., 1968) and the cerebellum (Koeppen et al., 2007). FRDA affects the central and peripheral nervous system, the musculoskeletal system, the heart and the endocrine pancreas. The ataxia is of mixed origin, resulting from spinocerebellar degeneration and an axonal peripheral sensory neuropathy with pyramidal signs (Delatycki & Corben, 2012). The neuropathology is characterized by mild cerebellar and DRG atrophy and a subsequent proliferation of the synaptic terminals of the dentate nucleus, that lead to loss of the dentate nucleus and its efferent fibres (Koeppen et al., 2007).

The development of the neuropathology involved in FRDA has been correlated with age at onset of disease, clinical severity and disease duration (Akhlaghi et al., 2011). The decrease in size and early atrophy of the DRG (Durr et al., 1996; Harding, 1981; Morral et al., 2010; Schols et al., 1997) has been linked to the FRDA clinical characteristics of progressive ataxia, scoliosis and cardiomyopathy (De Biase et al., 2007). Around two-thirds of all patients are found to have severe, life-threatening cardiomyopathy in the middle and late stages of the disease, making this an issue of tremendous clinical relevance (Durr et al., 1996; Harding, 1981; Payne et al., 2011). Indeed, progressive hypertrophic cardiomyopathy is the predominant cause of death in FRDA patients (Hanley et al., 2010; Tsou et al., 2011). The disease is caused by a deficiency of the protein frataxin, which was linked with the FRDA genetic defect discovered in 1996. The precise function of frataxin remains unclear, although it has been linked to changes in iron metabolism, mitochondrial respiration and reactive oxygen species (ROS) levels that have themselves been linked to aspects of FRDA

pathophysiology (Pandolfo & Pastore, 2009). However, no proven disease-modifying treatment exists for FRDA (Perlman, 2012; Wilson, 2012). This introductory chapter reviews the history and chronology of the evolving understanding of FRDA, including the discovery of its genetic basis; details the current understanding of pathogenic mechanisms of the disease; describes its clinical features; and places the aims of my study within the broader context of FRDA research.

## 1.2 Background

In 1863, Dr Nikolaus Friedreich performed what was to become the seminal study of Friedreich's ataxia. Ataxia is a Greek term (ατάξις) meaning 'lack of order'. Although the term has been in use since the time of Hippocrates in medical descriptions, it was not until the 19th century that it adopted its current meaning of incoordination due to neurological dysfunction. In a subgroup of six ataxic patients from two families, Friedreich observed that the form of ataxia he had discovered was hereditary, early-onset, and associated with a slow progression of disease involving an absence of sensory loss in its early stages (Friedreich 1863c, Friedreich 1863a, Friedreich 1863b). His clinical definition still characterises the classical FRDA phenotype. Friedreich observed fatty degeneration of heart tissue in three of his patients, and the early 20th century saw the first reports of cardiac involvement and electrocardiogram (ECG) changes in FRDA. Along with the further observation of diabetes in FRDA, this established FRDA as a multisystem disorder.

In the years since 1863, FRDA has been fully characterized as a unique disorder, with increasingly detailed descriptions of its genetic aetiology, pathophysiology and phenotype. Advances by the 1970s allowed for a reliable set of diagnostic criteria to be developed, in particular through Harding's seminal case series of 115 FRDA patients (Geoffroy et al., 1976; Harding, 1981). The genetic abnormality underlying the great majority of

FRDA cases, a GAA expansion mutation, was discovered in 1996 (Campuzano et al., 1996). This allowed for genotype-phenotype correlation, which in turn led to the discovery of a greater phenotypic spectrum than had been previously assumed. The original diagnostic criteria were thus found to have excluded more atypical FRDA cases that present with very early or late onset of disease, retained reflexes, spasticity and limited disease progression.

## 1.3 Genetics of Friedreich's Ataxia

FRDA is the most common inherited ataxia in Europe. Studies currently set the prevalence of the condition at between 1:20,000 and 1:125,000 in several western European populations (Filla et al., 1992; Vankan, 2013). The GAA expansion mutation has only been discovered among European, north African, Middle Eastern and Indian populations (Labuda et al., 2000). Estimates of the carrier frequency range between 1:60 and 1:110 (Cossee et al., 1997; Epplen et al., 1997; Filla et al., 1992; Harding & Zilkha, 1981; Romeo et al., 1983). Cases within families normally involve either an isolated individual or multiple siblings, indicating an autosomal recessive genetic disorder, although pseudodominance has also been observed (Harding & Zilkha, 1981). The disease occurs at equal frequency among males and females (Schols et al., 1997).

**Genetic Basis for FRDA**

The causative human frataxin gene (*FXN*) was first mapped by genetic linkage studies to chromosome 9p22 (Chamberlain et al., 1988), and then more fully described in 1996 as underlying an autosomal, recessively inherited condition (Campuzano et al., 1996). The discovery of the causative gene allowed for further extension and refinement of studies on the FRDA phenotype. The mutation responsible for the vast majority of FRDA cases was characterized by a homozygous, unstable genetic GAA triplet expansion, and was located in intron 1 of the *FXN* gene on the long arm of chromosome 9 (localized on 9q21.11) (Campuzano et al., 1996,

1997; Koutnikova et al., 1997). In general, these FRDA patients have between 70 and 1700 repeats in both alleles, clustering mostly between 600 and 900 repeats (Campuzano et al., 1996; Entezam et al., 2017; Epplen et al., 1997; Fig. 1). The largest case series to date, carried out on 592 EFACTS patients, gave an average GAA1 (smaller allele) size of 648 repeats and an average GAA2 (larger allele) size of 912 repeats (Reetz et al., 2015). All FRDA patients have at least one pathological triplet expansion in the first intron of the *FXN* gene. While most patients are homozygous for the expansion mutation, 1-3% are compound heterozygous for the GAA expansion in one allele and either a nonsense, missense, or deletion mutation in the other allele (Campuzano et al., 1996; Cossee et al., 1999; Gellera et al., 2007).

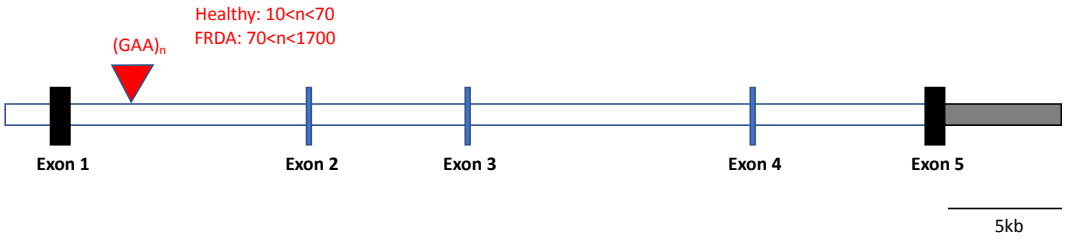


**Figure 1. FXN gene, chromosome 9q21.11.**

### Effect of mutations on *FXN* gene

The GAA expansion, associated with epigenetic changes (Festenstein, 2006), leads to transcriptional inhibition and partial silencing of the *FXN* gene, which in turn leads to pathological suppression of frataxin protein expression. The mechanisms of gene silencing have been studied at length in order to discover a method for targeting the initial gene and finding a viable therapy for FRDA. It is thought to occur due to GAA repeats forming R-loops and 'sticky DNA' triple helices containing non-Watson-Crick pairs, which could physically block transcription by impeding RNA polymerase II (Gacy et al., 1998; Sakamoto et al., 1999). Increased DNA methylation has also been observed upstream of the GAA repeat expansion in peripheral blood mononuclear cells from FRDA patients (Castaldo et al., 2008). The level of methylation is inversely correlated with *FXN* expression and age at onset, suggesting an important role in FRDA, most likely in abnormal

excessive heterochromatinisation leading to gene inactivation (Evans-Galea et al., 2012). Histones are also increasingly deacetylated in FRDA, leading to repressed gene expression (Yandim et al., 2013). These epigenetic studies into FRDA have already allowed histone deacetylase inhibition to be tested as a novel therapeutic strategy through the use of nicotinamide (Libri et al., 2014).

### Frataxin Protein

This gene codes for the protein frataxin, a small, globular, highly conserved, nuclear-encoded protein localized to the inner mitochondrial membrane (IMM) in eukaryotes (Puccio & Koenig, 2000). Frataxin is expressed ubiquitously, but its highest expression levels are in the cells of the heart and spinal cord, its intermediate levels in the cerebellum, liver, pancreas and muscle, and its lowest expression levels in the other organs of the body including the cerebral cortex (Campuzano et al., 1996). Thus, frataxin appears to be expressed more in organs or tissues with high energy demand, such as cardiomyocytes, sensory DRG neurons, pancreatic islet β-cells and cells of the cerebellar dentate nuclei and spinocerebellar tracts, which are all particularly affected in FRDA.

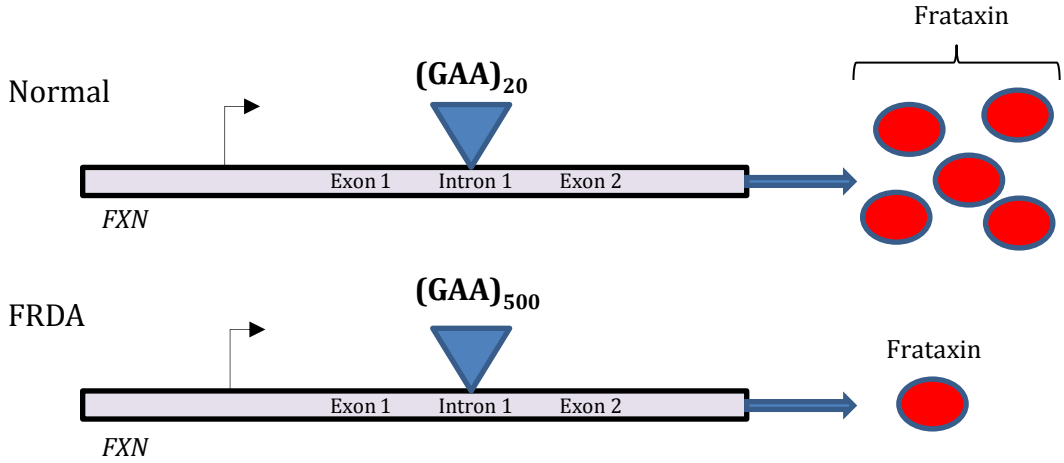


**Figure 2. Schematic representation of GAA expansion in FXN intron 1 causing decreased frataxin production.**

### Effects of FRDA mutations on frataxin protein levels

Studies comparing frataxin levels in FRDA patients against controls through methods such as lateral flow immunoassay of peripheral blood

mononuclear cells showed that the GAA expansion mutation leads to the partial yet significant reduction of frataxin to about 5-30% of original levels (Sacca et al., 2011; Willis et al., 2008; Fig. 2). Some clinical trials have attempted to simply restore frataxin levels in FRDA by using the glycoprotein erythropoietin, which has been shown to increase frataxin levels in FRDA models, but the trials have not displayed any clinical benefits (Mariotti et al., 2013; Nachbauer et al., 2011). The frataxin produced is structurally and functionally normal in typical FRDA (Gottesfeld, 2007; Schmucker & Puccio, 2010). On the other hand, the other rarer FRDA-associated mutations in *FXN* lead to non-functional or partially functional frataxin (Correia et al., 2008). This frataxin decrease is consistent with other loss-of-function, recessive genetic conditions. As shown in knockout animal models, complete absence of frataxin protein is lethal to the embryo in development (Cossee et al., 2000). In most cases, compound heterozygous patients are phenotypically similar to patients who are homozygous for the GAA expansion. However, some missense mutations, such as G130V, D122Y, R165P and L106S, cause an atypical form of FRDA, as do large deletion mutations (Cossee et al., 2000; Gellera et al., 2007). Homozygous point mutations have yet to be described in FRDA cases (Campuzano et al., 1996; Cossee et al., 1999; Gellera et al., 2007). Heterozygous carriers of the GAA expansion mutation, such as the parents of FRDA patients who are not compound heterozygotes, are thought to be clinically unaffected if they lack any other genetic abnormality (Andermann et al., 1976; Harding, 1981). However, these heterozygous carriers are known to produce significantly less frataxin than normal controls (Deutsch et al., 2010; Sacca et al., 2011; Willis et al., 2008). It is evident from these data that frataxin is essential for a healthy life, but its function remains to be fully elucidated.

**Genotype-Phenotype Correlation**

The FRDA phenotype is distinct, yet symptoms can be highly variable. Discovery of the causative gene allowed for further extension and refinement of studies on the FRDA phenotype (Campuzano et al., 1996). This allowed for atypical cases to be revealed via genotype-phenotype correlations following neurogenetic tests, where previously they might have

been misinterpreted based on clinical data. It was discovered in population studies that up to a quarter of genetically diagnosed patients did not fit the original diagnostic criteria proposed by Geoffroy and Harding (Durr et al., 1996; Filla et al., 2000; McCabe et al., 2000; Schols et al., 1997), expanding the phenotypic spectrum of FRDA. These atypical cases are normally either of early onset (before 15 years of age) or late onset (after 25 years of age).

The effect of the GAA expansion mutation on gene transcription has been shown to cause the FRDA phenotype, and the severity of the phenotype is related to the expansion size. The size has been correlated with incidence of cardiomyopathy and rate of progression of disease symptoms, and inversely correlated with age at onset and age of start of wheelchair use (Durr et al., 1996; Filla et al., 1996; Montermini et al., 1997; Rajagopalan et al., 2010). Specifically, around 50% of the variability in age at onset of FRDA has been shown to be accounted for by the size of the GAA expansion (Filla et al., 1996). This variability is caused by intergenerational instability of the GAA triplet expansion (Monros et al., 1997) as well as somatic mosaicism, fluctuations in expansion size during life, interruptions in the expansion and other modifying genetic or environmental elements (Pandolfo & Pastore, 2009).

In recent studies, the GAA expansion size has been statistically shown to account for only 40% of the symptoms in FRDA, which may explain the variability in FRDA symptoms that have been historically observed (Reetz et al., 2015, 2016). This is in contrast to dominant disorders caused by CAG repeats, where the correlation between expansion size and phenotype is considerably stronger. In FRDA, the correlation described is stronger with the smaller in size of the two expansions, GAA1 (Reetz et al., 2015; Schols et al., 1997). Most atypical presentations of FRDA are caused by extremely small or large GAA expansion sizes (particularly of GAA1), as well as by compound heterozygotes with point mutations (Parkinson et al., 2013). The smallest non-interrupted GAA1 expansion reported so far in a patient with FRDA was of 44 triplet repeats, only a little more than in the equivalent expansion size in controls, that has been shown to reach up to 33 repeats

(Sharma et al., 2002). Patients with late-onset atypical FRDA have in most cases between 100 and 500 repeats in the GAA1 allele (Bhidayasiri et al., 2005; Durr et al., 1996; Schols et al., 1997). It has also been shown that compound heterozygotes incorporating a missense point mutation on one allele located near the amino end of the carboxy-terminal domain of the protein may result in a milder FRDA phenotype (Cossee et al., 1999). A study by Saccà et al on white blood cells was the first to combine the determination of frataxin protein deficiency with an mRNA level decrease in FRDA and correlate the results with the genotype and disease severity of the patients. It discovered an inverse correlation between frataxin protein/mRNA levels and the length of both the shorter and longer GAA alleles, as well as a correlation between frataxin protein level, frataxin mRNA level and the age at onset of FRDA (Sacca et al., 2011). However, it should be noted that the vast majority of studies on FRDA patients measure white cell GAA expansion size, a tissue that is not clinically affected in FRDA.

**Frataxin Protein: translation and cleavage**

Frataxin is first translated in the cytoplasm into a 23.1kDa, 210-amino acid species known as frataxin precursor polypeptide ($FXN_{1-210}$) and is then targeted to the mitochondria (Campuzano et al., 1996). The amino acid terminal residues are then cleaved proteolytically by the mitochondrial processing peptidase (MPP). These amino acid residues most likely act as a mitochondrial targeting sequence in this case, and several studies have been carried out to determine which are involved. Although several cleavage sites have been elucidated in a variety of experiments, it is believed that the processing of frataxin precursor occurs in a two-stage process. Firstly, the mitochondrial signal peptide is cleaved (residues 1-42) to produce 18.8kDa, 169-amino acid long intermediate frataxin protein ($FXN_{42-210}$). Secondly, cleavage of the intermediate N-terminal tail (residues 42-81) creates the mature 14.2kDa, 130-amino acid protein ($FXN_{81-210}$) (Branda et al., 1999; Cavadini et al., 2000; Condo et al., 2007). The mature form of the protein is a large, twisted $\beta$-sheet made from a minimum of six anti-parallel $\beta$-strands ($\beta_1$-$\beta_6$) encircled by two α-helices ($\alpha_1$ & $\alpha_2$: Fig. 3).

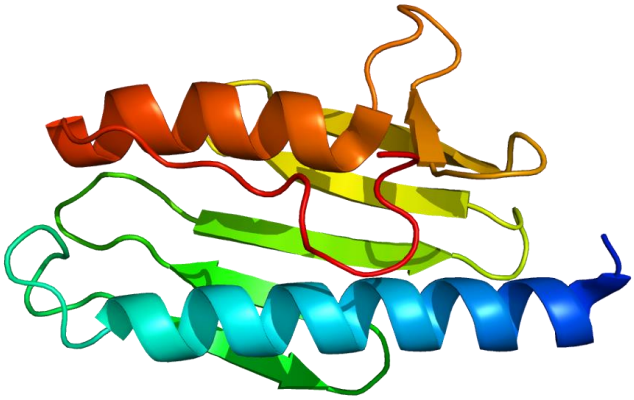

**Figure 3. Mature frataxin protein. α-helices shown as ribbons, β-strands as arrows and C-terminal tail in red. Image in public domain, based on PyMOL rendering.**

## 1.4 Pathophysiology of Friedreich's Ataxia

### 1.4.1 Role of Frataxin

Biopsy studies on FRDA individuals have uncovered three main biochemical features characterising the pathophysiology of the disease:

1. Intracellular iron deposits in the heart (Lamarche et al., 1980; Sanchez-Casis et al., 1976).
2. A deficit in mitochondrial iron-sulphur cluster (ISC)-containing enzymes such as aconitase and the mitochondrial respiratory chain complexes I, II and III in the heart (Rotig et al., 1997).
3. The presence of markers of oxidative damage in blood and urine samples (Bradley et al., 2004; Emond et al., 2000; Schulz et al., 2000).

We have yet to fully understand the precise function of the frataxin protein based on the biochemical features that result from its deficiency. It is now evident from studies, including on the yeast frataxin homolog Yfh1p, that free iron accumulates in the mitochondria, potentially causing oxidative

stress and lowering mitochondrial energy production (Babcock et al., 1997; Branda et al., 1999; Lodi et al., 2001). Some data suggests frataxin is a multifunctional protein involved in a variety of mitochondrial pathways, interacting with other proteins in iron-sulphur (Fe-S) cluster assembly (Shan et al., 2007), haem biosynthesis (Yoon & Cowan, 2004) and intracellular iron homeostasis (Huang et al., 2009). More recent *in vitro* and *in vivo* FRDA studies indicate that the major functional role of frataxin is in ISC biogenesis.

**Iron-Sulphur Clusters (ISCs)**

ISCs are small inorganic redox-active protein cofactors that play a role in fundamental cellular pathways including oxidative phosphorylation and metabolic processes such as enzyme catalysis. They are also involved in gene regulation. Enzymes involved in mitochondrial respiration that contain ISCs include aconitase and mitochondrial complexes I, II and III (Lill, 2009; Martelli et al., 2011). *De novo* ISC biogenesis is a highly conserved but still poorly understood process that occurs in the mitochondria of eukaryotes (Lill, 2009; Rouault, 2012). Upon the scaffold protein ISCU, the platform upon which the rest of the cluster is built, inorganic iron and sulphur form the ISC. The sulphur is produced, via a highly reactive persulphide intermediate, by a cysteine desulphurase (made up of a NFS1-ISD11 protein subcomplex). This enzyme catalyses the conversion of cysteine to alanine to produce the persulphide required to interact with the ionic iron and form the ISC (Pandolfo & Pastore, 2009; Prischi et al., 2010).

**Frataxin and ISCs: role as iron donor**

The Rötig study first associated frataxin with ISC-containing enzymes (Rotig et al., 1997). A time-dependent molecular and functional analysis of *MCK-Cre*, a conditional mouse model that reproduced the cardiomyopathy of FRDA (see Mouse Models section), also pointed towards an essential role of frataxin in ISC biogenesis (Puccio et al., 2001). This confirmed predictions made by a phylogenetic study into the frataxin interactome, which discovered two genes that co-occur with frataxin and whose expressed proteins are required in yeast mitochondria for ISC assembly

(Huynen et al., 2001). Later studies in yeast, where the yeast homolog of frataxin was depleted (Yfh1p), also indicated a key role for frataxin in ISC biogenesis (Duby et al., 2002; Muhlenhoff et al., 2002).

*In vitro* studies on bacterial, yeast and human frataxin made evident a low iron affinity of the protein. The iron was found to bind to a conserved acidic ridge in the $\alpha_1$-$\beta_1$ region of the mature frataxin protein (Cook et al., 2006; Nair et al., 2004). However, *in vivo* studies under physiological conditions have yet to demonstrate iron binding by frataxin. Nevertheless, a specific role for frataxin as an iron donor for the *in vivo* assembly of ISC clusters is indicated by:

1. The iron-dependent interaction of yeast frataxin with Nfs1 and Isu1, the yeast homologs of NFS1 and ISCU (Gerber et al., 2003).
2. *In vitro* reconstitution studies that reveal the ability of human frataxin to transfer iron to ISCU (Yoon & Cowan, 2003).
3. The capacity of CyaY (the bacterial homolog of frataxin) to contribute iron towards ISC formation (Layer et al., 2006).

**Frataxin and ISCs: interaction with ISCU-NFS1-ISD11 complex**

Frataxin has been described as interacting with both enzymes of the cysteine desulphurase sub-complex involved in producing the inorganic sulphur, NFS1 and ISD11, in addition to its apparent role as an iron donor (Gerber et al., 2003; Layer et al., 2006; Li et al., 2009; Shan et al., 2007). This interaction is essential for ISC assembly. More recent studies using mammalian immunoprecipitant and recombinant proteins revealed that frataxin interacts with NFS1, ISD11 and ISCU in a pre-packaged complex. This interaction also causes increased cysteine desulphurase activity, indicating that frataxin modulates the ability of NFS1 to provide sulphur for ISC biogenesis (Tsai & Barondeau, 2010; Schmucker et al., 2011). It has been shown that iron is not essential for interaction between frataxin and the ISCU-NFS1-ISD11 complex (Schmucker et al., 2011), despite iron being shown to improve the activation of NFS1 activity by frataxin (Tsai & Barondeau, 2010). However, data gathered using isothermal titration

calorimetry showed that the interaction of yeast homologs Yfh1p and Isu1 (in absence of Nfs1 and Isd11) depends on iron-binding (Cook et al., 2010), which indicates conversely that the binding of frataxin with iron is a fundamental part of the process culminating in ISC formation. The region of interaction with the complex was shown by an NMR study of Yfh1p to be the $\alpha_1$-$\beta_1$ region, previously observed to bind iron *in vitro*, as well as a large portion of the β-sheet (Cook et al., 2010). These results are supported by mutagenesis experiments determining the region of interaction between mouse frataxin and the ISCU-NFS1-ISD11 complex (Schmucker et al., 2011). However, the exact nature of the interaction remains to be established.

**Frataxin and ISCs: unclear role of frataxin**

It is clear from kinetics studies that eukaryotic frataxin increases the rate of ISC production. It facilitates the transfer of sulphur on the ISC assembly protein ISCU by acting as an allosteric modulator (Bridwell-Rabb et al., 2014). In addition, extramitochondrial frataxin regulates transfer of ISCs to cytosolic aconitase, and thereby exercises molecular control of a switch between enzymatic and RNA-binding cellular functions (Condo et al., 2010). However, how iron delivery and the modulation of NFS1 activity by frataxin are coordinated in the process of ISC biogenesis remains unclear. Some data obtained using the bacterial frataxin homolog can be used as an example of this uncertainty. CyaY has been shown to have a high affinity for the preformed IscS-IscU complex, the bacterial equivalent of the mammalian ISCU-NFS1-ISD11 complex (Prischi et al., 2010). However, *in vitro* reconstitution experiments made evident an inhibition of ISC biogenesis by CyaY, rather than an activation as expected based on previous data (Adinolfi et al., 2009). In stoichiometric conditions, CyaY specifically decreased IscS enzymatic activity in the presence of IscU. Thus, the effect of CyaY on IscS is opposite to that seen in the equivalent proteins of the mammalian system (Iannuzzi et al., 2011). An understanding of the basis for these differences, as well as an understanding of how this activation or inhibition precisely impacts upon the ability of the complex to form ISCs, is as yet unavailable. This understanding may be achieved

through *in vitro* biochemical experiments, as well as a 3D-structure determination of the eukaryotic and bacterial complexes using X-ray crystallography.

**Frataxins & ISCs: point mutation studies**

That frataxin appears to be both an iron donor and an activator of cysteine desulphurase activity, allows for studies to use FRDA missense mutations (see section 1.5.5 for more clinical information on FRDA point mutations) to assess the role and function of frataxin. Four different sets of frataxin point mutations were identified based on their biochemical properties (Bridwell-Rabb et al., 2011; Tsai et al., 2011; Yoon et al., 2012):

1. Genetic variants affecting both frataxin binding to the ISCU-NFS1-ISD11 complex and the cysteine desulphurase activity of the complex (Q153A, W155R)
2. Variants causing a greatly reduced frataxin binding ability, but an only mildly reduced cysteine desulphurase activity (R165C, N146K, W155A)
3. Variants which do not affect frataxin binding, but cause a greatly reduced cysteine desulphurase activity (Q148R)
4. Variants that have only mild defects in both frataxin binding ability and cysteine desulphurase activity (W155F, N146A, Q148G, I154F).

Results indicated however that missense mutations that affected the role of frataxin through different biochemical pathways all led to a very similar FRDA phenotype. An interesting further study could be to observe how point mutation variants that cause atypical presentation of FRDA affect the process of ISC formation (Cossee et al., 1999; Gellera et al., 2007).

**Proposed role of frataxin in other mitochondrial pathways**

In addition to its well-established role in ISC biogenesis, frataxin has been proposed to have other functions. This includes providing iron through direct protein-protein interactions with a variety of mitochondrial proteins,

including mitochondrial aconitase (Bulteau et al., 2004), ferrochelatase for haem biosynthesis (He et al., 2004; Yoon & Cowan, 2004) and succinate dehydrogenase, or respiratory chain complex II (Gonzalez-Cabo et al., 2005). However, as subsequent replication studies were unable to reproduce several of the protein-protein interactions, their relevance has been questioned. Further *in vivo* experiments using a murine fibroblast FRDA model containing human frataxin and deleted for endogenous frataxin, made evident a clear correlation between cellular viability and the ability of frataxin to interact with the ISCU-NFS1-ISD11 complex (Schmucker et al., 2011). This indicates that interaction with this complex is an essential function of frataxin in *in vivo* ISC biogenesis. Thus, although it cannot be excluded that direct protein-protein interactions involving frataxin occur in a particular biochemical context or under certain experimental conditions, the hypothesis of frataxin involvement in other mitochondrial pathways requires greater validation through complementary *in vivo* approaches in order to study the metabolic effects of frataxin deficiency.

**Frataxin and ISCs: Summary**

In order to fully decipher the cellular consequences of the frataxin knockdown, an understanding of its function is fundamental. Although the role of frataxin in ISC biogenesis is now clear, what remains unclear is the correlation between the role of frataxin in ISC biogenesis and the pathophysiology of FRDA. As ISC biogenesis is an essential pathway involved in many cellular processes, a ISC deficiency can lead to multiple and aggregating cellular dysregulations, and an increasing amount of diseases are linked to them (Lill, 2009). How exactly the cell senses the frataxin deficit also remains a challenging question for future studies to answer. Nevertheless, knowledge of the direct link between ISC biogenesis and frataxin levels has opened the door for novel investigations into the cellular and molecular pathophysiology of FRDA.

### 1.4.2 Iron Accumulation and Oxidative Stress in Friedreich's Ataxia

The first findings connecting frataxin directly with iron metabolism were made in yeast mitochondria from cells incorporating a deletion of the frataxin homolog gene, *YFH1*. An iron accumulation was observed in these mitochondria, in addition to a loss of mitochondrial respiratory chain function and aconitase dysfunction (Babcock et al., 1997). A further study on Yfh1p deficiency in yeast confirmed a strong link between frataxin and mitochondrial iron overload, with increasing susceptibility to oxidative stress (Branda et al., 1999). Lower frataxin levels have been found to lead to increased intracellular iron deposits in heart cells from both FRDA patients (Bradley et al., 2000; Lamarche et al., 1980; Sanchez-Casis et al., 1976) and mouse models (Al-Mahdawi et al., 2006; Puccio et al., 2001), with several studies also indicating that iron deposits mainly in mitochondria. The reduction in the activity of ISC-containing mitochondrial respiratory chain complexes I, II and III in endomyocardial biopsy analyses from FRDA patients revealed increased iron deposition in parallel (Rotig et al., 1997).

It is important to note that the role of intracellular iron accumulation in the FRDA cardiac pathology is better established than in the neuronal pathology, although it has been indicated to occur in glial cells supporting the dentate nucleus and dorsal root ganglia (Koeppen et al., 2012; Koeppen et al., 2016). Iron accumulation tends to cause an increase in oxidative stress, as iron is a highly redox-reactive metal whose regulation is critical. Indeed, a link between frataxin deficiency and impaired iron homeostasis leading to mitochondrial iron accumulation and oxidative stress is now well-established (Abeti et al., 2016; Bradley et al., 2004; Emond et al., 2000; Schulz et al., 2000). This is a potential key causal factor in the cell degeneration and death observed in affected tissues in FRDA (Schulz & Pandolfo, 2013; Wilson, 2012).

**Frataxin: role in iron accumulation**

The precise nature of the interaction of frataxin with iron remains controversial. Data from the yeast FRDA model first indicated that frataxin was involved in regulation of cellular iron levels, through its ability to directly bind iron (Adamec et al., 2000). This functional hypothesis was later expanded into considering frataxin as an iron storage protein akin to ferritin. This was based on reports that the frataxin protein formed large aggregates that retained iron in ferric ($Fe^{3+}$) form to help reduce iron toxicity in the cell (Cavadini et al., 2002; Yoon & Cowan, 2003). However, the protein also appears to act as an iron chaperone by providing bioavailable, labile ferrous ($Fe^{2+}$) iron to ISCs, a role that appears counterproductive to its other proposed role as an iron storage protein. For example, there is a correlation in all studied genomes in FRDA between the expression of the frataxin gene and the hscB gene in bacteria, which codes for a chaperonine that is part of the ISC machinery (Huynen et al., 2001). However, this role is yet to be fully proven physiologically.

**Mitochondrial iron accumulation: ISC deficit link**

Mitochondrial iron accumulation is claimed to result from defective ISC biosynthesis, following yeast studies that showed that iron accumulates in the mitochondria of all mutant cells with this ISC deficit (Chen et al., 2004; Radisky et al., 1999). In both animal and human models of FRDA, defects in Fe-S enzymes are detectable before mitochondrial iron accumulation (Puccio et al., 2001). However, the mechanism for this remains unclear. Through regulation of iron homeostasis, ISCs necessarily participate in reversible redox reactions, due to the ability of ionic iron to toggle valency between $Fe^{2+}$ and $Fe^{3+}$. The role of ISCs as a prosthetic group for mitochondrial aconitase and mitochondrial complexes I, II and III allows these proteins to become the site of redox reactions that are required for the correct functioning of the tricarboxylic acid cycle and the mitochondrial electron transport chain respectively (Johnson et al., 2005; Lill, 2009). Thus, the source of iron accumulation in FRDA may be in the dysregulation of these crucial redox reactions, as ROS generation can itself cause iron

accumulation. Furthermore, the iron-responsive element binding protein (IRP1) also contains ISCs. This protein binds to iron-responsive elements (IRE) on the mRNA of proteins with a role in iron metabolism.

Thus, defective ISC biosynthesis could lead to an increase in IRP1-mediated cellular iron uptake, and this has in fact been detected in frataxin-deficient cells (Lobmayr et al., 2005). A vicious cycle may be created with iron transported by transferrin receptor 1 to the mitochondria to increase ISC synthesis, and then accumulating there as the frataxin deficiency continues to block ISC biosynthesis (Pandolfo & Hausmann, 2013). Frataxin has also been shown to interact with a mitochondrial protein known as ferrochelatase, which mediates the insertion of iron into the porphyrin precursor during haem biosynthesis (Lesuisse et al., 2003). However, as faulty haem synthesis has never been observed as an important aspect of FRDA, its significance remains poorly understood. From these studies, it is evident that frataxin plays an essential, if still partially understood, role in mitochondrial iron metabolism.

**Frataxin and oxidative stress**

It is widely accepted that high free iron levels lead to increased ROS production and greater oxidative stress. In addition, lack of frataxin in affected cells causes changes in gene expression leading to down-regulation of proteins involved in mitochondrial ISC synthesis, as well as cytosolic and mitochondrial iron uptake. This iron dysregulation itself increases the fraction of labile redox-active iron in the mitochondria, inhibiting mitochondrial respiration and progressively enhancing ROS generation (Isaya, 2014). This can lead to mitochondrial dysfunction, oxidative stress and further mitochondrial iron accumulation (Pandolfo & Pastore, 2009). Frataxin deficiency has been shown to lead to oxidative damage in humans (Schulz et al., 2000), mice (Abeti et al., 2016; Abeti et al., 2015; Ristow et al., 2003), yeast (Karthikeyan et al., 2003) and *Caenorhabditis elegans* (Vazquez-Manrique et al., 2006). Specifically, in cerebellar granule neurons from a FRDA mouse model a mitochondrial energy imbalance between respiratory chain complexes I and II was

observed, leading to a basal excess of ROS and subsequent lipid peroxidation, glutathione depletion and cellular death (Abeti et al., 2016). In addition to mitochondrial iron accumulation, the frataxin-deficient yeast model (Babcock et al., 1997) and the FRDA patient fibroblast model (Wong et al., 1999) showed increased sensitivity to $H_2O_2$. The $H_2O_2$ molecule, through reaction with ferrous iron ($Fe^{2+}$) through the Fenton reaction, generates the highly toxic hydroxyl ($^{\cdot}OH$) radical. The frataxin deficiency causes both ingredients of the Fenton reaction to increase: the iron, through malfunctioning ISC biosynthesis, and the $H_2O_2$ via a decrease in respiratory chain function caused by impairment of the ISC-containing complexes I, II and III.

This pathway provides evidence that oxidative damage in both mitochondrial and nuclear DNA and to ISCs in aconitase and the electron transport chain (ETC) is at least worsened by the mitochondrial iron overload that results from frataxin deficiency (Babcock et al., 1997; Cavadini et al., 2002; Karthikeyan et al., 2002), even if the ISC defects appear to occur before the mitochondrial iron accumulation (Puccio et al., 2001). The evidence that frataxin-deficient cells are more sensitive to oxidative stress was increased by further studies (Condo et al., 2007; Tan et al., 2001), some of which showed a specific role for frataxin in protecting the cell against iron-induced oxidative damage (Gakh et al., 2006; O'Neill et al., 2005), a function that could be linked to the concept of frataxin as an iron chaperone or iron-storage molecule (Park et al., 2003).

**Therapeutic goals in FRDA Physiology Studies**

Therapeutic studies consequential to these physiological FRDA studies on downstream effects of frataxin deficiency logically included antioxidants such as idebenone and iron chelators such as deferiprone used alone or in combination, but although there has been halting progress, no clinical trial has stopped or reversed disease progression (Pandolfo et al., 2014; Parkinson et al., 2013). Therefore, more pathophysiological insights into FRDA are crucial. FRDA pathophysiology studies have yet to answer the following riddle: is the increased ROS production in FRDA primarily due to

a progressive reduction in ISC-containing enzymes via imbalanced oxidative phosphorylation, due to inhibition of the mitochondrial electron transport chain (ETC) complexes I, II and III? Or alternatively, is the increased ROS production due primarily to an accumulation of reactive iron in the mitochondria through the reduction in ISC biosynthesis, or a cellular or mitochondrial issue with $Ca^{2+}$ homeostasis, leading in turn to oxidative stress and a worsening of mitochondrial abnormalities (Fig. 4)? That the Abeti study was able to rescue the FRDA model mouse from its toxic oxidative pathophysiology not by correcting the upstream energy imbalance at the mitochondrial respiratory chain, but simply by preventing lipid peroxidation and activating antioxidant pathways within the mitochondria, offers some hope that therapeutic measures in FRDA need not necessarily address the ISC deficit directly (Abeti et al., 2015). Resolving these questions will be crucial for determining which of the multiple physiological pathways involved in FRDA is of most direct relevance to the clinical presentation of the disease, and therefore to an eventual disease therapy.

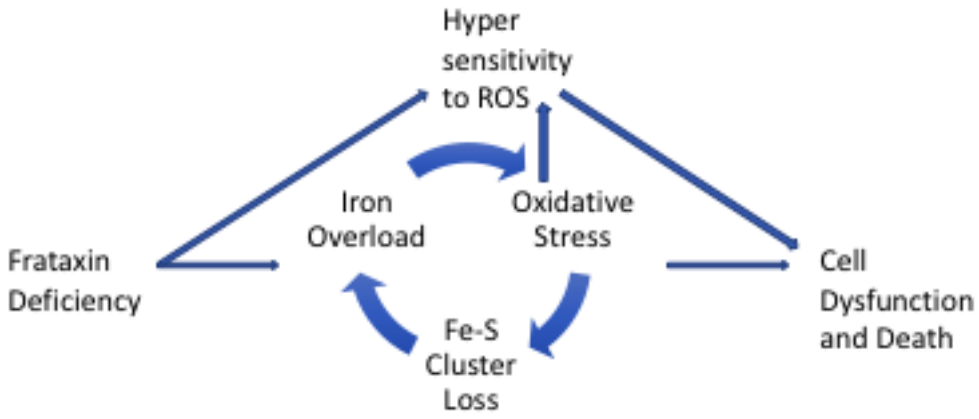


**Figure 4: Potential pathway for FRDA pathophysiology.**

A 'vicious cycle hypothesis', in which frataxin depletion leads to cell dysfunction and death through a pathophysiology rooted in iron overload, oxidative stress and/or ISC loss. For example, frataxin deficiency has been shown to lead to ISC deficiency, which usually precedes a mitochondrial iron overload. The iron overload leads to increased production of free radicals such as superoxide and hydrogen peroxide, which in turn affects ISC levels and ISC-containing proteins involved in mitochondrial function, leading to cellular dysfunction and death. Deficiency of antioxidant defences are also directly caused by loss of frataxin leading to a hypersensitivity to ROS of ISCs (which may itself also be directly

caused by frataxin deficiency). This again leads to mitochondrial iron accumulation and cellular dysfunction. It is important to note that all of these pathophysiological elements are interrelated, and likely to be at play in FRDA. However, one particular element of the pathway may be more responsible for the FRDA phenotype, and thus more therapeutically relevant.

### 1.4.3 $Ca^{2+}$ Signalling and Oxidative Stress in Cardiomyocytes

**$Ca^{2+}$ Studies in FRDA: introduction and future**

The established oxidative stress in FRDA has been associated with increased mitophagy, impaired cytoskeletal dynamics and mitochondrial transport, abnormal lipid metabolism, and abnormal $Ca^{2+}$ homeostasis (Gonzalez-Cabo & Palau, 2013). In studies of disorders other than FRDA, iron-induced oxidative stress has very often been associated with altered $Ca^{2+}$ homeostasis. In particular, it has been associated with reduced peak systolic $Ca^{2+}$ levels, slowed rates of $Ca^{2+}$ relaxation and elevated diastolic $Ca^{2+}$ levels in diseases such as hereditary haemolytic anaemia and other iron-overload conditions (Oudit et al., 2006; Schwartz et al., 2002). These can lead to arrhythmias and sudden death, both of which have also been found to occur in FRDA.

Although $Ca^{2+}$ homeostasis has been very rarely observed in FRDA studies, those that have been performed do indicate an altered $Ca^{2+}$ homeostasis in DRG neurons (Mincheva-Tasheva et al., 2014; Molla et al., 2017). The study by the Palau group in particular discovered dysfunctional mitochondria within axonal spheroids in frataxin-deficient sensory neurons of the DRG from the YG8R mouse models, and indicated that these axonal spheroids may be a direct consequence of $Ca^{2+}$ overload, alongside oxidative stress and mitochondrial depolarisation (Molla et al., 2017). These defects in $Ca^{2+}$ levels and in mitochondrial function had previously been experimentally related to retrograde axonal transport failure alongside an abnormal distribution of distal mitochondria, leading to dying-back

neuropathy in a Drosophila melanogaster larvae model with reduced frataxin expression (Shidara & Hollenbeck, 2010).

Frataxin overexpression in 3T3-L1 adipocytes increased mitochondrial buffer $Ca^{2+}$ capacity, as well as mitochondrial bioenergetics (Ristow et al., 2000). Conversely in an SH-SY5Y human neuroblastoma model incorporating stable frataxin silencing, mitochondrial buffer $Ca^{2+}$ capacity was decreased, associated with mitochondrial dysfunction (Bolinches-Amoros et al., 2014). A study of $Ca^{2+}$ homeostasis in FRDA model cardiomyocytes, which have a different pathophysiology to neurons, has only been carried out extremely recently in the Giunti lab where I have produced this thesis, to which I contributed several novel findings which are elucidated and discussed alongside other experiments performed by other scientists from the lab in Chapter 4 of this thesis (Abeti et al, 2018). Given the known association between iron-induced oxidative stress and altered $Ca^{2+}$ homeostasis, as well as the overlap in symptoms between FRDA and other iron-overload diseases, such studies could be of great benefit in unpicking the pathophysiological mechanism of FRDA in heart cells.

**Importance of the SR and RYR2 in $Ca^{2+}$ Signalling and E-C Coupling**

In order to form a hypothesis regarding the effect of $Ca^{2+}$ dysregulation in FRDA, we must first look at the fundamental role of $Ca^{2+}$ signalling in excitation-contraction coupling in cardiomyocytes. $Ca^{2+}$ homeostasis in cardiomyocytes is achieved through the integration of transsarcolemmal influx and efflux pathways. This homeostasis is modulated by membrane potential and by a system of intracellular $Ca^{2+}$ uptake and release controlled chiefly by the sarcoplasmic reticulum (SR). The crucial importance of the SR as the dynamic $Ca^{2+}$ store in cardiomyocytes, providing an essential source of $Ca^{2+}$ signals to cardiac muscle, is universally accepted. In cardiomyocytes, $Ca^{2+}$ influx mostly occurs through voltage-gated L-type $Ca^{2+}$ channels. Once in the cell, the $Ca^{2+}$ ions can then bind to the RYR2 protein, the cardiac isoform of the ryanodine receptor that is found in the sarcoplasmic reticulum membrane. This binding in turn leads to the release of $Ca^{2+}$ ions from the SR $Ca^{2+}$ store through the RYR2 into the cytosol (Fig.

5). This process is known as $Ca^{2+}$-induced $Ca^{2+}$ release (CICR), where the presence of $Ca^{2+}$ itself induces further $Ca^{2+}$ release from SR stores (Ramay et al., 2010). The $Ca^{2+}$ binds to the C domain of troponin, a complex of three proteins integral to muscle contraction in the heart. This shifts the tropomyosin protein to allow the myosin ATPase to bind to actin, and thereby cause cardiac muscle contraction (Berridge et al., 2003; Bootman et al., 2001).

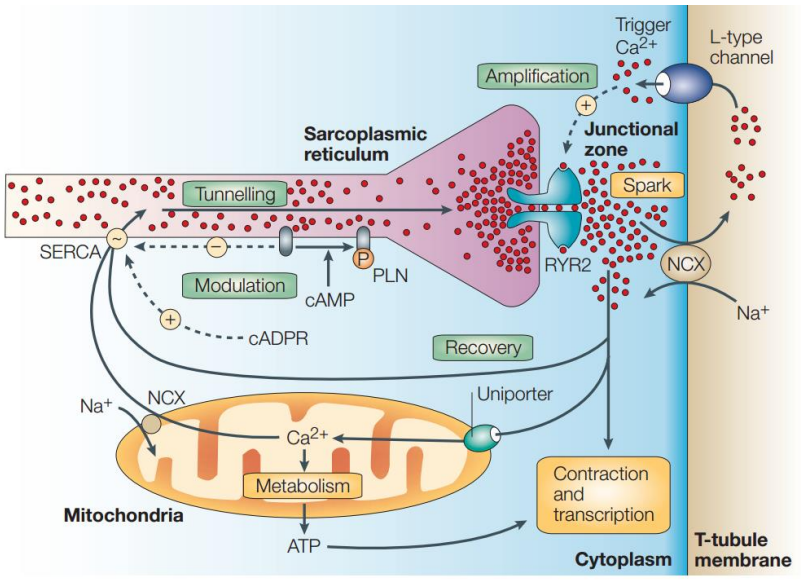


**Figure 5. Ca2+ Signalling in Cardiomyocytes.**

After an action potential depolarizes the cell membrane, the voltage-gated L-type channels are activated. The resulting $Ca^{2+}$ influx activates the RYR2 on the SR membrane, leading to CICR. This in turn results in a $Ca^{2+}$ spark that initiates muscle contraction and gene transcription. The role of the mitochondria as a $Ca^{2+}$ store, and the SR $Ca^{2+}$ ATPase (SERCA) and $Na^{+}$-$Ca^{2+}$ exchanger (NCX) as $Ca^{2+}$ transporters, is also visualised. Figure from Berridge *et al.*, 2003.

### SR-mitochondria microdomains and ROS regulation

In cardiac myocytes, the RYR2 proteins on the SR form regular microdomains with mitochondria. Within these microdomains, the mitochondria and SR can sustain local interorganellar $Ca^{2+}$ communication (Csordas et al., 2006; Garcia-Perez et al., 2008). As mitochondria are one of the major sources of intracellular ROS production, mitochondria-derived ROS could regulate $Ca^{2+}$ spark activity in intact cardiac myocytes. It has

been shown that mitochondrial ROS exerts bidirectional regulation of $Ca^{2+}$ sparks in a dose- and time-dependent manner (Yan et al., 2008).

**Oxidation-sensitive residues in receptors relevant to $Ca^{2+}$ Signalling**

Both the SR $Ca^{2+}$ ATPase (SERCA) pump, which pumps $Ca^{2+}$ into the SR at the expense of ATP, and the ryanodine receptors contain many free cysteine (Cys) residues that are sensitive to oxidation. For example, studies on rabbit cardiac and skeletal muscle first indicated that hydroxyl radicals bind to residues of the SERCA pump within the active site of the enzyme (Xu et al., 1997). From this it was later found that Cys674 appears to play a key and dual role in the oxidative regulation of the SERCA. Mild oxidative conditions lead to S-glutathionylation of Cys674 and increases pump activity. Extensive or extended exposure to oxidative stress leads to oxidation of other Cys residues and sulphonylation of Cys674, irreversibly inhibiting the pump (Adachi et al., 2004; Sharov et al., 2006). As the RyRs contain many free Cys residues, it has proved difficult to identify a specific target residue on which oxidative stress acts. However, S-glutathionylation and S-nitrosylation are two oxidative mechanisms that have been proposed as relevant to RYR2 regulation. In addition, it has been shown that oxidative stress leads to disulphide bonds forming between adjacent subunits in the RYR2, potentiating its activity (Zima & Mazurek, 2016). Thus, in the case of both the SERCA and the ryanodine receptor, distinct functional changes brought about by mild or severe oxidative stress illustrate that ROS can be either a signalling event or a harmful stress condition depending on the amount present.

**Effects of iron-induced Oxidative Stress in Cardiomyocytes**

For the purposes of my study, the possible effects on $Ca^{2+}$ homeostasis through the oxidative stress generated by iron overload in cardiomyocytes is of special interest. As previously mentioned, iron-induced oxidative stress in the heart and its effects are associated with hereditary haemolytic anaemia and other iron-overload conditions. Oxidative damage has also been shown to affect the electrical and contractile properties of cardiomyocytes through several key regulators of excitation-contraction

coupling that are highly sensitive to changes in the cellular redox state. These are specifically:

1. An increase in sarcoplasmic reticulum $Ca^{2+}$ leak through the cardiac ryanodine receptors in SR vesicles isolated from canine cardiac heavy muscle (Kawakami & Okabe, 1998) and rat ventricular cardiomyocytes (Cherednichenko et al., 2004).
2. Inhibition of activity of the SERCA pump in isolated SR vesicles from rabbit cardiac and skeletal muscle (Xu et al., 1997) and guinea pig ventricular cardiomyocytes (Goldhaber & Qayyum, 2000).
3. A reduction of L-type $Ca^{2+}$ channel current in guinea pig ventricular cardiomyocytes (Lacampagne et al., 1995), a finding corroborated in mouse cerebral cortical neurons (Shirotani et al., 2001).

### 1.4.4 Cellular and Animal Models of FRDA

In the 20-year span since the link between FRDA and the *FXN* gene mutation was identified, a variety of FRDA models have led to advancements in the understanding of frataxin protein function, FRDA pathophysiology and mechanisms of gene silencing and instability. Due to its high evolutionary conservation, the effect of frataxin has been modeled in a variety of organisms, including yeast (Babcock et al., 1997; Foury & Cazzalini, 1997), *Caenorhabditis elegans* (Vazquez-Manrique et al., 2006; Ventura et al., 2006; Zarse et al., 2007), *Drosophila melanogaster* (Anderson et al., 2008; Llorens et al., 2007) and mice (Al-Mahdawi et al., 2006; Miranda et al., 2002; Puccio et al., 2001). These models have confirmed mitochondrial dysfunction with iron accumulation and hypersensitivity to oxidative stress as relevant factors in FRDA.

The difficulty of replicating the triplet repeat nature of the common *FXN* mutation poses a problem in modeling FRDA in cell and animal models. As FRDA has a complex clinical phenotype and several species-specific disease pathways, mouse or other mammalian-based cell models are better suited to answering pathophysiological questions. Thus far, the generation of conditional and, increasingly, GAA-based mouse models have been more rewarding than the design of stable cellular models using cell types relevant to the disease, despite the limitations inherent to each model. Both methods remain however of great interest for understanding FRDA pathophysiology (Al-Mahdawi et al., 2006; Miranda et al., 2002; Puccio et al., 2001). Much current work in FRDA is focused on producing superior mouse models that accurately reproduce the partial frataxin deficiency to better model individual FRDA patients. This is usually done by introducing GAA expansion-containing constructs in either mouse or cellular models, or increasingly by the use of induced pluripotent stem cell (iPSC)-derived cells.

**Conditional and GAA-based mouse models of FRDA**

The first working FRDA mouse models were conditional knockout models, which reproduced the disease pathophysiology in the heart and nervous system and allowed for the testing of a variety of therapeutic approaches. These models produced a conditional ablation of the mouse *Fxn* gene by using the Cre-*loxP* recombination system for deletion of *Fxn* exon 4 from a conditional floxed allele ($Fxn^{L3}$) using tissue-specific (and sometimes inducible) Cre mouse lines. These lines include the cardiac-specific model *MCK-Cre* (Puccio et al., 2001), the neuronal model *NSE-Cre* (Puccio et al., 2001), and the neuronal model $Prp\text{-}CreER^{T}$ (Simon et al., 2004), which had a complete absence of the frataxin protein only in their respective target tissues.

GAA-based mouse models of FRDA instead incorporate a knock-in of a human *FXN* GAA expansion mutation into a mouse in which the native *Fxn* gene has been fully ablated. This means expression of frataxin is entirely dependent on the knock-in human gene and brings about a low level of

structurally normal frataxin protein in affected tissues that mimicks FRDA. These GAA-based models, generated both by the Pook lab (Al-Mahdawi et al., 2006) and the Pandolfo lab (Miranda et al., 2002), are more reliable mimics of the human disease than the previously produced conditional knockout models. This is because the progressive disease found in patients is the result of constant atypically low levels of frataxin, rather than the sudden, total tissue-specific frataxin deficit that occurs with the conditional knockout approach. The GAA-based model is also preferable as GAA expansions themselves could be a contributing factor in disease development. For example, the intrinsic somatic instability of long GAA tracts indicates they may have a role in the tissue specificity of FRDA. This model also allows for studies looking at how to increase transcription of the *FXN* gene. However, the phenotype of these animals is less severe than in the conditional knockout model. The models can also help to elucidate molecular and cellular mechanisms associated with GAA-mediated silencing of the *FXN* gene *in vivo*, as well as being crucial for the therapeutic evaluation of drugs that attempt to target this process precisely. However, generation of adequate GAA-based models that reproduce the FRDA phenotype is experimentally difficult for several reasons. These include the difficulty in generating a GAA expansion lengthy enough to cause pathogenesis, and also identifying the locus for genomic integration. The intrinsic instability of GAA tracts also leads to unaccounted contraction or elongation of the expansion.

Two major GAA-based mouse models have thus far been developed:

1. The KIKI/KIKO mouse model, obtained via a knock-in approach based on homologous recombination.
2. The YG8R mouse model, obtained via a human genomic yeast artificial chromosome (YAC) transgenic approach.

*KIKI/KIKO*

The knock-in (KIKI) mouse incorporates a homozygous 230 GAA-repeat expansion knock-in in both alleles and shows a 25% decrease in frataxin expression. The knock-in-knockout (KIKO) mouse is compound

heterozygous, with one allele fully deleted for frataxin: this model expresses 25 to 35% of wild-type mouse frataxin levels, which accurately reflects pathological levels in human patients (Miranda et al., 2002). However, no pathological phenotype was evident in the KIKO mice, despite some minor motor deficits upon rotarod testing and gait analysis. This suggests that despite the low frataxin levels, the transcriptional frataxin decrease does not reach the required threshold to induce FRDA. Despite this, transcriptome analysis of KIKI and KIKO mice showed transcriptional modifications that are significantly different from control mice (Coppola et al., 2009).

*YG8R*

Between the years 2001 and 2004, the Pook lab developed a new mouse model for improved replication of the FRDA phenotype. The human genomic YAC FRDA transgenic mice integrate the human *FXN* locus and its regulatory elements, inserted into the murine genome via a 370kb YAC on a genetic background in which the murine *Fxn* gene has been completely deleted. These unstable GAA-repeat expansions rescue the embryonic lethality of the *Fxn* knockout through expression of only human frataxin. Two pathological models have been developed, YG22 and YG8, which contain $GAA_{190}$ and $GAA_{190+90}$ respectively (Al-Mahdawi et al., 2006). The rescued YG8 mice, referred to as YG8R mice, display lower levels of human frataxin mRNA and frataxin protein, as well as mild motor coordination deficits, a progressive decrease in locomotor activity and increased weight. They also show large neurodegeneration vacuoles in the DRG and decreased aconitase activity in the cerebellum (Al-Mahdawi et al., 2006), reminiscent of features also found in the *NSE-Cre* and *Prp-CreER*$^{T}$ conditional FRDA mouse models (Puccio et al., 2001; Simon et al., 2004).

Although no severe heart dysfunction is seen in YG8R mice, studies of heart tissue revealed decreased aconitase activity, mitochondrial iron accumulation and evidence of lipid peroxidation indicative of ROS damage. They also revealed a non-significant reduction in the activities of mitochondrial respiratory chain complexes I, II and III. There are increased biomarkers of oxidative stress in brain, cerebellum and heart cells,

displayed through increased levels of oxidized proteins via oxyblot analysis, as well as through increased levels of malondialdehyde, a marker of lipid peroxidation (Al-Mahdawi et al., 2006). More recently, Abeti et al discovered that cerebellar granule neuronal cells from the YG8R mouse model have a mitochondrial energy imbalance between respiratory chain complexes I and II, leading to free radical production causing lipid peroxidation, glutathione depletion and cell death (Abeti et al., 2016), and that could be rescued with activation of mitochondrial antioxidant pathways and blocking lipid peroxidation (Abeti et al., 2015). This model has also proved very useful in studies into the instability of the GAA repeat in FRDA, as it reproduces the age-related somatic instability (particularly in the cerebellum) and intergenerational instability characteristic of the disease.

**Conclusion on GAA-based models**

Both the KIKI/KIKO and YG8R mice have proved extremely useful in studies into the mechanisms of GAA-mediated silencing and, in the case of YG8R, GAA somatic instability. The status of the YG8R model in particular as a good representation of FRDA was strengthened by further studies showing a similar epigenetic profile of DNA methylation in the brain, cerebellum and heart to patients with the disease (Al-Mahdawi et al., 2008), as well as an initial pathophysiological profile further developed by newer studies (Abeti et al., 2016; Abeti et al., 2015). Mouse models are currently being created with a larger GAA expansion size within the human *FXN* transgene in order to produce a more severe phenotype and more accurately mimic FRDA. To this end, bacterial artificial chromosomes (BACs) with the ability to incorporate the entire *FXN* locus with larger GAA expansions are being generated. These novel constructs will be valuable in further FRDA research.

**Mouse Models Summary/Future**

Many aspects of molecular FRDA pathophysiology remain to be addressed in molecular and cellular level studies using the different mouse models generated. For example, experiments on the YG8R FRDA mouse models

have shown that autophagy is certainly involved in the neurodegeneration of the large sensory neurons of the DRG, although the molecular and cellular mechanisms remain unknown (Al-Mahdawi et al., 2006; Simon et al., 2004). Increased autophagy has also been observed in the SH-SY5Y human neuroblastoma cell model silenced for frataxin, and proposed as a defence mechanism against oxidative stress (Bolinches-Amoros et al., 2014). Although the role of oxidative stress in pathology remains poorly understood, iron dysregulation is commonly observed in FRDA, usually through mitochondrial iron accumulation (Koeppen et al., 2007; Lamarche et al., 1980; Michael et al., 2006). Indeed, iron chelators are considered as potential therapeutic agents in FRDA (Richardson, 2003), and deferiprone is currently being tested in clinical trials. Mouse model-based FRDA studies will continue to be crucial in understanding the precise molecular mechanisms in the disease pathophysiology, as well as to assess potential therapeutic agents. They may also be crucial for understanding the long-term outcome in FRDA heart disease via *in vivo* and *in vitro* studies, and for developing therapies which ameliorate this aspect of the multisystem disorder.

**Cellular models of FRDA**

Cell culture models that replicate FRDA accurately are of crucial importance in further elucidating the molecular mechanisms of FRDA, as well as for use in novel therapeutic studies. The majority of cell culture-based studies into FRDA pathogenesis used patient-specific immortalized lymphoblasts, primary fibroblasts or peripheral lymphocytes, and these cell lines are still used in FRDA studies. These patient-derived cells reproduced several molecular features of FRDA, such as the epigenetic silencing of *FXN* expression. However, they develop none of the phenotypic characteristics of FRDA (Rotig et al., 1997; Sturm et al., 2005). A variety of cell lines (such as fibroblasts, neuronal cell lines and Schwann cells) have undergone siRNA- or shRNA-mediated silencing in order to reduce frataxin expression and attempt to generate a disease model with more relevant features (Lu et al., 2009; Napoli et al., 2007; Santos et al., 2001; Stehling et al., 2004; Zanella et al., 2008). However, these cell models have shown an

excessively variable phenotype in studies, most likely due to the variable efficiency of frataxin knockdown, ranging from almost complete knockout of frataxin expression to about 40% of normal frataxin levels. Thus, there is still a requirement for stable, disease-relevant cellular models in FRDA studies.

Two other strategies have also been developed in recent years to develop new FRDA cellular models:

1. Using murine fibroblasts to express a transgenic human frataxin gene incorporating various point mutations previously identified in compound heterozygous patients (G130V, I154F or N146K), prior to the deletion of endogenous *Fxn* (Calmels et al., 2009; Schmucker et al., 2011).
2. Generation of iPSCs from FRDA patient fibroblasts using newly developed techniques (Ku et al., 2010; Liu et al., 2011; Wu & Hochedlinger, 2011).

## 1.5 Clinical Features

**EFACTS**

The European Friedreich's Ataxia Consortium for Translational Studies (EFACTS) was founded in 2010 in order to form a single expert body in clinical neurology, biochemistry, molecular biology, genetics and bioinformatics for a more translational approach to the study of FRDA. A large, pan-European patient cohort with genetically confirmed FRDA was recruited. Their presentation and progression are recorded, forming a patient registry linked to a database of biological samples collected during study, which can be used in therapeutic trials and research studies. The

EFACTS program thus has the potential to increase our understanding of the clinical features of FRDA, and their relation to FRDA genetics (Reetz et al., 2015, 2016).

### 1.5.1 Early Onset Friedreich's Ataxia

Harding found that under 20% of FRDA patients developed symptoms prior to the age of 5, and such cases are now clinically classified as early onset Freidreich's ataxia (Harding, 1981). This minority of patients have a phenotype that is more severe and rapidly progressive than in classical FRDA and also involves a greater risk of cardiac symptoms, pes cavus and scoliosis. It is characterized by defective development instead of the degenerative phenotype associated with classical and late-onset FRDA: the patients are often undersized, with short limbs (Harding, 1981). Early onset Freidreich's ataxia patients are associated with a larger GAA1 expansion (Durr et al., 1996; Schols et al., 1997). Specifically, patients in the Durr study with over 780 GAA1 repeats had an average age at onset of 9.7 years, compared with a mean age at onset of 22.5 years in patients with a GAA1 expansion of fewer than 520 repeats (Durr et al., 1996). Compound heterozygosity with exonic deletions has also been shown to cause an earlier onset and more severe form of FRDA, although the rarity of this genetic form of FRDA in the literature currently suggests that it has little impact on the clinical picture of early onset FRDA (see section 1.6.2, Chapter 1).

### 1.5.2 Classical Friedreich's Ataxia

#### *Neurological Features*

**Age at Onset**

The typical age at onset of FRDA is around the beginning of puberty, between the ages of 10 and 16. Three major early case series testing mean age at onset gave a mean of 10.5±7.4 years (Harding, 1981), 11.6±4.5

years (Filla et al., 1990) and of 15.5±8 years of age (Durr et al., 1996). The modal age at onset is 10-12 years in one study (Harding, 1981) and 12-15 years in another (Filla et al., 1990). However, as the age at symptom onset is studied retrospectively, there is a possibility of inaccurate recall. Also, in case studies preceding the discovery of the genetic basis for FRDA, the clinical criteria were skewed toward an average age of onset that was earlier than the actual age, as many atypical FRDA cases were not included in the studies. In the largest case series so far, 592 EFACTS patients were tested giving a mean age at onset of 15.7±10.4 years of age (Reetz et al., 2015). Earlier onset cases tend to have a faster disease progression and display a higher frequency of non-neurological disease features such as cardiomyopathy and pes cavus.

**Symptom Introduction**

FRDA is a neurodegenerative disease characterized by slow, relentlessly progressive spinocerebellar and sensory ataxia. The classical phenotype regularly involves gait and limb ataxia, poor coordination and balance, leg weakness, sensory loss, areflexia, dysarthria, dysphagia, eye movement abnormalities, scoliosis, foot deformities, cardiomyopathy and diabetes. The most frequent presenting symptoms of FRDA are gait ataxia and clumsiness (Delatycki et al., 1999; Durr et al., 1996; Filla et al., 1990; Harding, 1981). A small number of patients also present with scoliosis alongside additional neurological features. FRDA is commonly confirmed by presence of pyramidal signs, muscular weakness, positive extensor plantar response and an absence of deep tendon reflexes (Harding, 1981; Pandolfo & Pastore, 2009). Gait and limb ataxia, dysarthria and lower limb areflexia are found in practically all cases, although their frequency may have been overestimated in early FRDA case series as they were required clinical features in diagnostic criteria before the discovery of the genetic basis of FRDA. It is important to clinically differentiate FRDA from other neurological disorders that are also characterized by early onset cerebellar ataxia and the presence of neuropathy in combination with non-neurological features such as spasticity. These similar disorders include ataxia with vitamin E

deficiency, ataxia with oculomotor apraxia types 1 and 2, ataxia with coenzyme $Q_{10}$ deficiency and late-onset Tay-Sachs disease. (Delatycki & Corben, 2012; Schulz et al., 2009).

**Gait & Limb ataxia**

Patients classically present with an unsteady gait, and have typically lost the ability to stand or walk due to loss of motor skills an average of 15.5 years after age at onset, ranging between 3 and 44 years (Harding, 1981). Patients also usually display truncal ataxia that causes swaying while sitting, and a positive Romberg's test. This requires progressively increasing levels of support, and most patients require a wheelchair within 10 to 15 years after disease onset (Durr et al., 1996; Harding, 1981; Schols et al., 1997). Distal upper limb wasting and loss of vibrational and joint position sense was usually present by 45 to 50 years after onset (Harding, 1981), and the mean age at onset of upper limb ataxia was of 19.8 years of age. (Schols et al., 1997). Limb ataxia leads to increasing difficulties with daily activities involving dexterity and coordination.

**Pyramidal weakness/Muscle weakness**

Pyramidal weakness is usually a relatively late sign in FRDA, present in the lower limbs by 25 to 30 years after onset (Harding, 1981). An underlying pyramidal pathology is however already present early in FRDA due to the frequency of extensor plantars as a sign. Upper limb strength is better maintained, with only mild distal upper limb weakness which can however affect fine manual dexterity. Distal muscle wasting is seen as a late sign in a significant amount of cases, although this issue does not apply to early-onset cases where muscle bulk may never establish itself in the first place (Durr et al., 1996; Filla et al., 1990; Harding, 1981).

**Areflexia**

Areflexia, especially in the lower limbs, is an early and extremely frequent FRDA sign in patients and is a reflection of the underlying peripheral neuropathy. Extensor plantar reactions are an early sign of FRDA present in between 73% and 89% of cases (Delatycki et al., 1999; Durr et al., 1996;

Harding, 1981). Muscle tone in the early stages is however usually normal or only slightly reduced. In more advanced stages when patients are wheelchair-bound, spasticity of the lower limbs can manifest, which can lead to muscle spasms and contractures. One study however used biomechanical methods to detect spasticity of the lower limbs in patients with disease durations of under 10 years, demonstrating once again the wide phenotypic range of FRDA (Milne et al., 2016).

**Dysarthria**

Dysarthria is a frequent sign of FRDA that is already present in many patients at onset and progresses during the course of disease, with over 90% of patients developing it at some stage. A study of 38 FRDA patients showed that 68% had mild dysarthria characterized by consonant imprecision, decreased pitch variation and impaired loudness maintenance (Folker et al., 2010). The mean age at onset of dysarthria was calculated at 20.8 years in one study, 6.6 years after the average age at onset (Schols et al., 1997), and all patients in another study developed dysarthria 10 to 15 after age at onset (Harding, 1981). Speech progressively becomes slower and more slurred, and intelligibility is impaired in severe or advanced cases.

**Dysphagia**

Mild dysphagia is also a common symptom of FRDA, and can become a serious clinical issue in later stages of the disease, where specific diets or even nasogastric feeding or gastrostomy may be required (Durr et al., 1996). Various case series give the frequency of dysphagia at between 27% and 74% (Durr et al., 1996; Filla et al., 1990; Schols et al., 1997).

**Sensory neuropathy**

Neurophysiological studies on the neuropathy in FRDA have shown severely reduced or even absent sensory action potentials that do not seem to change significantly over time. Peripheral nerve biopsies in FRDA patients have also shown an increase in the proportion of large myelinated fibres, which may be a compensatory mechanism against inefficient myelination. The severity of both of the above findings correlates with GAA

expansion size (Santoro et al., 1999). Thus, the sensory neuropathy present in FRDA is currently understood as a combination of inefficient myelination and slowly progressive axonopathy (Koeppen & Mazurkiewicz, 2013; Morral et al., 2010).

**Saccades/Nystagmus**

Oculomotor abnormalities, or abnormal eye movements, are a common early feature of FRDA. Fixation instability interrupted by frequent involuntary saccades (or 'square wave jerks') is the most usual sign. These jerks can occur in horizontal or vertical fixation (Fahey et al., 2008; Furman et al., 1983; Schols et al., 1997) and can also interrupt smooth pursuit movements and block the assessment of nystagmus, which is less frequent but also observed. It commonly presents as a horizontal gaze-evoked nystagmus on lateral gaze, and less usually on vertical gaze (Durr et al., 1996; Harding, 1981; Schols et al., 1997).

**Decreased visual acuity**

Decreased visual acuity is rarer in FRDA than eye movement abnormalities, although around two-thirds of patients show a clinical or subclinical optic neuropathy on assessment. Around 20% of patients have decreased acuity that progressively declines (Durr et al., 1996; Fahey et al., 2008; Geoffroy et al., 1976; Harding, 1981). Conversely, a small subpopulation of patients experiences acute bilateral vision loss (Fortuna et al., 2009). All FRDA patients show lowered retinal nerve fibre layer thickness in optical coherence tomography (OCT) scans, and pattern visual-evoked potentials show increased latency in 34% to 70% of patients (Carroll et al., 1980; Durr et al., 1996; Fortuna et al., 2009). These findings taken together indicate that, although few patients are clinically affected, the whole visual system is in some way affected in FRDA.

**Hearing Difficulties**

Hearing difficulties are due to auditory neuropathy caused by faulty central auditory processing. They are a frequent issue which carry severe social impacts, as the temporal distortion of stimuli can worsen verbal

communication problems (Rance et al., 2010). Hearing loss in several studies is measured at between 8% to 39% (Durr et al., 1996; Geoffroy et al., 1976; Harding, 1981; Schols et al., 1997). In the Harding study, hearing loss was adjudged to be mild in 5.2% of cases, moderate in 1.7% of cases and severe in 0.9% of cases.

**Sphincter Disturbance/Bowel problems**

Urinary urgency is increased, with 80% of patients showing lower urinary tract symptoms (Lad et al., 2017). Late onset FRDA patients report these symptoms more often, most likely due to longer disease duration. The increased bladder activity may also indicate pyramidal pathology. Although disturbance of the sphincter is poorly studied in FRDA, its prevalence has been shown to range between 7% and 41% in several case series (Andermann et al., 1976; Delatycki et al., 1999; Durr et al., 1996; Filla et al., 1990; Schols et al., 1997). Bowel problems such as constipation or incontinence have also been observed in 64% of FRDA patients (Lad et al., 2017) and may be related to FRDA corticospinal pathology.

## *Non-Neurological Features*

The primary non-neurological features of FRDA are hypertrophic cardiomyopathy, increased incidence of diabetes and scoliosis. There is evidence of cardiac abnormalities in virtually all FRDA cases upon diagnosis to a variable degree, even if the patient does not display cardiac symptoms (Durr et al., 1996; Harding, 1981; Malo et al., 1976). Cardiac hypertrophy affects both ventricles, particularly the left, involving focal necrosis and diffuse fibrosis (Hewer, 1969). Systole is usually relatively unaffected until shortly before death (Rajagopalan et al., 2010). Overt symptoms of heart failure are not common in FRDA: blood pressure and hypertension tend to be normal. Ischaemic heart disease also occurs very rarely in FRDA. However, in advanced FRDA, arrhythmias are sometimes reported which can affect systolic function leading to clinical heart failure, which is

responsible for over half the deaths of FRDA patients (Hanley et al., 2010; Tsou et al., 2011).

It is very rare for cardiac symptoms to develop before the neurological ones, although when they do heart transplantation can precede FRDA diagnosis (Leonard & Forsyth, 2001). Even in cases where a patient is initially referred to a cardiologist, on detailed examination neurological features are found that almost always precede the cardiological ones. An absence of any correlation between the severity of the neurological features and cardiac involvement in FRDA has also been reported, which may relate to the tissue-specific somatic instability and mosaicism of the GAA expansion observed in the disease (Weidemann et al., 2012). At least probable cardiac dysfunction accounted for 62% of the deaths in the largest study to date on FRDA mortality, a retrospective study of the clinical notes of 61 deceased FRDA patients. The mean age of death was 36.5 years (range between 12 and 87 years). Of the deaths caused by cardiac issues, most were due to congestive cardiac failure or arrhythmia (Tsou et al., 2011). Neuropathology has traditionally been the focus of FRDA clinical research, with over ten times as many publications on this subject compared with on cardiological issues. FRDA cardiopathology is however emerging as an important field in FRDA study, particularly as it is the primary cause of death among FRDA patients (Hanley et al., 2010).

**Symptoms Summary and Proposed Therapies**

The cardiopathology is characterized by a slow progression of left ventricular hypertrophy (LVH) as well as an increase in left ventricular dilatation. There is reduction in contractile sarcomeres, as well as the proliferation of mitochondria that contain electron-dense particles possibly indicating mitochondrial iron deposition (Michael et al., 2006). This finding is also corroborated in the heart of the FRDA MCK Cre-lox conditional KO mouse model (see Mouse Models section; Puccio et al., 2001). In the large case series studies that have been carried out so far, evidence of hypertrophic cardiomyopathy or LVH was found in 28% to 100% of cases although the definitions of these conditions varied between the studies

(Ackroyd et al., 1984; Delatycki et al., 1999; Durr et al., 1996; Filla et al., 1990; Geoffroy et al., 1976; McCabe et al., 2000; Schols et al., 1997). Significantly less myocardial energy generation in FRDA patients has been shown compared to controls, with the degree of energy reduction correlating with the degree of hypertrophy (Bunse et al., 2003). Idebenone, an antioxidant and coenzyme Q mimetic, has been used as a therapeutic strategy against this myocardial energy deficiency due to both its antioxidant properties and its ability to enhance electron transport within the mitochondria (Mariotti et al., 2003; Rustin et al., 2002). However, when carried out over a period longer than a year, idebenone therapeutic studies show no decrease in arrhythmias or disease progression, despite an apparent decrease in the visible hypertrophy (Pineda et al., 2008; Velasco-Sanchez et al., 2011). Antioxidant therapies have also not improved FRDA cardiac symptoms thus far, although extending the half-life of antioxidant agents may improve their therapeutic potential (Lynch et al., 2010).

**Echocardiogram**

Echocardiographic studies are very useful for evaluation of ventricular wall function and thickness over time. Abnormalities in the cardiac wall are present in a majority of FRDA patients, though these are often symptomless. The ventricles show retained systolic function and impaired diastolic filling, with 84% of 173 FRDA patients showing signs of diastolic dysfunction in one study (Dutka et al., 2000; Palagi et al., 1988). However, impaired systolic function alongside a relatively unaffected ejection fraction is instead observed early in disease progression (Kipps et al., 2009; Regner et al., 2012). A recent study showed FRDA patients dividing distinctly over a 10-year period into one group with slowly declining, normal ejection fraction, and another with a much sharper progressive decline (Pousset et al., 2015). The rate of ejection fraction decline is shown to be correlated with the size of the GAA1 repeat, although not with the hypertrophy itself (Dutka et al., 1999). Echocardiogram studies have generally been confirmed by cardiac MRI studies, which have also evidenced an increased left ventricular mass in FRDA that is greater in cases with a longer GAA expansion (Meyer et al., 2007; Rajagopalan et al., 2010; Weidemann et al.,

2012). A tendency towards left ventricular thinning due to dilation has also been observed in cases with longer disease duration, which may give the false indication that the ventricular defects have improved (Rajagopalan et al., 2010).

**Electrocardiogram**

Subtle electrocardiographic findings revealing repolarization abnormalities are often among the first signs of cardiomyopathy. The electrocardiogram (ECG) is abnormal in almost all FRDA cases, with the most typically observed anomaly being an inferolateral or widespread T-wave inversion. Other non-specific ST segment and T-wave abnormalities are also seen (Dutka et al., 1999; Schadt et al., 2012). Sinus rhythm and sinus tachycardia are also regularly found, and patients are troubled with paroxysmal or sustained arrhythmias in advanced FRDA, particularly atrial fibrillation which can become palpitations. However, patients rarely need insertion of a pacemaker or a defibrillator (Bourke & Keane, 2011). Evidence of LVH is only infrequently seen, and usually ECGs need to be combined with echocardiographic evidence as alone they are insufficient for FRDA diagnosis.

**Diabetes**

An association between FRDA and diabetes mellitus was first confirmed in a study of a cohort of 50 patients almost 100 years after the original disease discovery (Hewer & Robinson, 1968; Thoren, 1962). In several case series, diabetes mellitus was found in between 1% and 32% of cases (Andermann et al., 1976; Delatycki et al., 1999; Durr et al., 1996; Filla et al., 1990; Harding, 1981; McCabe et al., 2000; Reetz et al., 2015; Schols et al., 1997). The mechanism of the pathology remains unclear, but has been proposed to be a combination of decreased insulin secretion due to pancreatic β-cell apoptosis, and also increased insulin resistance in peripheral tissues (Finocchiaro et al., 1988). Diabetes, like cardiomyopathy, is associated with a longer pathological GAA expansion in both alleles, making diabetes more frequent in younger-onset cases as well as in more advanced FRDA (Filla et al., 1996). It has been shown that asymptomatic heterozygous carriers of

the GAA expansion may have increased incidence of insulin resistance (Fantus et al., 1991; Hebinck et al., 2000).

**Scoliosis and Foot Abnormalities**

Musculoskeletal abnormalities such as scoliosis, pes cavus and talipes equinovarus are frequently observed in FRDA. Scoliosis often requires surgical correction in earlier onset cases, although in less severe cases of later onset it may be mild and not require surgery (Tsirikos & Smith, 2012). Scoliosis of more than 10 degrees was found in 100% of patients in one study. Case series observing foot abnormalities show an incidence of 55% to 90% of cases with foot deformities (Ackroyd et al., 1984; Delatycki et al., 1999; Durr et al., 1996; Filla et al., 1990; Geoffroy et al., 1976; Harding, 1981; McCabe et al., 2000; Schols et al., 1997).

### 1.5.3 Late-Onset FRDA

**LOFA and Symptoms**

FRDA is typically classed as an early-onset disorder, and accounts for 75% of all ataxia patients who have an age at onset prior to 25 (Cossee et al., 1997). The literature describes two main forms of atypical FRDA: (i) Late-Onset (LOFA, defined as onset after 25) or Very Late-Onset Friedreich's Ataxia (VLOFA, defined as onset after 40), and (ii) FRDA with retained reflexes or FARR (Coppola et al., 1999; Klockgether et al., 1996; Parkinson et al., 2013; Verma & Gupta, 2012). LOFA/VLOFA is phenotypically distinct from classical FRDA, with a milder phenotype, slower disease progression and a more variable set of symptoms, also as patients with a longer disease duration do not always progress in a slow, regular manner. As with classical FRDA, the presenting features of LOFA in several case series are gait and limb ataxia (Bhidayasiri et al., 2005; Gellera et al., 1997). Contrary to classical FRDA, dysarthria develops later in the disease, although it is still

usually present. Pyramidal involvement is less understood in LOFA than in classical FRDA. Spasticity or retained reflexes are present in 30 to 40% of LOFA patients, although extensor plantar responses are present in 40 to 100% of atypical cases (Bhidayasiri et al., 2005; Coppola et al., 1999; De Michele et al., 1994; Gellera et al., 1997; Klockgether et al., 1993; Martinez et al., 2017; Montermini et al., 1997; Ragno et al., 1997).

In a recent study, a phenotypic and genotypic comparison between 44 LOFA patients, 30 VLOFA patients and 180 classical FRDA patients was carried out. It showed a reduced frequency of symptoms such as dysarthria, abolished tendon reflexes, extensor plantar reflexes, weakness, amyotrophy, cerebellar atrophy, scoliosis, and cardiomyopathy in delayed-onset FRDA patients compared to classical FRDA patients (Lecocq et al., 2016). Although little data has been collected on the presence of lower limb neuropathy in LOFA, one study showed that only 1 in 13 LOFA patients has an absence of any sensory neuropathy, which is invariably present in classical FRDA (Bhidayasiri et al., 2005). A further study showed abnormalities in peripheral sensory and motor conduction in 16 atypical FRDA cases, usually involving sensory axonal degenerative neuropathy (De Michele et al., 1994).

**VLOFA and Symptoms**

FRDA onset has been rarely observed after 50 years of age (Berciano et al., 2005; Galimanis et al., 2008). In VLOFA cases, spastic tetraparesis without marked ataxia is usually seen (Berciano et al., 2002; Labauge, 2002; Lhatoo et al., 2001). These patients have been reported to display subtle sensory neuropathy (Berciano et al., 2005; Lhatoo et al., 2001). All of these cases may more easily be misdiagnosed than other FRDA cases.

**Non-neurological Symptoms in LOFA**

Non-neurological aspects of the disease, such as pes cavus, scoliosis, cardiomyopathy and diabetes are much less common in LOFA/VLOFA (De Michele et al., 1996; Durr et al., 1996; Gellera et al., 1997; Reetz et al., 2015). Several studies have shown the presence of pes cavus to be

between 33 and 45%, while scoliosis is milder and present in under 40% of cases (Bhidayasiri et al., 2005; Coppola et al., 1999; De Michele et al., 1994; Durr et al., 1996; Gellera et al., 1997; Klockgether et al., 1993; Ragno et al., 1997; Schols et al., 1997). Two recent studies on the heart in over 350 LOFA/VLOFA FRDA patients showed an absence of cardiomyopathy in up to 40% of patients: where it was present, there was a correlation of the severity of the cardiac abnormalities with the size of the GAA1 allele (Regner et al., 2012; Weidemann et al., 2012). ECG studies show an abnormal ECG in which the characteristics of T-wave inversion, left axis deviation and repolarization abnormalities resemble those found in classical FRDA. The findings from LOFA echocardiogram studies also show abnormal findings in the atypical FRDA range (Bhidayasiri et al., 2005; Coppola et al., 1999; De Michele et al., 1994; Durr et al., 1996; Gellera et al., 1997; Schols et al., 1997). Despite these findings, mortality in LOFA/VLOFA is less related to cardiac symptoms than in classical FRDA.

**Protein and mRNA Expression in LOFA/VLOFA Patients**

Measuring frataxin protein, gene dosage, and mRNA expression levels could pick up atypical FRDA cases that remain undiagnosed through genetic techniques. The mean residual frataxin levels, compared with 100% in controls, are 35.8% in classical FRDA and 65.6% in LOFA, with an evident correlation between frataxin protein levels and GAA repeat size and an inverse correlation between frataxin protein levels and age at onset (Sacca et al., 2011). The GAA expansion size has also been found to negatively correlate with age at disease onset in LOFA/VLOFA patients, with the GAA1 allele accounting for 62.9% of age at onset variation and the larger GAA allele accounting for 15.6% of the variation (Lecocq et al., 2016). Studies of frataxin mRNA levels in LOFA have also shown reduced levels, ranging between 20 and 50% of controls (Pianese et al., 2004; Sacca et al., 2011). However, the same study also showed considerable overlap in frataxin protein and mRNA levels in FRDA between LOFA patients, controls and carriers. This indicates that frataxin protein and mRNA levels are not exclusive determinants of FRDA disease progression (Sacca et al., 2011).

**Conclusion**

FRDA patients have a distinct neurological and non-neurological phenotype, which varies between three established subtypes: early onset, classical and late onset FRDA. Early or late onset FRDA patients can now be clearly pinpointed by genetic and clinical analysis. Earlier disease onset is strongly associated with a more severe, quickly progressive, and developmental rather than degenerative phenotype. Late onset patients usually have a more benign phenotype and later age at onset, with a reduced frequency of symptoms such as dysarthria and areflexia. This is also true of non-neurological symptoms such as cardiomyopathy and diabetes, and this reduced severity has been linked to higher frataxin protein and mRNA levels in the cells of LOFA patients. From a consultant's point of view, to only have an understanding of the classical diagnostic criteria of FRDA is to ignore or misidentify atypical cases that do not fulfil all the criteria.

## 1.6 FRDA Compound Heterozygotes

### 1.6.1 Compound Heterozygotes with Point Mutations

The initial study of the genetic basis of Friedreich's ataxia discovered that around 1-3% of patients show, instead of the more common homozygosity for the GAA expansion in the *FXN* gene, a compound heterozygosity for a point mutation in the *FXN* gene in combination with the pathological GAA expansion (Campuzano et al., 1996). Since then, over 40 different point mutations from loci in all five exons of the frataxin gene transcript have been discovered. Among these are missense mutations caused by base pair substitutions, null mutations caused by base pair substitutions in the start codon that cause faulty translational initiation, and nonsense insertions, deletions and indels that produce frameshift variants leading to premature

termination. Intronic variants have also been discovered at all of the four splice-sites. No cases of homozygosity for FXN point mutations have yet been discovered (Campuzano et al., 1996; Cossee et al., 1999; Gellera et al., 2007).

**Studies on Point Mutations**

The first three *FXN* point mutations were discovered alongside the *FXN* GAA expansion, and included one missense (p. I154F), one nonsense (p. L106X), and one splice-site (g. IVS3-2A>G) mutation (Campuzano et al., 1996). The most common point mutation, p.G130V, was discovered soon after (Bidichandani et al., 1997). A comparative study was carried out on a series of five *FXN* compound heterozygotes. The study made evident the severe phenotype invariably associated with splice-site, nonsense and initiation codon mutations due to absence of functional frataxin, although the phenotype associated with missense mutations was more variable depending on which amino acid residue was affected (Forrest et al., 1998). A further study compared clinical features of 25 compound FRDA heterozygotes from 19 families with 196 FRDA patients with the homozygous GAA expansion. Patients with truncating or missense mutations in sequences encoding the carboxy-terminal half of frataxin protein had a phenotype that resembled the classic pathology of patients with homozygous GAA expansions. Patients who instead had a missense mutation in sequences encoding the amino-terminal half of the frataxin protein (e.g. D122Y/G130V) had a milder, more slowly progressive clinical phenotype (Cossee et al., 1999).

**Recurrent Point Mutations and Hot-Spots**

The majority of point mutations reported have been private mutations (Gellera et al., 2007). However, there are certain mutations that recur throughout studies. These include the following four missense mutations: p. G130V (Bidichandani et al., 1997; Cossee et al., 1999; Forrest et al., 1998), p. I154F (Campuzano et al., 1996; Cossee et al., 1999; Filla et al., 1996; Gellera et al., 2007), p. R165C (Forrest et al., 1998; McCormack et al., 2000) and p. W173G (Cossee et al., 1999; Gellera et al., 2007). Some of

these cases may share a common founder, and especially in the case of the p. G130V mutation, a later age at onset and slow progression may allow for generation of progeny and subsequent further spread of the mutation in a population.

**Point Mutation Study: Differing Severity**

A study by De Castro et al searched for pathological GAA expansions in *FXN* patients with early-onset spinocerebellar ataxia. Among the 175 in which a GAA expansion was discovered, seven (4%) had just one expansion, indicating their possible genetic status as compound heterozygotes based on their phenotype. Of the seven patients, four were confirmed as compound heterozygotes for four different point mutations: three nonsense mutations (p. W155X, p. E100fsX and p. R39fsX) and a splice-site variant (g. IVS3-2A>G). While the three patients with nonsense mutations had GAA expansion sizes of between 800 and 900 repeats that led to a classical FRDA phenotype with an early onset between ages 3 and 4, the patient with the splice-site variant had an expansion of only 250 repeats and a late-onset, slowly progressive phenotype. Thus, the size of the single pathological GAA expansion in point mutation compound heterozygotes determines FRDA severity (De Castro et al., 2000).

A larger study specifically explored the relationship between age at onset and GAA expansion size in 13 FRDA compound heterozygotes with point mutations and discovered a significant inverse correlation. The study also found a significant inverse correlation between GAA expansion size and frataxin protein expression, as measured by western blot analysis of lymphoblastoid cell lines derived from the patients (excluding two outliers), as well as a correlation between age at onset and frataxin expression. These results further confirmed the importance of the size of the single GAA expansion in determining frataxin production, and thus clinical severity in FRDA. This was particularly true for nonsense mutations, as the allele containing the GAA expansion becomes exclusively responsible for levels of frataxin production (Gellera et al., 2007).

**Large Study of the Effects of Point Mutations on Frataxin Structure**

Galea et al performed the largest study to date of *FXN* compound heterozygotes. This group specifically studied the effect of *FXN* point mutations on the tertiary structure of the frataxin protein, frataxin stability and protein function. It was discovered that amino acid residues that are deeper within the protein interior form a tightly packed hydrophobic core that stabilises protein structure, and that point mutations affecting residues within this core therefore had a more severe impact upon protein stability. Specifically, mutations generated steric clashes in the case of substitution by larger residues, cavities in the case of substitution by smaller residues and unfavourable interactions in the case of substitutions of hydrophobic residues for charged ones. The clinical effect of the different missense mutations was thus shown to be dependent on a variety of factors acting at the mutation site, and hence on the overall functionality of frataxin (Galea et al., 2016).

**Conclusion**

Out of the large range of *FXN* point mutations that have now been described, it is the splice-site, nonsense and initiation codon mutations that have the most severe clinical effects. Missense mutations, that usually occur in the last three exons of *FXN* (within the mature frataxin protein), have more variable effects depending on the how they impact upon the tertiary structure of the protein and upon the ability of frataxin to interact with other proteins. Also, GAA expansion size of the single allele of compound heterozygotes remains of great relevance to clinical severity, and this is particularly true when the point mutations lead to the GAA expansion becoming the sole driver of frataxin production, as is the case with null or nonsense mutations.

### 1.6.2 Compound Heterozygotes with Large Deletions

Recent developments in measuring gene dosage by multiplex ligation-dependent probe amplification (MLPA) have enabled identification of compound heterozygotes with large deletions in the frataxin gene (Deutsch et al., 2010). There have thus far only been twelve recorded cases, some of which present atypical features. The first case described involved a 2776 base pair deletion around exon 5a of *FXN*, by using a quantitative duplex PCR assay with exon-specific oligonucleotide probes analogous to MLPA, followed by sequencing of the 5a exon (g. 120032_122808del). Clinically, the patient had a typical FRDA phenotype, progressing from age of onset to wheelchair use in over six years (Zuhlke et al., 2004). Another lab described a further two cases: an individual with a deletion in exons 2 to 3 with a typical FRDA phenotype (aside from a lack of dysarthria) and a rapid progression from age at onset to wheelchair use in four years, and another case with a deletion of exon 5 and a classical, if severe FRDA presentation (Brigatti et al., 2012; Deutsch et al., 2010).

A further study described a large deletion of between 1603kbp and 2477kbp, including the entire *FXN* gene: poor probe coverage prevented knowledge of the exact length of the deletion. The individual had an unusual FRDA presentation, with chorea, intention tremor and very slow progression over almost thirty years (van den Ouweland et al., 2012).

The largest exonic *FXN* deletion case series was carried out by a collaboration of specialist centres in France and described six cases from five families. Four of these cases caused deletions in exons 4 and 5, one involved only exon 4 and the last involved exons 2 and 3. All cases had a young age at onset of between three and twelve years of age and a severe neurological phenotype, indicating a possible founder effect. One half had diabetes, 80% had scoliosis and 83% had cardiomyopathy, including one case of severe angina at only nine years of age (Anheim et al., 2012).

Another deletion was found in what is so far the only systematic study of exonic *FXN* deletions, carried out in the Norwegian population. The project contacted not only the three Norwegian laboratories that perform *FXN* gene testing, but also all of the 22 public hospitals of Norway that contain a paediatric and/or neurology unit, patient support organisations and the national centre for rare diagnoses. In all, 27 patients had genetically confirmed FRDA with homozygous GAA expansions, and a further four had clinical ataxia and one GAA expansion. Of these four, one was heterozygous for a point mutation, and another had a large deletion (of the remaining two, one had a mutation in the related OPA1 gene and the other remains without genetic diagnosis). The deletion was identical to the first ever *FXN* exonic deletion described by Zühlke et al, of 2776 base pairs around exon 5a. The patient had a relatively typical FRDA phenotype, including an age at onset of 7 with presenting symptoms of unsteadiness and gradual progression towards wheelchair use, cardiac symptoms, scoliosis, but no diabetes mellitus (Wedding et al., 2015).

A final case affected a patient from among a cohort of 41 FRDA patients, who had very early onset FRDA with hypertrophic cardiomyopathy, rapidly progressive gait instability and severe scoliosis, due to a complete exonic deletion of all exons from 1 to 5b. Although ‘exquisitely rare’, tests for FRDA exonic deletions are indicated by this study to be more appropriate in FRDA cases where the patient is of a particularly severe and early onset clinical phenotype (Hoffman-Zacharska et al., 2016).

Where a *FXN* exonic deletion is suspected, the MLPA test is recommended among relatives of that individual, to avoid a routine genetic test showing a single normal-sized GAA expansion being falsely interpreted as two normal sized expansions. Indeed, most patients with normal-sized alleles only have a single small band on the long-range PCR gel electrophoresis due to the small size of the triplet repeat, making misinterpretation potentially more common than when testing expanded alleles. Carrier status for the exonic deletion would be of great relevance to an individual’s genetic counseling, indicating that their partner should also be tested for FRDA carrier status.

**Conclusion**

Out of the very small number of *FXN* exonic deletions that have so far been described, almost all of the patients display a classical if severe FRDA clinical presentation. However, the number of cases studied is too few to consider the clinical phenotype fully characterized, and no systematic studies of their prevalence in a population have been performed. Oddly, the only exception to the phenotypic trend is the van den Ouweland case, where the patient, despite having a complete deletion of their *FXN* gene, had very slow disease progression, although alongside other unusual symptoms not usually observed in FRDA such as chorea.

In clinical diagnosis studies, GAA expansions are sized with the long-range PCR method by gel electrophoresis. It is interesting to note that when only a single band is visible on the gel corresponding to a pathological GAA expansion and there is no band corresponding to a normal sized GAA expansion, it is assumed by most diagnostic laboratories that the patient has two, equal-sized GAA expansions. Although this interpretation is very likely given the rarity of exonic deletions, it must be remembered that this result is by no means a confirmation that the patient indeed has two, equal-sized GAA expansions and it is possible that several cases of compound heterozygotes with large deletions are being missed. Correct results could have important implications for genetic counseling, as well as better understanding the underlying pathological mechanisms of FRDA. For example, in the case of the UK EFACTS cohort, the Université Libre de Bruxelles reported 15 of 147 patients for whom GAA sizing data was available as having equally sized pathological GAA expansions. Although the considerations made in this section are of relevance to these patients, they remain unscreened for exonic deletions in the *FXN* gene.

## 1.7 Justification for Current Study

FRDA is a highly complex, multisystem disorder, in which neurological signs are first observed, but the patient usually dies from cardiac complications. The crucial discovery of its genetic basis allowed FRDA research to directly investigate the underlying disease mechanisms and generate cellular and animal models of great usefulness. Further understanding of both FRDA molecular genetics and disease pathophysiology is of great importance, especially as at present there is no treatment available for FRDA.

I carried out two studies on FRDA, one with a translational scientific approach using molecular genetics techniques, and the other with a more basic approach using cell imaging techniques. In the translational study, an unprecedented 2000 ataxia patients were screened for the FRDA mutation to identify its percentage in an idiopathic late onset ataxia cohort. These patients are not routinely screened for FRDA as it is a paediatric disease: however, recently the FRDA mutation has been found in late onset ataxia patients. The results will improve the ataxia guidelines for genetic testing, making them more evidence-based. Correct diagnosis would also vastly improve patient care and genetic counselling.

In the basic science study, experiments were carried out in two separate FRDA cellular model populations, one atrial mouse adult (HL-1) and one ventricular rat neonatal line (H9c2). They modelled FRDA via knockdown of the frataxin gene using siRNA, and key results in these cells were confirmed using YG8R primary cells. These cells were used to test the novel hypothesis of $Ca^{2+}$ signaling dysfunction in conjunction with dysregulation of iron and ROS levels in FRDA, never previously studied in FRDA model heart cells. These mechanisms act through a great variety of bioenergetic pathways, mostly associated with ISC biogenesis and cellular and mitochondrial iron dynamics. Any potential clinical therapy, unless acting further upstream at the level of genetic or epigenetic repair of the mutation itself (no easy feat in a triplet repeat disorder), must address the multiple physiological pathways associated with FRDA if it is to be successful. The

primary aims of my study, subdivided into two separate sections for the FRDA genetics and physiological studies respectively, can be outlined thus:

Aims:

**Genetic Study:**

1. **To determine whether any of the cases of atypical FRDA are being missed by clinicians, due to the current clinical basis for FRDA referral.**
2. **To develop our understanding of the genotype-phenotype relationship in FRDA.**

**Physiological Study:**

1. **To explore the pathophysiology of cardiac cells in cellular and animal models of FRDA and gain insight into whether there is any effect on $Ca^{2+}$ homeostasis in these models.**
2. **To investigate whether any variation in $Ca^{2+}$ homeostasis may be linked to more well-established elements of FRDA pathophysiology, and whether any therapeutic avenue may be opened by new findings.**

# Chapter 2 : Methods

## 2.1 Genetic Screening Study of Ataxia Patients

### 2.1.1 Case Ascertainment

**Case Ascertainment and Sample Preparation**

The Neurogenetics Department of the National Hospital for Neurology and Neurosurgery (NHNN), a tertiary referral centre for inherited neurological diseases, has on its database samples received from neurological centres across the UK, including from EFACTS (see Chapter 1). This database was screened for two cohorts from among patients presenting with ataxia. One cohort was made from patients whose clinicians had requested *FXN* gene testing to observe for FRDA positivity. The other cohort of patients was comprised of those for whom *FXN* gene testing had not been requested by their clinician, and for whom, despite having been referred to hospital for spinocerebellar ataxia (SCA) testing, no clear genetic cause had been found. In the latter cohort, testing for GAA expansions was also carried out in the Neurogenetic Department of the NHNN using previously established techniques (Campuzano et al., 1996; Potdar & Raghu, 2013; Warner et al., 1996). Patient DNA is extracted in the NHNN using standard procedures and stored indefinitely at -80°C. All patients signed informed consent for genetic testing. The study was reviewed and approved by the UCL Joint Research Office.

### 2.1.2 Triplet-Primed Polymerase Chain Reaction

**Need for Molecular Diagnosis of Friedreich's Ataxia**

Polymerase chain reaction (PCR) is a simple and efficient technique that uses primers to amplify a desired region of DNA. Primers are short stretches of DNA designed to be complementary to specific DNA regions flanking the region of interest. These primers bind to those flanking regions and allow DNA polymerase to fill in the centre of the region with free nucleotides over a number of denaturation-synthesis cycles, vastly amplifying the concentration of that DNA region of interest. This product can then be analyzed by, for example, agarose gel electrophoresis.

**Triplet-Repeat Primed PCR**

The ultimate function of carrying out PCR experiments on the DNA of our 2000 patients was to test for pathological GAA expansions in each allele, which would allow for the diagnosis of FRDA. A two-stage PCR process was carried out, beginning with triplet-primed repeat PCR (TP-PCR). TP-PCR, a fast and robust technique, was ideal to apply en masse to the 2000 patient samples. However, it was necessarily a primary screening method, as it only answered the question of whether ataxia patients have the pathological GAA expansion in either allele (Fig. 6). Thus, any samples positive at the TP-PCR stage moved on to the next, more labour-intensive round of long range PCR testing. This allowed us to distinguish between FRDA expansion homozygous and heterozygous individuals, and fully test for FRDA positivity.

A study by Ciotti et al. showed 100% concordance between results obtained by TP-PCR and those by Southern Blot analysis and confirmed the TP-PCR method to be robust, fast and highly reproducible (Ciotti et al., 2004; Muthuswamy et al., 2013). TP-PCR detects GAA expansion using a set of three primers: FATP-P1, FATP-P3, and FATP-P4. P1 is a fluorescently labelled locus-specific primer that complements a section of DNA flanking the 5' end of the GAA sequence. P3 and P4 are reverse primers sharing a

common 5’ sequence. P4 contains a sequence complementary to the 3’ end of the repeat and binds to multiple sites within the repeat: its limited quantity means it runs out in the first cycles. The P3 primer amplifies from the end of the amplification products produced by the P4 primer. The P4 primer binds to multiple sites, so that products of many different sizes are produced, giving a characteristic trace when these undergo fragment size analysis by capillary electrophoresis (ABI-3730 fragment analyser, Applied Biosystems, ThermoFisher Scientific). The primer sequences used were:

FATP-P1: 5′-GCTGGGATTACAGGCGCGCGA-3′
FATP-P3: 5′- TACGCATCCCAGTTTGAGACG-3′
FATP-P4: 5′-6-FAM
TACGCATCCCAGTTTGAGACGGAAGAAGAAGAAGAAGAAGAA-3′

The desired samples of patient DNA were aliquoted, and DNA quality and concentration were determined using a NanoDrop ND-1000 spectrophotometer (ThermoScientific, Wilmington, DE, USA), using no less than 150 µg of genomic DNA per patient sample. A stock plate of the DNA samples was made up to be tested, and the plate was incubated at 55°C for two hours to ensure DNA homogeneity.

Then, the three primers were all resuspended in TE to 100 µM, and aliquots were made in TE at the following concentrations: FATP-P1 at 10 µM, and a mix containing FATP-P3 at 10 µM and FATP-P4 at 1 µM. Following this, a master mix was made containing 10 µL Amplitaq Gold 360 Master Mix (Applied Biosystems, ThermoFisher Scientific), 2 µL GC Enhancer (Applied Biosystems, ThermoFisher Scientific), 4 µL $H_2O$, 1 µL of the FATP-P3 primer (10 µM) and 1 µL of the primer mix FATP-P1 (10 µM) with FATP-P4 (1 µM) for each sample being analysed plus 10% for pipetting errors. This master mix was then centrifuged and added to the appropriate number of wells, of a 96-well plate, accounting for positive, negative and water controls. 2 µL of each DNA sample was taken from the stock plate and added to the appropriate wells. The resulting 20 µL solution was run on the following PCR program: an initial denaturation stage of 95°C for 10 minutes and then 35 cycles of 95°C for 1 minute, 58°C for 1 minute and 72°C for 1

minute. This was followed by a final extension stage of 72°C for 7 minutes, and then the samples were cooled to 4°C until ready to analyse.

After the PCR was completed, the capillary electrophoresis was carried out. A new master mix was made containing 12 µL Hi-Di formamide (Applied Biosystems, ThermoFisher Scientific) and 0.3 µL LIZ500 size standard (Applied Biosystems, ThermoFisher Scientific) per sample. The master mix was vortexed after adding the size standard, added to the appropriate number of wells in a new 96-well plate and 1 µL of PCR product for each sample was added to each of the wells. The plate was then heat-sealed, and the samples were heated to 95°C for 3 minutes on the thermocycler, and then rapidly cooled on ice for three minutes before transfer to the fragment analyser. Once the data was obtained, it was analysed using GeneMarker v2.2.0 (Soft Genetics, PA, USA), which generates a plot graphic for each sample.

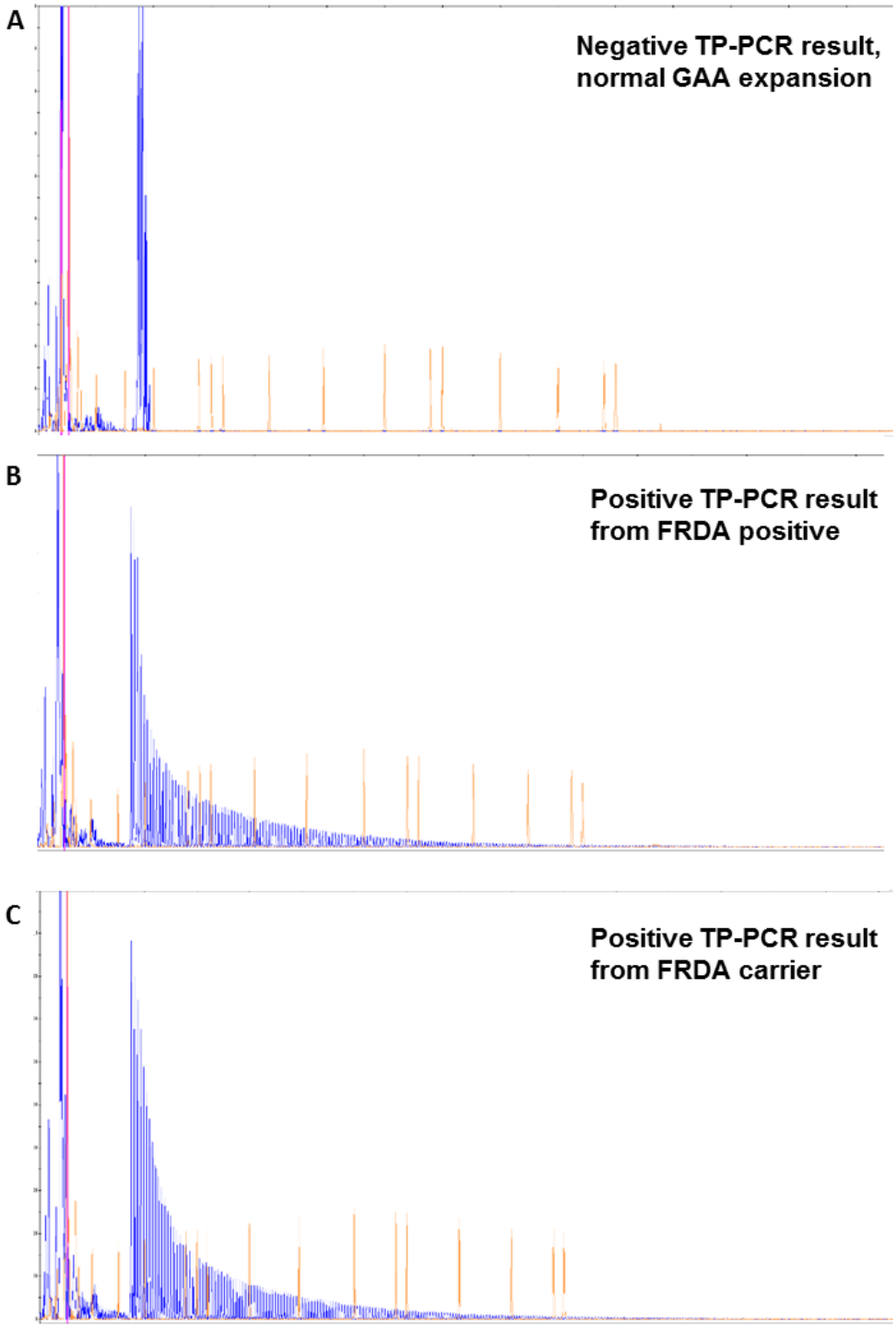


**Figure 6: TP-PCR results visualized by capillary electrophoresis, showing that TP-PCR does not distinguish between FRDA carriers and FRDA positives.**

A) Negative TP-PCR result, indicative of a normal GAA expansion. B) Positive TP-PCR result. This patient was later shown to be an FRDA positive by Long Range PCR. C) Positive TP-PCR Result. This patient was later revealed to be an FRDA carrier by Long Range PCR.

### 2.1.3 Long Range PCR

The second stage of the two-stage PCR process, following TP-PCR, was long range PCR, which asked the crucial final research question: do the patients positive at the TP-PCR stage have the FRDA pathological GAA repeat in both alleles or only one? Conventional PCR cannot produce fragments any larger than 3-4 kilobases (kb), as the Taq DNA polymerase error rate eventually stalls the lengthening of the DNA strand and leads to polymerase dissociation.

The long range PCR technique introduces a proofreading enzyme in tandem with the polymerase, which removes any misplaced bases and allows continuous amplification of the DNA strand up to 22 kb. This is ideal for amplification allowing for accurate sizing of the large FRDA GAA repeats. It has been used in several studies determining the relationship between the molecular and clinical phenotypes in FRDA. The GAA-R and GAA-F primers are those originally described by Campuzano and his colleagues in 1996 in their paper on the genetic basis for FRDA (Campuzano et al., 1996). The primer sequences used were:

GAAF: 5'- GGG ATT GGT TGC CAG TGC TTA AAA GTT AG-3'
GAAR: 5'-GAT CTA AGG ACC ATC ATG GCC ACA CTT GCC-3'

The accurate analysis of expansion size by long PCR originally linked the intronic homozygous GAA expansions in patients to the autosomal recessive mode of inheritance in FRDA, confirming this expansion mutation as the cause of disease (Campuzano et al., 1996; Lamont et al., 1997). It also allowed for the discovery that there is an inverse correlation between expanded repeat length and age at onset, and FRDA patients with diabetes or cardiomyopathy had larger expansions (Filla et al., 1996). Most relevantly for our study, a further study amplified the GAA expansion mutation in both healthy individuals and patients and showed that by observing the bands

after agarose gel electrophoresis, one could distinguish successfully between normal, heterozygous and homozygous alleles (Kocheva et al., 2008). Thus, the long range PCR protocol has been put forward as a genetic screening method to distinguish between FRDA patients and carriers.

The desired samples of patient DNA were aliquoted, and DNA quality and concentration were determined using a NanoDrop ND-1000 spectrophotometer (ThermoScientific, Wilmington, DE, USA). A stock plate of the DNA samples was made up to be tested, and the plate was incubated at 55°C for two hours to ensure DNA homogeneity. The two primers were all resuspended in TE to 100 µM, and a single aliquot was made at in TE incorporating both primers at the following concentrations: GAA-F at 5 µM and GAA-R at 5 µM The first of two master mixes was then made, (i) consisting of 2.5 µL of dATP, dTTP, dCTP and dGTP (Applied Biosystems, ThermoFisher Scientific) each of 100 mM concentration, 1 µL of the 5 µM GAA-F and 5 µM GAA-R primer mix, and 14 µL of $H_2O$ per sample plus 10% for pipetting errors. 1 µL DMSO was added if necessary at the expense of $H_2O$ to improve PCR amplification. 25 µL of master mix (i) was added to each well, followed by 1 µL of normalized DNA (DNA diluted x10 in $H_2O$). The plate was then centrifuged.

At this point, the second master mix was made, (ii) consisting of 5 µL of Expand Long Template Buffer 3 with 27.5 mM $MgCl_2$ and detergents 10x concentrated (Sigma-Aldrich), 0.75 µL Expand Long Template Enzyme Mix (Sigma-Aldrich), an enzyme mix that contains thermostable Taq DNA Polymerase and a thermostable DNA polymerase with proofreading activity, and 18.75 µL $H_2O$ per sample plus 10% for pipetting errors, and then kept on ice. The original mixture of master mix (i) and the DNA was subjected to a 'hot-start' PCR to reduce non-specific annealing and amplification. It was placed in the PCR machine once the temperature had reached 90°C, and only then was 24 µL of master mix (ii) added to each well quickly. The PCR programme proceeded as follows: an initial denaturation stage of 94°C for 7 minutes, then 10 cycles of 94°C for 10 seconds, 62°C for 30 seconds and 68°C for 3 minutes, and then 20 further cycles of 94°C for 10 seconds, 62°C

for 30 seconds and 68°C for 3 minutes with 20 second increments every cycle. This was followed by a final extension stage of 68°C for 10 minutes, and then the samples were cooled to 4°C until ready to analyse.

Following conclusion of the PCR, 10 µL of the 50 µL PCR product per sample was run on a 2% agarose minigel (2% was chosen to enhance the resolution of the DNA fragments) using a 1 Kb Plus ladder (Invitrogen, ThermoFisher Scientific) as a standard. The results were checked on the Gene Genius gel documentation system and recorded as a paper photograph after approximately 1, 2 and 3 hours at suitable exposure times. The gel electrophoresis allowed visualization of the expansion size of the PCR product. To calculate the number of GAA repeats, the required formula was allele size = (number of base pairs-457)/3. This is because the synthesised PCR products contain flanking sequences totalling 457 base pairs in addition to the GAA trinucleotide repeat expansion. Normal alleles run at approximately 500 base pairs, whereas affected alleles run at approximately 720 base pairs or above.

Capillary electrophoresis was also carried out as a confirmatory mechanism for the success of the original PCR. A new master mix was made containing 12 µL Hi-Di formamide (Applied Biosystems, ThermoFisher Scientific) and 0.3 µL ROX500 size standard (Applied Biosystems, ThermoFisher Scientific) per sample. The master mix was vortexed after adding the size standard, added to the appropriate number of wells in a new 96-well plate and 1 µL of PCR product for each sample was added to each of the wells. The plate was then heat-sealed, and the samples were heated to 95°C for 3 minutes on the thermocycler, and then rapidly cooled on ice for three minutes before transfer to the fragment analyser. Once the data was obtained, it was analysed using GeneMarker v2.2.0 (Soft Genetics, PA, USA), which generates a plot graphic for each sample.

The individuals who were determined experimentally to be either homozygous for the GAA expansion were thereby confirmed as having

FRDA, and their clinical details were subsequently gathered to examine the correlation between genotype and phenotype for each patient and the nature of any atypical presentations of FRDA. If the presence of at least one GAA expansion was detected, the samples were forwarded for point mutation and exonic deletion testing to determine whether they could be compound heterozygous FRDA patients.

### 2.1.4 Point Mutation Screening and Large Deletion Screening

Known cases of compound heterozygotes with point mutations were collected from the databases of the Neurogenetic Department of the NHNN and the European Friedreich's Ataxia Consortium for Translational Studies (EFACTS) registry. Relevant clinical data were gathered from patients' notes and the EFACTS registry. Whilst testing for repeat expansions was carried out in the Neurogenetics laboratory of NHNN (as described in the TP-PCR and Long range PCR methods section), sequencing for point mutations was undertaken in the Merseyside and Chesire Regional Molecular Genetics laboratory, Liverpool Women's Hospital, Liverpool, UK and the Université Libre de Bruxelles (Dr Myriam Rai & Prof. Massimo Pandolfo). In both laboratories, a previously published technique was made use of using the following primers (Pandolfo, 2006):

| | |
|---|---|
| Exon 1: | 5'-AGC ACC CAG CGC TGG AGG-3' (forward) |
| | 5'-CCG CGG CTG TTC CCG G-3' (reverse) |
| Exon 2: | 5'-AGT AAC GTA CTT CTT AAC TTT GGC-3' (forward) |
| | 5'-AGA GGA AGA TAC CTA TCA CGT G-3' (reverse) |
| Exon 3: | 5'-AAA ATG GAA GCA TTT GGT AAT CA-3' (forward) |
| | 5'-AGT GAA CTA AAA TTC TTA GAG GG-3' (reverse) |
| Exon 4: | 5'-AAG CAA TGA TGA CAA AGT GCT AAC-3' (forward) |
| | 5'-TGG TCC ACA ATG TCA CAT TTC GG-3' (reverse) |
| Exon 5a: | 5'-CTG AAG GGC TGT GCT GTG GA-3' (forward) |
| | 5'-TGT CCT TAC AAA CGG GGC T-3' (reverse) |

The technique involves a screening of exons 1 to 5a, covering the entire coding region of the most commonly expressed *FXN* transcript. It can also detect the pathogenic mutations in the promoter region, alternative exon 5b, the untranslated exon 6, the 3'-untranslated region, cryptic splice site mutations and somatic mosaicism.

### 2.1.5 Large Deletion Screening

Large deletions were detected using the multiplex ligation probe amplification (MLPA) technique, which has been used previously for the detection of exonic deletions (Anheim et al., 2012; Deutsch et al., 2010; van den Ouweland et al., 2012). The General Protocol issued by the manufacturer was followed (MRC-Holland, Amsterdam, Netherlands; version MDP-v002, 23.1.2012). The commercially available SALSA MLPA P136-B2 Recessive Ataxias Probemix was used (MRC-Holland, Amsterdam, Netherlands; lot 0511), which contains probes against the five coding exons in the *FXN* gene, but no probe for the non-coding exon 6. The probemix also contains probes against the nine exons of the APTX gene and the 26 exons of the SETX gene.

The probemix contains probes against nine reference exons from unrelated genes on different chromosomes, which act as a quality control mechanism. Patients are assumed to have no exonic deletions in any of these exons, or any point mutations at the site of probe binding: if they do, this will become apparent at the data analysis stage. The probemix also contains internal quality control fragments, the 'QDX2 control fragment set'. Among these is a 92-nucleotide control probe very similar to the other MLPA probes, used by the software as a comparison to other control fragments. Additionally, there are four 'Q-fragments', oligonucleotides containing both PCR primer sequences in a single molecule and therefore not dependent on the amplification of target DNA during the PCR process (see below). These are present in extremely low concentrations so that if enough target DNA is used, these Q-fragments are out-competed by the amplicons of MLPA

probes. Thus, if insufficient DNA has been used or if the ligation reaction failed, this is indicated to us by the height of the Q-fragments peaks being over one-third that of the 92-nucleotide probe on the software. There are two further 'D-fragments' from among this set of internal quality control fragments, which detect sequences within CpG islands, which are known to be harder to denature, and are usually located near mRNA transcription start locations in exon 1 of *FXN*. If the height of these peaks is less than 40% than that of the 92-nucleotide control probe, this is evidence that DNA denaturation was incomplete. This can lead to unreliable data for the probes detecting sequences in or within 5 kb from the CpG islands. Finally, there are probes that detect sequences within the X and Y chromosome that identify the gender of the sample and allow for a general identification of incorrect sample use.

**Table 1: Probes in MRC-Holland SALSA MLPA P316-B2 Recessive Ataxias Probemix.**

| FXN Exon | SALSA MLPA Probe | Length (nt) | Ligation Site | Start-End | Distance to next Probe | Left (5') Probe-Right (3') Probe |
|---|---|---|---|---|---|---|
| **1** | 10891-L11561 | 234 | 43nt before exon 1 | 70840233-70840293 | 10.9 kb | 5':CAGCAAGACAGCAGCTCCCAAGT<br>3':<br>TCCTCCTGTTTAGAATTTTAGAAGCGGCGGGCCACCAG |
| **2** | 10893-L11563 | 208 | 463-464 | 70851166-70851235 | 6.7 kb | 5':CAGAGTGTCTATTTGATGAATTTGAGGAAATCT<br>3':<br>GGAACTTTGGGCCACCCAGGGTAAGATAAAACACCTT |
| **3** | 10894-L13901 | 258 | 517-518 | 70857878-70857950 | 11.9 kb | 5':CTCTCTAGATGAGACCACCTATGAAAGACTAGCA<br>3':<br>GAGGAAACGCTGGACTCTTTAGCAGAGTTTTTTGAAGACCT |
| **4** | 14129-L15733 | 472 | 24nt after exon 4 | 70869764-70869842 | 8.3 kb | 5':CCATCCAGGTATGTAGGTATGTTCAGAAGTCA<br>3':<br>ACATATGTAATTCTTAAAGACTTCCGAAATGTGACATTGTGGACCAT |
| **5** | 10895-L11565 | 154 | 1448-1449[b] | 70878073-70878130 | - | 5':TGGCCTGCACTGGGTTGTCCA<br>3':<br>GGGAGACCTAGTGCTGTTTCTCCCACATATTCACATA |

Table based on MRC-Holland Product Descriptions v8 (7.3.12) & v11 (10.12.15).

**Table 2: QDX2 control fragments in MRC-Holland SALSA MLPA P316-B2 Recessive Ataxias probemix.**

| Length (nt) | Name | Gene | Chromosomal Location |
|---|---|---|---|
| **64** | 64nt Q-fragment | - | - |
| **70** | 70nt Q-fragment | - | - |
| **76** | 76nt Q-fragment | - | - |
| **82** | 82nt Q-fragment | - | - |
| **88** | 88nt D-fragment | *CARM1* | 19p13.2 |
| **92** | 92nt control fragment | *IL1B* | 2q13 |
| **96** | 96nt D-fragment | *JPH3* | 16q24.2 |
| **100** | 100nt X-fragment | *AMOT* | Xq23 |
| **105** | 105nt Y-fragment | *UTY* | Yq11.221 |

Table based on MRC-Holland Product Description v8 (7.3.12).

DNA quality and concentration were determined using a NanoDrop ND-1000 spectrophotometer (ThermoScientific, Wilmington, DE, USA), using no less than 150 µg of genomic DNA per patient sample. On day 1, for each sample, 5 µL of DNA solution in Tris-EDTA buffer (TE) was denatured at 98°C for 5 minutes and cooled to 25°C on a thermocycler (Applied Biosystems Gene Amp PCR System 9700, ThermoFisher Scientific, Waltham, MA, USA). Next, a hybridization master mix was prepared containing 1.5 µL of MLPA buffer and 1.5 µL of probemix for each reaction, and 3 µL of this mastermix was added to each 5 µL denatured DNA sample. The new samples were then hybridized through incubation for 1 minute at 95°C and then for 16-20 hours at 60°C of the thermocycler. On day 2, a ligase mastermix was prepared with 25 µL of distilled water, 3 µL of ligase buffer A, 3 µL of ligase buffer B and 1 µL of ligase-65 enzyme for each sample. The thermocycler temperature was lowered to 54°C, and 32 µL of ligase mastermix was added to each hybridised sample. The sample was ligated by incubation at 54°C for 15 minutes, and the enzyme inactivated by heating to 98°C for 5 minutes before cooling to 20°C. Following this, the ‘one-tube PCR’ protocol was followed. A polymerase mastermix was prepared containing 7.5 µL distilled water, 2 µL carboxyfluorescein-labelled

(6-FAM) SALSA PCR primer and 0.5 µL SALSA polymerase for each sample. 10 µL of this polymerase mastermix was added to each sample, and the whole 50 µL solution subjected to the following PCR programme: 35 cycles of 95°C for 30 seconds, 60°C for 30 seconds and 72°C for 60 seconds. The samples were then held at 72°C for another 20 minutes, and then cooled to 15°C (see Table 3).

On day 3, fragment size analysis was performed by capillary electrophoresis (ABI-3730 fragment analyser, Applied Biosystems, ThermoFisher Scientific). For this process, 0.2 µL GeneScan 500LIZ dye size standard (Applied Biosystems) and 9 µL Hi-Di formamide (Applied Biosystems) were added to 1 µL of each PCR product. The samples were heated to 80°C for 2 minutes on the thermocycler, and then rapidly cooled on ice for three minutes before transfer to the fragment analyser. Once the data was obtained, it was analysed using Coffalyser software (MRC-Holland) and GeneMarker v2.2.0 (Soft Genetics, PA, USA), which generates an EDQ or peak ratio for each probe using the negative control.

**Table 3: Thermocycler Program for MLPA Reaction.**

| Stage | Temperature | Time | |
|---|---|---|---|
| DNA Denaturation | 98°C | 5 minutes | |
| | 25°C | Pause | |
| Hybridization | 95°C | 1 minute | |
| | 60°C | Pause | |
| Ligation | 54°C | Pause | |
| | 54°C | 15 minutes | |
| | 98°C | 5 minutes | |
| | 20°C | Pause | |
| PCR Reaction | 95°C | 30 seconds | 35 cycles |
| | 60°C | 30 seconds | |
| | 72°C | 60 seconds | |
| | 72°C | 20 minutes | |
| | 15°C | Pause | |

Table based on MRC-Holland Product Description v8 (7.3.12).

## 2.2 Physiology of $Ca^{2+}$ in Cardiomyocytes in Friedreich's Ataxia

### 2.2.1 Cell Culture

Two immortal cardiomyocyte cell lines were employed for $Ca^{2+}$ imaging analysis and other physiological measurements. HL-1 cells are an atrial murine adult line, first developed by Dr William Claycomb (Claycomb et al., 1998) (a generous donation from the lab of Professor Sean Davidson, Hatter Institute, UCL). This was the first cell line developed that can maintain the contractile activity of the cardiomyocytes *in vitro*. HL-1 cardiomyocytes can be observed to contract, with this possibility more frequent at higher confluency. They can also be frozen using DMSO as a cryoprotectant, and also recovered from frozen stocks. The medium supported cell growth, maintaining the cells in a medium in which they could survive, grow and divide. Flasks or plates where the cells were to be plated were first pre-plated with the cell adhesive proteins gelatin and fibronectin in preparation for HL-1 plating. For passaging, 0.25% trypsin-EDTA was used to detach the cells from the surface of the flask. H9c2 cells (ATCC) were also used to corroborate data from the HL-1 cell line. These are immortalized ventricular neonatal rat myoblasts.

#### *Preparation of Complete Claycomb Medium*

Claycomb medium requires several supplements in order to nourish the HL-1 cells properly (FBS and L-Glutamine) as well as to maintain a differentiated phenotype in the cells and to stimulate their beating (Claycomb et al., 1998). They must be wrapped in aluminium foil as the ascorbic acid in the norepinephrine stock is light-sensitive. All supplements should be heated to 37°C. The Claycomb medium must incorporate the following reagents before being added to cells: Foetal Bovine Serum (FBS)

at 10% (Invitrogen), penicillin at 100 U/mL (Sigma Aldrich), streptomycin at 100 µg/mL (Sigma Aldrich), norepinephrine at 0.1 mM and L-glutamine at 2 mM. When referring to Claycomb medium during this methods section, this shall refer to complete Claycomb medium unless otherwise stated. Norepinephrine stock was made up to a 10mM concentration using ascorbic acid. Firstly, 25 mL of 30 mM ascorbic acid was made by adding 0.1475 g of ascorbic acid to 25 mL of cell culture grade distilled water. This mixture was covered in foil as ascorbic acid is light sensitive. Then, 80 mg of norepinephrine was added to the 25 mL of 30 mM ascorbic acid in a fume hood, taking the necessary precautions due to the toxicity and volatility of norepinephrine. This was then filter-sterilised using a 0.22 µm acrodisc syringe filter in the sterile hood, and aliquoted in 5 mL volumes for addition to the Claycomb medium (or stored at -20°C). The Claycomb medium itself was stored at 4°C and covered in aluminium foil due to the strong light-sensitivity of the medium.

### *Passaging of HL-1/H9c2 Cells*

HL-1/H9C2 cells were always handled under conditions of the utmost sterility. They were first plated into two T25 tissue culture flasks and maintained at 37°C and at 5% $CO_2$ in a humidified incubator for ideal cell growth conditions. Upon reaching 90-100% confluence, one of these flasks was split 1:2 into one T75 flask that was again split 1:3 into further T75 flasks (as many as required based on the experiments to be carried out) to become the 'working' set of cells. The other T25 flask was split 1:3 into a single T75 flask. Once the cells in this T75 flask were confluent, they were split into two T75 flasks, whose cells were frozen in liquid nitrogen upon reaching confluency for storage purposes (see separate 'freezing HL-1/H9c2 cells' section in methods).

Before plating the cells into flasks, these flasks must be coated with a pre-plating solution containing 0.02% gelatin and 5 µg/mL fibronectin (3 mL/T75 flask; 1 mL/T25 or 3 $cm^2$ dish/well) in tissue-culture grade $H_2O$. The solution must be autoclaved after the addition of gelatin for full dissolution of the

gelatin, after which the fibronectin is added in sterile conditions. The pre-plating solution must also be filter-sterilised prior to use in pre-plating, using a 0.22 µm acrodisc syringe filter in the sterile hood. The pre-plated flasks were incubated for at least two hours in the incubator. No pre-plating stage was required for the H9c2 cells, which were maintained in DMEM containing 10% FBS and 2mM L-glutamine. The T75 flask containing the HL-1/H9c2 cells to be passaged was first rinsed with 2 mL of 0.25% trypsin-EDTA (Sigma Aldrich), without pipetting directly over the surface of the cells. After removing this, 3 mL of the 0.25% trypsin-EDTA was added and the flask was left for 3 minutes inside the incubator, to harvest the cells. The 0.25% trypsin-EDTA detaches the cells from the surface of the flask. If the cells remained attached to the flask, the flask was lightly rapped on the benchtop, or the 3 mL of 0.25% trypsin-EDTA was removed and replaced with another 3 mL and incubated for 3 minutes as before: however, these procedures were kept to a minimum to avoid cell deterioration. As soon as possible following confirmation of cell detachment, the 3 mL 0.25% trypsin-EDTA containing the detached cells was collected and placed in a 15 mL falcon tube containing 3 mL of complete Claycomb medium (always pre-heated to 37°C before use). This inactivates the activity of trypsin, which if left active for too long can lead to cell deterioration and death. The tube containing 6 mL of solution was centrifuged at 700 rpm for 5 minutes.

Meanwhile, the pre-plating solution was removed from the T75 flasks that were due to be plated. After the centrifugation the cells formed into a pellet: the supernatant was removed, and the pellet was fully resuspended in 6 mL of incomplete Claycomb medium. 100 µL of this suspension was taken and added to a hemocytometer, along with 400 µL of 0.4% Trypan Blue, and the cells were counted. Following this, 12-13 mL of fresh complete Claycomb medium was added to each T75 flask due to be plated, followed by 2 mL of the cell suspension to achieve a 1:3 cell passage. A passage between 1:2 and 1:5 could also be performed depending upon experimental timing: any thinner than 1:5 was considered too thinly spread to reach full cell confluence. Alternately if the cells were being prepared for experiments,

they were plated in appropriate volumes onto 25mm glass coverslips stored within a 6 multi-well plate.

## *Isolation of Neonatal Cardiomyocytes*

In order to carry out $Ca^{2+}$ imaging experiments on primary cells, these had to be obtained by isolation of mouse neonatal cardiomyocytes from 6-day old YG8R and Y47R mice (Jackson Laboratories; this study was carried out in accordance with the recommendations of the Animal (Scientific Procedures) Act 1986, or ASPA). The protocol was approved by the UCL Animal Welfare and Ethical Review Body (AWERB). Mouse pups were obtained from mating couples of a YG8R/Y47R mouse colony. The YG8R is a mouse model that contains a human FXN YAC incorporating 190+90 GAA repeats on a mouse Fxn null background, recapitulating the FRDA progressive disease phenotype observed in humans (Al-Mahdawi et al., 2006; Pook et al., 2001). In order to isolate these cells they underwent several digestion cycles in a buffer containing collagenase, which breaks down the connective tissue in muscle cells, in a method previously described by Stephanou et al. (Stephanou et al., 1998). A two-step procedure is carried out, involving enzyme digestion followed by mechanical agitation of the ventricular tissue, and finally purification of the cardiomyocyte population. Neonatal cardiomyocytes are generally isolated from mice that are 4-6 days old. A number of hearts can be digested simultaneously to increase the myocyte yield. Mouse pups were decapitated, following which their hearts were excised and the cells dispersed in an isolation buffer.

**Table 4: Isolation Buffer**

| Isolation Buffer | Required concentration (mM) | $M_w$ | Volume added to 500 mL solution (g) |
|---|---|---|---|
| NaCl | 116 | 58.44 | 3.4 |
| HEPES | 20 | 238.30 | 2.38 |
| $NaH_2PO_4$ | 0.77 | 141.96 | 0.06 |
| Glucose | 5.5 | 180.16 | 0.5 |
| KCl | 5.4 | 5.4 | 0.2 |
| $MgSO_4$ | 0.4 | 0.4 | 0.05 |

Adjusted to pH 7.35 and filter-sterilised.

**Table 5: Digestion Buffer**

| Digestion Buffer | Volume required |
|---|---|
| Isolation Buffer | 100 mL |
| Collagenase type II (≈250units/mg) | 60 mg |
| Penicillin/Streptomycin | 1 mL |

Must be prepared fresh during each experiment.

When the pups were culled, their hearts were first rinsed in 70% EtOH and then isolated in a dish of isolation buffer, after which they were finely cut into small pieces. Meanwhile, the enzymatic digestion buffer containing collagenase type II enzyme (Worthington) and pancreatin was prepared, oxygenated for half an hour and filter-sterilised. The solution containing the finely chopped heart tissue for each mouse was then transferred to a 25 $cm^2$ flask containing 3 mL of digestion buffer enzyme solution and left to settle for 1-2 minutes. This digestion buffer was then slowly discarded, taking special care not to discard any of the heart tissue, and 3 mL of fresh digestion buffer was added. The flask was then kept at 37°C for 15 minutes. Following this, the flask was gently shaken, and the digestion buffer again discarded. The digestion at 37°C for 15 minutes was then repeated, after which the supernatant enzyme solution incorporating cardiomyocytes (and other cell types) was removed from the remaining chunks of tissue and suspended in 2 mL of FBS each. A fresh 3 mL of digestion buffer was then added to the tissue, and this procedure was repeated three times, until three 5 mL samples of cardiomyocyte-containing enzyme solution from each mouse heart have been collected (thus per pup, around 15 mL of digestion buffer is required).

The collected enzyme solutions were then centrifuged at 1000 rpm for 5 minutes, the supernatant discarded, and the cardiomyocyte fraction re-suspended in 2 mL plating medium with a syringe needle, after which the cells were plated using one well of a 6-well plate per cardiomyocyte fraction re-suspended in 2 mL of plating medium (15% FBS and 1% penicillin/streptomycin in DMEM+GlutaMAX medium). Thus, the cells from two hearts plated a 6-well plate, with each heart occupying three wells each. The 6-well plates contained 25 mm coverslips in each well (to allow for later analysis of the cells) and had been pre-plated with autoclaved and filter-sterilised 0.01% gelatin in PBS at 37°C for one hour in the incubator, after which the gelatin solution was removed, and the wells were ready for plating. The cells were left in plating medium overnight to attach to the surface, and the next day the medium was replaced with maintenance medium (1% FBS and 1% penicillin/streptomycin in DMEM+GlutaMAX medium).

### 2.2.2 Transfection of HL-1/H9c2 Cardiomyocytes

Transfection is the process of introducing foreign genetic materials into a eukaryotic cell in a non-viral manner. RNA interference (RNAi) is a technique whereby RNA is inserted into a cell to down-regulate the production of a specific protein by blocking translation, in this case frataxin. With effective introduction of an small interfering RNA (siRNA) construct, a single protein in a cell can be ‘silenced’, as the siRNA destroys the mRNA encoding that protein. As a good FRDA model requires a frataxin protein knockdown and not a full knockout, use of a small siRNA targeted to frataxin mRNA of 20-25 base pairs in length with no vector is ideal. siRNA is at first double-stranded, with 2 nucleotides on each 3’ overhang. Once it enters the cell however, it can be denatured by helicase, and then the sense and anti-sense siRNA strands and bound by the RISC (RNA-induced silencing complex)-related proteins. In the cells, the RISC complex containing the

anti-sense strand (which is the strand required to pair with the mRNA) uses the siRNA as a template for recognizing complementary mRNA. In this way, only specific mRNAs (such as frataxin) are selected for silencing by this method. If even one nucleotide on the siRNA does not correspond to the mRNA, the siRNA may not bind. Conversely, as few as 11 contiguous nucleotide matches with an unrelated mRNA can lead to off-target silencing. The active RISC complex is recycled and goes onto destroy other mRNA strands in the cell.

In the study, Lipofectamine 2000 was used as a transfection reagent. The lipofectamine reagent contains lipid subunits, which can form liposomes (the synthetic equivalent of the phospholipid bilayer of cell membranes) in an aqueous environment, which entrap nucleic acids. Transfection efficiency is increased due to the fact that the positive surface charge of the liposomes mediates the interaction of the negatively charged nucleic acid molecules and the cell membrane. This overcomes the electrostatic repulsion of the cell membrane and allows for the fusion of the liposome-nucleic acid transfection complex with the negatively charged cell membrane. The transfection complex is thought to enter the cell by endocytosis.

YFP-tagged plasmid DNA (pcDNA3-YFP) was co-transfected alongside the siRNA to act as a marker of cell transfection. This plasmid vector allows the cell to express YFP-tagged DNA using its own machinery. While the site of action for transfected RNA is in the cytoplasm, the DNA must be transported to the nucleus for effective transfection. There, the DNA is either transiently expressed for a short period of time or become incorporated into genomic DNA where the change induced is passed on to cells as they divide. In this case, the YFP-tagged DNA acts as a transiently expressed fluorescent marker that confirms cell transfection, and results in high expression levels that persist for 48 hours when the DNA is transfected.

The simultaneous transfection of cells with two unrelated, separate nucleic acid molecules carried out is known as a co-transfection. Theoretically, if

the cell takes up the siRNA construct, it is very likely to have taken up the YFP-DNA as well, and therefore YFP fluorescence can be used as a determination of successful co-transfection. There is a very small chance a transfected cell will express only the YFP-DNA plasmid and not the siRNA construct: however, if the experiment is repeated enough times, this chance will not be statistically significant. To knock-down frataxin mRNA in HL-1/H9c2 cardiomyocytes, a co-transfection of FXN-siRNA and YFP-tagged plasmid DNA was performed. Mm_Fxn_1 FlexiTube siRNA was used as the predesigned siRNA against mouse frataxin (SI01007139, Qiagen) in HL-1 cells, and Rat_Fxn FlexiTube siRNA (SI02902557, Qiagen) was used in H9c2 cells. This interferes with the expression of frataxin by targeting a short sequence around 450bp into the mouse FXN mRNA transcript from the 5' end (Gene accession no. NM_008044). For the negative control (siRNA-scrambled), AllStars Negative Control siRNA (1027418, Qiagen) was used for both cells.

100,000 HL-1/H9c2 cells were seeded per 35 mm well in a 6-well plate. On the next day, into each of the 6 wells went the following concentrations of siRNA and YFP-DNA (pcDNA3-YFP): 30 nM siRNA and 10 µg/mL YFP-DNA. To this end, solutions '$A_1$' and '$B_1$' were prepared in separate Eppendorf tubes. The negative control siRNA was used in the case of $A_1$, and Mm_Fxn_1 FlexiTube siRNA in the case of $B_1$, both of which were diluted to a 100 µM stock and then into 10 µM aliquots stored at -20°C before addition to the solutions. Each solution contained 9 µL siRNA from these aliquots, 15 µg (3.75 µL) YFP-DNA and 1.5 mL incomplete Claycomb medium. The solutions '$A_2$' and '$B_2$' were also made in separate Eppendorf tubes, each containing 30 µL Lipofectamine 2000 and 1.5 mL incomplete Claycomb medium.

After incubating these solutions separately for 5 minutes at room temperature, solution $KD_1$ was combined with $KD_2$ and solution $NC_1$ was combined with $NC_2$. The resulting 'Solution A' and 'Solution B' were mixed gently and incubated at room temperature for 20-30 minutes to allow DNA-liposome complexes to form. Prior to adding the transfection mix to the cells,

they were rinsed once with phosphate buffered saline (PBS) to remove any FBS, which inhibits the transfection process. Following this, 1 mL each of Solution A was added to three wells of the 6-well plate, and 1 mL each of Solution B was added to the other three and these were clearly labelled. The cells were incubated at 37°C for three hours (no more than this due to toxicity of the Lipofectamine 2000), and then the transfection mix was removed from the cells and replaced by fresh, complete Claycomb medium to allow the newly transfected cells to continue growing.

*Transfection Efficiency*

The transfection efficiency was calculated in HL-1 cells by measuring the amount of YFP-cells, which we used as a marker of successful co-transfection. Among cells transfected with siRNA control, 1946 out of 5772 cells were transfected with YFP, giving a transfection efficiency of 33.7±3.6%. Among cells transfected with FXN-siRNA, 1360 out of 4705 cells were transfected with YFP, giving a transfection efficiency of 28.9±3.6%. No significant difference was found between the two cell populations (Fig. 7). Transfection efficiency in H9c2 cells was observed to be of a very similar amount (data not shown).

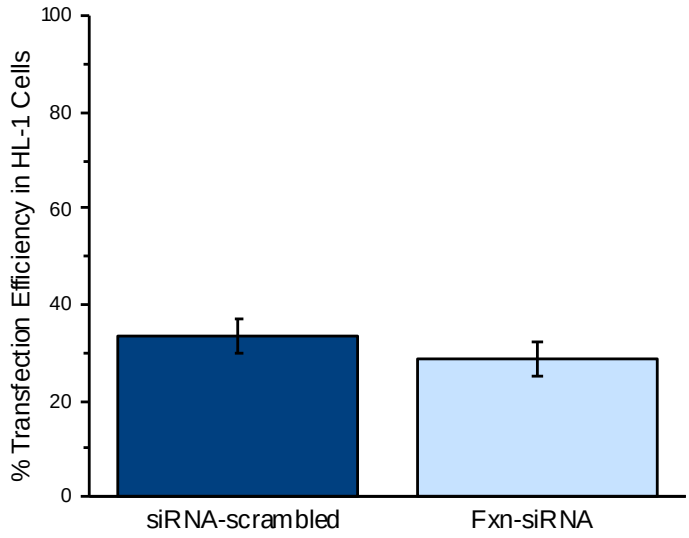


**Figure 7: Transfection Efficiency in HL-1 Cells.**

Transfection efficiency was measured at 34±4% in cells transfected with the scrambled siRNA, and 29±4% in cells transfected with the FXN-siRNA. There was no significant difference in transfection efficiency between the two groups.

### 2.2.3 Fluorescence Imaging

#### *Basics of Fluorescence*

Certain atoms or molecules can be excited at a certain wavelength of light specific to that atom/molecule, after which they emit light at a specific emission wavelength. This is known as luminescence, and fluorescence is a subcategory of luminescence where light is emitted from the atoms/molecules $10^{-8}$ s or less after absorption of light by the atoms/molecules. Compounds that emit fluorescence are known as fluorophores. Specifically, a molecule absorbing light causes its electron to move from the electronic ground state into an excited state. Fluorescence is caused by an electron returning to the electronic ground state, emitting a photon. This light can be detected by an epifluorescence microscope. The microscope is engineered for optimal fluorescence signal detection, and therefore excites the fluorophore at wavelengths very close to or at its

absorption peak, minimises the background signal, and detects as much fluorescence emission as possible.

### *CCD Microscopy*

Digital cameras are now used in fluorescence microscopy that incorporate a CCD photon detector, which allows for the transformation of light intensity information into information coded by localised electric charge that varies with changes in the light intensity. The detector is an integrated circuit etched onto a silicon surface forming light-sensitive elements called pixels. Photons incident on this surface generate charge that can be read by electronics, which can be quickly converted into a fluorescence intensity value for the corresponding location. Thus, the light signal is converted into quantitative, usable data based on its intensity in arbitrary units. The data of light patterns falling on the device is quantified digitally, allowing it to be reconstructed and displayed on a computer monitor. The capability for fluorescence imaging of a monochromatic CCD camera is tested by optimisation of the gain, offset and exposure time. CCDs have the highest light sensitivity of any light detection technique available. They can produce images with one input event, and therefore are ideal for picking up fluorescence events that change at speed (such as a change in $Ca^{2+}$ levels in a cardiomyocyte), in a way that a confocal microscope is unable to do due to the decreased signal intensity that it exchanges for increased optical resolution.

### *Confocal Microscopy*

The confocal microscope builds upon fluorescence microscopy techniques by using an optical imaging technique that improves optical resolution by adding a spatial pinhole at the confocal plane of the lens to eliminate out-of-focus light (see Fig. 8). As only light produced by fluorescence very close to the focal plane is detected, the optical resolution of the image is much

better than that of wide-field microscopes like the CCD camera, allowing for the observation of finer detail. However, the increased resolution is at the price of decreased signal intensity, so longer exposures are required. The confocal microscope illuminates a specimen using a point laser source, unlike the CCD camera which uses a light detection technique. Unlike the CCD camera, it enables three-dimensional reconstruction of an object from the superimposition of sets of images obtained at different depths, a process known as optical sectioning where the object is scanned in the x and y direction as well as the z-direction along the optical axis. The light signal is in this case converted by photomultiplier tubes (PMTs) into quantitative electrical signals based on light intensity in arbitrary units, which is then digitised and displayed as an image on a monitor for further analysis.

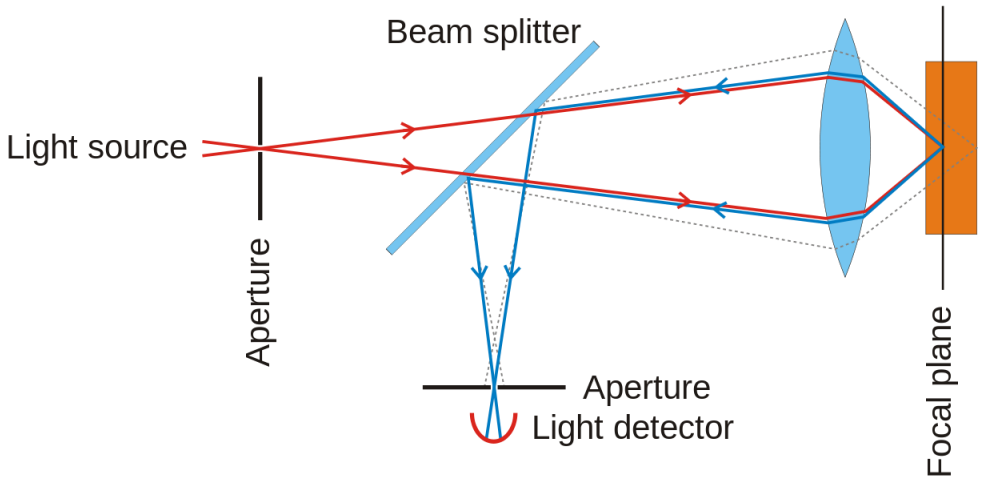


**Figure 8: Confocal Microscope.** Image in public domain.

## *$Ca^{2+}$ Imaging*

Once the cells were ready, the cells were analysed using the Fura-2-AM dye to measure $Ca^{2+}$ levels and their fluctuation following addition of caffeine and thapsigargin. Fura-2-AM is a ratiometric UV-light excitable dye, which emits light when excited at 340 nm in $Ca^{2+}$-bound form and at 380 nm in $Ca^{2+}$-unbound form. The acetoxymethyl (AM) form is useful for noninvasive intracellular loading. Fluorescence measurements were

obtained using a cooled charge-coupled device (CCD) camera (Hamamatsu, Orca ER).

Cytosolic $[Ca^{2+}]$ ($[Ca^{2+}]_c$) was observed in single cells using excitation light from a Xenon arc lamp, with the beam passing sequentially through 10 nm band pass filters centred at 340 nm and 380 nm placed inside a computer-controlled filter wheel. Emitted fluorescence light was reflected via a 510 nm long-pass filter to the CCD camera and digitised to 12-bit resolution (Digital Pixel Ltd, UK). All imaging data was analysed using Andor software (Belfast, UK).

To measure $[Ca^{2+}]_c$ in transfected HL-1/H9c2 cells or primary mouse cardiomyocytes, the cells plated on 25 mm diameter coverslips in 6-well plates were first loaded for 30 minutes in the cell incubator with 5 µM Fura-2-AM in 1 mL of HEPES-buffered salt solution (HBSS), so that the cells could take up the fluorophore. Incubation in the dark is crucial as Fura-2-AM is light-sensitive. Before adding the coverslips to the coverslip plates, the plates were washed for 5 minutes each in ethanol and $H_2O$ and dried thoroughly with a tissue. Meanwhile, the coverslips were transferred from the sterile incubator two at a time to maintain healthy cell conditions for as long as possible before the experiment.

The Claycomb medium was removed and the cells were rinsed with 1 mL of HBSS, and then washed again in 1 mL of HBSS for 3-5 minutes, following which this was removed and another 1 mL of HBSS was added. Then one coverslip was removed with sharp tweezers and added to the coverslip ring, which was carefully sealed and the appropriate amount of HBSS (i.e. the correct amount so that any solutions added later in the experiment containing precise concentrations of drugs would add up to a full total of 500 µL) was added as the recording medium. The CCD camera was turned on, beginning with turning on the computer and then progressively switching on the filter wheel and the monochromator, the noise of the filter wheel indicating that the camera was switched ‘on’ and the experiment could proceed. The Omega program was activated on the desktop.

When using the 40x objective, a drop of oil was added to the objective before placing the coverslip upon it; when using the 20x objective, no oil was added (using the 20x objective includes more cells in the field of vision but at the cost of a lower exactitude of measurement). Before the coverslip was placed on the objective and into the plateholder, the underside of the objective was cleaned with ethanol and dried with tissue. For measuring the intensity of the Fura-2-AM dye, a protocol was developed on the Omega software incorporating the 340 nm and 380 nm objective options in order to excite electrons alternately at 340 nm and 380 nm, allowing for a ratiometric measurement between the two Fura-2-AM intensities. The appropriate filter wheel was also selected for picking up emitted light, which was filter wheel 2, which picks up the light emission of Fura-2-AM at a wavelength of 510 nm.

In the case of HL-1 and H9c2 cells, successful transfection was marked by co-transfection of YFP-tagged plasmid DNA, and therefore only cells showing successful YFP-DNA co-transfection were selected for analysis in the experiment. Thus, the Omega software was also used in this case to create a 472 nm light wavelength of excitation (adjusting the available 490 nm objective option) in order to excite electrons at the appropriate wavelength for YFP, and thus provide an image of YFP-DNA fluorescence that could then be used for selecting which cells to analyse during the $Ca^{2+}$ imaging. The appropriate filter wheel was also selected for picking up emitted light, which was filter wheel 4, collecting the emission with the 525-536 nm band pass filter.

Before beginning the visualization of the cells using the Omega program, the microscope light path was turned on and the microscope was adjusted to ‘optical’ mode. An appropriate cluster of cells to measure was found by microscope observation. Then, the microscope light path was turned off and the microscope adjusted to ‘fluorescence’ mode, and the live imaging option was selected on the Omega program. The pixel binning was set to the ‘4x4’ setting. The focus, gain (amplification applied to the photon detection

system), offset (the threshold that defines the lowest intensity of brightness displayed) and exposure time were adjusted to produce an image of YFP-DNA fluorescence (if using HL-1 or H9c2 cells), and then of the Fura-2-AM fluorescence in the cells, that was crisp yet unsaturated at the 472 nm, 340 nm and 380 nm wavelengths. Once an appropriate image was established, appropriate regions of interest were set and the analysis was run, ensuring that the traces were measured as ratios of excitation between 340:380 nm, and not measured separately.

*Caffeine-based experiments*

Caffeine is a non-selective adenosine receptor antagonist that activates release of $Ca^{2+}$ from intracellular stores and can be used to assess SR $Ca^{2+}$ content in skeletal or cardiac muscle fibres (Endo & Thorens, 1975; Fabiato & Fabiato, 1975). The caffeine was used to elicit release of $Ca^{2+}$ from SR stores and compare the amplitude and peak shape of the ensuing $Ca^{2+}$ spike, our first step in the search for indications of any change in $Ca^{2+}$ homeostasis. Once a $[Ca^{2+}]_c$ baseline was established for the cell, 10 mM caffeine was added at a single interval using pre-prepared 50 mM or 100 mM aliquots of caffeine and the increase in $[Ca^{2+}]_c$ following activation of the ryanodine receptors on the SR. Images were collected and digitised at the fastest intervals possible based on the time exposure of the images, with a minimum of 1 second intervals.

*Thapsigargin-based experiments*

Thapsigargin, a potent inhibitor of the SERCA pump (Rogers et al., 1995), was also used to assess SR $Ca^{2+}$ content. In order to measure the effect of thapsigargin on the SERCA pump accurately, thapsigargin had to be added to the cells in a $Ca^{2+}$-free solution, instead of in regular HBSS solution. The $Ca^{2+}$-free recording medium was made using the following concentrations:

**Table 6: $Ca^{2+}$-free Medium.**

| Constituents of $Ca^{2+}$-free medium | Required concentration (M) |
|---|---|
| NaCl | 2 |
| KCl | 1 |
| $MgSO_4$ | 1 |
| $KH_2PO_4$ | 1 |
| D-Glucose | 1 |
| HEPES | 1 |
| EGTA | 0.5 |

N.B. The EGTA must be calibrated at pH 8.01, so instead of a volume of 50 mL a volume of 200 mL was used (with 38.04g of EGTA), so as to allow enough volume for pH calibration.

| $Ca^{2+}$-free medium | Stock concentration (M) | Final concentration (mM) |
|---|---|---|
| NaCl | 2 | 156 |
| KCl | 1 | 3 |
| $MgSO_4$ | 1 | 2 |
| $KH_2PO_4$ | 1 | 1.25 |
| D-Glucose | - | 10 |
| HEPES | 1 | 10 |
| EGTA | 0.5 | 0.5 |

The $Ca^{2+}$-free medium was then filter-sterilised and either used immediately in experiments using thapsigargin, or frozen at -20°C for later use. Before analysis with the cells bathed in HBSS in the coverslip dish under the CCD camera, the HBSS was replaced with 300 µL $Ca^{2+}$-free recording medium, after which the experiment was run on the camera and the $Ca^{2}$ baseline observed for 2 minutes. Then, thapsigargin pre-diluted in 200 µL $Ca^{2+}$-free recording medium (to aid admixture) at an amount achieving a final concentration in the 500 µL of medium of 2 µM thapsigargin, was added to the coverslip, and the effect on $Ca^{2+}$ levels recorded.

To calculate the fluorescence, following normalisation against the baseline value, the highest ratiometric (340/380) Fura-2 fluorescence value obtained during the peak was subtracted by the final value of the baseline fluorescence before peak onset. In an additional measurement, the experiments using thapsigargin to inhibit the SERCA pump were carried out

having preincubated the cells in 10 µM dantrolene for 2 hours, and then proceeding as usual. Dantrolene inhibits the ryanodine receptors, and thus its use in combination with thapsigargin helps distinguish whether the effects of the frataxin knockdown are causing damage to the ryanodine receptors themselves.

### *Measurements of ROS production*

The cells were also analysed for other physiological factors in addition to $Ca^{2+}$ levels in order to find potential links between any findings regarding $Ca^{2+}$ levels and other physiological events known to occur in FRDA. Using the CCD camera (as described in the $Ca^{2+}$ imaging section), dihydroethidium (Het; 5 µM; Thermo scientific), a superoxide indicator that exhibits blue fluorescence in the cytosol until oxidized where it intercalates within the cell's DNA and stains the nucleus a bright fluorescent red, was added in HBSS (Sigma) just before the start of the experiment to the HL-1/H9c2 cells and remained in the solution for the duration of the experiment. The dye was used ratiometrically to measure cytosolic superoxide levels, as the dye was excited in unoxidized form at 364 nm (blue fluorescence) and in oxidized form at 543 nm (red fluorescence), and emitted fluorescence was collected using the dual band filter. Data was collected every 5 seconds using the ratio 543/364nm. This was then normalised through averaging the first 10 ratiometric values and dividing each value by this baseline. The rate of fluorescent units/second was calculated to allow for a comparison between the disease and control cell groups. Mitochondrial ROS was calculated following addition of 1 µM CM-H2Xros (Thermo scientific) 20 minutes before beginning the experiment.

## *Measurement of NAD(P)H Autofluorescence*

The autofluorescence of NAD(P)H (or NADH and NADPH together) was imaged in cardiomyocyte cultures using the cooled CCD camera. The setting up of the experiment regarding transfer and preparation of cells for analysis using the CCD camera is as described in the $Ca^{2+}$ imaging section. The autofluorescence that these pyridine nucleotides emit in their reduced forms was excited at 360 nm, with the emission collected by the 525-536 nm band pass filter. After the transfected cells had been selected for by testing for YFP, cells were exposed to first the uncoupling agent carbonyl cyanide 4-(trifluoromethoxy) phenylhydrazone (FCCP, 1 µM), to stimulate respiration and achieve maximum NADH oxidation, and then to NaCN (1 mM), to inhibit respiration and achieve maximum NADH reduction. This was done in order to measure the full range of the autofluorescence signal, in relation to the full mitochondrial NADH pool, and thus to allow for normalisation of the data (Abeti et al, 2011). The following formula was used to normalise the NADH autofluorescence measurements:

$$\Delta F_{normalised} = (F - F_{fccp}) / (F_{cn} - F_{fccp})$$

## *Measurement of Mitochondrial Membrane Potential ($\Delta\psi_m$)*

Tetramethyl rhodamine, methyl ester (TMRM) is a cationic, cell-permeant red-orange fluorescent dye readily sequestered by active mitochondria. It was used to estimate the dynamic signal $\Delta\psi_m$ in HL-1/H9c2 cell mitochondria, and to observe the fluctuations in the membrane potential when caffeine was added. FCCP, which is an uncoupling agent that disrupts ATP synthesis, was added at the end to fully dissipate the $\Delta\psi_m$. In order to measure small fluctuations in $\Delta\psi_m$, de-quenching mode was used. The cells were incubated for 20 minutes with 500 nM TMRM, and then prepared in a coverslip chamber and imaged using the cooled CCD camera (as described in the $Ca^{2+}$ imaging section). The dye must be kept continuously in solution at 500 nM, as otherwise it will wash out of the cells immediately. The cells were observed in 300 µl of HBSS medium. After the transfected cells had

been selected for by testing for YFP-DNA expression, the TMRM was visualised using an excitation wavelength of 560 nm with a long pass filter using the 810 Zeiss confocal microscope. Depolarisation was indicated by an increase of $\Delta\psi_m$. Once the experiment had begun and a TMRM baseline value established among the cells selected, 10 mM caffeine was added, and 1 µM FCCP was added after a 10-minute interval from the start to complete the experiment.

### *Immunofluorescence*

Immunofluorescence techniques were used to visualize the frataxin mRNA knockdown achieved by the HL-1/H9c2 cells siRNA transfection. To do this, a Zeiss 810 UV-vis confocal laser scanning microscope (CLSM) was used to obtain the images. Immunofluorescence is a semi-quantitative method that uses the specificity of antibodies to their antigen to target fluorescent dyes to specific molecular targets within the cell, thereby allowing visualization of the target molecule throughout the sample. It is an example of immunostaining (using antibodies to stain proteins). In this experiment, the unlabelled primary antibody specifically binds the target molecule, and the secondary antibody carrying the fluorophore recognizes the primary antibody and binds to it. Secondary antibodies must be against the host species of the primary antibody being used.

Following transfection of the cells in 6-well plates as described above, the Claycomb medium was removed by aspiration and the coverslips were washed twice in PBS 1x. The wash buffer was aspirated, and the cells fixed by addition of 4% paraformaldehyde (PFA). The PFA was prepared in PBS at 60°C and in 1 M NaOH in order to dissolve the paraformaldehyde. The cells were incubated in PFA for 10-15 minutes, after which the PFA was removed by aspiration and the cells washed thoroughly three times (for 5, 10 and 5 minutes) with PBS 1x. After the last wash was aspirated, the cells were permeabilised by addition of 0.1% Triton X-100 in PBS 1x and incubation for 30 minutes at room temperature. After this detergent solution

was removed by aspiration, the coverslips were again washed in PBS 1x three times as before. After the last wash was aspirated, blocking solution made from 3% bovine serum albumin (BSA) and 10% goat serum in 0.1% Triton X-100 in PBS 1x was added, and the cells were incubated in this solution for 1 hour at room temperature. After the blocking solution was aspirated, the primary antibody solution was added to the coverslip. The primary antibody used was the mouse monoclonal anti-frataxin antibody [17A11] ab113691 (Abcam) at a concentration of 1 µg/mL for immunofluorescence. The primary antibody was provided at 1 mg/mL and was therefore diluted 1:1000 in 3% BSA and 10% goat serum in 0.1% Triton X-100 in PBS 1x, using enough solution to cover the entire coverslip (25-50 µL).

The cells with the primary antibody applied were incubated at room temperature for 1 hour (keeping the lid on the 6-well plate to avoid evaporation) or overnight in a humidified chamber at 4°C. The specificity of the immunoreactions was controlled by adding buffer rather than primary antibodies in a control coverslip(s), which did not result in immunostaining. Following this, the coverslips were washed three times in PBS 1x, then drained and applied with the secondary antibody. The secondary reagent used was Alexa Fluor 568 goat anti-mouse IgG (A-11004, Thermo Fisher Scientific), diluted 1:1000 for one hour beforehand in 3% BSA and 10% goat serum in 0.1% Triton X-100 in PBS 1x. The coverslips were incubated for a minimum of 45 minutes in darkness, after which the coverslips were washed three times in PBS 1x. On the final wash in PBS, 300 nM DAPI was added for 5 minutes in order to stain the nuclei to allow for their detection, and the cells were incubated at room temperature in the dark for 2-5 minutes. The cells were washed three times in PBS 1x again. Then, a drop of mounting medium was placed on a microscope slide and the coverslip was placed upon the drop, cell side down. The coverslip was sealed and the cells were wrapped in foil and kept at 4°C until ready for viewing with the confocal microscope. Confocal images were obtained using a Zeiss 810 UV-vis CLSM equipped with a META detection system and a 40x oil immersion

objective. Illumination intensity was kept as low as possible to avoid phototoxicity and the pinhole was set to give an optical slice of 2 µm.

### 2.2.4 DNA Analysis of YG8R/Y47R/WT mice

Mice pups were obtained from mating couples of a YG8R/Y47R mouse colony. In order to genotype these pups or any mice of interest from the colony that could be used in matings, a sample had to be obtained from them and analysed by PCR methods. Briefly, PCRs were carried out in a 25 µL volume containing 200-500 ng of genomic DNA from the mice, 2.5 pmol of each primer, and the Extract-N-Amp tissue PCR kit (Sigma-Aldrich).

Genomic DNA was isolated from ear or tail biopsies of mice. PCR analysis was carried out using GAA-F and GAA-R primers (Campuzano et al., 1996). DNA extraction was performed as follows: each ear/tail was first placed in a 0.5 mL Eppendorf tube, and 100 µL of Extraction solution was added, as well as 25 µL of tissue preparation solution, and the solution was mixed by pipetting. The sample was then incubated at room temperature for 10 minutes, after which it was incubated at 95°C for three minutes on a heat block. Then, 100 µL of Neutralisation solution B was added to the sample, which was then mixed by vortexing and centrifuged for 5-10 seconds. All the solutions were from the Extract-N-Amp tissue PCR mix. These DNA extractions from mouse tails or ears were either used immediately in a PCR experiment or stored at 4°C for later use. Meanwhile, the following PCR mix was prepared on ice:

**Table 7: PCR Mastermix for DNA Analysis of YG8R/Y47R Mice.**

| PCR mastermix reagents | Volume per sample (µL) |
|---|---|
| Extract-N-Amp Polymerase | 12 |
| PCR-grade $dH_2O$ | 8 |
| GAA-F (from 100µM stock) | 0.5 |

| | |
|---|---|
| GAA-R (from 100µM stock) | 0.5 |

The primers used were those from the original Campuzano paper that details them (Campuzano et al., 1996):

GAAF: 5'- GGG ATT GGT TGC CAG TGC TTA AAA GTT AG-3'
GAAR: 5'-GAT CTA AGG ACC ATC ATG GCC ACA CTT GCC-3'

The PCR mastermix was prepared for n+1 samples, with each sample prepared in duplicate and including positive controls for the three transgenic genotypes Y47R, YG8R and Y47R/YG8R and an $H_2O$ control. 21 µL was then added to the pre-labelled 250 µL Fischer PCR tubes, and 4 µL of the appropriate DNA extraction mix was added to each. The tubes were quickly agitated and centrifuged, and then added to the PCR machine using the following PCR amplification cycle:

**Table 8: PCR Cycles for DNA Analysis of YG8R/Y47R Mice.**

| Cycles | Stage | Temp | Time |
|---|---|---|---|
| **1 cycle** | denaturation | 94°C | 3 minutes |
| **10 cycles** | denaturation | 94°C | 10 seconds |
| | annealing | 62°C | 30 seconds |
| | elongation | 68°C | 3 minutes |
| **20 cycles** | denaturation | 94°C | 10 seconds |
| | annealing | 62°C | 30 seconds |
| | elongation | 68°C | 3 minutes + 20 second increments per cycle |
| **1 cycle** | | 68°C | 10 minutes |
| | | 4°C | pause |

Following completion of the PCR reaction, 10 µL of PCR product was added to a 1.5% agarose gel made using 1xTBE, using 5 mL of Invitrogen 1kb ladder, and gel electrophoresis was performed. The gel was run at 80V for 1 hour in the large tanks after which the gel was checked, and then for a further 2 hours and 20 minutes in order to size the bands. In the smaller minigel trays the gel was run at 40V for 40 minutes to 1 hour. Band sizes are 457 base pairs + 3x the GAA repeat number of the sample.

### 2.2.5 Statistical Analysis

Data were generated from a minimum of three independent experiments (three sets of three coverslips). Statistical analysis was carried out with the OriginPro 2015 software (OriginLab Corporation). The data is expressed in the form mean ± standard error of the mean (SEM).

# Chapter 3 : Genetic Screening Study of Ataxia Patients for Friedreich's Ataxia

## 3.1 Introduction

FRDA is a complex, multisystem disorder that displays varying rates of progression in patients. This divergence in progression has been addressed in several case studies. Through comparing the age at onset, timespan between age at onset and first use of wheelchair and first onset of various common symptoms such as dysarthria and lower limb and upper limb weakness, these studies developed a clearer understanding of FRDA progression (Harding, 1981; Schols et al., 1997). These studies provided evidence for a general timescale for FRDA from age at onset to death. However, the amount of variation in age at onset as well as rate of progression was high enough to elicit studies into the frequency and nature of atypical forms of FRDA, such as late-onset or very-late onset FRDA (LOFA/VLOFA), as well as a potential genetic basis for their occurrence.

The discovery of the genetic basis for Friedreich's ataxia (Campuzano et al., 1996) crucially allowed for a full clinical description of atypical cases of the disease. Many of these had previously been misdiagnosed due to being outside the established clinical diagnostic criteria (Durr et al., 1996; Filla et al., 2000; Geoffroy et al., 1976; Harding, 1981; Schols et al., 1997). These cases had a less severe disease phenotype, involving a later onset of disease, milder or absent neurological symptoms, slower progression and an absence of non-neurological symptoms (Bhidayasiri et al., 2005; Coppola et al., 1999; De Michele et al., 1994; Gellera et al., 1997; Klockgether et al., 1993; Montermini et al., 1997; Ragno et al., 1997). Indeed, onset can rarely even be in a very late age range after 50, making misdiagnosis more probable for these patients (Berciano et al., 2005; Galimanis et al., 2008). Patients with an age at onset after 50 are

characterized as VLOFA, whereas patients with an age at onset between 25 and 50 are characterized as LOFA.

There is a well-established correlation between the rate of progression/severity of FRDA and the size of the GAA1 allele, with very small sizes below 100 GAA repeats often responsible for atypical FRDA (Schols et al., 1997; Sharma et al., 2002). Atypical FRDA can also present due to compound heterozygosity. This can involve a point mutation in one *FXN* allele alongside the GAA expansion in the other (Campuzano et al., 1996; Cossee et al., 1999; Gellera et al., 2007), with atypical symptoms particularly common in cases involving the p.G130V missense mutation (Bidichandani et al., 1997; Cossee et al., 1999; Forrest et al., 1998). Very rarely an exonic deletion is present instead of a point mutation, which has also been shown to lead to an unusual presentation of FRDA in one case (van den Ouweland et al., 2012).

Thus, it is crucial for clinicians to understand the difference between classical FRDA and LOFA/VLOFA, in order to correctly diagnose FRDA even when it presents atypically. This chapter concerns a study I carried out regarding the frequency of atypical FRDA cases in the disease, in order to understand to what extent FRDA cases were being missed by clinicians. Specifically, a consecutive series of 2000 ataxic patients who lacked a genetic diagnosis after having been referred for the major spinocerebellar ataxias (SCA1, 2, 3, 6, 12 and 17) and who had not been originally referred for a FRDA test, presumably as their symptoms were atypical for the disease, were screened for FRDA. This chapter details this study and places it in the context of:

1. Previous studies on FRDA disease progression and on atypical FRDA, including late-onset/very-late onset Friedreich's Ataxia and the influence of GAA expansion size and compound heterozygosity on patient phenotype.
2. A previous study by Dr M.H. Parkinson, which studied genotype-phenotype correlation in 1768 patients from the same database as the 2000 patients in my study, but who had already been referred for

FRDA testing by their clinicians, and thus presumably had symptoms that fit the diagnostic criteria for FRDA.

## 3.2 Results

### 3.2.1 Genetic Analysis

A consecutive series of 2000 patients from the UK who 1) presented with ataxia, 2) lacked a genetic diagnosis after having been tested for the major spinocerebellar ataxias (SCA1, 2, 3, 6, 12 and 17), and 3) had not been referred for FRDA testing, were tested for FRDA using DNA samples from the patients that had been taken between the years 1996 and 2013. The DNA from all relevant patients was obtained from the NHNN Department of Neurogenetics. The vast majority of neurogenetics labs test for the presence of pathological GAA expansions by the two-stage molecular diagnostic process of 1) triplet-primed PCR and 2) long-range PCR. Using this two-stage PCR process, 2000 cases were screened for FRDA in the laboratory. If two GAA expansions are discovered after stage 2, a genetic diagnosis of FRDA can be made. Twenty cases tested positive at the TP-PCR stage, which confirmed the presence of a *FXN* GAA triplet repeat expansion in at least one allele for each sample (refer to Methods, section 1.2). At the long PCR stage, 3 cases were shown to have triplet repeat expansions in both alleles and were thus newly diagnosed as being FRDA-positive (0.15% of cases; Fig. 10). The number of pathological GAA expansions for each allele in the three FRDA-positive patients determined following long-range PCR are given in Table 10. The intermediate zone between ‘normal’ and ‘pathologically’ expanded repeats as classified and used in the Neurogenetics laboratory of the NHNN is between 35 and 89 GAA repeats. In all three patients, the number of GAA repeats in each allele is over the threshold and thus pathological for FRDA. However, although individuals affected with FRDA commonly have GAA expansion sizes between 600 and 900 GAA repeats (Campuzano et al., 1996; Entezam et

al., 2017; Epplen et al., 1997), the number of GAA repeats is lower for the GAA1 allele of each of the three patients. Patient 3 has a GAA expansion size that is very close to the upper threshold for the non-pathological intermediate zone in FRDA: 100 GAA repeats in each allele. Patient 1 has 170 repeats in GAA1 and 550 repeats in GAA2, respectively. Such a small amount of GAA repeats indicates a likely late-onset, very slowly progressive disease course, particularly in patient 3. Patient 2, on the other hand, has two divergent pathological GAA expansions of 420 and around 2000 GAA repeats (for the larger amounts, it becomes difficult to set an exact measurement based on the gel reading). Although the GAA1 allele is still well below the usual amount of 600-900 GAA repeats in FRDA patients, the larger size of the GAA2 allele indicates a potential earlier age at onset and faster course of disease compared to patient 1 and patient 3, respectively. The allele sizes of all three patients indicate late-onset atypical FRDA with its accompanying phenotype of slower progression and more variable symptoms, where patients usually have between 100 and 500 repeats in the GAA1 allele (Bhidayasiri et al., 2005; Durr et al., 1996; Schols et al., 1997). Furthermore, for patient 3, the number of GAA repeats is indistinguishable in each allele, as shown by the presence of only a single band on the gel indicating pathological GAA expansion, and no corresponding control band (Fig. 10). There is an extremely small chance that this patient could be compound heterozygous for a single pathological GAA expansion and a large deletion, although this has never been discovered in a FRDA patient. Nevertheless, it is standard laboratory procedure to assume the far more likely scenario that this single band comprises the DNA from two pathological GAA expansions, and not screen this patient for exonic deletions. These first conclusions drawn from the genetic data are placed in the context of clinical data in Section 3.3, where a full genotype-phenotype correlation is performed on the three FRDA-positive patients discovered in this study.

Of the other 17 cases that tested positive at the triplet-primed PCR stage and were subsequently tested by long range PCR, a further 12 cases were shown to have a pathological GAA repeat expansion in only one allele, while

in the other 5, no result was attainable using this process due most likely to DNA degradation (Fig. 10). These samples were thus referred for further testing for compound heterozygosity status by searching for possible *FXN* point mutations and exonic deletions. If only one expansion is found in an individual with ataxic symptoms, the DNA is first put through sequence analysis to test for pathological point mutations. The samples were sent off for external sequence analysis at Royal Liverpool University Hospital and all returned negative for any of the relevant FRDA point mutations.

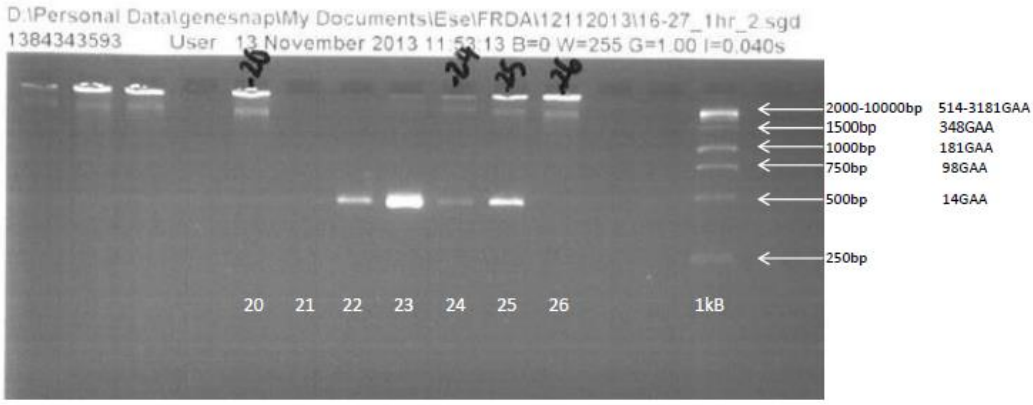


**Figure 9: Long-range FXN PCR Example Photo.**

Lane 20 = FRDA patient. Lane 21 = no DNA control. Lanes 22/23 = Negative (GAA-/-) controls. Lanes 24/25 = Carriers (GAA+/-). Lane 26 = Positive control (GAA+/+). 1kb size ladder (Promega, Madison, WI, USA) with equivalent GAA sizes. To calculate the number of GAA repeats, the required formula was allele size = (number of base pairs-457)/3. The reasoning behind this calculation is that the synthesised PCR products contain flanking sequences totalling 457 base pairs in addition to the GAA trinucleotide repeat expansion. Normal alleles run at approximately 500 base pairs, whereas affected alleles run at approximately 720 base pairs or above. *Gel courtesy of Dr Robyn Labrum and Dr Ese Mudanohwo, also used in M. H. Parkinson thesis.*

**A**

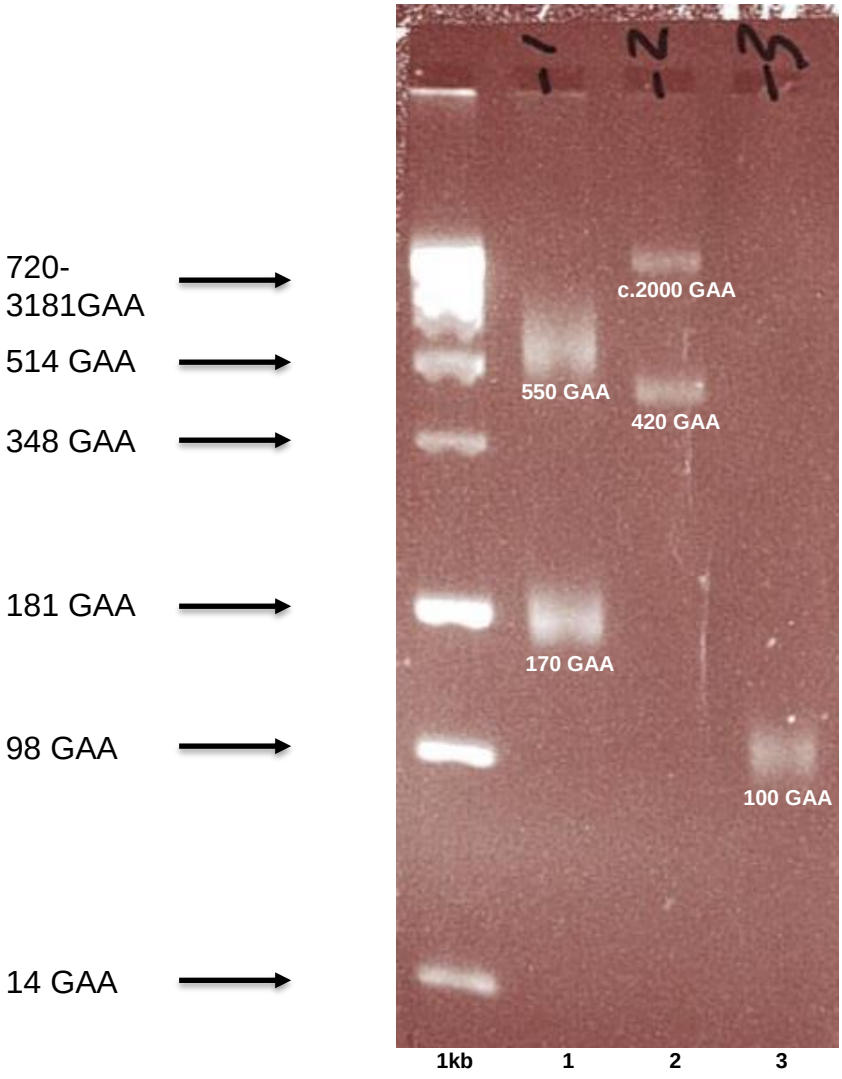
720-
3181GAA
514 GAA
348 GAA
181 GAA
98 GAA
14 GAA
1
2
3
c.2000 GAA
550 GAA
420 GAA
170 GAA
100 GAA
1kb
1
2
3

**B**

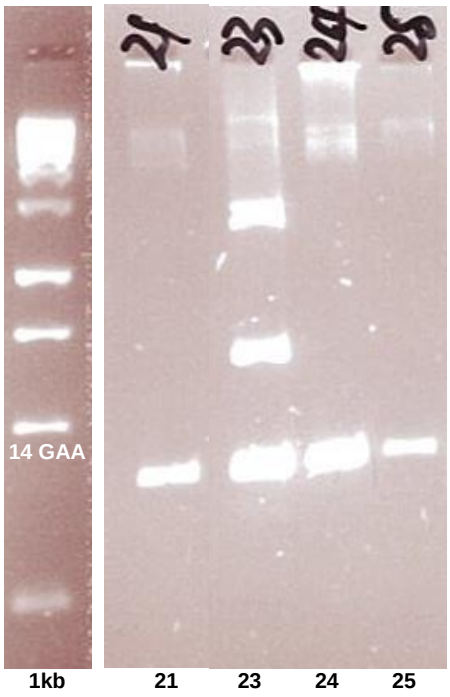


**C**

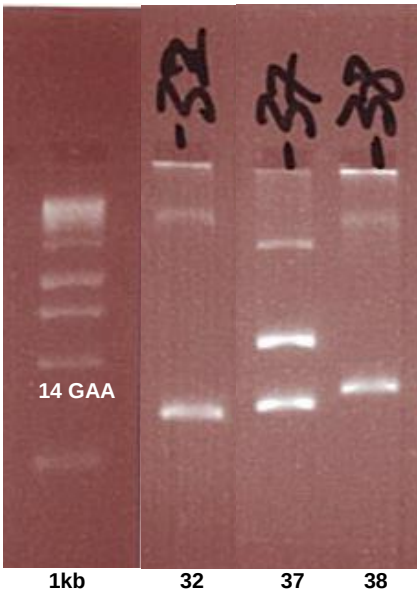

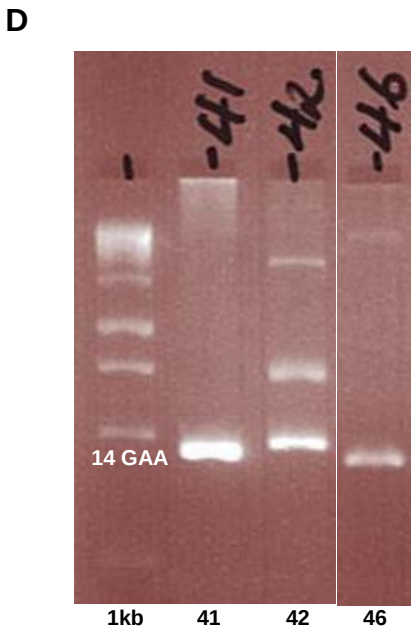


**Figure 10. Long Range PCR: FRDA Positive and Carrier Data.**

**A**) The FRDA-positive data for patients 1, 2 and 3 obtained by Long-range PCR, visualized on a 2% agarose gel following electrophoresis, with GAA sizes indicated. **B**), **C**), **D**) 10 of the 12 FRDA carriers displayed in lanes 21, 23, 24, 25, 32, 37, 38, 41, 42 and 46. 1kb size ladder (Promega, Madison, WI, USA) with equivalent GAA sizes was used.

### 3.2.2 MLPA Testing

The multiplex ligation-dependent probe amplification (MLPA) process measures gene dosage and allows identification of FRDA patients incorporating large deletions in the *FXN* gene (Deutsch et al., 2010). As well as the 12 patients to be screened, a negative control used by the NHNN laboratory was used that was clinically confirmed as lacking pathological GAA expansions and thus being FRDA-negative. The MLPA GeneMapper software uses this negative control to calculate an 'Exon Dosage Quotient' (EDQ) score for the disease exons by creating peaks based on the patient sample and control sample exon size, and then comparing the ratio (Fig. 11

& Fig. 12). A non-DNA containing control containing TE buffer was also included to test for contamination by extraneous DNA of any of the reactions during the experiment. The MLPA reaction 'failed' for the TE control, indicating no contamination of the MLPA reaction reagents. In the MLPA results, an EDQ of 1±0.25 shows no evidence of exon deletion or duplication in any of the five exons that the MLPA reaction is designed to study. A result of 0.5±0.25 shows heterozygous deletion, while a result of 0±0.25 shows homozygous deletion. Conversely, a result of 1.5±0.25 shows heterozygous duplication, and a result of 2±0.25 shows homozygous duplication. In theory an exon triplication could also occur, but this has never yet been observed in any FRDA patient.

For all 12 GAA+/- cases discovered by the previous two-stage PCR process, the EDQ score for exons 1 to 5 were all within the 1±0.25 range, indicating that exon deletion or duplication at each of the probe sites was absent (Table 9). Using GAA+/- patient 8 as an example, Figure 11 shows the signal intensity of peaks for each of the probes for this patient in blue and for the negative control in red for comparison, with the five *FXN* exon probes labelled. The ratio of blue to red peaks generates the EDQ. As can be observed, they are all of approximately equal height, and so the EDQ ratios are all in the 0.75-1.25 range. Figure 12 shows the EDQs for GAA+/- patient 8 with the disease probes in green and the reference probes in blue, and the five *FXN* exon probes again labelled. All the values can be clearly seen to be within the 0.75 to 1.25 'normal' range, indicating the absence of exonic deletions or duplications in the *FXN* gene.

As none of the 12 GAA+/- individuals were positive for any point mutations or exonic deletions in the *FXN* gene, they were confirmed as FRDA carriers. The carrier rate was calculated at 0.6%, or 1 in 167, in the full cohort. A large variation has previously been seen in carrier frequency, with which the carrier frequency of this study is broadly compatible (Cossee et al., 1997; Epplen et al., 1997; Filla et al., 1992; Harding & Zilkha, 1981; Romeo et al., 1983). Finally, the other 5 cases remaining that also tested positive at the triplet-primed PCR stage showed no result after either gel or capillary

electrophoresis at the long-range PCR stage, due to probable degraded or low-quality DNA.

**Table 9: FXN Exon Dosage Quotients (EDQ) for 12 GAA+/- samples and controls.**

| Sam-ple | Pre-test status | EDQ Exon 1 | EDQ Exon 2 | EDQ Exon 3 | EDQ Exon 4 | EDQ Exon 5 |
|---|---|---|---|---|---|---|
| **1** | GAA +/- | 0.954 | 0.998 | 0.996 | 0.882 | 1.067 |
| **2** | GAA +/- | 0.897 | 1.093 | 0.943 | 1.051 | 0.969 |
| **3** | GAA +/- | 0.998 | 0.919 | 1.057 | 1.164 | 0.920 |
| **4** | GAA +/- | 1.013 | 1.000 | 1.024 | 0.975 | 1.047 |
| **5** | GAA +/- | 1.057 | 0.997 | 0.967 | 0.864 | 1.008 |
| **6** | GAA +/- | 0.923 | 1.085 | 1.052 | 1.073 | 1.027 |
| **7** | GAA +/- | 0.885 | 0.995 | 0.964 | 0.998 | 1.017 |
| **8** | GAA +/- | 0.981 | 0.984 | 1.015 | 0.909 | 1.068 |
| **9** | GAA +/- | 0.967 | 0.982 | 0.937 | 1.027 | 1.014 |
| **10** | GAA +/- | 1.103 | 1.010 | 0.943 | 0.820 | 1.001 |
| **11** | GAA +/- | 1.150 | 1.053 | 0.968 | 0.924 | 0.962 |
| **12** | GAA +/- | 1.251 | 1.121 | 1.029 | 1.130 | 0.933 |
| **13** | GAA -/- | 1.000 | 1.000 | 1.000 | 1.000 | 1.000 |
| **14** | TE control | - | - | - | - | - |
| **15** | GAA +/+ | 1.108 | 1.086 | 1.004 | 0.893 | 0.985 |
| **16** | GAA +/+ | 1.162 | 1.113 | 1.174 | 1.138 | 0.968 |
| **17** | GAA +/+ | 0.908 | 1.087 | 1.062 | 1.126 | 1.051 |
| **Mean± SD** | All GAA +/- | 1.006± 0.093 | 1.020± 0.060 | 0.991± 0.045 | 0.985± 0.108 | 1.003± 0.046 |
| **Range** | | 0.885-1.150 | 0.919-1.121 | 0.937-1.057 | 0.820-1.164 | 0.920-1.068 |
| **Mean± SD** | All values | 1.015± 0.095 | 1.033± 0.060 | 1.008± 0.062 | 0.998± 0.108 | 1.002± 0.042 |
| **Range** | | 0.992-1.151 | 0.919-1.121 | 0.937-1.174 | 0.820-1.164 | 0.920-1.068 |

GAA +/- one GAA expansion (symptomatic carrier)
GAA -/- no GAA expansions (negative control)
GAA +/+ two GAA expansions (known FRDA patient reported as having two identically sized expansions)
TE=Tris-EDTA buffer (no DNA control)
SD=standard deviation

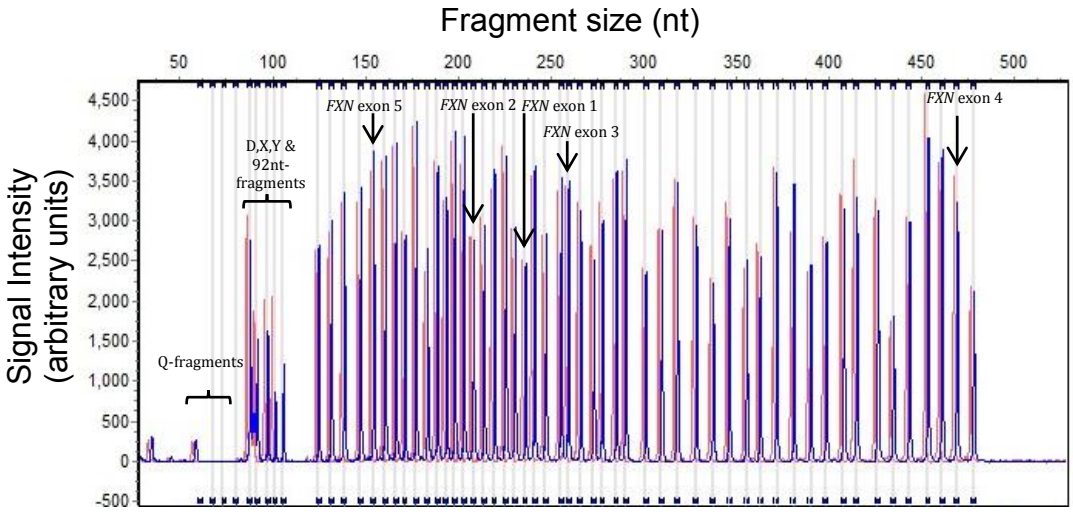


**Figure 11: Peak height comparison chart for patient 8.**

Chart generated by GeneMarker software. Blue peaks = patient samples; red peaks = control samples. 64-82 peaks=Q-fragments; 88-105 peaks=D,X,Y & 92bt control fragments; 128-481 peaks=*FXN, SETX, APTX* & 9 control genes including *FXN* peaks at 154, 208, 234, 258 & 472. The ratio of the red peaks:blue peaks was used to calculate the peak ratios (EDQ) in Figure 10.

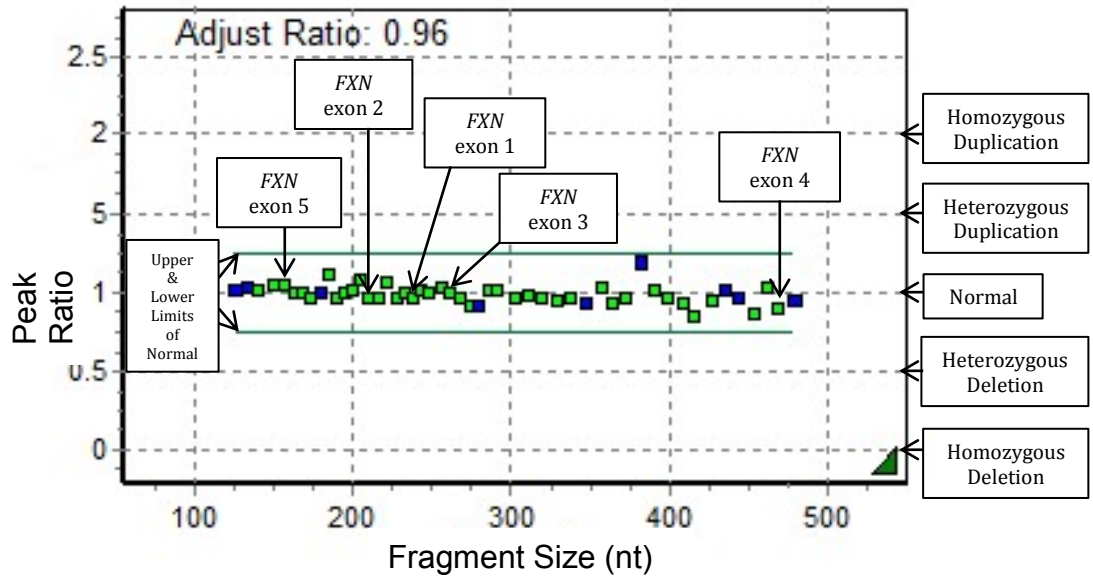


**Figure 12: Peak ratios (EDQ) for patient 8.**

Chart generated by GeneMarker software. Peak ratio (EDQ) for disease (green) and reference (blue) probes. The five *FXN* gene probes are highlighted (154, 208, 234, 258 & 472nt). The remainder are for *SETX* and *APTX*. All values are within the upper and lower limits of normal, indicating no evidence for deletions or duplications of any *FXN* exon.

**Table 10: General summary of FRDA-positive cases from ataxic patient screening study.**

| Patient no. | Age at Onset | Expansion size, allele 1 | Expansion size, allele 2 | Symptoms summary |
|---|---|---|---|---|
| 1 | 50 | 170 | 550 | Cerebellar ataxia, very slowly progressive gait and truncal ataxia, mild dysarthria, impaired balance |
| 2 | 25 | 420 | 2000 | Progressive gait ataxia, impaired balance, paresthesias in hands and feet, areflexia, reduced vibration and joint position sense, mild dysarthria, blackouts |
| 3 | 55 | 100 | 100 | Progressive gait ataxia, brisk lower limb reflexes, extensor plantars, dysarthria, reduced vibration sense |

### 3.2.3 Clinical Features

Three patients out of the cohort of 2000 patients screened were confirmed through the two-stage PCR process as being positive for FRDA via the most common homozygous recessive genotype. A further twelve were confirmed via additional point mutation and exonic deletion testing as having a FRDA carrier status (Fig. 13). The clinical features of all FRDA-positive patients that have been derived from available medical notes and clinic letters are summarised in Table 10 and detailed more fully in Table 11 and Table 12 respectively. The mean±SD age at onset for the three patients was 43.3±16.1 (range 25 to 55). The incompleteness of patient data for all three patients does not allow for a complete clinical description, but there are many interesting clinical findings that provide an understanding of the reason for the original misdiagnoses.

#### *Very Late-onset Patient 1: Intrafamilial Variability*

Patient 1, a right-handed male, had a very slowly progressive gait and truncal ataxia, with mild dysarthria and retained reflexes. He swayed to either side and was positive for the Romberg test. However, his fine motor functions were still intact, and he had no numbness, weakness, or

impairment of the visual, auditory or any other neurological system. His records showed no reports of any non-neurological symptoms or wheelchair use. Thus, his symptoms were almost exclusively cerebellar in nature, unlike the usual FRDA combination of cerebellar and sensory ataxia. There was no family medical history of note, with one fascinating exception. It is speculated in patient 1's clinical notes that his elder brother had been tentatively diagnosed with multiple sclerosis in his mid-20s. Over the next 10 to 15 years his brother's fine motor function deteriorated, and he was eventually confined to a wheelchair. Over another 15 years, his ability to move deteriorated further, and he died in his 60s. He was not excessively rigid, nor did he have dysarthria or any significant problems with any neurological systems. The FRDA diagnosis of patient 1 greatly increases the probability that his brother is also a FRDA case, given also the slowly progressive nature of his disease and the lack of any previous family history. However, a potential FRDA re-diagnosis is unfortunately not possible as DNA is not available from the brother. If the brother was to be retrospectively interpreted as FRDA-positive, the intrafamilial variability of age at onset of 25 years would indicate instability of the FRDA expansion mutation and great intrafamilial clinical heterogeneity in FRDA.

### *Patient 2: Borderline LOFA case*

Patient 2, a right-handed female patient, was referred for a progressive neuropathy at age 27. The patient's predominantly insidious symptoms had onset in her early 20s and had worsened from age 25. In addition, her past medical history was positive for blackouts from age 17. On referral she had a wide-based ataxic gait, impairment of balance, mild dysarthria and gradually progressive numbness and paresthesia in her hands and feet. However, she had normal eye movement and cranial nerves on examination. Her Romberg's test was positive, and she had areflexia, reduced joint position sense in her knees and elbows and bilateral finger-nose incoordination. She was confined to a wheelchair in her early 30s. Although the comparatively earlier onset points to a genetic cause of neuropathy, she had no significant past medical family history of note: only

one maternal uncle was diagnosed with multiple sclerosis in his 20s and died at 31. A sural nerve biopsy was carried out that showed no clear evidence of inflammatory change in the nerve itself. Thus, the relatively mild sensory deficit was thought to be not severe enough to cause her ataxia. Her MRI scan was normal. Thus, the patient showed progressive sensory neuropathy and a mix of sensory and cerebellar ataxia.

### *Very Late-onset Patient 3: A Clinical Conundrum*

Patient 3, a male, presented with late onset cerebellar ataxia at 55 years of age. He had progressive balance problems, slurred speech, incoordination and dysphagia. As he was a heavy drinker, regularly consuming up to 100 units of alcohol a week for 30 years of his life, it was suggested that his cerebellar syndrome was all alcohol-related, and undeniably his alcohol intake will have contributed to his condition. However, on cutting his alcohol intake drastically, his physical signs continued to progress gradually with age, which can occur in alcoholic cerebellar degeneration but may also imply possible alternative explanations for his disease. He had high blood pressure and pleural calcification on chest radiograph. On examination he presented with cerebellar dysarthria, nystagmus, finger-nose and heel-shin ataxia and an ataxic broad-based gait. He had pyramidal signs and reduced vibration sense in the legs, as well as brisk lower limb reflexes and upgoing plantars. His power and reflexes were otherwise normal, and his records showed no reports of any non-neurological symptoms or wheelchair use.

## 3.2.4 Comparison of Clinical Data

Two of the three FRDA positive cases had VLOFA, with ages of onset of 55 (Patient 3) and 50 (Patient 1) respectively. Neither patient showed any ancestral history of ataxia, indicative of a recessive condition. The results from the long-range PCR for the two VLOFA patients indicate the GAA1 expansion sizes in both alleles were extremely close to the mimimum diagnostic threshold for FRDA (Patient 1, 170 GAA repeats; Patient 3, 100

GAA repeats), which may well account for the extremely late onset of disease in the two patients (Table 10). Both male, they presented with gait ataxia, as is common in both classical and late-onset FRDA (Bhidayasiri et al., 2005; Gellera et al., 1997). As expected, they had an extremely slow disease progression and showed symptoms of mild dysarthria. Overall, patient 3 showed the less benign phenotype of the two patients, presenting with pyramidal signs and reduced vibration sense in the legs, upgoing plantars and nystagmus, which were all either absent or unreported in patient 1. Both showed an absence of several symptoms expected in FRDA, such as all the non-neurological symptoms, pes cavus and sensory neuropathy. Although subtle sensory neuropathy is usually present in VLOFA (Berciano et al., 2005; Lhatoo et al., 2001), it may not have been picked up clinically due to misdiagnosis. Spastic tetraparesis is often observed in VLOFA (Berciano et al., 2002; Labauge, 2002; Lhatoo et al., 2001), but patient 3 shows brisk reflexes only in the lower limbs, while in patient 1 even the fine motor functions are still intact. Surprisingly, the symptoms of patient 1 indicate a pure cerebellar ataxia rather than the typical mix of cerebellar and sensory ataxia in FRDA, which may go some way to explain the misdiagnosis of this patient. Patient 3 has symptoms which may appear more indicative of FRDA at first glance, but his original diagnosis of pure alcohol-induced ataxia due to his lifestyle, although partially correct, was evidently responsible for his FRDA not being diagnosed for many years.

In the case of patient 2, a threshold LOFA patient with onset in her early to mid-twenties, the long-range PCR gave *FXN* GAA expansion sizes of around 420 repeats in the smaller allele and somewhere between 1500-2500 repeats in the larger allele. This would increase the probability of a more severe phenotype and an earlier age of onset, as is indeed the case in the results. As the smaller GAA1 allele accounts for 62.9% of age at onset variation and the larger GAA2 allele accounts for 15.6% of the variation in LOFA patients (Lecocq et al., 2016), the expanded allele of 420 GAA repeats is probably more relevant phenotypically than the allele with the larger pathological expansion. This patient displayed areflexia and reduced

joint position sense in knees and elbows, unlike the two VLOFA patients, and was confined to a wheelchair in her early 30s. Her presenting symptom was also a progressive neuropathy accompanied by blackouts, although it was later concluded that her sensory deficit was too mild to be the cause of her ataxia. This patient conforms to a general LOFA milder phenotype with more variable symptoms, and it is possible that the unusual presenting features for FRDA including the blackouts may have initially misled clinicians.

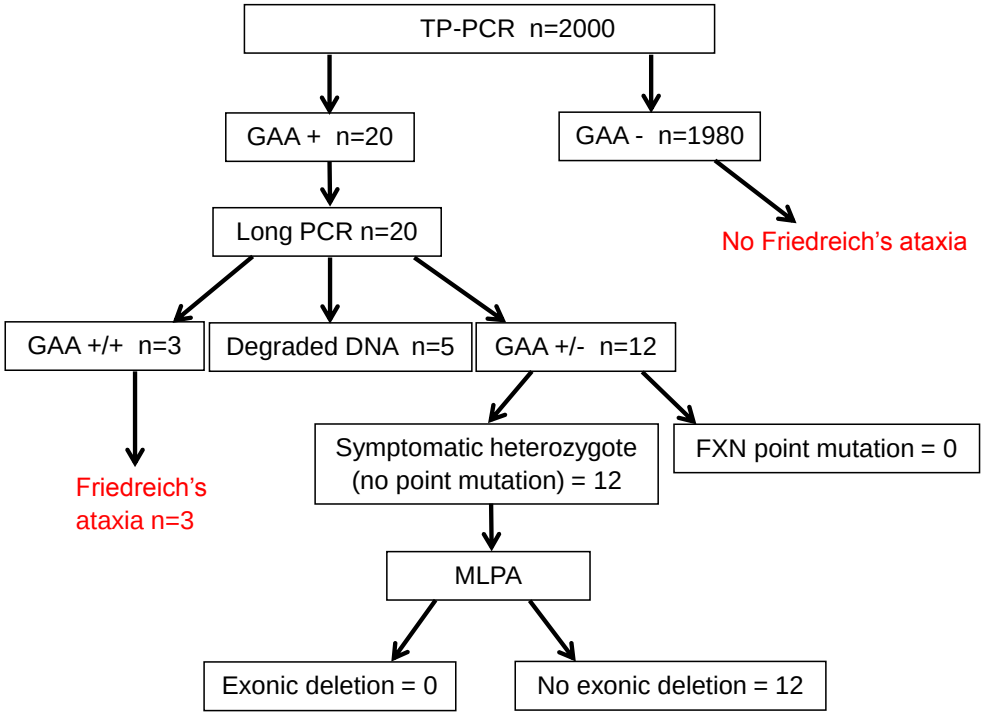


**Figure 13: Flowchart summary of genetic results in 2000-patient two-stage PCR study.**

GAA+/+ two GAA expansions; GAA+/- one GAA expansion; GAA-/- no GAA expansions. MLPA = multiplex ligand-dependent probe amplification.

### 3.2.5 FRDA Carrier Clinical Details

Clinical details were obtained for 9 out of 12 FRDA carriers, who were all originally referred for idiopathic ataxia. As none of these patients were compound heterozygous for an FRDA point mutation or exonic deletion, they are not FRDA-positive or expected to have FRDA-like symptoms (Andermann et al., 1976; Harding, 1981). I provide their clinical details for the purpose of comparing their phenotype with the FRDA-positive patients,

and better understanding the potential clinical difficulty in diagnosis and selecting which patients to refer for FRDA testing among the thousands of patients referred with ataxic symptoms to diagnostic clinics in the UK.

Patient 1, a female, had eye movement disorder and dizziness, triggered by a virus. Her age of onset for these symptoms was 32.

Patient 2, a female, developed a cerebellar syndrome with some episodic features and severe nystagmus after she had suffered renal failure during an acute illness at age 50. She also had a mild gait ataxia, although her eye movement abnormality was more severe than her ataxia. It was uncertain whether her episodic ataxia had a progressive course. It is also unknown whether her renal symptoms could have had a neurological basis.

Patient 3, a female, presented with severe dysphagia. She experienced falls beginning at age 65, and her very late onset ataxia was slowly progressive. Her symptoms included a cerebellar atrophy consistent with progressive supra-nuclear palsy, dysarthria, extended neck, visual hallucinations, horizontal nystagmus and bradykinesia.

Patient 4, a left-handed male, had spastic paraplegia, possibly hereditary. His mother had a progressive gait disturbance.

Patient 5, a male, had a progressive alteration in sensation in both feet from age 48. His hands also became less sensitive in making fine movements, and he was diagnosed with a painful sensory neuropathy of uncertain cause. Following further analysis, he was diagnosed with small fibre neuropathy, with possible corticospinal tract features. He had non-sustained left horizontal nystagmus, but brisk reflexes and a lack of cerebellar ataxia. He also had a slowly progressive dysfunction of thermal perception. He had no family history of neurological disease.

Patient 6, a male, had partial epilepsy and secondary generalisation cerebral and cerebellar atrophy. He experienced his first seizure age 19, and thereafter suffered from complex partial and secondary generalised

seizures, at the rate of around 15 per year. He had an ataxic, broad-based gait.

Patient 7, a female, was diagnosed at age 25 with oscillopsia and finger-nose ataxia. She veered to the right when walking and had the sensation of vertigo on awakening. At age 50, she was diagnosed with temporomandibular joint disturbance, nystagmus, bilateral extensor plantar responses, dizzy spells, poor balance, severe depression, mild cerebellar signs on examination, and increasingly poor vision. It was felt likely that the patient had demyelination of the vertebral column, commonly the first episode in multiple sclerosis. This patient was indeed later diagnosed with multiple sclerosis.

Patient 8, a female, presented with impaired mobility and became wheelchair bound. This patient was later diagnosed with multiple sclerosis.

Patient 9, a left-handed female, developed seizures from age 2, consisting of absence-like attacks of a few seconds. Her conditioned worsened, and at 19 she had cryptogenic partial epilepsy as well as learning disability. Her epilepsy involved complex partial seizures, secondary generalised tonic-clonic seizures and regular daily absences. Her EEG displayed epileptiform activity.

## Table 11: Clinical features of FRDA-positive cases from ataxic patient screening study, Part 1.

Y = Yes; N = No; N/R = No Result; UL = Upper Limb; LL = Lower Limb

| Patient no. | Symptom at onset | Ataxia | Tone | Pyramidal weakness | UL weakness | LL weakness | Small hand muscle weakness | UL areflexia | LL areflexia | Extensor plantar response | Touch sensation loss | Vibration/position al loss | Dysarthria | Dysphagia |
|---|---|---|---|---|---|---|---|---|---|---|---|---|---|---|
| 1 | Poor balance | Y | Normal | Y | N | Y | N | N | N | Y | N | Y | Y | N/R |
| 2 | Swaying to either side | Y | Normal | N | N | N | N | N | N | N/R | N | N | Y | N/R |
| 3 | Progressive neuropathy, blackouts | Y | N/R | N/R | N | N | N/R | Y | Y | N/R | Y | Y | Y | N/R |

## Table 12: Clinical features of FRDA-positive cases from ataxic patient screening study, Part 2.

| Patient no. | Polyneuropathy | Trunkal ataxia (gait, stance, sitting) | Limb ataxia (dysmetria, intentional tremor) | Nystagmus | Square Wave Jerks | Optic atrophy | Hearing Loss | Scolioisis | Foot abnormalities | Diabetes | Cardiomyopathy | Echocardiogram | ECG | Bladder | Bowel |
|---|---|---|---|---|---|---|---|---|---|---|---|---|---|---|---|
| 1 | N/R | Y | Y | Y | N | N | N/R | N/R | N/R | N | N/R | N/A | N/A | N/R | N/R |
| 2 | N | Y | N/R | N | N | N | N | N/R | N/R | N | N/R | N/A | N/A | N/R | N/R |
| 3 | Y | Y | Y | N | N | N | N/R | N/R | N/R | N | N/R | N/A | N/A | N/R | N/R |

### 3.2.6 Comparison to FRDA-referred Cohort Study*

* *I thank Dr Michael Parkinson for gathering the genetic data from patients referred for FRDA, and Dr Hector Garcia and Ms Katarina Manso for gathering the comparative clinical data on patients from this cohort.*

The data gathered in this study were compared to a previously gathered cohort of 1768 genetically undiagnosed ataxia patients who, contrary to the 2000 I tested, had already been referred for a FRDA test (M. Parkinson, unpublished data). These 1768 patients underwent a genetic screening for FRDA at the NHNN between 2003 and 2013. 196 cases (11.1%) were shown to have homozygous pathological GAA expansions within the *FXN* gene and were therefore classified as FRDA-positive. Of the 40 which were found to carry a single pathological expansion, 11 were found to have pathological point mutations associated with FRDA after sequencing, increasing the number confirmed as FRDA-positive to 207 (11.7%).

This proportion of FRDA-positive cases is, as expected, far higher than in my study, as patients referred for FRDA are more likely to have typical symptoms of the disease. Among the other 29 cases, inspection of clinical records revealed that 9 were asymptomatic carriers, most likely referred for predictive clinical testing or partner testing in order to inform reproductive choices. The other 20 cases were symptomatic carriers, and thus subjected to an MLPA test in order to determine whether any cases were compound heterozygous for an exonic deletion. 18 were not positive for exonic deletions, while there was no DNA available for the other two patients. Thus, 29 patients of the cohort were confirmed after the appropriate genetic tests

to be FRDA carriers, a carrier rate of 1.6%. This is considerably higher than the carrier rate in my study, although both are within the normal range based on previous studies (Cossee et al., 1997; Epplen et al., 1997; Filla et al., 1992; Harding & Zilkha, 1981; Romeo et al., 1983). Figure 14 details the flowchart for these 1768 patients and the diagnostic pathway through which FRDA patients and carriers are identified by the NHNN Neurogenetics department. Figure 15 gives the combined flowchart for my own study and the M. H. Parkinson study, and Figure 16 shows the respective proportions of FRDA positives and carriers discovered in my study and in M.H. Parkinson's study in pie chart form.

The clinical features for 106 of the 207 FRDA-positive cases from this cohort are given in full in Tables 13-16. These were derived in 80 cases from the EFACTS assessment (Tables 13-14), whereas in another 26 cases, information was derived from the available or traceable medical notes and clinic letters (Tables 15-16). In general, the 80 EFACTS patients are more completely clinically characterized than the other 26, although it was also not always possible to obtain the entirety of FRDA-relevant clinical data from each patient even in the EFACTS cohort. Although the number of FRDA positives in my study is too few to make a meaningful statistical analysis with the clinical data from the referred samples in the M.H. Parkinson study, there does still appear to be a trend to toward increased disease severity and a more 'classical FRDA' phenotype with the samples referred for FRDA. The mean±SD age at onset for the 103 referred patients for which data was available was 14.3±10.5 (range 1 to 51), corresponding to the typical age at onset of FRDA. This was significantly younger than the mean±SD age at onset for the 3 FRDA positive patients from my study, which was 43.3±16.1 (range 25 to 55) and indicative of LOFA/VLOFA.

The proportion of patients from the samples referred for FRDA with the presence of certain key clinical characteristics for which data were available were catalogued in Table 17. Almost all of these patients for whom data is available present with areflexia (96.2%), vibrational sensory loss (99%) and dysarthria (92.4%). All three FRDA-positive patients not originally referred

for FRDA also had dysarthria, which is very common even in LOFA/VLOFA patients. However, only 1 in 3 showed any signs of areflexia and 2 in 3 showed vibrational sensory loss, indicative of the less severe phenotype and greater variability of symptoms in delayed-onset FRDA. Similarly, although 81.6% of patients from the Parkinson study had symptoms of square wave jerks and 57.3% showed signs of nystagmus, the only eye movement deficits reported among the FRDA positives in my study was nystagmus in 1 patient out of 3. Similarly, paresis and extensor plantars were observed in the lower limbs of only 1 in 3 patients from my study, but in 88.7% and 73.8% of patients in the Parkinson study, respectively.

There was also no mention of any non-neurological signs in the 3 FRDA-positive patients from my study, whereas 56.7% of FRDA-positive patients in the other study had cardiomyopathy and 9.5% had diabetes. Only one patient in my study became wheelchair-bound, compared to 67.9% of those in the other study. Overall, the three FRDA-positive cases not originally referred for FRDA display had a significantly later age of onset and an overall less severe ataxia phenotype than the cohort of 106 FRDA-positive cases that were clinically referred for an FRDA test and for which clinical data were available. The small size of the GAA1 expansions in the three FRDA-positive patients from my study is most likely the cause of the later age at onset and the less severe phenotype. The implications of the data from both studies will be considered together in the discussion.

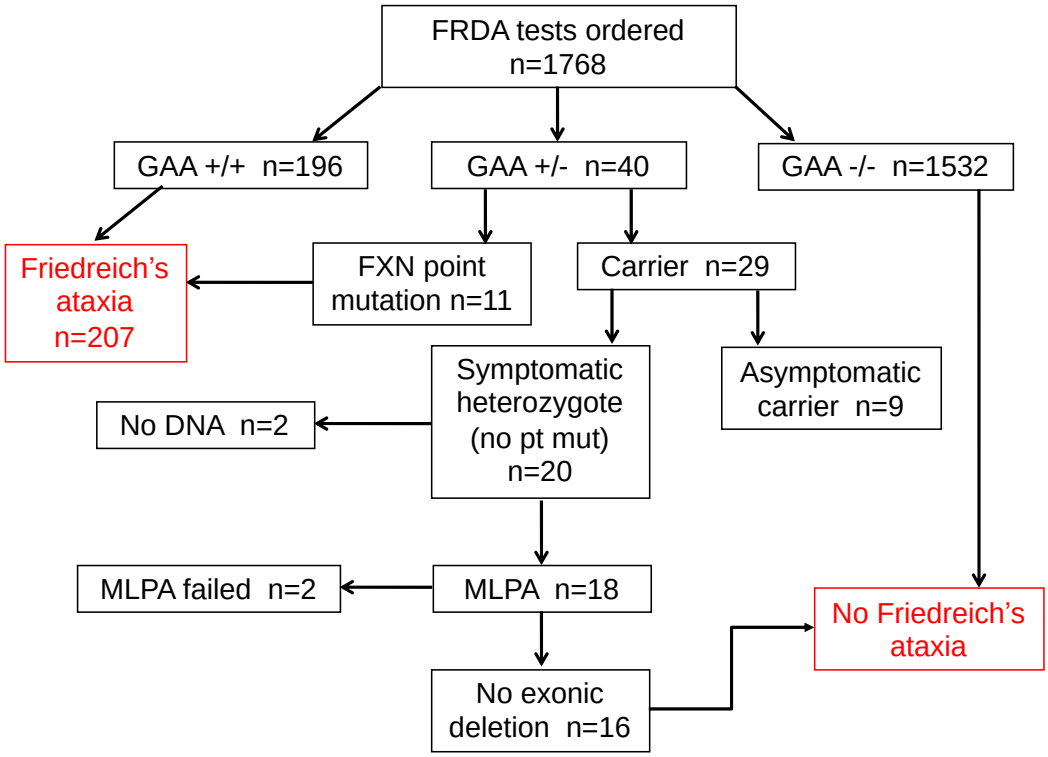


**Figure 14: Flowchart summary of genetic results in M.H. Parkinson study.**

GAA+/+ two GAA expansions; GAA+/- one GAA expansion; GAA-/- no GAA expansions. MLPA = multiplex ligand-dependent probe amplification. With thanks to Dr M.H. Parkinson for the figure.

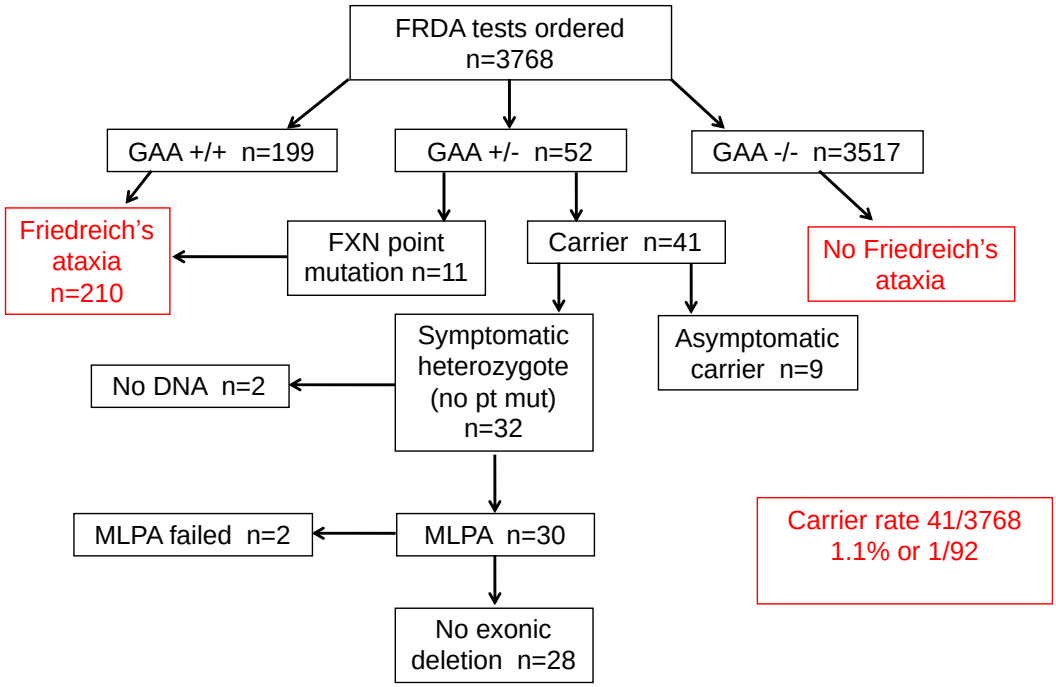


**Figure 15: Flowchart summary of genetic results in both 2000-patient two-stage PCR study and M. H. Parkinson study combined.**

GAA+/+ two GAA expansions; GAA+/- one GAA expansion; GAA-/- no GAA expansions. MLPA = multiplex ligand-dependent probe amplification.

A

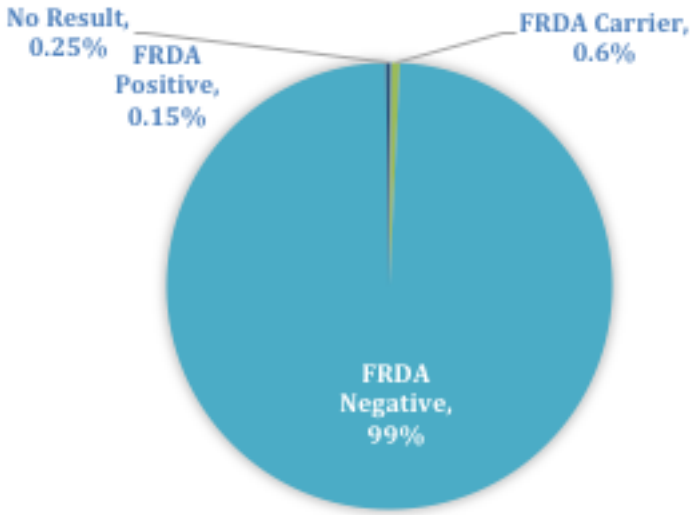


B

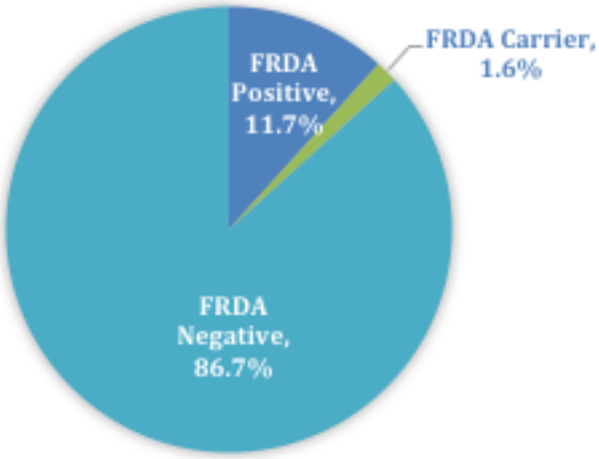


**Figure 16: Proportion of FRDA positives, carriers, no result and negatives among screened cohorts of A) ataxia patients not referred for FRDA, and B) ataxia patients referred for FRDA (M.H. Parkinson).**

**Table 13: Clinical features of EFACTS FRDA patients from M.H. Parkinson study, Part 1.**

| Patient no. | Symptom at onset | Ataxia | Tone | Pyramidal weakness | UL weakness | LL weakness | Small hand muscle weakness | UL areflexia | LL areflexia | Extensor plantar response | Touch sensation loss | Vibration/positional loss | Dysarthria | Dysphagia |
|---|---|---|---|---|---|---|---|---|---|---|---|---|---|---|
| **1** | Unsteadiness (unable to ice skate) | Y | Increased | N | N | Y | N | Y | Y | Y | N | Y | Y | Y |
| **2** | Unsteadiness, clumsiness | Y | Increased | N | Y | Y | Y | Y | Y | Y | Y | Y | Y | Y |
| **3** | Unsteadiness (extreme reaction to alcohol) | Y | Normal | N | N | Y | Y | Y | Y | Y | Y | Y | Y | Y |
| **4** | Hand tremors, leg pains | Y | Increased | N | Y | Y | Y | Y | Y | N | N/R | Y | Y | Y |
| **5** | Unsteadiness, falls | Y | Normal | Y | Y | Y | Y | Y | Y | Y | Y | Y | Y | Y |
| **6** | Unsteadiness, clumsiness | Y | Decreased | Y | Y | Y | Y | Y | Y | N | N | Y | Y | Y |
| **7** | Unsteadiness | Y | Normal | Y | Y | Y | Y | Y | Y | Y | N | Y | Y | Y |
| **8** | Unsteadiness, altered sensation in both legs, scoliosis | Y | Normal | N | Y | Y | Y | Y | Y | Y | Y | Y | Y | N |
| **9** | Unsteadiness | Y | Increased | N | Y | Y | Y | Y | Y | Y | N | Y | Y | Y |
| **10** | Unsteadiness | Y | Normal | N | Y | Y | Y | Y | Y | N | Y | Y | Y | Y |
| **11** | Unsteadiness | Y | Normal | N | Y | Y | Y | Y | Y | N | N/R | Y | Y | Y |
| **12** | Shaky hands, poor handwriting, falls | Y | Increased | Y | Y | Y | Y | Y | Y | Y | Y | Y | Y | Y |
| **13** | Scoliosis. Unsteadiness | Y | Normal | Y | N | Y | Y | Y | Y | Y | Y | Y | Y | Y |
| **14** | Falls | Y | Increased | Y | Y | Y | Y | Y | Y | Y | Y | Y | Y | Y |

| | | | | | | | | | | | | | | |
|---|---|---|---|---|---|---|---|---|---|---|---|---|---|---|
| **15** | Unsteadiness | Y | Normal | Y | N | Y | N | Y | Y | Y | Y | Y | Y | Y |
| **16** | Unsteadiness | Y | Increased | N | Y | Y | Y | Y | Y | Y | N | Y | Y | Y |
| **17** | Clumsiness (in playing football and guitar) | Y | Increased | Y | N | Y | N | Y | Y | Y | Y | Y | Y | Y |
| **18** | Unsteadiness, falls | Y | Increased | Y | Y | Y | Y | Y | Y | N | Y | Y | Y | Y |
| **19** | Unsteadiness | Y | Normal | N | Y | Y | Y | Y | Y | Y | Y | Y | Y | Y |
| **20** | Clumsiness (bumping into things) | Y | Increased | Y | N | Y | N | Y | Y | Y | Y | Y | Y | Y |
| **21** | Unsteadiness | Y | Increased | N | N | Y | N | N | N | Y | N | Y | Y | Y |
| **22** | Unsteadiness, falls | Y | Increased | N | Y | Y | Y | Y | Y | Y | N | Y | Y | Y |
| **23** | Unsteadiness, clumsiness | Y | Increased | Y | N | Y | N | N | N | Y | N | Y | Y | Y |
| **24** | Unsteadiness | Y | Increased | Y | N | Y | N | Y | Y | Y | N | Y | Y | N |
| **25** | Unsteadiness (especially with gymnastics) | Y | Increased | Y | Y | Y | Y | Y | Y | Y | Y | Y | Y | Y |
| **26** | Unsteadiness | Y | Normal | N | Y | Y | Y | Y | Y | Y | N | Y | Y | Y |
| **27** | Unsteadiness | Y | Increased | N | Y | Y | Y | Y | Y | N | Y | Y | Y | N |
| **28** | Unsteadiness, dysarthria | Y | Increased | N | N | Y | N | Y | Y | Y | N | Y | Y | Y |
| **29** | Scoliosis | Y | Increased | Y | N | Y | N | Y | Y | Y | Y | Y | Y | N |
| **30** | Unsteadiness | Y | Increased | N | Y | Y | Y | Y | Y | N | Y | Y | Y | Y |
| **31** | Unsteadiness | Y | Normal | Y | N | Y | N | Y | Y | Y | Y | Y | Y | N |
| **32** | Unsteadiness, falls | Y | Increased | N/R | Y | Y | Y | Y | Y | Y | N/R | N/R | Y | N |
| **33** | Unsteadiness | Y | Normal | N/R | N | Y | N | Y | Y | N | N/R | N/R | Y | N |
| **34** | Unsteadiness | Y | Normal | N | Y | Y | Y | Y | Y | N | Y | Y | Y | Y |
| **35** | Falls, clumsiness with handwriting | Y | Normal | N | N | N | N | Y | Y | N | N | Y | N | N |
| **36** | Scoliosis | Y | Increased | Y | N | Y | N | Y | Y | N | Y | Y | Y | Y |
| **37** | Unsteadiness | Y | Increased | Y | Y | N | Y | Y | N | Y | N | Y | Y | Y |
| **38** | Unsteadiness | Y | Normal | Y | N | Y | N | Y | Y | Y | N | Y | Y | Y |
| **39** | Unsteadiness | Y | Increased | N | Y | Y | Y | Y | Y | Y | Y | Y | Y | Y |

| | | | | | | | | | | | | | | |
|---|---|---|---|---|---|---|---|---|---|---|---|---|---|---|
| **40** | Unsteadiness | Y | Normal | Y | Y | Y | Y | Y | Y | Y | N | Y | Y | Y |
| **41** | Unsteadiness | Y | Increased | N | N | Y | N | Y | Y | Y | Y | Y | Y | Y |
| **42** | Unsteadiness, falls | Y | Normal | N | Y | Y | Y | Y | Y | Y | Y | Y | Y | Y |
| **43** | Falls | Y | Increased | N | N | Y | N | Y | Y | Y | N | Y | N | Y |
| **44** | Unsteadiness | Y | Normal | N | Y | Y | Y | Y | Y | Y | Y | Y | Y | Y |
| **45** | Unsteadiness. Fatigue on prolongued walking | Y | Increased | Y | N | Y | N | Y | Y | Y | Y | Y | Y | Y |
| **46** | Unsteadiness | Y | Normal | N | Y | Y | Y | Y | Y | Y | N | Y | Y | N |
| **47** | Unsteadiness | Y | Normal | Y | Y | Y | Y | Y | Y | N | Y | Y | Y | Y |
| **48** | Unsteadiness, falls | Y | Increased | N | N | Y | N | Y | Y | Y | N | Y | Y | Y |
| **49** | Clumsiness | Y | Increased | N | Y | Y | Y | Y | Y | N | Y | Y | Y | Y |
| **50** | Scoliosis. Unsteadiness | Y | Increased | Y | Y | Y | Y | Y | Y | Y | Y | Y | Y | Y |
| **51** | Unsteadiness | Y | Increased | Y | Y | Y | Y | Y | Y | Y | Y | Y | Y | Y |
| **52** | Unsteadiness | Y | Normal | N | N | N | N | Y | Y | Y | Y | Y | N | N |
| **53** | Unsteadiness | Y | Normal | N | Y | Y | Y | Y | Y | Y | N/R | Y | Y | Y |
| **54** | Unsteadiness | Y | Normal | N | N | Y | N | Y | Y | Y | Y | Y | N | Y |
| **55** | Unsteadiness | Y | Increased | N | Y | Y | Y | Y | Y | N | Y | Y | Y | Y |
| **56** | Unsteadiness | Y | Increased | N | Y | Y | Y | Y | Y | N | N/R | Y | Y | Y |
| **57** | Unsteadiness | Y | Increased | N | Y | Y | Y | Y | Y | Y | Y | Y | Y | Y |
| **58** | Unsteadiness. Cardiomyopathy | Y | Increased | N | Y | Y | Y | Y | Y | Y | Y | Y | Y | Y |
| **59** | Clumsiness | Y | Normal | N | N | N | N | Y | Y | Y | Y | Y | N | Y |
| **60** | Scoliosis | Y | Increased | N | Y | Y | Y | Y | Y | Y | Y | Y | N | Y |
| **61** | Unsteadiness | Y | Increased | Y | Y | Y | Y | Y | Y | Y | N | Y | Y | Y |
| **62** | Unsteadiness | Y | Normal | N | N | Y | N | Y | Y | Y | Y | Y | Y | Y |
| **63** | Cardiomyopathy | Y | Normal | N | Y | Y | Y | Y | Y | Y | Y | Y | Y | Y |
| **64** | Unsteadiness | Y | Normal | N/R | Y | Y | Y | Y | Y | N | N/R | Y | Y | Y |

| | | | | | | | | | | | | | | |
|---|---|---|---|---|---|---|---|---|---|---|---|---|---|---|
| **65** | Unsteadiness, falls | Y | Increased | N | Y | Y | Y | Y | N | N | N | Y | Y | N |
| **66** | Falls | Y | Increased | N | Y | Y | Y | Y | Y | Y | N/R | Y | Y | Y |
| **67** | Unsteadiness | Y | Normal | N/R | N | Y | N | Y | Y | N | N/R | Y | Y | Y |
| **68** | Clumsiness | Y | Increased | N | Y | N | N | Y | N | Y | N | Y | Y | N |
| **69** | Scoliosis | Y | Normal | N | Y | Y | Y | Y | Y | Y | Y | Y | Y | N |
| **70** | Unsteadiness | Y | Increased | N | N | N | N | N | N | N | N/R | Y | Y | Y |
| **71** | Clumsiness | Y | Normal | N | Y | Y | Y | Y | Y | Y | Y | Y | N | N |
| **72** | Unsteadiness | Y | Increased | N | N | N | N | Y | Y | Y | N/R | Y | Y | N |
| **73** | Unsteadiness | Y | Increased | N | Y | Y | Y | Y | Y | Y | N | Y | Y | N |
| **74** | Falls | Y | Normal | N/R | N | N | N | Y | Y | Y | N/R | Y | Y | Y |
| **75** | Unsteadiness. Falls | Y | Normal | N | N | N | N | Y | Y | N | N | Y | Y | N |
| **76** | Falls | Y | Increased | Y | Y | Y | Y | Y | Y | Y | N/R | Y | Y | N |
| **77** | Unsteadiness | Y | Normal | N | N | N | N | N/R | N/R | N/R | N/R | N/R | Y | N |
| **78** | Unsteadiness | Y | Normal | N | N | N | N | Y | Y | N | N/R | Y | N | N |
| **79** | Unsteadiness | Y | Increased | N | Y | Y | Y | Y | Y | Y | N/R | Y | Y | Y |
| **80** | Unsteadiness | Y | Increased | N | Y | Y | Y | Y | Y | Y | Y | Y | Y | Y |

N.B. With thanks to Ms **Katarina Manso** and Dr **Hector Garcia** for the phenotypic data gathered on all the FRDA-positive patients from the Parkinson study in Tables 13-16.

**Table 14: Clinical Features of EFACTS FRDA Patients from M. H. Parkinson Study, Part 2.**

| Patient no. | Polyneuropathy | Trunkal ataxia | Limb ataxia | Nystagmus | Square Wave Jerks | Optic atrophy | Hearing Loss | Scolioisis | Foot abnormalities | Diabetes | Cardiomyopathy | Echocardiogram | ECG | Bladder | Bowel |
|---|---|---|---|---|---|---|---|---|---|---|---|---|---|---|---|
| **1** | N | Y | Y | N | Y | N | N | Y | PC | N | Y (Palpitations) | Normal | LVH, T inverted in inferolateral leads | Y | N |
| **2** | Y | Y | Y | N | Y | Y | Y | Y | TE | N | Y (Ventricular tachycardia, AF, ICD) | Hypertrophy, small left ventricular cavity with normal wall thickness with longitudinal dysfunction | Inferolateral T wave changes | Y | Y |
| **3** | Y | Y | Y | N | Y | N | Y | N | N | N | Y | Normal LV size and function, mild diastolic dysfunction, mildly dilated LA size | T wave inversion I, II, aVF, V3-V6 | Y | N |
| **4** | N | Y | Y | N | Y | N/R | Y | Y | TE | N | Y | Mild concentric hypertrophy | LVH | Y | N |
| **5** | Y | Y | Y | Y | Y | N/R | Y | Y | PC | N | Y | Mild hypertrophic cardiomyopathy | Dyspnoea | Y | Y |
| **6** | N | Y | Y | Y | Y | N | Y | Y | N | N | Y (Vasovagal syncope) | Hypertrophic cardiomyopathy | LVH | N | Y |
| **7** | N | Y | Y | Y | Y | N | N | Y | N | N | Y | Concentric LVH, mild diastolic dysfunction | T wave inversion II, III, aVF, V5, V6), dyspnoea | N | N |
| **8** | Y | Y | Y | Y | Y | N | N | Y | PC | N | N | Normal | Repolarization abnormalities, LVH | N | N |

| | | | | | | | | | | | | | | | |
|---|---|---|---|---|---|---|---|---|---|---|---|---|---|---|---|
| **9** | N | Y | Y | Y | Y | N | Y | Y | PC | N | Y (Paroxysmal AF) | Mild concentric LVH | T wave inversions in leads V3-V6, I, II, III, aVL, aVF | Y | N |
| **10** | Y | Y | Y | Y | Y | Y | Y | Y | PC | N | Y (AF, ICD) | Moderately dilated LV and RV, severe systolic dysfunction | Abnormal (ventricular paced rhythm, tachycardia). | Y | N |
| **11** | N | Y | Y | N | Y | Y | Y | Y | N | N | Y | LV moderate concentric hypertrophy, low-normal systolic function | T wave inversion in the inferolateral leads, incomplete RBBB | Y | Y |
| **12** | Y | Y | Y | Y | Y | Y | Y | Y | PC | N | N | Normal | Normal | N | Y |
| **13** | Y | Y | Y | Y | Y | N/R | N | Y | PC | N | N | Normal | Normal | Y | Y |
| **14** | Y | Y | Y | Y | Y | Y | N | Y | PC & TE | N | Y | LVH | Widespread T-wave inversion (I-III, aVF, V1-V6) | Y | N |
| **15** | Y | Y | Y | Y | Y | N | Y | N | PC | N | N | N/R | N/R | N | N |
| **16** | N | Y | Y | Y | Y | N | N | Y | PC & TE | N | Y | Concentric LVH | Repolarization abnormalities | Y | Y |
| **17** | Y | Y | Y | N | Y | N | N | N | PC & TE | N | N | Normal | T wave inversion in I, II, aVL, V4-V6 | N | Y |
| **18** | Y | Y | Y | Y | Y | N | Y | Y | PC | N | Y (AF) | Mild concentric hypertrophy | T wave inversion all leads, right axis deviation | Y | N |
| **19** | Y | Y | Y | Y | Y | N | Y | Y | PC | Y | Y (AF) | Left ventricular hypertrophy with severely impaired systolic function, severe tricuspid regurgitation | T wave inversions in the precordial leads, right axis deviation | Y | N |
| **20** | Y | Y | Y | Y | Y | Y | Y | Y | PC | N | N | Normal | Lateral T wave changes | Y | Y |
| **21** | N | Y | Y | Y | Y | N | N | Y | PC | N | N | Normal | Normal | Y | N |
| **22** | N | Y | Y | Y | Y | N | N | Y | PC | N | Y | N/R | N/R | N | N |
| **23** | N | Y | Y | Y | Y | N | N | N | N | N | N | Normal | Repolarization abnormalities | Y | N |
| **24** | N | Y | Y | Y | Y | N | N | N | N | N | N | Normal | T wave inversion in I, II, aVL, V5, V6, LV hypertrophy | Y | N |
| **25** | Y | Y | Y | Y | Y | N | Y | Y | PC & TE | N | Y | Mild hypertrophic cardiomyopathy | N/R | Y | N |
| **26** | N | Y | Y | Y | Y | N | Y | Y | TE | N | N | Normal | Normal | Y | N |
| **27** | Y | Y | Y | Y | Y | Y | Y | Y | PC | N | N | N/R | N/R | Y | N |
| **28** | N | Y | Y | N | Y | N | N | Y | N | N | Y | Hypertrophic cardiomyopathy | Repolarization abnormalities | Y | N |

| | | | | | | | | | | | | | | | |
|---|---|---|---|---|---|---|---|---|---|---|---|---|---|---|---|
| **29** | Y | Y | Y | Y | Y | N | Y | Y | PC | N | Y | Mild concentric LVH | Negative T waves in the inferior and the lateral leads | N | N |
| **30** | Y | Y | Y | Y | N | Y | Y | Y | PC | N | Y | N/R | T wave inversion in II, III, aVF, V6 | N | N |
| **31** | Y | Y | Y | Y | Y | N | N | N | N | N | N | N/R | N/R | N | N |
| **32** | N/R | Y | Y | N | Y | N | N | Y | PC | N | Y | N/R | N/R | N | N |
| **33** | N/R | Y | Y | N | Y | N | N | Y | N | N | N | N/R | N/R | N | N |
| **34** | Y | Y | Y | Y | Y | N | Y | N | PC | N | N | Normal | Flattened T waves | N | N |
| **35** | N | Y | Y | Y | Y | N | N | N | N | N | Y (AF, Myocardial ischaemia) | Hypertrophic cardiomyopathy | T wave inversion | N | N |
| **36** | Y | Y | Y | Y | Y | N | N | Y | PC | N | Y | Mild septal hypertrophy | T wave inversion in inferolateral leads | Y | N |
| **37** | N | Y | Y | N | Y | N | N | Y | N | N | N | Normal | Normal | Y | N |
| **38** | N | Y | Y | N | Y | N | N | N | N | N | N | Normal | Normal | Y | N |
| **39** | Y | Y | Y | N | Y | N | N | Y | N | N | N | N/R | T wave inversion I, aVL, V3-V6 | Y | N |
| **40** | N | Y | Y | N | Y | Y | N | N | N | N | Y | LVH | Non-specific T wave flattening inferolaterally | Y | N |
| **41** | Y | Y | Y | N | Y | N | N | Y | PC | N | Y | Mild concentric LV hypertrophy | T wave inversion in I, II, aVL, V5, V6 | N | N |
| **42** | Y | Y | Y | N | Y | N | Y | Y | PC | N | Y (intermittent atrial tachyarrhythmia) | Hypertrophic cardiomyopathy | Repolarization abnormalities, Hypertrophy | Y | N |
| **43** | N | Y | Y | Y | Y | N | N | Y | PC | N | N | Normal | Normal | Y | N |
| **44** | Y | Y | Y | N | Y | N | Y | Y | PC | N | Y | LVH | N/R | N | N |
| **45** | Y | Y | Y | N | Y | N | N | Y | N | N | Y | Mild concentric LVH | Normal | Y | N |
| **46** | N | Y | Y | N | Y | N | N | Y | PC | N | N | Normal | Normal | N | N |
| **47** | Y | Y | Y | Y | Y | N | Y | Y | PC | N | Y | Hypokinetic basal postero-inferior wall, left atrial size mildly dilated | Inferolateral T wave inversion, Inferioposterior Q-waves | Y | N |
| **48** | N | Y | Y | N | Y | N | N | Y | PC | N | Y (Permanent AF) | Dilated LV/RV with severe systolic dysfunction, thinning of basal, posterior and inferior wall | AF, T-wave inversion | Y | N |
| **49** | Y | Y | Y | Y | Y | Y | Y | Y | PC | N | N | Normal | T negative wave V4-V6 | Y | N |

| | | | | | | | | | | | | | | | |
|---|---|---|---|---|---|---|---|---|---|---|---|---|---|---|---|
| **50** | Y | Y | Y | Y | Y | N | N | Y | PC | N | Y | N/R | N/R | Y | Y |
| **51** | Y | Y | Y | Y | Y | N | N | Y | N | N | N | Normal | Non-specific T wave flattening | Y | N |
| **52** | Y | Y | Y | N | N | N | N | N | N | Y | N | N/R | N/R | N | N |
| **53** | N | Y | Y | Y | N | N | Y | Y | PC | N | Y | Ventricular hypertrophy | N/R | Y | N |
| **54** | Y | Y | Y | Y | Y | N | Y | N | N | N | N | Normal | Normal | Y | N |
| **55** | Y | Y | Y | Y | Y | Y | Y | N | PC | N | N | Normal | Flat T wave in lateral leads | Y | N |
| **56** | N | Y | Y | Y | Y | N/R | Y | Y | PC | N | Y (Paroxysmal AF) | Normal | Repolarization abnormalities | Y | N |
| **57** | Y | Y | Y | N | Y | Y | N | Y | PC | N | Y (Paroxysmal AF) | Mild LVH | Negative T waves in the anterolateral leads | Y | N |
| **58** | Y | Y | Y | Y | Y | Y | Y | Y | PC | Y | Y (Previous myomectomy, AF) | Hypertrophic Cardiomyopathy, Hypokinetic lateral wall | Q waves V1-V3 | Y | N |
| **59** | Y | Y | Y | N | N | N | N | N | N | N | Y | Mild LVH | Repolarization abnormalities | N | N |
| **60** | Y | Y | Y | N | Y | N | N | Y | PC | Y | Y (Paroxysmal AF) | Mild hypertrophy | T wave inversion in II, III, aVF, V3-V6 | Y | N |
| **61** | N | Y | Y | Y | N | N | Y | N | PC | N | N | Normal | T wave inversion in leads II, III, aVF, V3-V6 | Y | N |
| **62** | Y | Y | Y | N | Y | N | N | N | N | N | N | Normal | Repolarization changes | N | N |
| **63** | Y | Y | Y | N | Y | N | Y | Y | PC | N | N | Normal | N/R | N | N |
| **64** | N/R | Y | Y | Y | Y | N | N | Y | PC | N | Y | Mild concentric LVH, moderate mid-ventricular obstruction, Mid/apical LV cavity obliteration | Negative T waves I, II, III, aVF, V4-V6 | N | N |
| **65** | N | Y | Y | Y | N | N | N | N | N | N | Y | N/A | Hypertrophy | N | N |
| **66** | N/R | Y | Y | N | Y | N | Y | N | N | N | Y | LV basal septal hypertrophy | Slow R wave progression, T-wave abnormalities | Y | N |
| **67** | N/R | Y | Y | N | Y | N | N | Y | N | Y | N | Normal | Normal | Y | N |
| **68** | N | Y | Y | Y | Y | N | Y | Y | PC | N | Y | LVH | Repolarization abnormalities, hypertrophy | N | N |
| **69** | Y | Y | Y | N | Y | N | Y | Y | PC | N | N | N/R | N/R | N | N |
| **70** | N/R | Y | Y | N | N | N | N | N | N | N | N | Normal | Mild repolarization abnormalities | Y | N |

| | | | | | | | | | | | | | | | |
|---|---|---|---|---|---|---|---|---|---|---|---|---|---|---|---|
| **71** | Y | Y | Y | N | N | N | N | N | PC | N | N | Normal | Normal | N | N |
| **72** | N/R | Y | Y | N | Y | N | N | Y | N | N | N | N/R | N/R | Y | N |
| **73** | N | Y | Y | N | Y | Y | N | Y | PC | N | Y (Supraventricular tachycardia) | Apical hypertrophy | Small inverted T waves laterally | Y | N |
| **74** | N/R | Y | Y | N/A | N/A | Y | Y | Y | N | N | Y (Paroxysmal AF) | Impaired LV systolic function | LVH | N | N |
| **75** | N | Y | Y | Y | Y | N | N | N | N | N | N | N | T wave inversion V3-V6 | Y | N |
| **76** | N/R | Y | Y | N | Y | N | N | Y | PC | Y | Y (Intracardiac thrombus) | N/R | N/R | Y | N |
| **77** | N/R | Y | Y | N | N | N | N | Y | PC | N | N | N/R | N/R | N | N |
| **78** | N/R | Y | Y | N | Y | N | N | N | N | N | N | Normal | N/R | N | N |
| **79** | N/R | Y | Y | N | Y | N | N | Y | PC | N | Y | Normal | Inverted T wave laterally | Y | N |
| **80** | Y | Y | Y | Y | Y | N | Y | Y | PC | N | Y | Mild concentric LVH | T wave inversion in most of the leads | N | N |

N/A = Not Applicable; LVH = Left Ventricular Hypertrophy; PC = Pes Cavus; TE = Talipes Equinovarus; AF = Atrial Fibrillation; ICD = Implantable Cardioverter Defibrillator; LV/RV = Left/Right Ventricular; LA/RA = Left/Right Atrial; aVL/aVR = Augmented Vector Left/Right; RBBB = Right Bundle Branch Block; V1-V6 = Types of Electrodes in ECG

**Table 15: Clinical features of non-EFACTS FRDA patients from M.H. Parkinson study, Part 1.**

| Patient no. | Symptom at onset | Ataxia | Tone | Pyramidal weakness | UL weakness | LL weakness | Small hand muscle weakness | UL areflexia | LL areflexia | Extensor plantar response | Touch sensation loss | Vibration/positional loss | Dysarthria | Dysphagia |
|---|---|---|---|---|---|---|---|---|---|---|---|---|---|---|
| 1 | Clumsiness, poor balance | Y | N/R | N/R | Y | Y | N/R | Y | Y | Y | N/R | N/R | Y | N |
| 2 | Poor coordination, unsteadiness | Y | N/R | Y | N/R | Y | N/R | Y | Y | Y | N/R | Y | Y | N/R |
| 3 | Unsteadiness | Y | Increased | N/R | Y | Y | N/R | Y | Y | Y | N/R | Y | Y | Y |
| 4 | Falls, unsteadiness | Y | Normal | N/R | Y | Y | Y | Y | Y | Y | N | Y | Y | N |
| 5 | Unsteadiness, clumsiness | Y | Normal | Y | N | Y | N | Y | Y | N | N | N | Y | N |
| 6 | Unsteadiness, incoordination UL | Y | Increased | Y | Y | Y | Y | Y | Y | Y | Y | Y | Y | Y |
| 7 | Unsteadiness | Y | Increased | Y | N | Y | N | Y | Y | Y | Y | Y | Y | N |
| 8 | Unsteadiness | Y | Normal | N | Y | N | Y | Y | Y | N | N | Y | Y | N/R |
| 9 | Clumsiness of both arms | Y | Normal | Y | Y | Y | Y | Y | Y | Y | Y | Y | Y | Y |
| 10 | Clumsiness | Y | N/R | N | N | N | N | Y | Y | Y | N/R | N/R | Y | N |
| 11 | Unsteadiness | Y | Normal | N | Y | Y | Y | Y | Y | N | Y | Y | Y | Y |
| 12 | Unsteadiness, clumsiness | Y | Increased | N | Y | Y | Y | Y | Y | Y | Y | Y | Y | Y |
| 13 | Unsteadiness | Y | Decreased | N | N | N | N | N | Y | N | N | Y | Y | Y |
| 14 | Unsteadiness, clumsiness | Y | N/R | Y | Y | Y | N | Y | Y | Y | N | Y | Y | N |
| 15 | Clumsiness | Y | N/R | Y | N | Y | N/R | Y | Y | Y | Y | Y | Y | Y |

| | | | | | | | | | | | | | | |
|---|---|---|---|---|---|---|---|---|---|---|---|---|---|---|
| 16 | Unsteadiness | Y | N/R | N | Y | Y | Y | Y | Y | N | N/R | Y | Y | Y |
| 17 | Clumsiness, repeated falls | Y | Increased | N | Y | Y | Y | Y | Y | Y | Y | Y | Y | Y |
| 18 | Unsteadiness | Y | Normal | Y | N | Y | N | N | N | Y | Y | Y | Y | Y |
| 19 | Unsteadiness, falls | Y | Normal | N | Y | Y | Y | Y | Y | Y | Y | Y | Y | Y |
| 20 | Unsteadiness | Y | Increased | Y | Y | Y | Y | Y | Y | Y | Y | Y | Y | Y |
| 21 | Unsteadiness, fatigue | Y | Normal | Y | Y | Y | Y | Y | Y | Y | Y | Y | Y | Y |
| 22 | Unsteadiness | Y | Normal | N | N | N | N | Y | Y | Y | Y | Y | Y | Y |
| 23 | Unsteadiness | Y | N/R | Y | N | Y | N | Y | Y | N | N/R | N/R | N/R | N/R |
| 24 | Unsteadiness | Y | Increased | Y | Y | Y | Y | Y | Y | Y | N/R | Y | Y | N |
| 25 | N/R | Y | N/R | N | Y | Y | Y | N/R | N/R | N/R | N/R | N/R | Y | N/R |
| 26 | N/R | Y | Normal | N | N | Y | N | N | Y | N/R | Y | Y | Y | N |

**Table 16: Clinical features of non-EFACTS FRDA patients from M.H. Parkinson study, Part 2.**

| Patient no. | Polyneuropathy | Trunkal ataxia | Limb ataxia | Nystagmus | Square Wave Jerks | Optic atrophy | Hearing Loss | Scolioisis | Foot abnormalities | Diabetes | Cardiomyopathy | Echocardiogram | ECG | Bladder | Bowel |
|---|---|---|---|---|---|---|---|---|---|---|---|---|---|---|---|
| 1 | N/R | N/A | N/R | N/R | N/R | Y | Y | Y | Y | N | Y (Congestive failure, AF) | N/A | N/A | Y | Y |
| 2 | N/R | Y | Y | Y | Y | N/R | N/R | Y | N/R | N | Y (Biventricular hypertrophy, AF) | N/A | N/A | N/R | N/R |

| | | | | | | | | | | | | | | | |
|---|---|---|---|---|---|---|---|---|---|---|---|---|---|---|---|
| 3 | N | Y | Y | N | Y | Y | N/R | Y | Y | Y | Y (Dilated myocardiopathy, AF) | Wall thinning | N/A | Y | N |
| 4 | N | Y | Y | N | Y | N | N/R | N/R | N/R | N | N/R | N/A | Axonal sensory neuropathy | Y | N |
| 5 | N | Y | Y | N | N | N | N/R | Y | N/R | N | Y | LV thickening | N/A | N/R | N/R |
| 6 | Y | Y | Y | N | N | Y | Y | Y | Y | Y | N | N/A | Sensory neuropathy | Y | N/R |
| 7 | Y | Y | Y | N | N | N | N | N | N | N | N | Normal | Symmetrical sensory axonal neuropathy | Y | Y |
| 8 | Y | Y | Y | N | N | N | N/R | N/R | N/R | N | N | N/A | Sensory neuropathy | N/R | N/R |
| 9 | Y | Y | Y | Y | Y | N | N | N/R | N/R | N | Y (Palpitations) | LVH | Sensory axonal neuropathy | Y | N |
| 10 | N/R | Y | Y | N | N | N | N/R | N/R | N | N | Y | N/R | N/A | N/R | N/R |
| 11 | Y | Y | Y | Y | Y | N/R | N | Y | N | N | Y (Faint episodes x3) | LVH, mild diastolic dysfunction | N/A | N | N |
| 12 | Y | Y | Y | Y | N | Y | N | Y | N | Y | Y (Recurrent chest pain) | LVH, apex wall thickening | Sensory neuropathy | Y | N |
| 13 | N | Y | Y | Y | Y | N | N | N | N | N | N | N/A | Sensory/motor axonal neuropathy | Y | N |
| 14 | N | Y | Y | N | N | Y | Y | Y | N/R | N | N | N/A | N/A | N | N |
| 15 | Y | Y | Y | Y | Y | Y | N/R | Y | N/R | N | Y (Palpitations) | Mild hypertrophic cardiomyopathy | N/A | Y | Y |
| 16 | N | Y | Y | Y | N | N | Y | Y | N | Y | N | N/A | N/A | N | Y |
| 17 | Y | Y | Y | Y | Y | N | N/R | N/R | N/R | N/R | N | N/A | Sensory axonal neuropathy (absent radial and sural SAN) | Y | N |
| 18 | Y | Y | Y | Y | Y | N | N | Y | N | N | Y (Dyspnoea) | N/R | N/A | Y | N |
| 19 | Y | Y | Y | Y | Y | N/R | N | Y | Y | N | Y (Palpitations) | Mild concentric LVH | N/A | Y | N |
| 20 | Y | Y | Y | Y | Y | N/R | N | Y | N | N | Y (Dyspnoea) | Normal | N/A | Y | N |
| 21 | Y | Y | Y | Y | Y | Y | N | Y | Y | N | N | N/R | N/A | Y | Y |
| 22 | Y | Y | Y | Y | N | N | N | Y | N/R | N | N | Normal | N/A | Y | N |
| 23 | N/R | Y | N/R | N/R | N/R | N | N | Y | N/R | N | Y | Mild, asymmetric septal hypertrophy morphology | N/A | N/R | Y |

| | | | | | | | | | | | | | | | |
|---|---|---|---|---|---|---|---|---|---|---|---|---|---|---|---|
| 24 | N | Y | Y | Y | Y | Y | Y | Y | N | N | Y | Concentric LVH with some apical non-compaction | N/A | N/R | N |
| 25 | N/R | Y | Y | Y | Y | N/R | N/R | N/R | N/R | N | N/R | N/A | N/A | N/R | N/R |
| 26 | Y | Y | Y | Y | N | N/R | N/R | N/R | N/R | N | N | Normal | N/A | N | Y |

**Table 17: Clinical Features in FRDA Patients, M. H. Parkinson Study.**

| Feature | FRDA patients | | |
|---|---|---|---|
| | No. | % | *n* |
| **Paresis** | 94 | **88.7** | 106 |
| **Spasticity** | 54 | **55.1** | 98 |
| **Areflexia** | 100 | **96.2** | 104 |
| **Extensor plantars** | 76 | **73.8** | 103 |
| **Vibrational sensory loss** | 98 | **99** | 99 |
| **Square wave jerks** | 84 | **81.6** | 103 |
| **Nystagmus** | 59 | **57.3** | 103 |
| **Diabetes** | 10 | **9.5** | 105 |
| **Cardiomyopathy** | 59 | **56.7** | 104 |
| **Dysarthria** | 97 | **92.4** | 105 |
| **Dysphagia** | 74 | **72.5** | 102 |
| **Wheelchair-bound** | 72 | **67.9** | 106 |

### 3.2.7 Results Summary

We carried out a study of a consecutive series of 2000 ataxia patients lacking a genetic basis for their symptoms following referral for all the major SCAs, and who had not been referred for an FRDA test, presumably as their symptoms were atypical for the disease. This was the largest study of its kind ever done. Out of 2000 patient DNA samples tested, only three were identified as having two pathological GAA expansions and thus as being FRDA-positive, accounting for 0.15% of our population (Fig. 13). Clinical information showed atypical phenotypes for all three FRDA-positive cases, two of which were very-late onset. The FRDA-positive results, although too few to analyse in any statistical fashion, are consistent with previous reports, which show that the size of the pathological GAA expansion is inversely correlated with age at onset and positively correlated with severity of symptoms in FRDA. The three FRDA-positive

patients display atypical symptoms, consistent with the greater variety of symptoms seen in LOFA/VLOFA.

My study also located 12 patients with the pathological GAA expansion in only one allele (Fig. 13). No point mutations and no exonic deletions were discovered among the 12 individuals with only one pathological GAA expansion. Thus, these 12 were confirmed as FRDA gene carriers, all of which were symptomatic for separate ataxic disorders. This gives a carrier rate of 0.6%, or 1/167. All available clinical information is detailed in the following results section and explored in the discussion.

This study complemented a previous one by Dr M.H. Parkinson, which collected the clinical data of 1768 undiagnosed ataxia patients who had been referred for an FRDA test (Fig. 14). Among those that had been referred, 207 (11.7%) tested positive for FRDA. The carrier rate in this population was of 1.6%, or 1 in 63, within the expected limits of carrier frequency (Cossee et al., 1997; Epplen et al., 1997; Filla et al., 1992; Harding & Zilkha, 1981; Romeo et al., 1983). 11 FRDA patients were compound heterozygotes with rare point mutations: the proportion of these among the FRDA–positive cases was 5.3%, which is above the expected amount (M.H. Parkinson, unpublished data). When combined with the previous data, this gave from a total of 3768 patients screened an FRDA positive rate of 5.6% (210/3768) and a carrier rate of 1.1% (41/3768; Fig. 15). A comparison of clinical data in these respective studies indicated that phenotypes of FRDA-positive patients who had been referred for an FRDA test by their consultants were more in line with classical FRDA than those who had not been referred (Tables 13-17).

Overall, the study indicates that although the probability that a FRDA case is missed during the consultant referral and genetic testing process is extremely low, it can occur, adding important clinical data on atypical FRDA. Despite this, in general an ataxic patient who displays symptoms atypical for FRDA is indicated by this study to be extremely unlikely to have FRDA. This therefore reinforces the current diagnostic model in which the

FRDA test is only carried out upon consultant referral, making it more evidence-based.

## 3.3 Discussion

Since the discovery of the genetic basis for FRDA in 1996, natural history studies have been performed on large cohorts of genetically confirmed FRDA patients that provide the frequencies of clinical features. These have been of vital importance in further understanding the underlying molecular pathology, planning interventional clinical trials, and providing prognostic information for the patients (Delatycki et al., 1999; Durr et al., 1996; McCabe et al., 2000; Schols et al., 1997). Some of these studies also showed that the original diagnostic criteria proposed by Geoffroy and Harding before the FRDA gene was discovered proved to be inadequate for up to a quarter of genetically diagnosed FRDA patients (Durr et al., 1996; Filla et al., 2000; Schols et al., 1997). The criteria typically excluded atypical cases presenting with very early or late onset FRDA, retained reflexes and very slow or limited disease progression (Geoffroy et al., 1976; Harding, 1981). The literature describes specific cases of atypical FRDA in its main, often overlapping forms of LOFA/VLOFA and FRDA with retained reflexes (Coppola et al., 1999; Klockgether et al., 1996; Parkinson et al., 2013; Verma & Gupta, 2012). However, no systematic study has ever been carried out on a cohort of ataxic patients to determine the frequency of FRDA cases among patients not originally referred for FRDA. This is particularly relevant clinically as atypical FRDA patients not picked up by consultants may never be diagnosed, and thus not receive the medical care appropriate to them in the present or the future.

The aim of the work described in this chapter was therefore to provide a thorough genetic and clinical assessment of atypical, late-onset FRDA

patients discovered through the largest screening to date of individuals presenting with ataxia not originally referred for FRDA by their consultants, and also compare the data with a previous study of FRDA frequency in ataxia cases who were originally referred for FRDA, which was also the largest study to date of its kind (M.H. Parkinson, unpublished data). The specific objective of the genetic assessment was to assess the frequency of FRDA among a 2000-strong consecutive series of SCA-negative ataxic patients that were not referred for a FRDA test across a 17-year period (1996-2013), presumably as they had a clinical history that did not induce clinicians to consider an FRDA screening necessary.

The rate of FRDA-positive cases in my cohort was 0.15% (Fig. 13). This indicates that although the probability that a FRDA case is missed during the consultant referral and genetic testing process is extremely low, it can occur. Despite this, it is clear that an ataxic patient who displays symptoms atypical for FRDA is evidently extremely unlikely to have FRDA. When compared to the Parkinson study, the frequency of FRDA-positives is as expected far higher among ataxic patients referred for FRDA, at 11.7% (Fig. 14). The extreme comparative paucity of FRDA cases in the diagnostic results from my genetic study indicates that a patient with FRDA tends to have a phenotype that is very consistent and diagnosable. Despite our knowledge of LOFA/VLOFA and the phenotypic variability in the disease, 50% of which is accounted for by the GAA expansion size (in particular GAA1; Filla et al., 1996), which can undergo intergenerational instability as well as somatic mosaicism (Monros et al., 1997; Pandolfo & Pastore, 2009), it appears from this study that our understanding of the clinical variability of FRDA and its atypical forms is strong enough to allow for correct diagnosis in almost all cases presenting with ataxia. These findings, alongside the expected highly atypical nature of the disease exhibited by the very few FRDA-positive patients discovered in my study, reinforce the current diagnostic model where the FRDA test is only carried out upon consultant referral. The alternative, testing all patients presenting with ataxia for FRDA, is not cost-effective or time-effective given the scarcity of FRDA-positive cases.

Furthermore, 12 GAA+/- individuals were also discovered out of the cohort of 2000 ataxic patients, none of which tested positive for compound heterozygosity point mutations or exonic deletions and thus were confirmed as FRDA carriers. In the Parkinson study, one of the largest ever performed to systematically screen a consecutive series of ataxia patients for *FXN* point mutations and exonic *FXN* deletions, the prevalence of *FXN* point mutations among FRDA patients referred for an FRDA screening has been calculated as 5.3% (11 out of 207; M.H. Parkinson, unpublished data), which is approximately the same as when the two studies are compared (11 out of 210). Comparatively, the point mutation rate per patient was 4.3% (11 out of 258) in a previous study (Campuzano et al., 1996) and 3.5% (25 out of 719) in another (Cossee et al., 1999). Thus, pathological GAA expansions are present in approximately 97-98% of chromosomes from FRDA patients studied. The absence of *FXN* point mutations discovered in the 2000-patient cohort, particularly given the eventual finding of only three positive FRDA cases, is completely consistent with previous data. This is despite the fact that atypical presentation of FRDA is sometimes accounted for by compound heterozygosity with point mutations (Parkinson et al., 2013), in particular the p. G130V mutation that leads to a late-onset, atypically mild disease phenotype (Bidichandani et al., 1997; Cossee et al., 1999; Forrest et al., 1998). Thus, despite the negative results for FRDA point mutations in this study, previous evidence supports testing for FRDA point mutations in atypical FRDA cases.

Ataxic patients have been referred to major tertiary referral centres for neurogenetics specialising in hereditary ataxia across the world for decades. However, the MLPA test for exonic deletions is only requested in very specific cases due to its perceived rarity. Compound heterozygosity with exonic deletions has been found in 11 confirmed cases, two from the USA and nine from western Europe. The majority of previous described FRDA cases with exonic deletions in the *FXN* gene have been discovered through a convergence of suspected FRDA with inconclusive genetic data

(van den Ouweland et al., 2012; Zuhlke et al., 2004). Additional findings of these mutations in FRDA patients would indicate that GAA+/- symptomatic individuals should be more regularly tested for exonic deletions. However, given the absence of FRDA-associated exonic deletions in the very large cohorts of both my study and the Parkinson study, the current understanding that compound heterozygous FRDA patients with an exonic deletion are extremely rare is retained. The results add to the bulk of evidence regarding whether testing for exonic deletions is indicated in FRDA patients. They reinforce the current diagnostic screening method for ataxia patients, where the MLPA test for exonic deletions is not offered routinely but only in cases where a single pathological GAA mutation or FRDA-associated point mutation is found in an individual who also exhibits clear clinical symptoms of FRDA.

There is an extremely small chance that FRDA patients with exonic deletions may not have been detected due to a small deletion preventing the binding of one or both of the GAA primers to the GAA repeat, or a large deletion to one of the splice sites. Ideally in future, alternative techniques to assess the exact breakpoints of a deletion should be adopted in addition to the MLPA technique, which could also be revised to provide more coverage to the larger exons 1 and 5b. However, given the complete absence of cases of exonic deletions thus far in individuals from the UK who present with compound heterozygote FRDA, and given also the more severe FRDA phenotype that usually occurs in cases of FRDA compound heterozygotes with exonic deletion (Brigatti et al., 2012; Deutsch et al., 2010), a mistake in the data is extremely unlikely, certainly among the 8 FRDA carriers for which clinical data was successfully retrieved. There is only one discovered case of FRDA with exonic deletion where the patient had an atypical mild FRDA phenotype that slowly progressed over 30 years (van den Ouweland et al., 2012), which is not enough to be able to draw any diagnostic conclusions. Frataxin protein or mRNA levels could also be measured in future to help guide further genetic testing.

The 12 FRDA carriers confirmed in my cohort gave a carrier rate of 0.6% or 1 in 167 (Fig. 13). The earlier Parkinson study to which our study is compared in this chapter has a carrier rate of 1.6% which is equivalent to 1 in 63 (M.H. Parkinson, unpublished data; Fig. 14). When combined together, these studies give an overall carrier rate of 1.1% (Fig. 15). No systematic study of FRDA carrier rate has been carried out in the UK, although Harding & Zilkha estimated it at approximately 1 in 110 (Harding & Zilkha, 1981). However, all studies produced prior to 1996 rely on clinical, not genetic diagnoses, making them potentially less accurate. Previous European studies range from a higher frequency of 1 in 85 in France (Cossee et al., 1997) and between 1 in 60 and 1 in 90 in Germany (Epplen et al., 1997), to a lower frequency of 1/191 in the Piedmont region of northern Italy (Leone et al., 1990) and 1 in 196 in the entire population of Norway (Wedding et al., 2015). A large variation can be seen in carrier frequency between studies, with which the carrier frequency of this study is broadly compatible. An interesting further study would be to update the understanding of different carrier rates among different European populations. The considerably greater carrier frequency in the Parkinson cohort compared to my cohort may be partially explained by the fact that it included 9 asymptomatic carriers who were probably referred for predictive clinical testing for potential presymptomatic FRDA, or else they were partners tested to inform reproductive choices. The present samples are not representative of the UK population as a whole, and thus cannot be considered as a full epidemiological study: however, this is the largest study of its kind carried out so far, using patient data from across the country.

The clinical features of the three FRDA-positive patients are too small a sample size to statistically analyse. However, they are consistent with the size of the pathological GAA expansion being inversely correlated with age at onset and positively correlated with severity of symptoms in FRDA (Durr et al., 1996; Filla et al., 1996; Montermini et al., 1997; Rajagopalan et al., 2010). The symptoms of especially patient 1 and patient 3 have a LOFA/VLOFA symptom characterization that conforms fully with their

extremely small GAA expansion sizes (Tables 11-12). The average age at onset of FRDA in the three patients is typical for LOFA (and tending towards VLOFA), while the average age at onset for the patients in the Parkinson study conforms fully with typical age at onset in classical FRDA (Durr et al., 1996; Filla et al., 1990; Harding, 1981; Reetz et al., 2015), meaning that considered together (Fig. 15) they have a phenotype very characteristic of classical FRDA.

The absence of non-neurological symptoms in any of the three FRDA-positive patients may be explained by these symptoms being far less common in late-onset FRDA (De Michele et al., 1996; Durr et al., 1996; Filla et al., 1996; Gellera et al., 1997). They all have dysarthria, which often presents later in LOFA cases. Its presence on disease presentation may be explained by the VLOFA status of the patients. In classical FRDA patients, dysarthria tends to exhibit prior to pyramidal weakness, which itself presents before loss of vibrational or joint position sense and muscle weakness (Harding, 1981), but the FRDA-positive patients in the 2000-patient study were clinically assessed so late that it is difficult to build a clear picture of disease progression from case notes. Indeed, the whole topic of disease progression has proved difficult to study in the three FRDA-positives and therefore its role in the Parkinson study is also not analysed in this chapter. Retrospective analyses of case histories of this kind necessarily aim for quantity of patients, as the clinical data are often not consistently and completely available.

The paucity of FRDA-positives from my cohort of 2000 ataxic patients suggests that the clinical symptoms of the FRDA-positives are likely to be extremely atypical for FRDA. The extremely small size of the GAA1 repeat expansion in patients 1 and 3 is entirely consistent with this hypothesis (Tables 11-12). Although both patients have VLOFA, the phenotype is only particularly unusual for FRDA in patient 1, who displays an even milder phenotype, lacking even the nystagmus and pyramidal signs present in patient 3 despite having a marginally larger GAA1 expansion size.

Nevertheless, there are understandable and interesting reasons for why patients 2 and 3 may not have been referred by their consultant on referral.

In the case of patient 3, it is quite clear that his very high alcohol intake is crucially responsible for creating diagnostic confusion, as well as likely worsening his ataxic symptoms. Aside from the alcohol intake, he displays symptoms fairly typical for LOFA/VLOFA such as dysarthria, nystagmus, finger-nose ataxia, gait ataxia, pyramidal signs and reduced vibration sense in the legs, whilst retaining power and reflexes and lacking any confirmed sign the non-neurological features of FRDA, meaning it is quite likely he would have been correctly diagnosed had it not been for the alcohol abuse.

In the case of patient 2, the GAA expansion sizes are smaller but still in the expected LOFA range, and the more phenotypically relevant GAA1 size (420 repeats; Lecocq et al., 2016) is considerably smaller than the GAA2 size (c. 2000 repeats). This genotype provides a slightly more severe phenotype, with a borderline classical/LOFA age at onset of around 25 (although the clinical notes indicate it may have been in her early twenties) and additional symptoms not seen in patients 1 and 2 such as areflexia and confinement to wheelchair in her early thirties. Her symptoms were not unduly atypical for FRDA/LOFA. However, her presenting symptoms of neuropathy and blackouts were highly unusual for FRDA and her sensory ataxia was not severe. Both of these findings may have hindered a correct diagnosis of FRDA. The lack of clinical distinction between LOFA and VLOFA claimed recently (Lecocq et al., 2016) cannot be appropriately studied here due to the small sample size available.

The clinical symptoms of the elder brother of patient 3, originally diagnosed as multiple sclerosis, may also be radically reinterpreted following this study. The elder brother experienced a progressive loss of motor function and confinement to a wheelchair, passing away in his 60s. Although dysarthria or specific neurological symptoms are not reported, the very benign nature and progression of the FRDA-like symptoms in his brother

increases the possibility that the original patient diagnosis of multiple sclerosis was mistaken. His lack of previous family history is characteristic of autosomal recessive disease and indicates a possible missed FRDA diagnosis, although this does not itself preclude the original multiple sclerosis diagnosis. The FRDA diagnosis of patient 3 allows us to re-interpret the clinical data in a new light in both the patient and his brother. The symptoms in both siblings are / would be unusual for FRDA. If the elder brother of patient 3 is indeed FRDA positive, this would indicate a strong intrafamilial variability in age at onset of 25 years. As the largest FRDA phenotype study to date showed an only 40% correlation between GAA expansion and severity of clinical symptoms (Reetz et al., 2015), such variability would not be inconsistent with FRDA literature. Other factors affecting FRDA phenotype might involve somatic mosaicism, expansion interruptions, intergenerational instability of the FRDA expansion (Monros et al., 1997) or other genetic and environmental elements (Pandolfo & Pastore, 2009). Further study of intrafamilial cases may shed greater light on the clinical heterogeneity of FRDA and its complex, multisystemic nature.

The Parkinson study of FRDA frequency in patients clinically referred for FRDA, unlike my study, reveals a cohort of FRDA patients with a clinical spectrum typical of classical FRDA (Tables 13-17). For example, the frequency of symptoms such as areflexia, extensor plantars, dysarthria, dysphagia and vibrational sensory loss all conform to previous large case series studies carried out on FRDA patients (Delatycki et al., 1999; Harding, 1981). Square wave jerks are found more frequently than nystagmus, as in previous literature (Durr et al., 1996; Harding, 1981; Schols et al., 1997). The previous data concerning non-neurological features such as cardiomyopathy and diabetes are not precise enough to establish a comparison with the data in this study, and data for GAA repeat size in each allele was not consistently available for the Parkinson study. However, it may be reasonably assumed, based on their classical FRDA symptoms and age at onset, that the majority of FRDA patients detected in the Parkinson study had a considerably higher number of GAA repeats

than those of the three FRDA patients detected in the more recent study. Thus, the clinical symptoms in both patient cohorts presented in this chapter further bear out the original implications of the genetic findings, which were that the FRDA patient phenotype is very consistent and diagnosable, with a natural phenotypic variation that is well accounted for by the genotypic-phenotypic characterization of LOFA/VLOFA.

# Chapter 4 : Reduced $Ca^{2+}$ Levels in Cardiomyocytes in Friedreich's Ataxia Models

## 4.1 Introduction

Frataxin is a mitochondrial protein involved in the biogenesis of iron-sulphur clusters (ISCs). It has been shown to be involved in various physiological functions such as response to oxidative stress (Abeti et al., 2016; Babcock et al., 1997; Condo et al., 2007; Gakh et al., 2006; O'Neill et al., 2005) and most recently, regulation of cellular $Ca^{2+}$ homeostasis (Bolinches-Amoros et al., 2014; Molla et al., 2017; Abeti et al, 2018). The reduction of frataxin in FRDA patient biopsies has been associated with intracellular iron deposits (Lamarche et al., 1980; Sanchez-Casis et al., 1976), mitochondrial dysfunction associated with a deficit in ISC-containing enzymes involved in mitochondrial respiration (Rotig et al., 1997) and oxidative damage (Bradley et al., 2004; Emond et al., 2000; Schulz et al., 2000). It has been proposed that the modifications in iron metabolism are themselves the cause of the inhibition of mitochondrial respiration and the promotion of ROS generation that lead to the physiological dysfunctions described (review: Pandolfo & Pastore, 2009).

Frataxin deficiency has been shown to lead to mitochondrial dysfunction with iron accumulation and hypersensitivity to oxidative damage in mice (Abeti et al., 2016; Abeti et al., 2015; Al-Mahdawi et al., 2006; Ristow et al., 2003), yeast (Babcock et al., 1997; Karthikeyan et al., 2003), *Caenorhabditis elegans* (Vazquez-Manrique et al., 2006) and *Drosophila melanogaster* (Llorens et al., 2007). Frataxin has been shown to interact physically with components of the ISC assembly complex (Stemmler et al., 2010) and also specifically with complex II of the electron transport chain

(ETC; Gonzalez-Cabo et al., 2005), directly associating frataxin with mitochondrial structure, function and bioenergetics (Lodi et al., 1999; Ristow et al., 2000). Frataxin has also been proposed to protect the cell against oxidative damage (Gakh et al., 2006; O'Neill et al., 2005), which has itself been linked to the mitochondrial iron overload that results from frataxin deficiency (Babcock et al., 1997; Cavadini et al., 2000; Karthikeyan et al., 2002).

The effect of oxidative stress on $Ca^{2+}$ homeostasis is well-established (Ermak & Davies, 2002). Although $Ca^{2+}$ regulation is strongly linked with mitochondrial function in the cell, few studies of FRDA have explored this link. Stable frataxin deficiency in dorsal root ganglia (DRG) neurons has been shown to lead to mitochondrial failure, in association with oxidative stress and $Ca^{2+}$ dysregulation (Mincheva-Tasheva et al., 2014; Molla et al., 2017). It is also known that frataxin expression levels directly correlate with mitochondrial buffer $Ca^{2+}$ capacity (a marker of mitochondrial function), which increases with frataxin overexpression in 3T3-L1 adipocytes (Ristow et al., 2000) and decreases with frataxin downregulation in SH-SY5Y human neuroblastoma cells (Bolinches-Amoros et al., 2014).

The effects on $Ca^{2+}$ homeostasis by the oxidative stress generated through iron overload in cardiomyocytes is also of great interest for clarifying the pathophysiological mechanism of FRDA cardiomyocytes. The early embryonic lethality that results from total frataxin knockout in mouse models occurs without significant mitochondrial iron accumulation during embryonic resorption (Cossee et al., 2000), and this accumulation has been shown to occur after onset of FRDA pathology in frataxin-deficient neuronal and cardiac murine cell lines (Puccio et al., 2001). This suggests that a subtle increase in redox-active mitochondrial iron is more likely to play a key role in FRDA pathogenesis than a general mitochondrial iron accumulation. Studies of other diseases such as hereditary haemolytic anaemia and other iron-overload conditions associate iron-induced oxidative stress with imbalanced $Ca^{2+}$ handling, which can lead to arrhythmias and sudden death as have also been observed in FRDA. In

these studies on other iron-overload conditions, the oxidative stress has been linked with lower peak systolic $Ca^{2+}$ levels, higher diastolic $Ca^{2+}$ levels, as well as slowed rates of $Ca^{2+}$ relaxation (Oudit et al., 2006; Schwartz et al., 2002). Due to the overlap in key symptoms between FRDA and some of these other iron-overload conditions, an investigation into $Ca^{2+}$ signaling in FRDA heart cells could shed light on certain unknown aspects of FRDA pathophysiology (Isaya, 2014).

In cardiomyocytes, most $Ca^{2+}$ influx occurs via voltage-gated L-type $Ca^{2+}$ channels. Although many of the FRDA neuronal-based studies cited above observe $Ca^{2+}$ channel function in the plasma membrane, in FRDA cardiomyocyte pathology the role of the SR as the key dynamic $Ca^{2+}$ store could also be of great relevance. Cardiac-specific ryanodine receptors (RYR2) on the SR surface allow for release of $Ca^{2+}$ from SR stores regulated by $Ca^{2+}$-induced $Ca^{2+}$-release (CICR), where this $Ca^{2+}$ release is stimulated by the presence of $Ca^{2+}$ itself. This event is a crucial part of the cyclical process causing cardiac muscle contraction, as the released $Ca^{2+}$ then binds to the C domain of troponin (Ramay et al., 2010), highlighting the fundamental role of $Ca^{2+}$ signaling and homeostasis in cardiac excitation-contraction coupling. Mitochondria are crucial for regulating local interorganellar $Ca^{2+}$ communication and ROS levels and form tightly linked microdomains with the RYR2, which indicates that they are highly likely to be affected by an SR pathology (Csordas et al., 2006; Garcia-Perez et al., 2008).

Oxidative damage could specifically affect $Ca^{2+}$ levels in FRDA cardiomyocytes via oxidation-sensitive Cys residues on the RYR2 or the sarcoplasmic reticulum $Ca^{2+}$ ATPase (SERCA) pumps (Adachi et al., 2004; Cherednichenko et al., 2004; Goldhaber & Qayyum, 2000; Sharov et al., 2006; Ying et al., 2008; Zima & Mazurek, 2016). For example, the oxidative damage could potentiate the RYR2, leading to an increased probability and duration of RYR2 channel opening, and thereby causing an increased $Ca^{2+}$ leak from the SR (Zima & Mazurek, 2016).

## 4.2 Results

***With great thanks to Dr R. Abeti for obtaining the data on mitochondrial energy imbalance, as well as the H9c2 cell caffeine response and H9c2 immunofluorescence data.**

### 4.2.1 Fxn-siRNA-induced Knockdown

The focus of the work described in the present chapter was to investigate the role of $Ca^{2+}$ in cardiomyocytes to elucidate FRDA pathophysiology. To do so I employed two cardiac cell lines to conduct my experiments. HL-1 and H9c2 are the only available cell lines that can substitute primary cardiomyocytes as disease models. HL-1 cells are adult atrial murine cardiomyocytes, while H9c2 cells are neonatal ventricular cardiomyocytes from rats. I modelled FRDA in these cells via siRNA-induced knockdown of frataxin. One neonatal line and one adult line were used, which allowed for insight into FRDA pathophysiology at different stages of cardiac development. I also used neonatal heart cells from the YG8R FRDA mouse model to confirm findings made in the cell lines.

YFP was co-transfected alongside the siRNA to provide a fluorescent marker of successful transfection, and therefore of frataxin mRNA knockdown (Fig. 17 A-B). I co-transfected one set of cells with YFP-DNA and scrambled siRNA as my control cells, and another set of cells with YFP-DNA and mouse Fxn-siRNA. The efficiency of transfection was assessed by immunofluorescence using an antibody against frataxin protein. The fluorescence parameters are indicated in Fig. 17 A-B. Cells in all experiments were selected if, in addition to Fura-2 fluorescence, they also emitted YFP fluorescence, which confirmed their transfected status. In order to observe if siRNA transfection against Fxn had achieved knockdown, I calculated the relative fluorescence level of frataxin in the transfected cells in the FXN-siRNA group when the frataxin fluorescence in the siRNA-scrambled group was set at 100%. The results showed a significant ~40 % decrease in frataxin expression in Fxn-siRNA HL-1 cells when compared to control cells (Fig. 17 C) and a significant ~70%

decrease in frataxin expression in Fxn-siRNA H9c2 cells compared to control cells (Fig. 17 D; **H9c2 data in collaboration with Dr R. Abeti**).

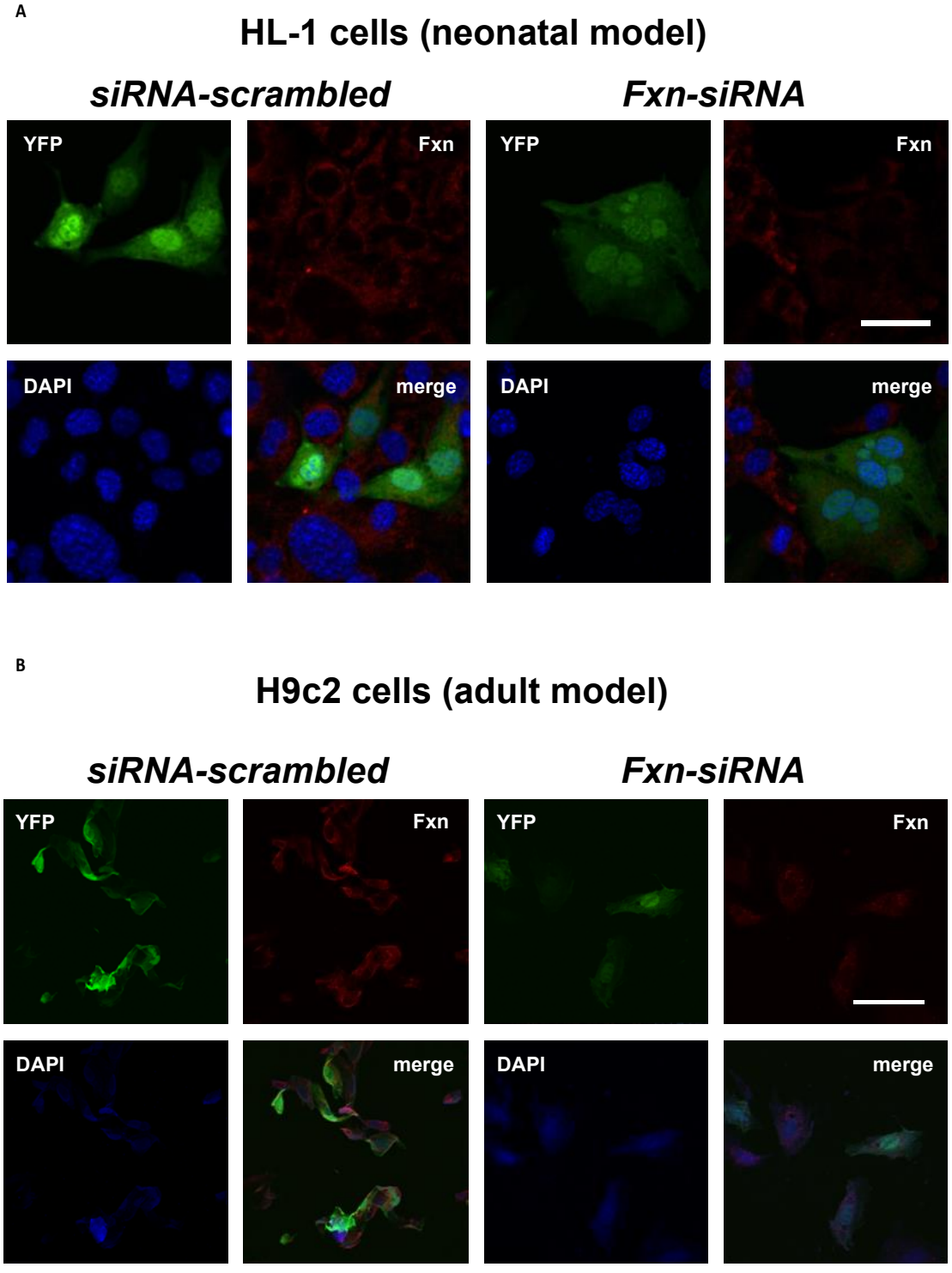

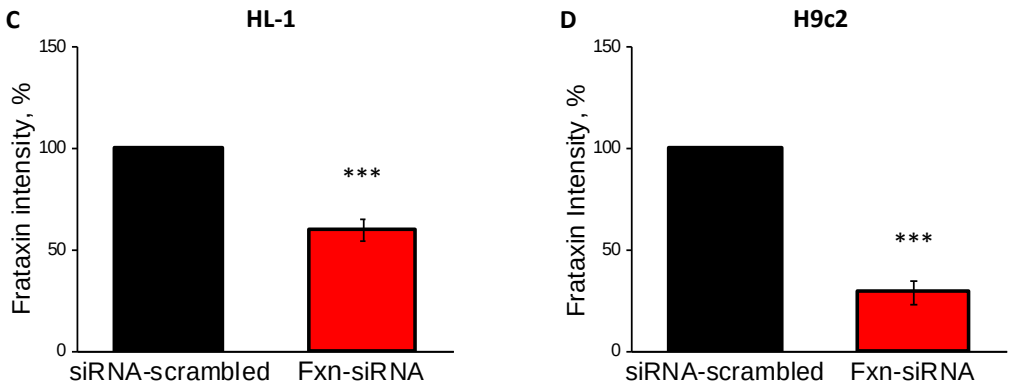


**Figure 17: Immunofluorescence Experiments on HL-1 and H9c2 cells: knock-down of endogenous frataxin in cardiac cell lines using siRNA.**

**A**) A comparison between siRNA-scrambled-transfected and Fxn-siRNA-transfected HL-1 cells. The top left images show YFP fluorescence in green in siRNA-scrambled cells, and cells labelled with Fxn antibody showing with red fluorescence. The bottom left images show DAPI labelling the nuclei in blue, and the merged image. The top right images show YFP fluorescence in siRNA-transfected cells, with the equivalent Fxn antibody fluorescence being very low. The bottom right images show DAPI labelling the nuclei in blue, and the merged image. **B**) A comparison between siRNA-scrambled-transfected and Fxn-siRNA-transfected H9c2 cells. The top left images show YFP fluorescence in green in siRNA-scrambled cells, and cells labelled with Fxn antibody showing red fluorescence. The bottom left images show DAPI labelling the nuclei in blue, and the merged image. The top right images show YFP fluorescence in siRNA-transfected cells, with the equivalent Fxn antibody fluorescence being very low. The bottom right images show DAPI labelling the nuclei in blue, and the merged image. **C**) Frataxin immunofluorescence levels in HL-1 cardiomyocytes in cells transfected with the siRNA-scrambled and transfected with Fxn-siRNA. The histogram shows the quantified red fluorescence from both groups of cells. When the anti-frataxin fluorescence level of the control cells was set at 100%, the frataxin level of the cells transfected with Fxn-siRNA (n= 3 independent experiments) was 60±5%, a significant decrease compared to control cells (***p<0.001). SEM was used to calculate the error. **D**) Frataxin immunofluorescence levels in H9c2 cardiomyocytes in cells transfected with siRNA-scrambled and transfected with Fxn-siRNA. The histogram shows the quantified red fluorescence from both groups of cells. When the anti-frataxin fluorescence level of the control cells was set at 100%, the frataxin level of the cells transfected with Fxn-siRNA was 29±5%, a significant decrease compared to control cells (n= 3 independent experiments; ***p<0.001; **data in collaboration with R. Abeti**). SEM was used to calculate the error. Scale bar = 20µm.

### 4.2.2 Increased ROS in Fxn KD HL-1 and H9c2 cells

Increased oxidative stress is a hallmark of frataxin-deficient cells (Abeti et al., 2016; Abeti et al., 2015; Navarro et al., 2010; Pastore & Puccio, 2013) and any study of $Ca^{2+}$ signalling in the disease must also include an observation of ROS levels. After analyzing transfection and knockdown efficiency of Fxn-siRNA, I investigated ROS levels in the two cell models.

Dihydroethidium (Het) is a superoxide indicator that displays blue fluorescence in the cytosol until oxidized: it then intercalates into the nuclear DNA and emits red fluorescence. The rate of fluorescence measures superoxide production, which is a function of the rate of cytosolic ROS generation. In the example data presented, for HL-1 cells the red fluorescence indicates cytosolic ROS levels 1500 seconds following incubation in cells transfected with siRNA-scrambled (top left, Fig. 18 A) and Fxn-siRNA (bottom left, Fig. 18 A). 10 µM Het was added at the beginning of each experiment. The data gathered suggests that superoxide production at cell resting condition, and therefore ROS generation in the cytosol, is increased in frataxin-deficient cells in both HL-1 (Fig. 18 B & D) and H9c2 cells (Fig. 18 C & E).

Oxidative stress was also assessed by measuring mitochondrial ROS levels through adding 20 nM of the CM-H2Xros dye to the HL-1 cells, with the rate of fluorescence measuring mitochondrial ROS production (Fig. 19 A). These data also suggest an increase in rate of ROS production in frataxin-deficient cells based on the kinetic trace recordings (Fig. 19 B-C). The data indicates that an increase in mitochondrial ROS levels may be occurring simultaneously with a general increase in cytosolic ROS levels in the frataxin-deficient cardiomyocytes. Taken together, this indicates a potential pathological increase in ROS levels and thus oxidative stress resulting from frataxin deficiency, which may affect $Ca^{2+}$ signaling and homeostasis in the cardiomyocyte model. I therefore moved to assessments of $Ca^{2+}$ homeostasis.

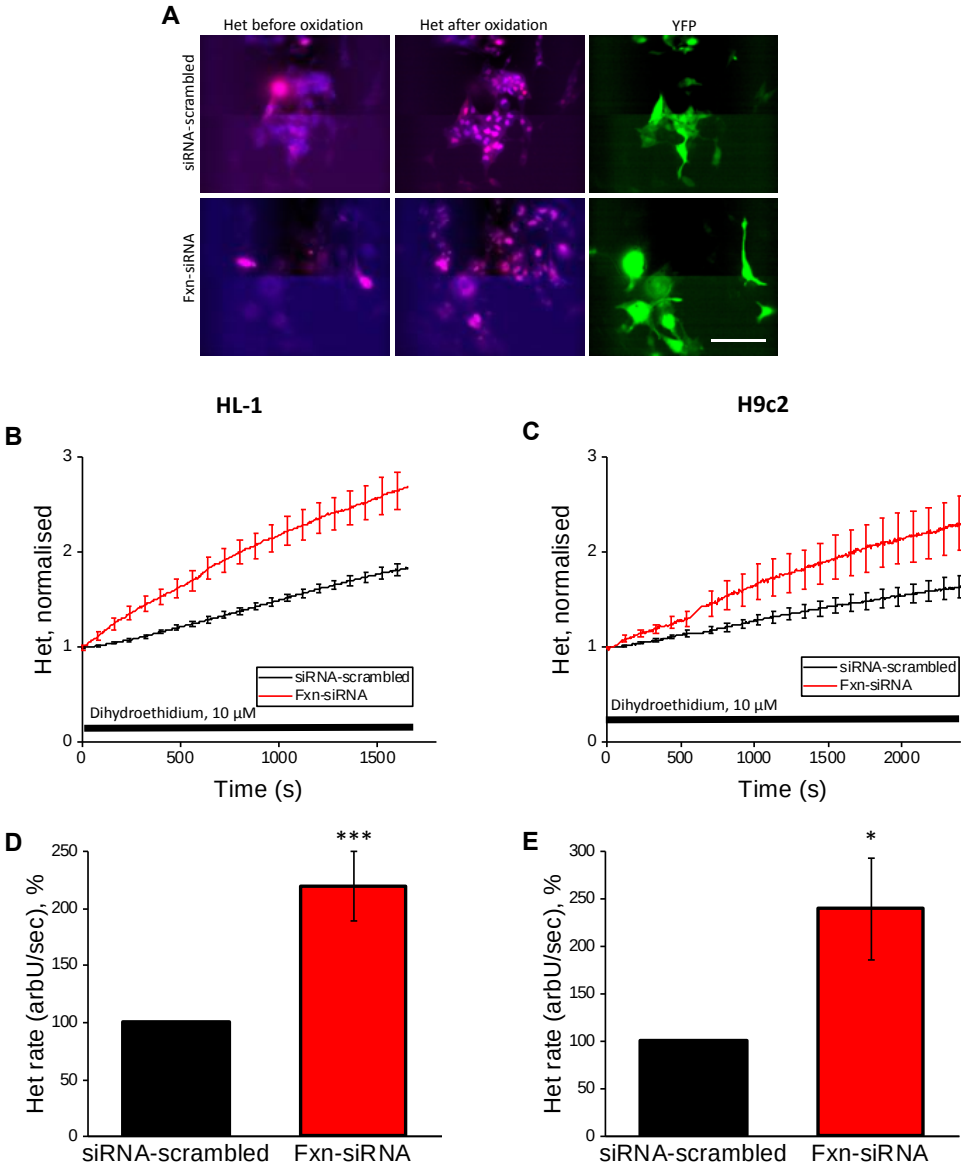


**Figure 18: Increased rate of generation of cytosolic reactive oxygen species (cROS) over time in frataxin-deficient cells from two FRDA cell models.**

**A**) Ratiometric Het and YFP signal in HL-1 transfected cells. The data shows cells loaded with 10 µM Het and excited at 364 (blue signal) and 543 nm (red signal), with the red signal indicating oxidation of the Het. YFP fluorescence for the equivalent cells is also shown. **B**) Average kinetic curve showing the average increase in ratiometric Het fluorescence (and therefore increase in cytosolic ROS levels) in HL-1 cardiomyocytes normalized to 1, with the siRNA-scrambled trace in black and the FXN-siRNA trace in red. **C**) Average kinetic curve showing the average increase in ratiometric Het fluorescence in H9c2 cardiomyocytes normalized to 1, with the siRNA-scrambled trace in black and the FXN-siRNA trace in red. **D**) The histogram shows the quantified red fluorescence from both groups of cells. The rate of dihydroethidium fluorescence increase in HL-1 cells transfected with siRNA-scrambled was normalised to 100%. The data shows a significant increase in the fluorescent unit increase per second in FXN-siRNA cells (219±31; n= 3 independent experiments) compared with siRNA-scrambled cells. The difference is statistically significant (***p<0.001). SEM was used to calculate the error. **E**) The histogram shows the quantified red fluorescence from both groups of cells. The rate of

dihydroethidium fluorescence increase in H9c2 cells from 2 coverslips transfected with siRNA-scrambled was normalised to 100%. The data shows a significant increase in the fluorescent unit increase per second in FXN-siRNA cells (240±54; n= 3 independent experiments) compared with siRNA control cells. The difference is statistically significant (*p<0.05). SEM was used to calculate the error. Scale bar = 20µm.

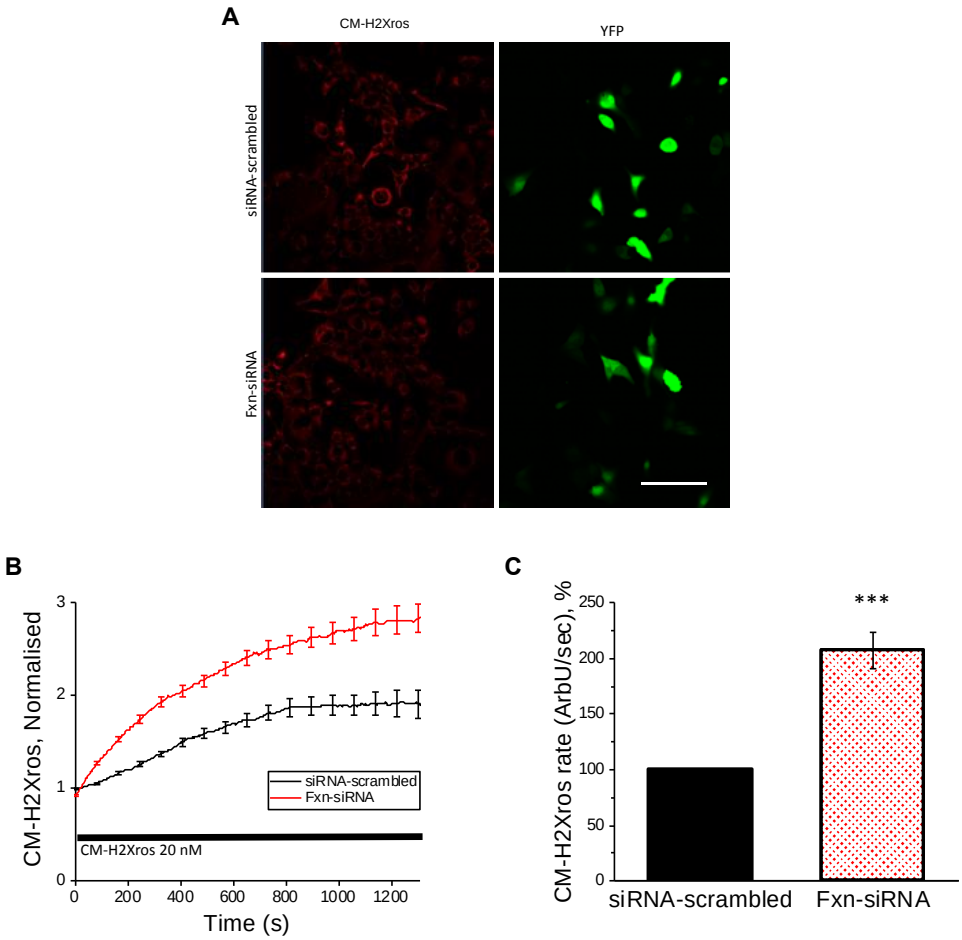


**Figure 19: Increased rate of generation of mitochondrial reactive oxygen species (mROS) over time in HL-1 cells with lower frataxin levels.**

**A**) CM-H2Xros and YFP signal in HL-1 cells. Top left: siRNA-scrambled CM-H2Xros levels; top right: siRNA-scrambled YFP levels; bottom left: Fxn-siRNA CM-H2Xros levels; bottom right: Fxn-siRNA YFP levels. **B**) Average kinetic curve showing the average increase in CM-H2Xros fluorescence (and therefore mitochondrial ROS levels) normalised to 1 in HL-1 cardiomyocytes, with the siRNA-scrambled trace in black and the FXN-siRNA trace in red. **C**) The rate of CM-H2Xros fluorescence increase in HL-1 cells from 2 coverslips transfected with siRNA-scrambled was normalised to 100%. The HL-1 cell data shows a significant increase in the normalized fluorescent unit increase per second in FXN-siRNA cells (208±16; n= 3 independent experiments) compared with siRNA-scrambled cells. The difference is extremely statistically significant (***p<0.001). SEM was used to calculate the error. Scale bar = 20µm.

### 4.2.3 Decreased NADH Redox Index in Fxn KD HL-1 and H9c2 cells

During energy production, the function of the mitochondrion is crucial to providing ATP via the metabolism of substrates, and this may be affected in FRDA (Gonzalez-Cabo et al., 2005; Rotig et al., 1997; Stemmler et al., 2010). The tricarboxylic acid cycle provides substrates like NADH and $FADH_2$, electron carriers that donate electrons to the mitochondrial electron transport chain (ETC). The oxidized form of NADH is NAD+. The levels of NADH, which donates its electrons to complex I of the ETC, can be estimated by NAD(P)H autofluorescence, from which an NADH redox index can be obtained that gives an indication of mitochondrial ETC activity. This redox index is estimated by observing the difference in the fluorescence values between application of FCCP, which drives mitochondrial respiration to the maximum and thereby stimulates maximum NADH oxidation, and NaCN, which via inhibition of mitochondrial respiration stimulates maximum NADH reduction.

The mitochondrial NADH autofluorescence is visualized in Fig. 21 A-B. The NADH maximal oxidation is achieved with FCCP (set at 0%) and the maximal reduction with NaCN (set at 100%). The redox index is calculated based on these parameters by measuring the percentage at baseline prior to FCCP addition, and this normalization is done cell by cell. A reduction in redox index was found following Fxn knockdown (Fig. 20 A-B).

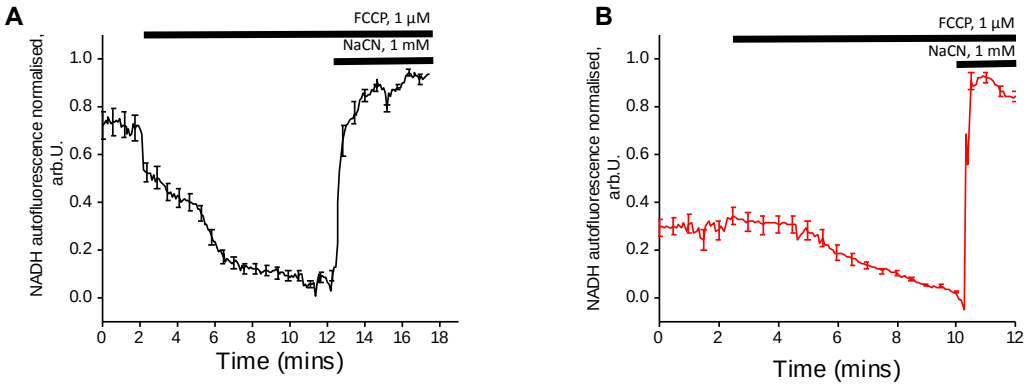


**Figure 20: Representative NADH level traces in HL-1 cells following FCCP and NaCN addition, showing decreased redox index in Fxn-siRNA cells.**

**A**) Representative kinetic trace showing average NADH level in HL-1 cells from a siRNA-scrambled coverslip. The greatest extent of the response to FCCP and NaCN are set as '0' and '1', the mitochondrial NADH redox index. **B**) Representative trace showing average NADH level in HL-1 cells from a Fxn-siRNA coverslip.

The redox index was statistically confirmed to be significantly decreased in HL-1 cells transfected with FXN-siRNA (Fig. 21 C). In H9c2 cells, the redox index was also significantly decreased in Fxn-siRNA cardiomyocytes (Fig. 21 D). These data indicate a changed $NAD^+$/NADH ratio in frataxin-deficient cells compared to controls, with decreased $NAD^+$ levels. This depletion of the $NAD^+$ substrate necessary for NADH production and mitochondrial complex I activity is an indication of energy imbalance within the cell.

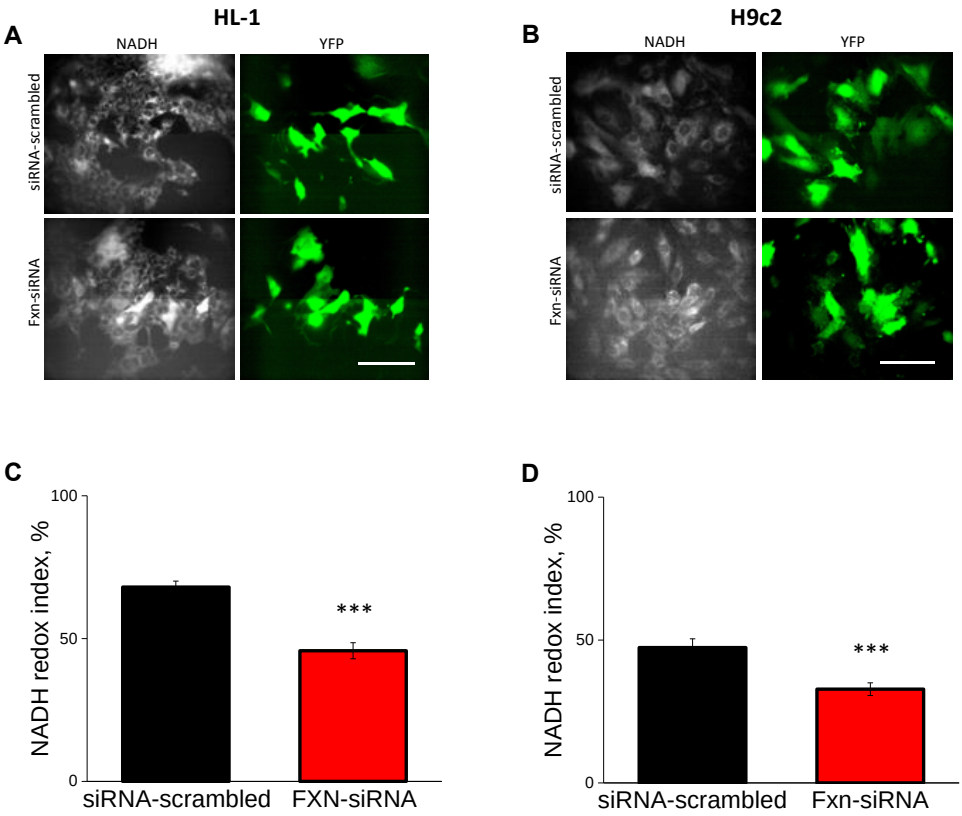


**Figure 21: NADH Levels: Decrease in cells with lower frataxin levels.**

**A**) NADH and YFP signal in HL-1 cells. **B**) NADH and YFP signal in H9c2 cells. **C**) Average redox index in HL-1 cells, showing a redox index of 68±2% in siRNA-scrambled cells and of 46±3% in Fxn-siRNA cells (n= 3 independent experiments; ***p<0.001). **D**) Average redox index in siRNA-scrambled and Fxn-siRNA cells among H9c2 cells, showing a value of showing a value of 47±3% redox index in siRNA-scrambled cells and a 33±2% redox index in Fxn-siRNA cells (n= 3 independent experiments; ***p<0.001). Scale bar = 20µm.

### 4.2.4 Mitochondrial Energy Imbalance in FRDA Pathophysiology (from Abeti et al., 2018)

Mitochondria are crucial in regulating $Ca^{2+}$ homeostasis, as after a physiological response they take up $Ca^{2+}$ to restore cytosolic $Ca^{2+}$ levels to resting conditions. The mitochondrial membrane potential ($\Delta\psi_m$) is susceptible to changes during this process. This was measured during the application of caffeine in order to observe any potential changes in mitochondrial function. In both the HL-1 and H9c2 cell lines, a depolarisation in $\Delta\psi_m$ was found corresponding with the caffeine response in control cells, as the mitochondria actively uptake $Ca^{2+}$ to rebalance $Ca^{2+}$

homeostasis following $Ca^{2+}$ release into the cytosol. This depolarisation was significantly reduced in Fxn-siRNA cells (Fig. 22 A-B).

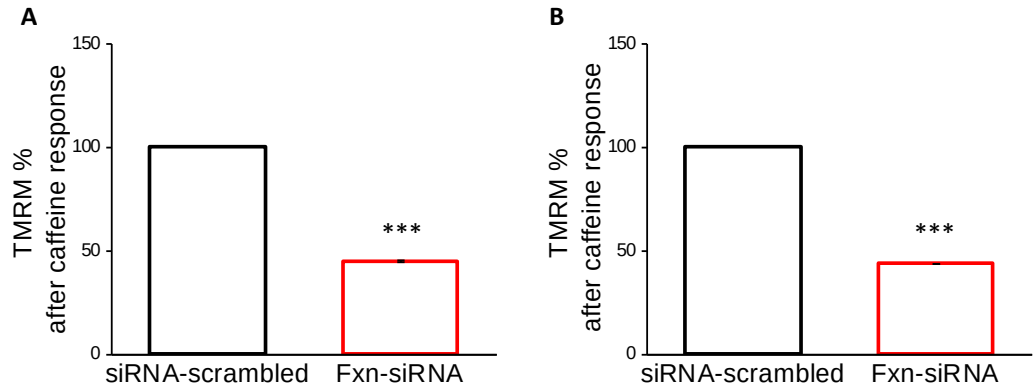


**Figure 22: Comparison of TMRM levels during caffeine response in HL-1 and H9c2 cells: abnormal bioenergetics response to caffeine in both cell lines (from Abeti et al, 2018).**

**A)** The average depolarisation was set at 100% for the siRNA-scrambled cells in both cell lines. The average equivalent TMRM fluorescence percentage for Fxn-siRNA-transfected HL-1 cells was 45±1% (n= 3 independent experiments; ***p<0.001). SEM was used to calculate the error. **B**) The average equivalent TMRM fluorescence percentage for Fxn-siRNA-transfected H9c2 cells was 44±1% (n= 3 independent experiments; ***p<0.001). The depolarisation response in the frataxin-deficient cells of both cell lines is reduced, indicating inefficient mitochondrial $Ca^{2+}$ uptake. SEM was used to calculate the error.

### 4.2.6 Caffeine-Induced $Ca^{2+}$ Response Decrease in Fxn KD Cells

I then indirectly observed SR $Ca^{2+}$ levels via the response to caffeine addition in my cardiomyocyte models. Caffeine is an agonist that is used to activate the ryanodine receptor in cardiomyocytes (RYR2), inducing $Ca^{2+}$ release from the SR of the cardiomyocytes. This causes a rise in $[Ca^{2+}]_c$, and any variation in the $Ca^{2+}$ response to caffeine may indicate a change in SR $Ca^{2+}$ content or perhaps a potentiation or inhibition of the RYR2 that regulate that content. I loaded the cells with 5 µM Fura-2 and recorded the fluorescence each second. $Ca^{2+}$ was found to be released from SR stores consistently in HL-1 cells on application of 10mM caffeine.

I compared $[Ca^{2+}]_c$ levels between HL-1 cells transfected with Fxn-siRNA and those transfected with the siRNA-scrambled control.

In summary, there was a significant decrease in the caffeine-induced $Ca^{2+}$ response in HL-1 and H9c2 cells with Fxn knockdown, as compared to those incorporating siRNA-scrambled (Fig. 23 B-E). There was a large difference in level of decrease between the HL-1 and H9c2 cells, however, which could indicate either an increased potentiation of RYR2 function in H9c2 cells leading to a lower SR $Ca^{2+}$ level due to increased leak, or alternatively an inhibition of SERCA pump function in H9c2 cells causing less $Ca^{2+}$ to enter the SR in the first place. The CICR amplitude and frequency at first increased in the HL-1 FRDA-model cells, before abruptly stabilising above its baseline, indicating a probable energetic collapse of the CICR process (Fig. 24 A-B). There was no secondary phase of $Ca^{2+}$ signaling in H9c2 cells due to their adult, non-beating nature.

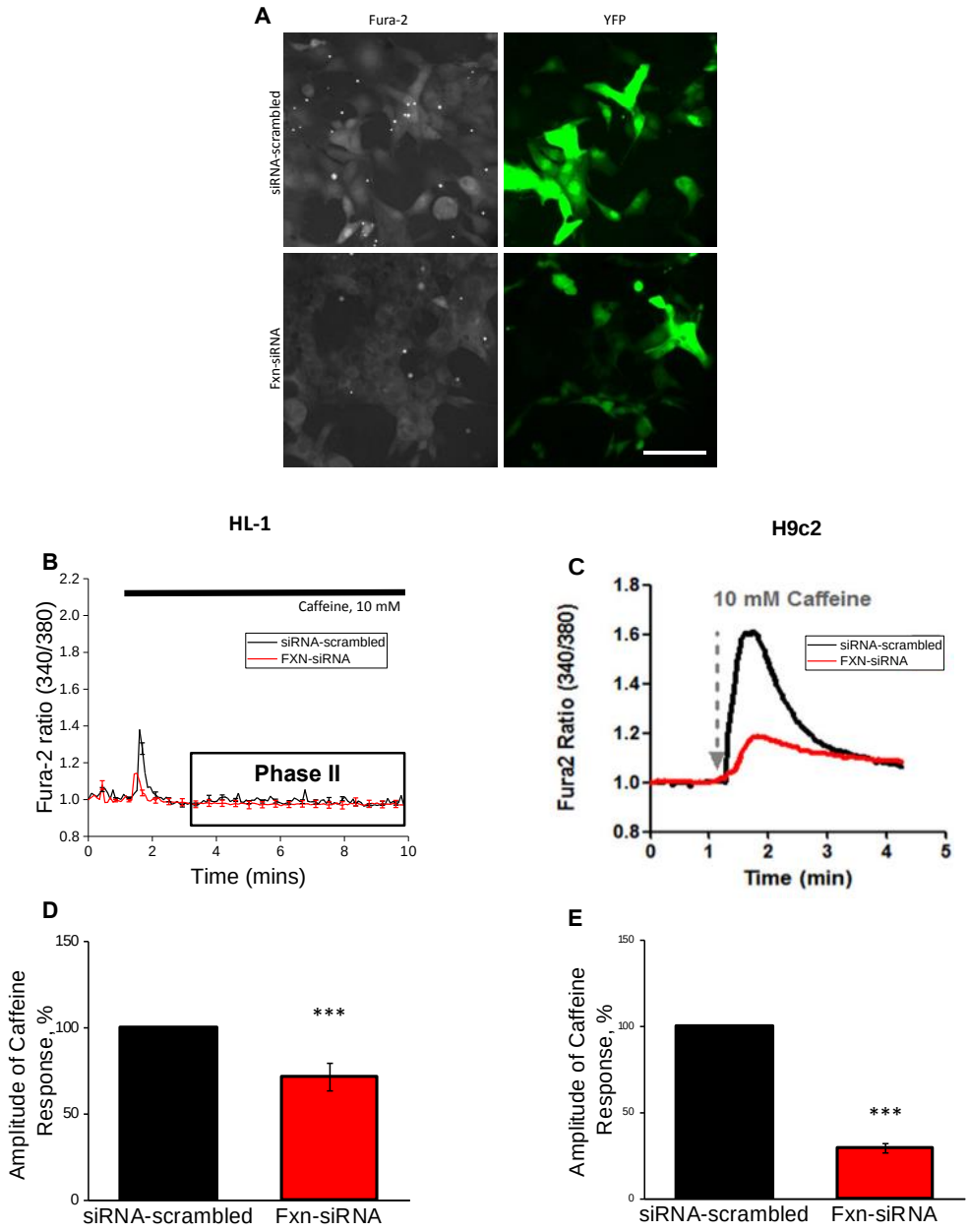


**Figure 23: Caffeine-Induced Ca2+ Transient Amplitude: decrease in cells with lower frataxin levels.**

Average amplitude of caffeine-induced $[Ca^{2+}]_c$ peak in HL-1 and H9c2 cells. **A**) Fura-2 and YFP fluorescence in HL-1 cells. Top left: siRNA-scrambled Fura-2 levels; top right: siRNA-scrambled YFP levels; bottom left: Fxn-siRNA Fura-2 levels; bottom right: Fxn-siRNA YFP levels. **B**) Average kinetic curve representing Fura-2 ratio showing the difference between the caffeine-induced $[Ca^{2+}]_c$ transient in HL-1 cells transfected with siRNA-scrambled and FXN-siRNA. The siRNA-scrambled trace is in black and the FXN-siRNA trace is in red. The box indicating phase II of the caffeine response is highlighted, and further analysed in Figure 22. **C**) Average kinetic curve representing Fura-2 ratio showing the difference between the caffeine-induced $[Ca^{2+}]_c$ transient in H9c2 cells transfected with siRNA-scrambled and FXN-siRNA. The siRNA-scrambled trace is in black and the FXN-siRNA trace is in red. **Graph from Abeti et al, 2018. D**) The corresponding average % caffeine-

induced $[Ca^{2+}]_c$ amplitude of siRNA-transfected HL-1 cells. The average amplitude of cells transfected with siRNA-scrambled was normalized to 100%. The corresponding average amplitude from cells transfected with FXN-siRNA was 72±8% (***p<0.001; n= 3 independent experiments). SEM was used to calculate the error. **E**) The corresponding average % caffeine-induced $[Ca^{2+}]_c$ amplitude of siRNA-transfected H9c2 cells. The average amplitude of cells transfected with siRNA-scrambled was normalized to 100%. The corresponding average amplitude of cells transfected with FXN-siRNA was 30±3% (***p<0.001; n= 3 independent experiments). **Graph from Abeti et al, 2018.** SEM was used to calculate the error. Scale bar = 20µm.

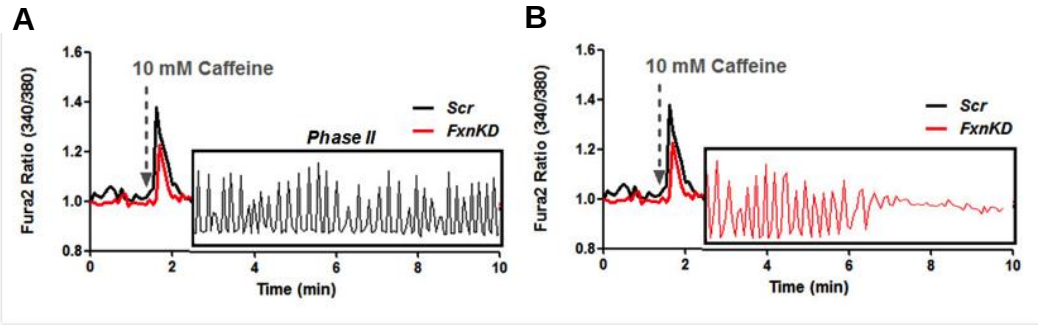


**Figure 24: Phase II of the caffeine-induced $Ca^{2+}$ signalling response in HL-1 cells (from Abeti et al, 2018).**

Phase II response to caffeine. **A**) The phase II response of the siRNA-scrambled cells is displayed above in the black box, and **B**) the phase II response of the Fxn-siRNA cells is displayed below in the red box. Both the amplitude and frequency of response is increased in Fxn-siRNA cells, and over 7 minutes of recording following caffeine addition, Fxn-siRNA-transfected cells end their caffeine response early, most likely due to bioenergetic failure of CICR.

## 4.2.7 Thapsigargin Experiments

### *Thapsigargin Response Indicates Reduced SR $Ca^{2+}$ Levels in Fxn KD HL-1 and H9c2 cells*

To get further data on SR $Ca^{2+}$ levels, I carried out experiments on HL-1 and H9c2 cells using thapsigargin, which works by blocking the SERCA pump allowing for measurement of the subsequent $Ca^{2+}$ leak from the SR. Data gathered from thapsigargin experiments on HL-1 cells and H9c2 cells showed a significant decrease in the estimation of the SR $Ca^{2+}$ level in Fxn knockdown-transfected cells (Fig 25 C-F). This confirmed the findings from the caffeine data, indicating a lower SR $Ca^{2+}$ content in cells incorporating a frataxin mRNA knockdown.

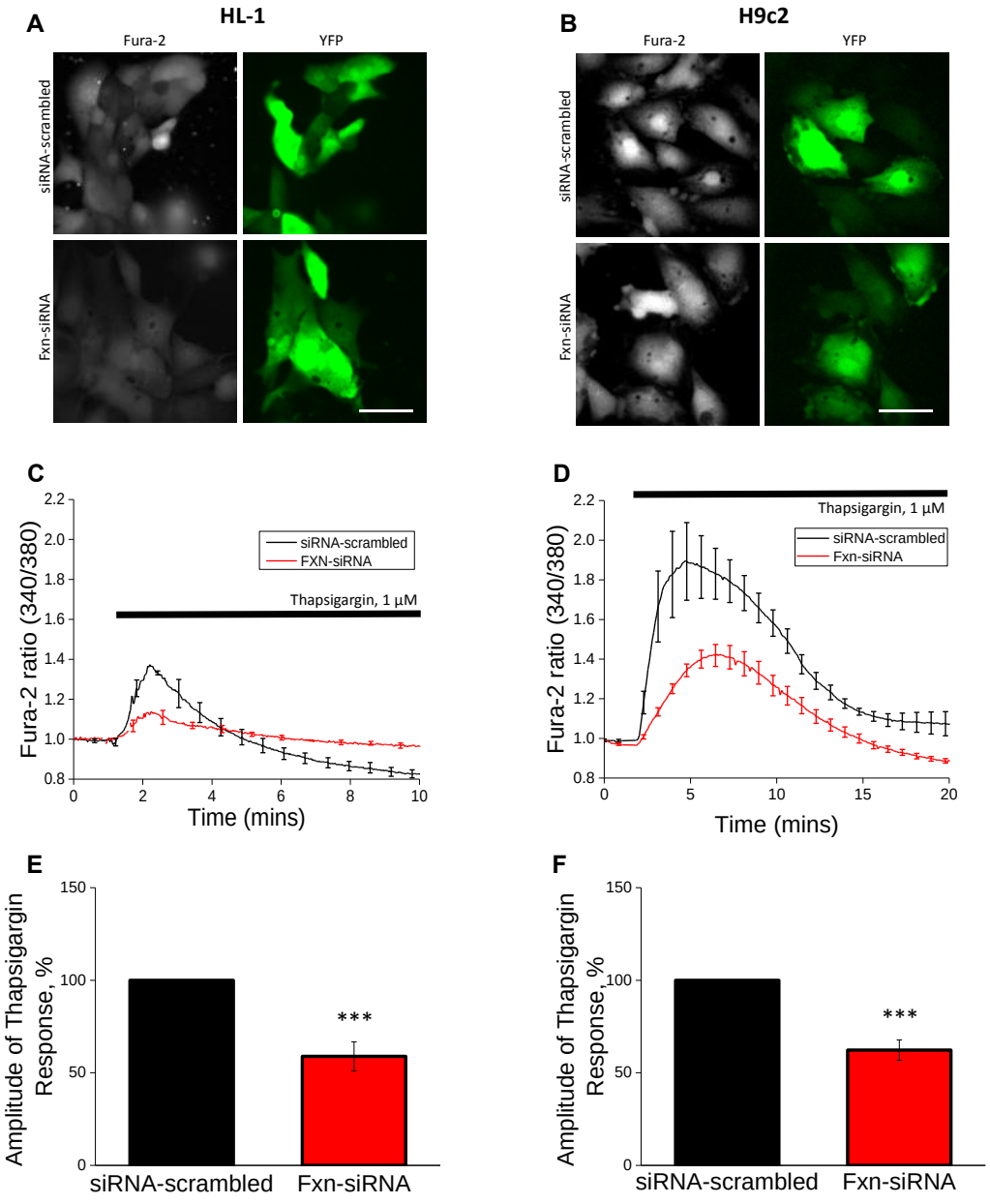


**Figure 25: Thapsigargin-Induced Ca2+ Transient Amplitude: decrease in cells with lower frataxin levels in both FRDA cell models.**

**A**) Fura-2 and YFP fluorescence in HL-1 cells. Top left: siRNA-scrambled Fura-2 levels; top right: siRNA-scrambled YFP levels; bottom left: Fxn-siRNA Fura-2 levels; bottom right: Fxn-siRNA YFP levels. **B**) Fura-2 and YFP signal in H9c2 cells. Top left: siRNA-scrambled

Fura-2 levels; top right: siRNA-scrambled YFP levels; bottom left: Fxn-siRNA Fura-2 levels; bottom right: Fxn-siRNA YFP levels. **C**) Average kinetic curve representing Fura-2 ratio showing the difference between the thapsigargin-induced $[Ca^{2+}]_c$ transient in HL-1 cells transfected with siRNA-scrambled and FXN-siRNA. The siRNA-scrambled trace is in black and the FXN-siRNA trace is in red. **D**) Average kinetic curve representing Fura-2 ratio showing the difference between the thapsigargin-induced $[Ca^{2+}]_c$ transient in H9c2 cells transfected with siRNA-scrambled and FXN-siRNA. The siRNA-scrambled trace is in black and the FXN-siRNA trace is in red. **E**) The corresponding average % thapsigargin-induced $[Ca^{2+}]_c$ amplitude of siRNA-transfected HL-1 cells. The average amplitude of cells transfected with siRNA-scrambled was normalized to 100%. The corresponding average amplitude from cells transfected with FXN-siRNA was 58.9±7.8% (***$p<0.001$; n= 3 independent experiments). SEM was used to calculate the error. **F**) The corresponding average % thapsigargin-induced $[Ca^{2+}]_c$ amplitude of siRNA-transfected H9c2 cells. The average amplitude of cells transfected with siRNA-scrambled was normalized to 100%. while the corresponding average amplitude of cells transfected with FXN-siRNA was 62.3±5.5% (***$p<0.001$; n= 3 independent experiments). SEM was used to calculate the error. Scale bar = 20μm.

## *Dantrolene Increases Amplitude of Thapsigargin-Induced $Ca^{2+}$ Response in both Control and Fxn KD HL-1 and H9c2 cells*

Dantrolene is an inhibitor of ryanodine receptor function. Its use allowed for an understanding of whether the RYR2 were already inhibited or not, which could give me more insight into the specific pathological role of the RYR2. The cells were preincubated with 20 μM dantrolene for two hours, and then thapsigargin was added. The data displays an extremely significant difference between the cells transfected with scrambled-siRNA and Fxn-siRNA in both cells lines, despite the use of dantrolene (Fig. 26 C-F).

In figure 27 (**data produced in collaboration with Dr R. Abeti**), Part A provides a summary and comparison of the $Ca^{2+}$ responses to thapsigargin and thapsigargin-dantrolene in HL-1 cells described in Figs. 25-26, while part B compares the average amplitude of the thapsigargin-induced $Ca^{2+}$ response with and without dantrolene incubation in HL-1 cells. Frataxin-deficient cells without dantrolene have an average amplitude of 41±14%, compared to an average amplitude in frataxin-deficient cells with dantrolene of 77±7%, showing a significant increase in average amplitude

in dantrolene-treated cells (*p<0.05). Thus, comparison of the data in figs. 25-26 shows how preincubation with dantrolene increases the amplitude of the thapsigargin-induced $Ca^{2+}$ response in both control and frataxin-deficient cells (Fig. 27 A-B).

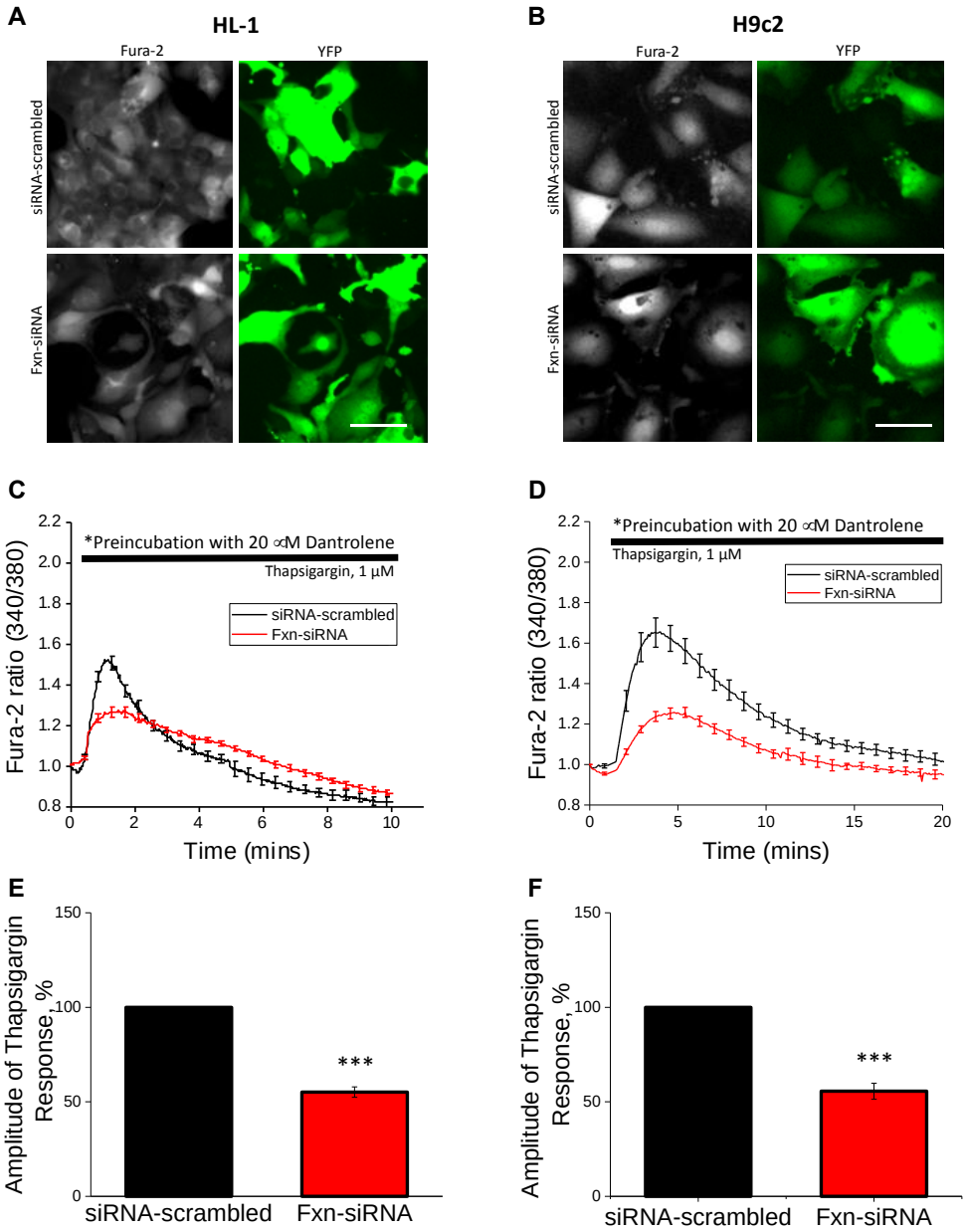


**Figure 26: Thapsigargin-Induced $Ca^{2+}$ Transient Amplitude Following Pre-Incubation with Dantrolene: decrease in cells with reduced frataxin levels in the HL-1 FRDA cell model.**

Average amplitude of thapsigargin-induced $[Ca^{2+}]_c$ peak in HL-1 cells following preincubation with dantrolene. **A**) Fura-2 and YFP fluorescence in HL-1 cells. Top left: siRNA-scrambled Fura-2 levels; top right: siRNA-scrambled YFP levels; bottom left: Fxn-siRNA Fura-2 levels; bottom right: Fxn-siRNA YFP levels. **B**) Fura-2 and YFP fluorescence in H9c2 cells, following same pattern as A). **C**) Average kinetic curve

representing Fura-2 ratio showing the difference between the thapsigargin-induced $[Ca^{2+}]_c$ transient in HL-1 cells transfected with siRNA-scrambled and FXN-siRNA. The siRNA-scrambled trace is in black and the FXN-siRNA trace is in red. **D**) Average kinetic curve representing Fura-2 ratio in H9c2 cells. **E**) The corresponding average % of thapsigargin-induced $[Ca^{2+}]_c$ amplitude of siRNA-transfected HL-1 cells. The average amplitude of cells transfected with siRNA-scrambled was normalized to 100%. The corresponding average amplitude of cells transfected with FXN-siRNA was 55±3% (***p<0.001; n= 3 independent experiments). SEM was used to calculate the error. **F**) The corresponding average % of thapsigargin-induced $[Ca^{2+}]_c$ amplitude of siRNA-transfected HL-1 cells. The average amplitude of cells transfected with siRNA-scrambled was normalized to 100%. The corresponding average amplitude of cells transfected with FXN-siRNA was 62±6% (***p<0.001; n= 3 independent experiments). SEM was used to calculate the error. Scale bar = 20µm.

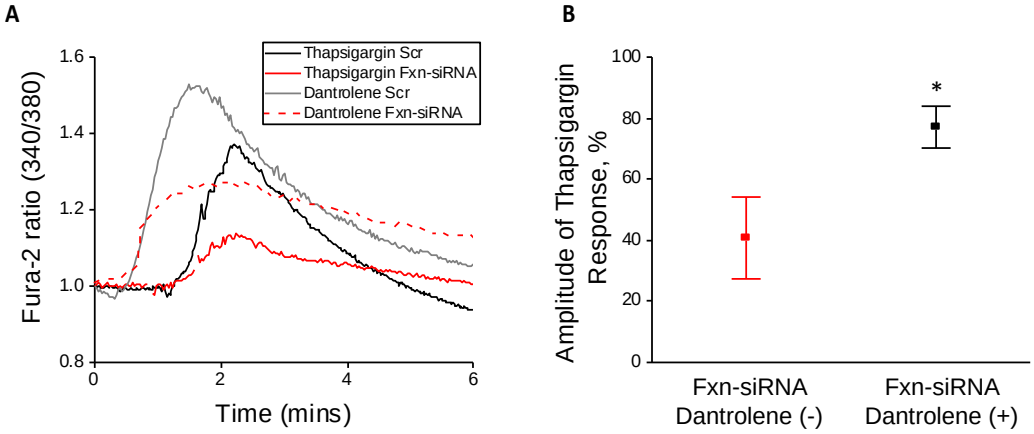


**Figure 27: Thapsigargin-Induced $Ca^{2+}$ Transient Amplitude: increase in average amplitude in dantrolene-treated frataxin-deficient HL-1 cells.**

**A**) Average kinetic curve representing Fura-2 ratio summarising the difference between the thapsigargin-induced $[Ca^{2+}]_c$ transient in HL-1 cells transfected with FXN-siRNA and not pre-incubated with dantrolene (Fig. 23), and those undergoing the same treatment and also pre-incubated with dantrolene (Fig. 24). Non-dantrolene: the siRNA-scrambled trace is in black and the FXN-siRNA trace is in red. Dantrolene: the siRNA-scrambled trace is in grey and the FXN-siRNA trace is the dashed line in red. **B**) A comparison of the average amplitude of thapsigargin response in frataxin-deficient cells without dantrolene (41±14%), and with dantrolene (77±7%), showing a significant increase in average amplitude in dantrolene-treated cells (*p<0.05). SEM was used to calculate the error. **Data produced in collaboration with Dr R. Abeti.**

### 4.2.8 Primary Cell Data

#### *Caffeine-Induced $Ca^{2+}$ Response Decreased in YG8R Mouse Model Cells*

To complement my data from the two heart cell lines, I studied cells from the YG8R FRDA mouse (Al-Mahdawi et al., 2006), in order to see firstly if we could obtain less heterogeneous results using caffeine to stimulate the ryanodine receptors. This was achieved in primary cells from a YG8R mouse (n=4) and was compared with control cells from primary cultures obtained from wild-type mice of the equivalent breed, C57/BL6. The data indicated an extremely significant decrease in SR $Ca^{2+}$ content due to the FXN knockdown, confirming the data from the two FRDA-like cardiomyocyte models (Fig. 28 A-B). Data specifically from the Y47R control mouse model may be required for a more complete picture. Although my primary cell data appears to agree with my hypothesis that there will be significantly less $Ca^{2+}$ in the SR, the smaller amount of data currently accumulated from primary cells mean that accumulation of more primary cell data and additional experimental techniques such as using thapsigargin are a crucial next step.

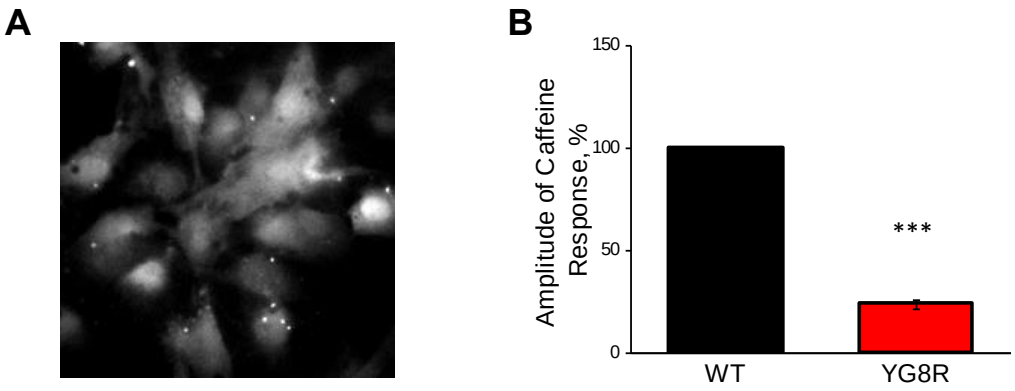


**Figure 28: Thapsigargin-Induced Ca2+ Transient Amplitude: decrease in YG8R primary cells with lower frataxin levels.**

**A)** Fura-2 fluorescence in YG8R mouse primary cells. **B)** The average % caffeine-induced $[Ca^{2+}]_c$ amplitude of WT/YG8R cells. The average amplitude of WT cells from the B57/C6 breed of mice was set at 100%. The corresponding average amplitude from cells from the YG8R mouse model was 24±2% (n=3 independent experiments; ***p<0.001), indicating a significant decrease in the SR $Ca^{2+}$ content.

### 4.2.9 Results Summary

It is known that changes in iron metabolism, oxidative stress and mitochondrial dysfunction result from frataxin deficiency, and that these lead to a pathophysiological phenotype in the heart as well as affected neural tissue. However, very few FRDA studies have been carried out into the potential relevance of $Ca^{2+}$ homeostasis, which is intimately linked with mitochondrial function and ROS levels, and none at all have been performed using a FRDA cardiomyocyte model. Therefore, I undertook the first study of $Ca^{2+}$ signalling using two different FRDA heart cell lines, the murine adult atrial cell line HL-1 and the rat ventricular neonatal cell line H9c2.

I began by characterising my FRDA cell models through testing well-established physiological effects of FRDA, and then investigated the $[Ca^{2+}]_c$ levels in two cardiomyocyte cell lines representative of a neonatal and an adult phenotype. The increase in ROS levels observed in both FRDA cell models (Figs. 18-19) was consistent with that found in previous FRDA models (Abeti et al., 2016; Bradley et al., 2004; Emond et al., 2000;

Lamarche et al., 1980; Puccio et al., 2001). A decreased NADH redox index was found in both FRDA cell models, indicating depletion of the $NAD^+$ substrate for mitochondrial complex I activity and a general energy imbalance due to frataxin depletion (Fig. 20-21). I specifically focused on the SR $Ca^{2+}$ content, and thus RYR2/SERCA activity, in the cardiac FRDA model cells to see if these could be affected compared to the control cells.

Reduced $Ca^{2+}$ levels due to increased leakage from the SR through the ryanodine receptors leading to a lower SR $Ca^{2+}$ content, was established using caffeine and thapsigargin, respectively (Figs. 23-25). The findings of this study allow for the hypothesis that $Ca^{2+}$ homeostasis is impaired by oxidative stress caused by reduced levels of frataxin in FRDA. More work is now necessary to establish a causal link between them. I also collected important preliminary data from FRDA model YG8R mouse primary cells on the thapsigargin-induced $Ca^{2+}$ response that, crucially, supported the data from the cell models (Fig. 28). However, additional $Ca^{2+}$ level measurements, ROS activity measurements and NADH level measurements will be required to complete the physiological picture in primary cells.

In conclusion, the novel finding of a decreased SR $Ca^{2+}$ content has been discovered in FRDA model cardiomyocytes alongside the more established increase in ROS levels. This change in $Ca^{2+}$ homeostasis is most likely caused by RYR2 potentiation, causing a leakier SR. These data, together with additional data gathered by Dr Abeti that found $\Delta\psi_m$ depolarization (presented in this results section) and $[Ca^{2+}]_m$ uptake inhibition which was reversed by vitamin E administration in these same FRDA model cardiomyocytes (Abeti et al, 2018), are part of the first steps indicating how modulation of $Ca^{2+}$ in cardiomyocytes could be a novel therapeutic strategy in FRDA.

## 4.3 Discussion

Frataxin deficiency is known to cause oxidative stress through the generation of iron free radicals and an imbalance in mitochondrial bioenergetics (Abeti et al., 2016; Bradley et al., 2004; Puccio et al., 2001; Puccio & Koenig, 2000). Hypertrophic cardiomyopathy is a key symptom in FRDA, and the function of frataxin in general appears to be more relevant in tissues with a higher energy demand such as the heart (Puccio et al., 2001). $Ca^{2+}$ homeostasis has been assessed in a small amount of FRDA cellular models such as neuronal cell lines, some of which have established a link between $Ca^{2+}$ levels and the mitochondrial dysfunction and oxidative stress previously established in FRDA pathophysiology (Bolinches-Amoros et al., 2014; Mincheva-Tasheva et al., 2014; Molla et al., 2017; Ristow et al., 2000; Wong et al., 1999). This link has been established in particular in DRG neurons from the YG8R FRDA mouse model used in this study (Molla et al., 2017). However, despite the heart defects associated with FRDA that can lead to arrhythmia and sudden death, $Ca^{2+}$ homeostasis has never been studied in FRDA model cardiomyocytes.

Shifts in $Ca^{2+}$ homeostasis can lead to changes in heart contraction and relaxation, and ultimately to cardiac failure (Limbu et al., 2015). As the heart defects in FRDA have strong similarities with other disorders involving iron-induced oxidative stress and $Ca^{2+}$ dysregulation in cardiomyocytes (Oudit et al., 2006; Schwartz et al., 2002), a study of $Ca^{2+}$ homeostasis in an FRDA cardiac model could increase the knowledge of the pathophysiological mechanisms of FRDA, with a view to potential therapies. In order to understand the role of $Ca^{2+}$ homeostasis in cardiomyocytes in FRDA, we used two heart cell models of FRDA, as well as primary cardiomyocytes from a mouse model. In particular I aimed to study the effect of frataxin deficiency on the SR, as the major regulator of intracellular $Ca^{2+}$ uptake and release in heart cells, as well as to test any potential therapeutic measures based on the results obtained.

This report showed that frataxin knockdown in cardiomyocytes increases both cytosolic and mitochondrial ROS levels (Fig. 18). I then showed that my hypothesis that $Ca^{2+}$ homeostasis is affected in FRDA cardiomyocytes was supported. Specifically, a decrease in the SR $Ca^{2+}$ pool was fully established through two experimental procedures using measurement of cytosolic $Ca^{2+}$ levels. Caffeine was added to the cells to elicit the emptying of $Ca^{2+}$ from the SR via RYR2 receptors, and this established a decreased release of $Ca^{2+}$ from the SR in frataxin-deficient cells compared to controls (Fig. 23). Thapsigargin, a SERCA pump inhibitor, was used to prohibit the SR $Ca^{2+}$ pool from increasing, and indirectly confirmed a decrease in the SR $Ca^{2+}$ pool by observing reduced $Ca^{2+}$ leak through the ryanodine receptors in FRDA cells (Fig. 25). This decrease in SR $Ca^{2+}$ leak via ryanodine receptors had previously been observed in specific iron-overload conditions but not FRDA (Cherednichenko et al., 2004; Kawakami & Okabe, 1998). Finally, thapsigargin was used following a preincubation of the cells with dantrolene, a ryanodine receptor inhibitor, in order to assess the role of RYR2 dysfunction in the change in SR $Ca^{2+}$ content. Use of dantrolene maintained the significant difference in $Ca^{2+}$ response between control and FRDA-deficient cells observed using thapsigargin without dantrolene, but it significantly increased the amount of $Ca^{2+}$ in the SR store compared to sole use of thapsigargin (Figs. 26-27). These results showed that the RYR2 were not pathologically inhibited by dantrolene but are perhaps potentiated in FRDA as the SR $Ca^{2+}$ levels were nearly restored by dantrolene. Thus, the SR $Ca^{2+}$ pool decrease in FRDA was indicated to be at least partially caused by a defect in the RYR2.

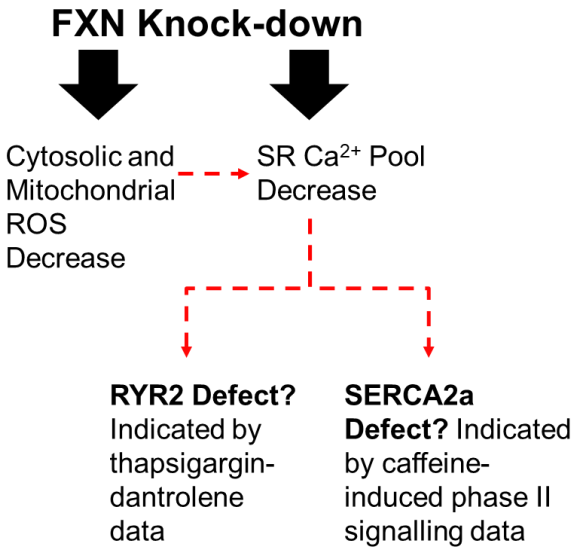


**Figure 29. Summary of Key Findings in FRDA Ca2+ Pathophysiology.**

These data were fully established in both the HL-1 and H9c2 cell FRDA models, but remain incompletely characterized in the primary cell models, although the preliminary data obtained thus far support the findings obtained in the cell models (Fig. 28). HL-1 cells, as adult cardiomyocytes, are a useful point of comparison with data from the H9c2 cells and the neonatal primary cells from the mouse model. That both cell models, and the data gathered on primary cells thus far, produce similar results shows that the FRDA pathophysiology associated with $Ca^{2+}$ level dysregulation may be present from an early age in patients, despite lack of symptoms until adolescence and early adulthood. This is supported by previous studies where the early embryonic lethality caused by total frataxin knockout in mouse models was not associated with mitochondrial iron accumulation (Cossee et al., 2000; Simon et al., 2004), indicating that FRDA pathogenesis is primarily determined by a subtle, early increase in redox-active mitochondrial iron. Given the indications from my study of $Ca^{2+}$ signalling in HL-1 and H9c2 cells, further data in primary cells from neonatal mice will be of great importance in confirming my original findings, as well as for developing potential novel FRDA therapies involving pharmacological manipulation of cellular $Ca^{2+}$ levels.

The SR $Ca^{2+}$ store depletion established in the FRDA-like cells is associated with and may be explained by the increase in both cytosolic and mitochondrial ROS levels in the two cell models, indicating increased oxidative stress (Figs. 18-19). FRDA cells are known to display an increased sensitivity to oxidative stress (Babcock et al., 1997; Condo et al., 2007; Tan et al., 2001; Wong et al., 1999), and in one case this has been linked to $Ca^{2+}$ dysregulation within the cell (Wong et al., 1999). Depressed SERCA2a function, leak through RYR2 on the SR surface and increased $Na^{+}$-$Ca^{2+}$ Exchanger (NCX) expression have previously been linked with SR $Ca^{2+}$ store depletion, cardiac contractile dysfunction and the resulting systolic heart failure and may be responsible for the cardiac symptoms of FRDA (Zima & Mazurek, 2016). The NCX may thus be another potential avenue of study in FRDA cardiac pathophysiology.

Several studies have detailed the sensitivity to oxidation of certain free cysteine (Cys) residues in the active site of both SERCA and RYR2 proteins, to which hydroxyl radicals can bind (Diaz et al., 2005; Marx et al., 2000; Xu et al., 1997; Ying et al., 2008; Zima & Mazurek, 2016). In cardiomyocytes, RYR2 are particularly important for SR $Ca^{2+}$ homeostasis, and it is known that a reduction in SR $Ca^{2+}$ content can be exacerbated by increased $Ca^{2+}$ leak through RYR2. RYR2 potentiation is indicated by the phase II $Ca^{2+}$ signalling after caffeine-response in HL-1 cells, indicating a probable energetic collapse of the $Ca^{2+}$-Induced $Ca^{2+}$-Release (CICR) process (Fig. 24). RYR2 potentiation is indicated as reducing SR $Ca^{2+}$ levels in this study. This may primarily be due to hyperphosphorylation of the RYR2, which has been associated with oxidative stress and shown to increase the probability of RyR opening (Zima & Mazurek, 2016). RYR2 potentiation may also be associated with increased oxidation, which has also been shown to enhance $Ca^{2+}$ release from cardiomyocytes (Oda et al., 2015).

A reduction in the SERCA2a paralog is strongly correlated with heart failure (Diaz et al., 2005), and thus may be involved in the intracellular $Ca^{2+}$ dysregulation. The Cys674 residue of the SERCA pump has been

observed to be a particularly crucial residue for oxidative regulation (Adachi et al., 2004; Sharov et al., 2006). Decreased SERCA function may be indicated by a compensatory increase in SERCA protein levels in HL-1 and H9c2 frataxin-deficient cells, although preliminary attempts to study this via Western blot experiments are not presented in this study due to unclear data. A further comparative measurement of the specific levels of the crucial Cys674 residue between control and frataxin-deficient cells would also be of great use in physiologically defining the precise role of the SERCA2a protein in the $Ca^{2+}$ dysregulation in FRDA. It will be important to establish whether the SR $Ca^{2+}$ content is primarily reduced by excessive $Ca^{2+}$ efflux through RYR2, or if both the RYR2 and SERCA pump have a pathological role in FRDA (Fig. 29). Given the nature of the direct link between decreased frataxin and increased sensitivity to oxidative stress, the data gathered thus far indicate that the iron-induced ROS pathway may play the dominant role in FRDA pathophysiology.

The results in this study can be corroborated with those of my colleague Dr Rosella Abeti, who discovered a partial inhibition of $[Ca^{2+}]_m$, as had been previously seen in other FRDA models (Bolinches-Amoros et al., 2014; Abeti et al, 2018). As thapsigargin had been shown to cause a gradual, detectable $Ca^{2+}$ leak from the SERCA into the cytosol, we wanted to see if mitochondrial $Ca^{2+}$ uptake was affected due to the SR-mitochondria microdomains (Csordas et al., 2006; Garcia-Perez et al., 2008). Together with the mitochondrial ROS data and TMRM data showing increased oxidative stress and increased mitochondrial depolarization in frataxin-deficient cells respectively (Fig. 19 & Fig. 22), this finding indicates that there may be an element of the cellular $Ca^{2+}$ dysregulation that will need to be explained at the mitochondrial level.

As cellular $Ca^{2+}$ homeostasis is intimately linked to mitochondrial function, bioenergetics impairment has also been claimed as the primary cause of FRDA cardiomyopathy (Perdomini et al., 2014; Puccio et al., 2001). However, this impairment may be fully mechanistically linked to the iron-induced ROS increase in FRDA. ROS levels were also shown to be

increased in the mitochondria in our study, which may also affect the mitochondrial $Ca^{2+}$ uniporter 1 (MCU), crucial for $[Ca^{2+}]_m$ uptake and known to be affected by high levels of oxidative stress (Dong et al., 2017). The RYR2 on the SR form microdomains with mitochondria in cardiomyocytes, which interact with and control local interorganellar $Ca^{2+}$ signalling in the cell (Csordas et al., 2006; Garcia-Perez et al., 2008). Thus, both the change in the SR $Ca^{2+}$ pool and the increase in oxidative stress discovered in this report is likely to affect mitochondrial function, including its role as the secondary cellular $Ca^{2+}$ buffer after the SR. It is also known that RYR2-mediated $Ca^{2+}$ fluxes control mitochondrial $Ca^{2+}$ and ATP levels in the cell (Bround et al., 2013), which may account for the changes in $[Ca^{2+}]_m$ observed.

Further studies on the effect of RYR2 alteration on mitochondrial $Ca^{2+}$ levels may be necessary to fully characterize the role of the RYR2 in the FRDA pathophysiological mechanism. Mitochondrial dysfunction is likely to both be at least partially responsible for and affected by the increased ROS levels observed in frataxin-deficient cardiomyocytes. The decreased mitochondrial ISC synthesis resulting from frataxin deficiency (Rotig et al., 1997) is expected to lead to reduced or faulty respiratory chain function and consequent ROS production due to the key role of the clusters in the structure and function of respiratory complexes I, II and III, and the protein aconitase. Decreased ISC synthesis has been directly associated with increased mitochondrial iron levels (Chen et al., 2004; Radisky et al., 1999), which itself can lead to increased free radical generation (Babcock et al., 1997; Cavadini et al., 2002) and create a vicious cycle alongside decreased respiratory chain function, leading to decreased ATP synthesis and cell death. Progressive cardiomyopathy in FRDA has also been proposed to result from iron-catalysed mitochondrial dysfunction (Michael et al., 2006).

$Ca^{2+}$ itself is known to stimulate three proteins of the tricarboxylic acid cycle, and thereby the electron transport chain, driving ATP synthesis. Thus, a $Ca^{2+}$ signaling defect in the cell could in theory be the cause, as

well as the consequence of mitochondrial dysfunction and an increase in ROS levels. A recent study by the Palau group indicated that $Ca^{2+}$ overload, in conjunction with oxidative stress and mitochondrial defects, may be directly responsible for neurological symptoms in FRDA (Molla et al., 2017). Mitochondrial ROS and a cellular dysregulation of $Ca^{2+}$ homeostasis via the SR may work in tandem to produce the FRDA cardiac phenotype. The $Ca^{2+}$- and ROS-based findings in this study are corroborated with the finding of a decreased NADH redox index in both FRDA cell models, indicating an $NAD^+$ depletion. The potential decrease in mitochondrial complex I activity could indicate a lower mitochondrial ETC activity, although more direct experiments on the production and activity of the mitochondrial complexes are needed in this FRDA model (Fig. 20-21). The NADH data should also be further corroborated with data on $FADH_2$ levels to obtain a more complete picture of the extent of mitochondrial ETC activity in FRDA cells. This finding allows the $Ca^{2+}$ levels to be considered alongside both the established FRDA physiological marker of mitochondrial dysfunction as well as that of oxidative stress, although more work is necessary to establish a causal link between them. Thus, the mechanics of the bioenergetics pathway must be further explored alongside the iron overload pathway in elucidating the precise role of $Ca^{2+}$ homeostasis in FRDA pathophysiology.

The iron-induced oxidative stress could lead to reduced peak systolic $Ca^{2+}$ levels, slowed rates of $Ca^{2+}$ relaxation, and elevated diastolic $Ca^{2+}$ levels, as observed in studies of other heart conditions associated with iron overload (Oudit et al., 2006; Schwartz et al., 2002). Although no conclusive findings were obtained regarding these symptoms in this study, increased spontaneous heart activity levels in HL-1 cells with the frataxin knockdown incorporated was observed via repeating $Ca^{2+}$ spikes. This has been shown to underlie arrhythmias and sudden death often in combination with a slowed $Ca^{2+}$ re-uptake in the sarcoplasmic reticulum (Payne et al., 2011). Unfortunately, a full comparative study of this effect necessitated a beating monolayer of cardiomyocytes in every cell type. This was only possible in an inconsistent manner in the early passages of HL-1 cell culture, and not

possible at all in the neonatal H9c2 cells and the neonatal primary cell cultures, which did not form beating monolayers. No difference was evident in basal $Ca^{2+}$ levels following Fxn knockdown either. Thus, further studies of potential pathological differences in $Ca^{2+}$ spike frequency as well as shifts in the pattern of $Ca^{2+}$ signaling during systole and diastole may require electrophysiological experiments and *in vivo* tests on primary cells or other cell models.

One potential further avenue for the study of $Ca^{2+}$ homeostasis imbalance in FRDA cardiomyocytes, in addition to study of the SR or RYR2, is looking at $Ca^{2+}$ flux in L-type $Ca^{2+}$ channels on the plasma membrane. In iron-overload conditions, free non-transferrin-bound iron has been shown to permeate through L-type $Ca^{2+}$ channels. The permeation of 0.5mM $Fe^{2+}$ (reactive ferrous iron) through the cardiac L-type $Ca^{2+}$ channels has been shown to cause a slowing of the $Ca^{2+}$ current inactivation, resulting in a 50% increase in net $Ca^{2+}$ influx and in the time integral of the $Ca^{2+}$ current in iron overload studies using cardiomyocytes (Lacampagne et al., 1995; Oudit et al., 2003; Shirotani et al., 2001). This may be a factor in the impaired diastolic function that occurs in early-stage iron overload. Higher concentrations of ferrous iron (2-4mM) elicit instead a reduction in the $Ca^{2+}$ current due to increased competition with the $Fe^{2+}$, leading to the systolic dysfunction seen in late-stage iron cardiomyopathy (Lacampagne et al., 1995). These findings may be of great relevance to the mechanism of cardiomyopathy in FRDA.

In addition, there is new potential for FRDA therapies that perform a pharmacological manipulation of cellular $Ca^{2+}$ levels. One potential therapy involves the lipid-soluble antioxidant vitamin E, that in conjunction with coenzyme Q10 (CoQ10) has shown a beneficial effect on mitochondrial bioenergetics in cardiomyocytes and muscle cells (Hart et al., 2005; Lodi, Rajagopalan, et al., 2001). Further experiments by Dr Rosella Abeti showed that the inhibition of $[Ca^{2+}]_m$ was rescued by application of the antioxidant vitamin E post-thapsigargin response in HL-1 frataxin-deficient cells (Abeti et al, 2018). Although these experiments are not presented in

this thesis, they greatly emphasise how oxidative stress and $Ca^{2+}$ deregulation are related in the FRDA model. A series of TUNEL experiments also indicated increased apoptosis following hypoxia-reoxygenation injury in frataxin-deficient cells compared to controls, and also showed prevention of apoptosis in these cells following vitamin E administration (Abeti et al, 2018). These results indicate a greater propensity for FRDA-like cells to suffer from hypoxia-reoxygenation injury, as occurs in FRDA (Payne et al., 2011), as well as a possible therapeutic role of vitamin E in treating the cardiac aspects of the disease.

Although vitamin E has been proposed as a therapy for the symptoms of FRDA cardiomyopathy, it was not previously considered due to a lack of natural history studies specifically on the cardiac symptoms of FRDA (Cooper & Schapira, 2007). A common current treatment for FRDA patients presenting with cardiac abnormalities is bisoprolol, which blocks beta-adrenergic receptors that are activated by the sympathetic nervous system. The sympathetic nervous system is activated during heart dysfunction in order to increase ionotropic support (including $Ca^{2+}$), which also increases oxidative stress leading to the potentiation of ryanodine receptor function (Rehsia & Dhalla, 2010). This mechanism is entirely consistent with the data from this study, and consequently a key therapeutic concern is to protect the heart muscle from oxidative stress and RYR2 potentiation via use of an antioxidant. These results support the hypothesis that defects in RYR2 function are the major contributor to the $Ca^{2+}$ dysregulation observed in the FRDA cardiomyocyte model used (Bolinches-Amoros et al., 2014; Mincheva-Tasheva et al., 2014; Zima & Mazurek, 2016), and adds weight to the proposal for vitamin E as a therapeutic factor in FRDA cardiomyopathy.

There is some indication in FRDA model DRG neurons that a cellular or mitochondrial $Ca^{2+}$ overload is specifically occurring, and therapies involving $Ca^{2+}$ chelators have been proposed in this model to prevent the dying-back neurodegeneration that occurs in FRDA DRG cells (Molla et al., 2017). However, the subtle, dynamic nature of $Ca^{2+}$ homeostasis in

heart cells, due to its crucial function in excitation-contraction coupling, makes a basic modulation of cellular $Ca^{2+}$ levels highly unlikely to be of use in restoring normal $Ca^{2+}$ homeostasis. Furthermore, $Ca^{2+}$ levels appear to be reduced in the cytosol and mitochondria in FRDA-like heart cells, not overloaded. Future potential therapies may need to be directed towards subcellular targets, such as modulating the function of $Ca^{2+}$ buffer organelles such as the SR and the mitochondria. The tight interconnection of the SR-mitochondrial network and its importance in heart function makes it likely that a successful therapy will be directed at this level. Therapy may become possible if specific residues or active sites of the SR or RYR2 are discovered that are affected by high ROS levels in FRDA model cardiomyocytes, which can then be specifically targeted to restore function alongside use of antioxidants such as idebenone or vitamin E to combat the symptoms of FRDA (Payne et al., 2011). Alternatively, due to the interconnection of dysregulated $Ca^{2+}$ levels with ROS levels and mitochondrial dysfunction, modulation of $Ca^{2+}$ levels may not be the only or necessary therapeutic target in resolving the cardiac phenotype in FRDA.

# Chapter 5 : Final Discussion

Over the around 150 years since the disease was first characterised as a unique disorder, the description of its genetic aetiology, pathophysiology and phenotype has developed. However, it was only in the 1970s that the understanding of the FRDA phenotype became detailed enough for a specific set of reliable diagnostic criteria to be drawn up (Geoffroy et al., 1976; Harding, 1981). It is only since the discovery of the genetic basis of the disease (Campuzano et al., 1996) that we have been able to perform genotype-phenotype correlations for FRDA patients, which revealed that the phenotype spectrum previously proposed for FRDA left out up to a quarter of FRDA cases due to their atypical symptoms. These symptoms included very early or very late disease onset, retained reflexes, spasticity and limited disease progression (Durr et al., 1996; Filla et al., 1997; McCabe et al., 2000; Schols et al., 1997). These genetic advancements also led to a more accurate genotype-phenotype characterisation, improving diagnostic accuracy and genetic counselling at a clinical level.

In the genetics study, out of a total of 2000 DNA samples from genetically undiagnosed ataxia patients not referred by their clinicians for an FRDA test (the largest study of its kind ever performed), only three were identified as having two pathological GAA expansions, and thus as positive for FRDA (0.15% of the cohort). This indicates that the risk that an ataxic patient, with symptoms atypical for FRDA, in fact has the FRDA genotype is extremely low, confirming my hypothesis made in Chapter 1. These data strengthen the current diagnostic model where the FRDA test is only carried out upon consultant referral. No point mutations and no exonic deletions were discovered among the 12 individuals with only one pathological GAA expansion, which was consistent with previous data. Thus, these 12 were confirmed as FRDA gene carriers, all of which were symptomatic for separate ataxic disorders. This gives a carrier rate of 0.6%, or 1/167. A large variation has previously been seen in carrier frequency, with which the carrier frequency of this study is broadly compatible.

The three FRDA-positive patients display atypical symptoms for classical FRDA, and their late age at onset also suggests that disease progression is slower in these patients. This is all consistent with a diagnosis of LOFA (in one patient, who had an age of onset of around 25) and VLOFA (in the other two patients, who both had ages of onset of over 50). This FRDA variant is phenotypically distinct from classical FRDA, and is characterised by a milder phenotype, slower disease progression and a more variable set of symptoms, all of which are the case in the three FRDA-positive patients. In one case, the ataxia was attributed to excessive alcoholism, and in the other two it is possible unusual symptoms such as blackouts may have confused the clinicians. Nevertheless, it could be argued that these patients should have been referred for an FRDA test in any case, especially when environmental factors may obscure the role of any genetic factor, as with the patient suffering from alcoholism. The well-being of the patient, as well as any potential therapeutic benefit in future, rests upon a correct diagnosis.

There is an extremely small chance that FRDA patients with exonic deletions may not have been detected, and alternative testing may need to be carried out in future to rule out this possibility with certainty. The extremely small expansion size in five of the six alleles from my three FRDA-positive patients is a confirmation of the strong correlation between expansion size and disease severity (including incidence of cardiomyopathy), and its inverse correlation with age at onset (Durr et al., 1996; Filla et al., 1997; Montermini et al., 1997; Rajagopalan et al., 2010). This is broadly compatible with the knowledge that 50% of variability in age at onset has been shown to be caused by expansion size (Filla et al., 1997). The great variety in the age at onset between one of the FRDA patients in my study and their sibling indicated that further study of intrafamilial cases may shed light on the clinical heterogeneity of FRDA and the importance of other factors in determining the severity. However, the sibling was originally diagnosed with multiple sclerosis, and although an actual FRDA diagnosis is extremely likely retrospectively (see Chapter 3, Discussion), it is not yet confirmed by the data. Intrafamilial variety in

GAA expansion size may be explained by somatic mosaicism and interruptions in the expansion as well as other reasons (Pandolfo, 1999), all of which warrant further study in FRDA genetic research. Ultimately however, the clinical symptoms presented in my genetic screening, in addition to the study performed on the other cohort of patients who were originally referred for FRDA by Dr M. H. Parkinson, bear out the theory that the FRDA patient phenotype is almost fully accounted for by the current genotype-phenotype characterisation of FRDA, including crucially its variant LOFA/VLOFA form. Despite the clinical heterogeneity of FRDA, it is consistent and diagnosable enough to make the risk of misdiagnosing atypical FRDA patients very low indeed. The data also strengthens the already well-established point that atypical cases of FRDA are almost always caused by extremely small or large GAA expansion sizes (Parkinson et al., 2013).

This thesis also describes an expansion and clarification of the current knowledge of the pathways involved in FRDA pathophysiology. Although frataxin is a multifunctional protein, it was known that the major functional role of frataxin is in ISC biogenesis (Puccio et al., 2001; Rotig et al., 1997). ISC deficiency is linked to an increasing amount of diseases as it can lead to multiple, aggregating cellular dysfunctions (Lill, 2009). Mitochondrial iron accumulation is linked with ISC deficiency in yeast studies (Chen et al., 2004; Radisky et al., 1999), although it is detected after the original ISC defects (Puccio et al., 2001). This mitochondrial iron accumulation has been more established in FRDA cardiac pathology studies than in ones focusing on the neurology. It is in turn linked with increased oxidative stress (Abeti et al., 2016; Bradley et al., 2004; Emond et al., 2000; Schulz et al., 2000), the potential major causal factor in the cell degeneration and death that presents in FRDA (Chen et al., 2004; Schulz & Pandolfo, 2013). Oxidative stress has more recently been associated with abnormal $Ca^{2+}$ homeostasis in FRDA (Gonzalez-Cabo & Palau, 2013).

This has been explored for the first time in cardiomyocytes in this thesis, which has established a key role for cellular $Ca^{2+}$ dysregulation in FRDA

cell degeneration and death (confirming my original hypothesis in Chapter 1), that is partially rescued with the administration of vitamin E. All experiments were carried out and compared in two separate FRDA rodent cellular model populations, one neonatal (H9c2) and one adult (HL-1). They modelled FRDA via knockdown of the frataxin gene using siRNA. A lower $Ca^{2+}$ leak from the sarcoplasmic reticulum through the ryanodine receptors and a lower sarcoplasmic reticulum $Ca^{2+}$ content was established using caffeine and thapsigargin respectively. These data can be inserted into the current framework of FRDA research, given my other findings of an increase in ROS levels in both models indicating that the $Ca^{2+}$ deregulation may be due to the effect of pathological levels of oxidative stress previously observed in the disease. These findings are among the first that have found a change in $Ca^{2+}$ levels alongside the established oxidative stress data in FRDA. More work is now necessary to establish a causal link between them. I also collected important data from FRDA model YG8R mouse primary cells on the thapsigargin-induced $Ca^{2+}$ response: however, ROS activity and NADH level measurements will be required to complete the physiological picture in those cells. Given the indications from my study of $Ca^{2+}$ signalling in FRDA-like cell lines, these further data in FRDA model primary cells from neonatal mice will be of great importance in verifying my original findings.

The finding of a decreased SR $Ca^{2+}$ content in FRDA-like cardiomyocytes corresponded with previous findings in heart cells following oxidative damage, including an increased SR $Ca^{2+}$ leak through RYR2 in SR vesicles isolated from canine cardiac muscle (Kawakami & Okabe, 1998) as well as from rat ventricular cardiomyocytes (Cherednichenko et al., 2004). An imbalance in $[Ca^{2+}]_m$ and a decreased depolarisation in $\Delta\psi_m$ was also discovered by my colleague Dr Abeti in frataxin-deficient cells, which could be rescued by preincubating the cells with vitamin E (Abeti et al, 2018). A link between $Ca^{2+}$, mitochondrial dysfunction and oxidative stress has already been detected in studies on FRDA model DRG neurons (Molla et al., 2017), indicating a possible future research avenue in FRDA cardiomyopathy studies. However, as it is also known the heart defects

present in FRDA are associated with iron-induced oxidative stress and $Ca^{2+}$ dysregulation in other disorders relevant to my study (Oudit et al., 2006; Schwartz et al., 2002), it will be important to understand the precise pathophysiological mechanism of $Ca^{2+}$ dysregulation in the disease. It is still unclear whether the primary pathological result of frataxin deficiency is directly oxidative stress and increased ROS hypersensitivity leading to ISC loss, iron overload, and cell death, or whether oxidative stress is only an indirect result of iron overload or indeed ISC loss itself (Figure 4, Chapter 1). A role for the directly increased ROS sensitivity of frataxin-deficient cells is implied but not confirmed by my results concerning RYR2 function in the heart, which indicate that specific residues of the protein may be particularly sensitive to severe oxidation. It is already known that frataxin has a specific role in protection against iron-induced oxidative damage (Gakh et al., 2006; O'Neill et al., 2005).

Future studies should focus more specifically on the cysteine residues of the SERCA (such as Cys674) and RYR2 which are directly affected by oxidative stress, in order to confirm the crucial pathophysiological role of ROS hypersensitivity in FRDA, understand which residues are most crucial to the FRDA pathology, and clarify what role the SERCA pump has in FRDA in addition to the role of the RYR2. The potential discovery of a role in FRDA for specific residues in the RYR2 and SERCA also has clear therapeutic benefits. Given the close relationship between the SR and the mitochondria in heart muscle cells, further studies linking the effect of RYR2 potentiation with mitochondrial $Ca^{2+}$ levels may be highly useful in more fully characterising the role of the RYR2 in the FRDA pathophysiological mechanism. The decrease in the SR $Ca^{2+}$ pool is likely to affect the role of the mitochondria as the secondary cellular $Ca^{2+}$ buffer after the SR, as also indicated by the increased mitochondrial ROS levels. The potentially pathological difference in the phase II response of $Ca^{2+}$ spike frequency following caffeine application indicates a potential difference in electrical spark activity in the heart that may be further understood through future electrophysiological studies and *in vivo* tests, which may be able to explain specific shifts in the pattern of $Ca^{2+}$ signalling

during heart systole and diastole better than physiological experiments. Hypoxia-reoxygenation injury was accentuated in frataxin-deficient cells, and experiments by my colleague Dr Abeti showed that this could be partially rescued by vitamin E administration (Abeti et al, 2018). Thus, vitamin E, for which former proposals as a therapeutic route for FRDA cardiomyopathy had lacked robustness due to a lack of natural history studies on that aspect of the condition, emerged more strongly as a potential FRDA therapy (Cooper & Schapira, 2007). This study supports the hypothesis that $Ca^{2+}$ homeostasis is affected in FRDA and forms a gateway to further work alongside the recent Mollá paper (Molla et al., 2017).

The data showing a decrease in intracellular $Ca^{2+}$ levels corresponds with previous studies carried out in FRDA-like DRG neurons (Mincheva-Tasheva et al., 2013; Molla et al., 2017). The data showing a decreased $[Ca^{2+}]_m$ with lower frataxin levels in heart cells corresponds with previous data in 3T3-L1 adipocytes, which showed a direct correlation between frataxin levels and mitochondrial $Ca^{2+}$ buffer capacity (Bolinches-Amoros et al., 2014). Although this is a notable step forward, there are various directions future FRDA research could take to build upon our current knowledge. Oxidative stress has been shown to incur SERCA pump inhibition in SR vesicles isolated from rabbit cardiac and skeletal muscle (Xu et al., 1997) as well as guinea pig ventricular cardiomyocytes (Goldhaber & Qayyum, 2000). Further experiments on SERCA pump function could prove useful for understanding the relative responsibility for the RYR2 defect in FRDA pathophysiology. Oxidative stress has also elicited a reduced L-type $Ca^{2+}$ current in guinea pig ventricular cardiomyocytes (Lacampagne et al., 1995). As $Ca^{2+}$ influx occurs mostly through L-type $Ca^{2+}$ channels in cardiomyocytes, it will be important to study whether the $Ca^{2+}$ influx rate or perhaps L-type channel function itself is affected in FRDA. Also, a previous study showed that mitochondrial ROS levels can function as a bidirectional regulator of $Ca^{2+}$ sparks in both a dose- and time-dependent manner (Yan et al., 2008). As mitochondrial

ROS levels appear to increase in FRDA-like cardiomyocytes, it would be interesting to more closely study the relationship between ROS levels and $Ca^{2+}$ spark frequency and observe if mitochondrial ROS levels are particularly related to the $Ca^{2+}$ dysregulation observed. The ROS generation and associated $Ca^{2+}$ dysregulation may also itself cause iron accumulation, meaning a study of iron levels in FRDA-like cardiomyocytes could provide more detail concerning the precise pathophysiology of the disease in heart cells.

Ultimately, studies previously carried out by the Giunti group (Abeti et al., 2016; Abeti et al., 2015) had already shown that a potential FRDA therapy need not address the ISC deficit directly, as FRDA model mouse cerebellar granular neurons were rescued from their toxic ROS-based pathophysiology by blocking lipid peroxidation and activation of mitochondrial antioxidant pathways. A further publication by myself and my colleagues in the Giunti group may be added to this thesis as the initation of the study of $Ca^{2+}$ signaling in FRDA-model heart cells (Abeti et al, 2018). In neurons as in heart cells, it may be that the most clinically relevant of the multiple physiological pathways in FRDA is that driven by increased oxidative stress. In the heart, this pathway is intimately connected with $Ca^{2+}$ dysregulation at the level of the SR-mitochondria microdomain, and now more work is needed to understand its precise pathophysiology.

# References


Abeti, R., Brown, A. F., Maiolino, M., Giunti, P. (2018). Calcium deregulation: novel insights to understand Friedreich's ataxia pathophysiology. *Frontiers in Neuroscience*, *12,* 264. https://doi.org/10.3389/fncel.2018.00264

Abeti, R., Parkinson, M. H., Hargreaves, I. P., Angelova, P. R., Sandi, C., Pook, M. A., … Abramov, A. Y. (2016). "Mitochondrial energy imbalance and lipid peroxidation cause cell death in Friedreich's ataxia". *Cell Death & Disease*, *7*, e2237. https://doi.org/10.1038/cddis.2016.111

Abeti, R., Uzun, E., Renganathan, I., Honda, T., Pook, M. A., & Giunti, P. (2015). Targeting lipid peroxidation and mitochondrial imbalance in Friedreich's ataxia. *Pharmacological Research*, *99*, 344–350. https://doi.org/10.1016/j.phrs.2015.05.015

Ackroyd, R. S., Finnegan, J. A., & Green, S. H. (1984). Friedreich's ataxia. A clinical review with neurophysiological and echocardiographic findings. *Archives of Disease in Childhood*, *59*(3), 217–221.

Adachi, T., Pimentel, D. R., Heibeck, T., Hou, X., Lee, Y. J., Jiang, B., … Cohen, R. A. (2004). S-glutathiolation of Ras mediates redox-sensitive signaling by angiotensin II in vascular smooth muscle cells. *The Journal of Biological Chemistry*, *279*(28), 29857–29862. https://doi.org/10.1074/jbc.M313320200

Adamec, J., Rusnak, F., Owen, W. G., Naylor, S., Benson, L. M., Gacy, A. M., & Isaya, G. (2000). Iron-dependent self-assembly of recombinant yeast frataxin: implications for Friedreich ataxia. *American Journal of Human Genetics*, *67*(3), 549–562. https://doi.org/10.1086/303056

Adinolfi, S., Iannuzzi, C., Prischi, F., Pastore, C., Iametti, S., Martin, S. R., … Pastore, A. (2009). Bacterial frataxin CyaY is the gatekeeper of iron-sulfur cluster formation catalyzed by IscS. *Nature Structural & Molecular Biology*, *16*(4), 390–396. https://doi.org/10.1038/nsmb.1579

Akhlaghi, H., Corben, L., Georgiou-Karistianis, N., Bradshaw, J., Storey, E., Delatycki, M. B., & Egan, G. F. (2011). Superior cerebellar peduncle atrophy in Friedreich's ataxia correlates with disease symptoms. *Cerebellum (London, England)*, *10*(1), 81–87. https://doi.org/10.1007/s12311-010-0232-3

Al-Mahdawi, S., Pinto, R. M., Ismail, O., Varshney, D., Lymperi, S., Sandi, C., … Pook, M. (2008). The Friedreich ataxia GAA repeat expansion mutation induces comparable epigenetic changes in human and transgenic mouse brain and heart tissues. *Human Molecular Genetics*, *17*(5), 735–746. https://doi.org/10.1093/hmg/ddm346

Al-Mahdawi, S., Pinto, R. M., Varshney, D., Lawrence, L., Lowrie, M. B., Hughes, S., … Pook, M. A. (2006). GAA repeat expansion mutation mouse models of Friedreich ataxia exhibit oxidative stress leading to progressive neuronal and cardiac pathology. *Genomics*, *88*(5), 580–590. https://doi.org/10.1016/j.ygeno.2006.06.015

Andermann, E., Remillard, G. M., Goyer, C., Blitzer, L., Andermann, F., & Barbeau, A. (1976). Genetic and family studies in Friedreich's ataxia.

*The Canadian Journal of Neurological Sciences. Le Journal Canadien Des Sciences Neurologiques*, *3*(4), 287–301.
Anderson, P. R., Kirby, K., Orr, W. C., Hilliker, A. J., & Phillips, J. P. (2008). Hydrogen peroxide scavenging rescues frataxin deficiency in a Drosophila model of Friedreich's ataxia. *Proceedings of the National Academy of Sciences of the United States of America*, *105*(2), 611–616. https://doi.org/10.1073/pnas.0709691105
Anheim, M., Mariani, L.-L., Calvas, P., Cheuret, E., Zagnoli, F., Odent, S., … Koenig, M. (2012). Exonic deletions of FXN and early-onset Friedreich ataxia. *Archives of Neurology*, *69*(7), 912–916. https://doi.org/10.1001/archneurol.2011.834
Babcock, M., de Silva, D., Oaks, R., Davis-Kaplan, S., Jiralerspong, S., Montermini, L., … Kaplan, J. (1997). Regulation of mitochondrial iron accumulation by Yfh1p, a putative homolog of frataxin. *Science (New York, N.Y.)*, *276*(5319), 1709–1712.
Berciano, J., Infante, J., Garcia, A., Polo, J. M., Volpini, V., & Combarros, O. (2005). Very late-onset Friedreich's ataxia with minimal GAA1 expansion mimicking multiple system atrophy of cerebellar type. *Movement Disorders : Official Journal of the Movement Disorder Society*, *20*(12), 1643–1645. https://doi.org/10.1002/mds.20644
Berciano, J., Mateo, I., De Pablos, C., Polo, J. M., & Combarros, O. (2002). Friedreich ataxia with minimal GAA expansion presenting as adult-onset spastic ataxia. *Journal of the Neurological Sciences*, *194*(1), 75–82.
Berridge, M. J., Bootman, M. D., & Roderick, H. L. (2003). Calcium signalling: dynamics, homeostasis and remodelling. *Nature Reviews. Molecular Cell Biology*, *4*(7), 517–529. https://doi.org/10.1038/nrm1155
Bhidayasiri, R., Perlman, S. L., Pulst, S.-M., & Geschwind, D. H. (2005). Late-onset Friedreich ataxia: phenotypic analysis, magnetic resonance imaging findings, and review of the literature. *Archives of Neurology*, *62*(12), 1865–1869. https://doi.org/10.1001/archneur.62.12.1865
Bidichandani, S. I., Ashizawa, T., & Patel, P. I. (1997, May). Atypical Friedreich ataxia caused by compound heterozygosity for a novel missense mutation and the GAA triplet-repeat expansion. *American Journal of Human Genetics*. United States.
Bolinches-Amoros, A., Molla, B., Pla-Martin, D., Palau, F., & Gonzalez-Cabo, P. (2014). Mitochondrial dysfunction induced by frataxin deficiency is associated with cellular senescence and abnormal calcium metabolism. *Frontiers in Cellular Neuroscience*, *8*, 124. https://doi.org/10.3389/fncel.2014.00124
Bootman, M. D., Lipp, P., & Berridge, M. J. (2001). The organisation and functions of local Ca 2 + signals, *3*.
Bourke, T., & Keane, D. (2011). Friedreich's Ataxia: a review from a cardiology perspective. *Irish Journal of Medical Science*, *180*(4), 799–805. https://doi.org/10.1007/s11845-011-0744-y
Bradley, J. L., Blake, J. C., Chamberlain, S., Thomas, P. K., Cooper, J. M., & Schapira, A. H. (2000). Clinical, biochemical and molecular genetic correlations in Friedreich's ataxia. *Human Molecular*

*Genetics*, *9*(2), 275–282.
Bradley, J. L., Homayoun, S., Hart, P. E., Schapira, A. H. V, & Cooper, J. M. (2004). Role of oxidative damage in Friedreich's ataxia. *Neurochemical Research*, *29*(3), 561–567.
Branda, S. S., Cavadini, P., Adamec, J., Kalousek, F., Taroni, F., & Isaya, G. (1999). Yeast and human frataxin are processed to mature form in two sequential steps by the mitochondrial processing peptidase. *The Journal of Biological Chemistry*, *274*(32), 22763–22769.
Bridwell-Rabb, J., Fox, N. G., Tsai, C.-L., Winn, A. M., & Barondeau, D. P. (2014). Human frataxin activates Fe-S cluster biosynthesis by facilitating sulfur transfer chemistry. *Biochemistry*, *53*(30), 4904–4913. https://doi.org/10.1021/bi500532e
Bridwell-Rabb, J., Winn, A. M., & Barondeau, D. P. (2011). Structure-function analysis of Friedreich's ataxia mutants reveals determinants of frataxin binding and activation of the Fe-S assembly complex. *Biochemistry*, *50*(33), 7265–7274. https://doi.org/10.1021/bi200895k
Brigatti, K. W., Deutsch, E. C., Lynch, D. R., & Farmer, J. M. (2012). Novel diagnostic paradigms for Friedreich ataxia. *Journal of Child Neurology*, *27*(9), 1146–1151. https://doi.org/10.1177/0883073812448440
Bround, M. J., Wambolt, R., Luciani, D. S., Kulpa, J. E., Rodrigues, B., Brownsey, R. W., … Johnson, J. D. (2013). Cardiomyocyte ATP production, metabolic flexibility, and survival require calcium flux through cardiac ryanodine receptors in vivo. *The Journal of Biological Chemistry*, *288*(26), 18975–18986. https://doi.org/10.1074/jbc.M112.427062
Bulteau, A.-L., O'Neill, H. A., Kennedy, M. C., Ikeda-Saito, M., Isaya, G., & Szweda, L. I. (2004). Frataxin acts as an iron chaperone protein to modulate mitochondrial aconitase activity. *Science (New York, N.Y.)*, *305*(5681), 242–245. https://doi.org/10.1126/science.1098991
Bunse, M., Bit-Avragim, N., Riefflin, A., Perrot, A., Schmidt, O., Kreuz, F. R., … Osterziel, K. J. (2003). Cardiac energetics correlates to myocardial hypertrophy in Friedreich's ataxia. *Annals of Neurology*, *53*(1), 121–123. https://doi.org/10.1002/ana.10419
Calmels, N., Schmucker, S., Wattenhofer-Donze, M., Martelli, A., Vaucamps, N., Reutenauer, L., … Puccio, H. (2009). The first cellular models based on frataxin missense mutations that reproduce spontaneously the defects associated with Friedreich ataxia. *PloS One*, *4*(7), e6379. https://doi.org/10.1371/journal.pone.0006379
Campuzano, V., Montermini, L., Lutz, Y., Cova, L., Hindelang, C., Jiralerspong, S., … Koenig, M. (1997). Frataxin is reduced in Friedreich ataxia patients and is associated with mitochondrial membranes. *Human Molecular Genetics*, *6*(11), 1771–1780.
Campuzano, V., Montermini, L., Molto, M. D., Pianese, L., Cossee, M., Cavalcanti, F., … Pandolfo, M. (1996). Friedreich's ataxia: autosomal recessive disease caused by an intronic GAA triplet repeat expansion. *Science (New York, N.Y.)*, *271*(5254), 1423–1427.
Carroll, W. M., Kriss, A., Baraitser, M., Barrett, G., & Halliday, A. M. (1980). The incidence and nature of visual pathway involvement in Friedreich's ataxia. A clinical and visual evoked potential study of 22

patients. *Brain : A Journal of Neurology*, *103*(2), 413–434.
Castaldo, I., Pinelli, M., Monticelli, A., Acquaviva, F., Giacchetti, M., Filla, A., … Cocozza, S. (2008). DNA methylation in intron 1 of the frataxin gene is related to GAA repeat length and age of onset in Friedreich ataxia patients. *Journal of Medical Genetics*, *45*(12), 808–812. https://doi.org/10.1136/jmg.2008.058594
Cavadini, P., Adamec, J., Taroni, F., Gakh, O., & Isaya, G. (2000). Two-step processing of human frataxin by mitochondrial processing peptidase. Precursor and intermediate forms are cleaved at different rates. *The Journal of Biological Chemistry*, *275*(52), 41469–41475. https://doi.org/10.1074/jbc.M006539200
Cavadini, P., O'Neill, H. A., Benada, O., & Isaya, G. (2002). Assembly and iron-binding properties of human frataxin, the protein deficient in Friedreich ataxia. *Human Molecular Genetics*, *11*(3), 217–227.
Chamberlain, S., Shaw, J., Rowland, A., Wallis, J., South, S., Nakamura, Y., … Williamson, R. (1988). Mapping of mutation causing Friedreich's ataxia to human chromosome 9. *Nature*, *334*(6179), 248–250. https://doi.org/10.1038/334248a0
Chen, O. S., Crisp, R. J., Valachovic, M., Bard, M., Winge, D. R., & Kaplan, J. (2004). Transcription of the yeast iron regulon does not respond directly to iron but rather to iron-sulfur cluster biosynthesis. *The Journal of Biological Chemistry*, *279*(28), 29513–29518. https://doi.org/10.1074/jbc.M403209200
Cherednichenko, G., Zima, A. V, Feng, W., Schaefer, S., Blatter, L. A., & Pessah, I. N. (2004). NADH oxidase activity of rat cardiac sarcoplasmic reticulum regulates calcium-induced calcium release. *Circulation Research*, *94*(4), 478–486. https://doi.org/10.1161/01.RES.0000115554.65513.7C
Ciotti, P., Maria, E. Di, & Bellone, E. (2004). Triplet repeat primed PCR (TP PCR) in molecular diagnostic testing for Friedreich ataxia. *… of Molecular Diagnostics*, *6*(4), 285–289. Retrieved from http://www.sciencedirect.com/science/article/pii/S1525157810605235
Claycomb, W. C., Lanson, N. A. J., Stallworth, B. S., Egeland, D. B., Delcarpio, J. B., Bahinski, A., & Izzo, N. J. J. (1998). HL-1 cells: a cardiac muscle cell line that contracts and retains phenotypic characteristics of the adult cardiomyocyte. *Proceedings of the National Academy of Sciences of the United States of America*, *95*(6), 2979–2984.
Condo, I., Malisan, F., Guccini, I., Serio, D., Rufini, A., & Testi, R. (2010). Molecular control of the cytosolic aconitase/IRP1 switch by extramitochondrial frataxin. *Human Molecular Genetics*, *19*(7), 1221–1229. https://doi.org/10.1093/hmg/ddp592
Condo, I., Ventura, N., Malisan, F., Rufini, A., Tomassini, B., & Testi, R. (2007). In vivo maturation of human frataxin. *Human Molecular Genetics*, *16*(13), 1534–1540. https://doi.org/10.1093/hmg/ddm102
Cook, J. D., Bencze, K. Z., Jankovic, A. D., Crater, A. K., Busch, C. N., Bradley, P. B., … Stemmler, T. L. (2006). Monomeric yeast frataxin is an iron-binding protein. *Biochemistry*, *45*(25), 7767–7777. https://doi.org/10.1021/bi060424r

Cook, J. D., Kondapalli, K. C., Rawat, S., Childs, W. C., Murugesan, Y., Dancis, A., & Stemmler, T. L. (2010). Molecular details of the yeast frataxin-Isu1 interaction during mitochondrial Fe-S cluster assembly. *Biochemistry*, *49*(40), 8756–8765. https://doi.org/10.1021/bi1008613

Cooper, J. M., & Schapira, A. H. V. (2007). Friedreich's ataxia: coenzyme Q10 and vitamin E therapy. *Mitochondrion*, *7 Suppl*, S127-35. https://doi.org/10.1016/j.mito.2007.04.001

Coppola, G., De Michele, G., Cavalcanti, F., Pianese, L., Perretti, A., Santoro, L., … Filla, A. (1999). Why do some Friedreich's ataxia patients retain tendon reflexes? A clinical, neurophysiological and molecular study. *Journal of Neurology*, *246*(5), 353–357.

Coppola, G., Marmolino, D., Lu, D., Wang, Q., Cnop, M., Rai, M., … Geschwind, D. H. (2009). Functional genomic analysis of frataxin deficiency reveals tissue-specific alterations and identifies the PPARgamma pathway as a therapeutic target in Friedreich's ataxia. *Human Molecular Genetics*, *18*(13), 2452–2461. https://doi.org/10.1093/hmg/ddp183

Correia, A. R., Pastore, C., Adinolfi, S., Pastore, A., & Gomes, C. M. (2008). Dynamics, stability and iron-binding activity of frataxin clinical mutants. *The FEBS Journal*, *275*(14), 3680–3690. https://doi.org/10.1111/j.1742-4658.2008.06512.x

Cossee, M., Durr, A., Schmitt, M., Dahl, N., Trouillas, P., Allinson, P., … Pandolfo, M. (1999). Friedreich's ataxia: point mutations and clinical presentation of compound heterozygotes. *Annals of Neurology*, *45*(2), 200–206.

Cossee, M., Puccio, H., Gansmuller, A., Koutnikova, H., Dierich, A., LeMeur, M., … Koenig, M. (2000). Inactivation of the Friedreich ataxia mouse gene leads to early embryonic lethality without iron accumulation. *Human Molecular Genetics*, *9*(8), 1219–1226.

Cossee, M., Schmitt, M., Campuzano, V., Reutenauer, L., Moutou, C., Mandel, J. L., & Koenig, M. (1997). Evolution of the Friedreich's ataxia trinucleotide repeat expansion: founder effect and premutations. *Proceedings of the National Academy of Sciences of the United States of America*, *94*(14), 7452–7457.

Csordas, G., Renken, C., Varnai, P., Walter, L., Weaver, D., Buttle, K. F., … Hajnoczky, G. (2006). Structural and functional features and significance of the physical linkage between ER and mitochondria. *The Journal of Cell Biology*, *174*(7), 915–921. https://doi.org/10.1083/jcb.200604016

De Biase, I., Rasmussen, A., Endres, D., Al-Mahdawi, S., Monticelli, A., Cocozza, S., … Bidichandani, S. I. (2007). Progressive GAA expansions in dorsal root ganglia of Friedreich's ataxia patients. *Annals of Neurology*, *61*(1), 55–60. https://doi.org/10.1002/ana.21052

De Castro, M., Garcia-Planells, J., Monros, E., Canizares, J., Vazquez-Manrique, R., Vilchez, J. J., … Palau, F. (2000). Genotype and phenotype analysis of Friedreich's ataxia compound heterozygous patients. *Human Genetics*, *106*(1), 86–92.

De Michele, G., Di Maio, L., Filla, A., Majello, M., Cocozza, S., Cavalcanti, F., … Campanella, G. (1996). Childhood onset of

Friedreich ataxia: a clinical and genetic study of 36 cases. *Neuropediatrics*, *27*(1), 3–7. https://doi.org/10.1055/s-2007-973740

De Michele, G., Filla, A., Cavalcanti, F., Di Maio, L., Pianese, L., Castaldo, I., … Campanella, G. (1994). Late onset Friedreich's disease: clinical features and mapping of mutation to the FRDA locus. *Journal of Neurology, Neurosurgery, and Psychiatry*, *57*(8), 977–979.

Delatycki, M. B., & Corben, L. A. (2012). Clinical features of Friedreich ataxia. *Journal of Child Neurology*, *27*(9), 1133–1137. https://doi.org/10.1177/0883073812448230

Delatycki, M. B., Paris, D. B., Gardner, R. J., Nicholson, G. A., Nassif, N., Storey, E., … Forrest, S. M. (1999). Clinical and genetic study of Friedreich ataxia in an Australian population. *American Journal of Medical Genetics*, *87*(2), 168–174.

Deutsch, E. C., Santani, A. B., Perlman, S. L., Farmer, J. M., Stolle, C. A., Marusich, M. F., & Lynch, D. R. (2010). A rapid, noninvasive immunoassay for frataxin: utility in assessment of Friedreich ataxia. *Molecular Genetics and Metabolism*, *101*(2–3), 238–245. https://doi.org/10.1016/j.ymgme.2010.07.001

Diaz, M. E., Graham, H. K., O'neill, S. C., Trafford, A. W., & Eisner, D. A. (2005). The control of sarcoplasmic reticulum Ca content in cardiac muscle. *Cell Calcium*, *38*(3–4), 391–396. https://doi.org/10.1016/j.ceca.2005.06.017

Dong, Z., Shanmughapriya, S., Tomar, D., Siddiqui, N., Lynch, S., Nemani, N., … Madesh, M. (2017). Mitochondrial Ca(2+) Uniporter Is a Mitochondrial Luminal Redox Sensor that Augments MCU Channel Activity. *Molecular Cell*, *65*(6), 1014–1028.e7. https://doi.org/10.1016/j.molcel.2017.01.032

Duby, G., Foury, F., Ramazzotti, A., Herrmann, J., & Lutz, T. (2002). A non-essential function for yeast frataxin in iron-sulfur cluster assembly. *Human Molecular Genetics*, *11*(21), 2635–2643.

Durr, A., Cossee, M., Agid, Y., Campuzano, V., Mignard, C., Penet, C., … Koenig, M. (1996). Clinical and genetic abnormalities in patients with Friedreich's ataxia. *The New England Journal of Medicine*, *335*(16), 1169–1175. https://doi.org/10.1056/NEJM199610173351601

Dutka, D. P., Donnelly, J. E., Nihoyannopoulos, P., Oakley, C. M., & Nunez, D. J. (1999). Marked variation in the cardiomyopathy associated with Friedreich's ataxia. *Heart (British Cardiac Society)*, *81*(2), 141–147.

Dutka, D. P., Donnelly, J. E., Palka, P., Lange, A., Nunez, D. J., & Nihoyannopoulos, P. (2000). Echocardiographic characterization of cardiomyopathy in Friedreich's ataxia with tissue Doppler echocardiographically derived myocardial velocity gradients. *Circulation*, *102*(11), 1276–1282.

Dyck, P. J., Gutrecht, J. A., Bastron, J. A., Karnes, W. E., & Dale, A. J. (1968). Histologic and teased-fiber measurements of sural nerve in disorders of lower motor and primary sensory neurons. *Mayo Clinic Proceedings*, *43*(2), 81–123.

Emond, M., Lepage, G., Vanasse, M., & Pandolfo, M. (2000). Increased levels of plasma malondialdehyde in Friedreich ataxia. *Neurology*,

*55*(11), 1752–1753.
Endo, M., & Thorens, S. (1975). Release of calcium from the sarcoplasmic reticulum induced by hypotonic solutions. *Nihon Seirigaku Zasshi. Journal of the Physiological Society of Japan*, *37*(12), 422–424.
Entezam, M., Amirfiroozi, A., Togha, M., & Keramatipour, M. (2017). Comparison of Two Different PCR-based Methods for Detection of GAA Expansions in Frataxin Gene. *Iranian Journal of Public Health*, *46*(2), 222–228.
Epplen, C., Epplen, J. T., Frank, G., Miterski, B., Santos, E. J., & Schols, L. (1997). Differential stability of the (GAA)n tract in the Friedreich ataxia (STM7) gene. *Human Genetics*, *99*(6), 834–836.
Ermak, G., & Davies, K. J. A. (2002). Calcium and oxidative stress: from cell signaling to cell death. *Molecular Immunology*, *38*(10), 713–721.
Evans-Galea, M. V, Carrodus, N., Rowley, S. M., Corben, L. A., Tai, G., Saffery, R., … Sarsero, J. P. (2012). FXN methylation predicts expression and clinical outcome in Friedreich ataxia. *Annals of Neurology*, *71*(4), 487–497. https://doi.org/10.1002/ana.22671
Fabiato, A., & Fabiato, F. (1975). Contractions induced by a calcium-triggered release of calcium from the sarcoplasmic reticulum of single skinned cardiac cells. *The Journal of Physiology*, *249*(3), 469–495.
Fahey, M. C., Cremer, P. D., Aw, S. T., Millist, L., Todd, M. J., White, O. B., … Delatycki, M. B. (2008). Vestibular, saccadic and fixation abnormalities in genetically confirmed Friedreich ataxia. *Brain : A Journal of Neurology*, *131*(Pt 4), 1035–1045. https://doi.org/10.1093/brain/awm323
Fantus, I. G., Janjua, N., Senni, H., & Andermann, E. (1991). Glucose intolerance in first-degree relatives of patients with Friedreich's ataxia is associated with insulin resistance: evidence for a closely linked inherited trait. *Metabolism: Clinical and Experimental*, *40*(8), 788–793.
Festenstein, R. (2006, October). Breaking the silence in Friedreich's ataxia. *Nature Chemical Biology*. United States. https://doi.org/10.1038/nchembio1006-512
Filla, A., De Michele, G., Barbieri, F., & Campanella, G. (1992). Early onset hereditary ataxias of unknown etiology. Review of a personal series. *Acta Neurologica*, *14*(4–6), 420–430.
Filla, A., De Michele, G., Cavalcanti, F., Pianese, L., Monticelli, A., Campanella, G., & Cocozza, S. (1996). The relationship between trinucleotide (GAA) repeat length and clinical features in Friedreich ataxia. *American Journal of Human Genetics*, *59*(3), 554–560.
Filla, A., De Michele, G., & Cocozza, S. (1997, April). Genetic abnormalities in Friedreich's ataxia. *The New England Journal of Medicine*. United States.
Filla, A., De Michele, G., Coppola, G., Federico, A., Vita, G., Toscano, A., … Cocozza, S. (2000). Accuracy of clinical diagnostic criteria for Friedreich's ataxia. *Movement Disorders : Official Journal of the Movement Disorder Society*, *15*(6), 1255–1258.
Filla, A., DeMichele, G., Caruso, G., Marconi, R., & Campanella, G.

(1990). Genetic data and natural history of Friedreich's disease: a study of 80 Italian patients. *Journal of Neurology*, *237*(6), 345–351.
Finocchiaro, G., Baio, G., Micossi, P., Pozza, G., & di Donato, S. (1988). Glucose metabolism alterations in Friedreich's ataxia. *Neurology*, *38*(8), 1292–1296.
Folker, J., Murdoch, B., Cahill, L., Delatycki, M., Corben, L., & Vogel, A. (2010). Dysarthria in Friedreich's ataxia: a perceptual analysis. *Folia Phoniatrica et Logopaedica : Official Organ of the International Association of Logopedics and Phoniatrics (IALP)*, *62*(3), 97–103. https://doi.org/10.1159/000287207
Forrest, S. M., Knight, M., Delatycki, M. B., Paris, D., Williamson, R., King, J., … Nicholson, G. A. (1998). The correlation of clinical phenotype in Friedreich ataxia with the site of point mutations in the FRDA gene. *Neurogenetics*, *1*(4), 253–257.
Fortuna, F., Barboni, P., Liguori, R., Valentino, M. L., Savini, G., Gellera, C., … Carelli, V. (2009). Visual system involvement in patients with Friedreich's ataxia. *Brain : A Journal of Neurology*, *132*(Pt 1), 116–123. https://doi.org/10.1093/brain/awn269
Foury, F., & Cazzalini, O. (1997). Deletion of the yeast homologue of the human gene associated with Friedreich's ataxia elicits iron accumulation in mitochondria. *FEBS Letters*, *411*(2–3), 373–377.
Friedreich, N. (1863a) Ueber Degenerative Atrophie der Spinalen Hinterstränge. *Archiv. Path. Anat. Physiol. Klin. Med.,* **26,** 433-459.
Friedreich, N. (1863b) Ueber Degenerative Atrophie der Spinalen Hinterstränge. *Archiv. Path. Anat. Physiol. Klin. Med. ,* **27,** 1-26.
Friedreich, N. (1863c) Ueber Degenerative Atrophie der Spinalen Hinterstränge. . *Archiv. Path. Anat. Physiol. Klin. Med.,* **26,** 391-419.
Furman, J. M., Perlman, S., & Baloh, R. W. (1983). Eye movements in Friedreich's ataxia. *Archives of Neurology*, *40*(6), 343–346.
Gacy, A. M., Goellner, G. M., Spiro, C., Chen, X., Gupta, G., Bradbury, E. M., … McMurray, C. T. (1998). GAA instability in Friedreich's Ataxia shares a common, DNA-directed and intraallelic mechanism with other trinucleotide diseases. *Molecular Cell*, *1*(4), 583–593.
Gakh, O., Park, S., Liu, G., Macomber, L., Imlay, J. A., Ferreira, G. C., & Isaya, G. (2006). Mitochondrial iron detoxification is a primary function of frataxin that limits oxidative damage and preserves cell longevity. *Human Molecular Genetics*, *15*(3), 467–479. https://doi.org/10.1093/hmg/ddi461
Galea, C. A., Huq, A., Lockhart, P. J., Tai, G., Corben, L. A., Yiu, E. M., … Evans-Galea, M. V. (2016). Compound heterozygous FXN mutations and clinical outcome in friedreich ataxia. *Annals of Neurology*, *79*(3), 485–495. https://doi.org/10.1002/ana.24595
Galimanis, A., Glutz, L., Burgunder, J.-M., Spiegel, R., & Kaelin-Lang, A. (2008, May). Very-late-onset Friedreich ataxia with disturbing head tremor and without spinal atrophy--a case report. *Movement Disorders : Official Journal of the Movement Disorder Society*. United States. https://doi.org/10.1002/mds.21946
Garcia-Perez, C., Hajnoczky, G., & Csordas, G. (2008). Physical coupling supports the local Ca2+ transfer between sarcoplasmic reticulum subdomains and the mitochondria in heart muscle. *The Journal of*

*Biological Chemistry*, *283*(47), 32771–32780. https://doi.org/10.1074/jbc.M803385200
Gellera, C., Castellotti, B., Mariotti, C., Mineri, R., Seveso, V., Didonato, S., & Taroni, F. (2007). Frataxin gene point mutations in Italian Friedreich ataxia patients. *Neurogenetics*, *8*(4), 289–299. https://doi.org/10.1007/s10048-007-0101-5
Gellera, C., Pareyson, D., Castellotti, B., Mazzucchelli, F., Zappacosta, B., Pandolfo, M., & Di Donato, S. (1997). Very late onset Friedreich's ataxia without cardiomyopathy is associated with limited GAA expansion in the X25 gene. *Neurology*, *49*(4), 1153–1155.
Geoffroy, G., Barbeau, A., Breton, G., Lemieux, B., Aube, M., Leger, C., & Bouchard, J. P. (1976). Clinical description and roentgenologic evaluation of patients with Friedreich's ataxia. *The Canadian Journal of Neurological Sciences. Le Journal Canadien Des Sciences Neurologiques*, *3*(4), 279–286.
Gerber, J., Muhlenhoff, U., & Lill, R. (2003). An interaction between frataxin and Isu1/Nfs1 that is crucial for Fe/S cluster synthesis on Isu1. *EMBO Reports*, *4*(9), 906–911. https://doi.org/10.1038/sj.embor.embor918
Goldhaber, J. I., & Qayyum, M. S. (2000). Oxygen free radicals and excitation-contraction coupling. *Antioxidants & Redox Signaling*, *2*(1), 55–64. https://doi.org/10.1089/ars.2000.2.1-55
Gonzalez-Cabo, P., & Palau, F. (2013). Mitochondrial pathophysiology in Friedreich's ataxia. *Journal of Neurochemistry*, *126 Suppl*, 53–64. https://doi.org/10.1111/jnc.12303
Gonzalez-Cabo, P., Vazquez-Manrique, R. P., Garcia-Gimeno, M. A., Sanz, P., & Palau, F. (2005). Frataxin interacts functionally with mitochondrial electron transport chain proteins. *Human Molecular Genetics*, *14*(15), 2091–2098. https://doi.org/10.1093/hmg/ddi214
Gottesfeld, J. M. (2007). Small molecules affecting transcription in Friedreich ataxia. *Pharmacology & Therapeutics*, *116*(2), 236–248. https://doi.org/10.1016/j.pharmthera.2007.06.014
Hanley, A., Corrigan, R., Mohammad, S., & MacMahon, B. (2010). Friedreich's ataxia cardiomyopathy: case based discussion and management issues. *Irish Medical Journal*, *103*(4), 117–118.
Harding, A. E. (1981). Friedreich's ataxia: a clinical and genetic study of 90 families with an analysis of early diagnostic criteria and intrafamilial clustering of clinical features. *Brain : A Journal of Neurology*, *104*(3), 589–620.
Harding, A. E., & Zilkha, K. J. (1981). "Pseudo-dominant" inheritance in Friedreich's ataxia. *Journal of Medical Genetics*, *18*(4), 285–287.
Hart, P. E., Lodi, R., Rajagopalan, B., Bradley, J. L., Crilley, J. G., Turner, C., … Cooper, J. M. (2005). Antioxidant treatment of patients with Friedreich ataxia: four-year follow-up. *Archives of Neurology*, *62*(4), 621–626. https://doi.org/10.1001/archneur.62.4.621
He, Y., Alam, S. L., Proteasa, S. V, Zhang, Y., Lesuisse, E., Dancis, A., & Stemmler, T. L. (2004). Yeast frataxin solution structure, iron binding, and ferrochelatase interaction. *Biochemistry*, *43*(51), 16254–16262. https://doi.org/10.1021/bi0488193
Hebinck, J., Hardt, C., Schols, L., Vorgerd, M., Briedigkeit, L., Kahn, C.

R., & Ristow, M. (2000). Heterozygous expansion of the GAA tract of the X25/frataxin gene is associated with insulin resistance in humans. *Diabetes*, *49*(9), 1604–1607.
Hewer, R. (1969). The heart in Friedreich's ataxia. *British Heart Journal*, *31*(1), 5–14.
Hewer, R. L., & Robinson, N. (1968). Diabetes mellitus in Friedreich's ataxia. *Journal of Neurology, Neurosurgery, and Psychiatry*, *31*(3), 226–231.
Hoffman-Zacharska, D., Mazurczak, T., Zajkowski, T., Tataj, R., Gorka-Skoczylas, P., Polatynska, K., … Bal, J. (2016). Friedreich ataxia is not only a GAA repeats expansion disorder: implications for molecular testing and counselling. *Journal of Applied Genetics*, *57*(3), 349–355. https://doi.org/10.1007/s13353-015-0331-4
Huang, M. L.-H., Becker, E. M., Whitnall, M., Suryo Rahmanto, Y., Ponka, P., & Richardson, D. R. (2009). Elucidation of the mechanism of mitochondrial iron loading in Friedreich's ataxia by analysis of a mouse mutant. *Proceedings of the National Academy of Sciences of the United States of America*, *106*(38), 16381–16386. https://doi.org/10.1073/pnas.0906784106
Huynen, M. A., Snel, B., Bork, P., & Gibson, T. J. (2001). The phylogenetic distribution of frataxin indicates a role in iron-sulfur cluster protein assembly. *Human Molecular Genetics*, *10*(21), 2463–2468.
Iannuzzi, C., Adinolfi, S., Howes, B. D., Garcia-Serres, R., Clemancey, M., Latour, J.-M., … Pastore, A. (2011). The role of CyaY in iron sulfur cluster assembly on the E. coli IscU scaffold protein. *PloS One*, *6*(7), e21992. https://doi.org/10.1371/journal.pone.0021992
Isaya, G. (2014). Mitochondrial iron-sulfur cluster dysfunction in neurodegenerative disease. *Frontiers in Pharmacology*, *5*, 29. https://doi.org/10.3389/fphar.2014.00029
Johnson, D. C., Dean, D. R., Smith, A. D., & Johnson, M. K. (2005). Structure, function, and formation of biological iron-sulfur clusters. *Annual Review of Biochemistry*, *74*, 247–281. https://doi.org/10.1146/annurev.biochem.74.082803.133518
Karthikeyan, G., Lewis, L. K., & Resnick, M. A. (2002). The mitochondrial protein frataxin prevents nuclear damage. *Human Molecular Genetics*, *11*(11), 1351–1362.
Karthikeyan, G., Santos, J. H., Graziewicz, M. A., Copeland, W. C., Isaya, G., Van Houten, B., & Resnick, M. A. (2003). Reduction in frataxin causes progressive accumulation of mitochondrial damage. *Human Molecular Genetics*, *12*(24), 3331–3342. https://doi.org/10.1093/hmg/ddg349
Kawakami, M., & Okabe, E. (1998). Superoxide anion radical-triggered Ca2+ release from cardiac sarcoplasmic reticulum through ryanodine receptor Ca2+ channel. *Molecular Pharmacology*, *53*(3), 497–503.
Kipps, A., Alexander, M., Colan, S. D., Gauvreau, K., Smoot, L., Crawford, L., … Blume, E. D. (2009). The longitudinal course of cardiomyopathy in Friedreich's ataxia during childhood. *Pediatric Cardiology*, *30*(3), 306–310. https://doi.org/10.1007/s00246-008-9305-1

Klockgether, T., Chamberlain, S., Wullner, U., Fetter, M., Dittmann, H., Petersen, D., & Dichgans, J. (1993). Late-onset Friedreich's ataxia. Molecular genetics, clinical neurophysiology, and magnetic resonance imaging. *Archives of Neurology*, *50*(8), 803–806.

Klockgether, T., Zuhlke, C., Schulz, J. B., Burk, K., Fetter, M., Dittmann, H., … Dichgans, J. (1996). Friedreich's ataxia with retained tendon reflexes: molecular genetics, clinical neurophysiology, and magnetic resonance imaging. *Neurology*, *46*(1), 118–121.

Kocheva, S. A., Plaseska-Karanfilska, D., Trivodalieva, S., Kuturec, M., Vlaski-Jekic, S., & Efremov, G. D. (2008). Prenatal diagnosis of spinal muscular atrophy in Macedonian families. *Genetic Testing*, *12*(3), 391–393. https://doi.org/10.1089/gte.2007.0112

Koeppen, A. H., & Mazurkiewicz, J. E. (2013). Friedreich ataxia: neuropathology revised. *Journal of Neuropathology and Experimental Neurology*, *72*(2), 78–90. https://doi.org/10.1097/NEN.0b013e31827e5762

Koeppen, A. H., Michael, S. C., Knutson, M. D., Haile, D. J., Qian, J., Levi, S., … Lamarche, J. B. (2007). The dentate nucleus in Friedreich's ataxia: the role of iron-responsive proteins. *Acta Neuropathologica*, *114*(2), 163–173. https://doi.org/10.1007/s00401-007-0220-y

Koeppen, A. H., Ramirez, R. L., Becker, A. B., & Mazurkiewicz, J. E. (2016). Dorsal root ganglia in Friedreich ataxia: satellite cell proliferation and inflammation. *Acta Neuropathologica Communications*, *4*(1), 46. https://doi.org/10.1186/s40478-016-0288-5

Koeppen, A. H., Ramirez, R. L., Yu, D., Collins, S. E., Qian, J., Parsons, P. J., … Feustel, P. J. (2012). Friedreich's ataxia causes redistribution of iron, copper, and zinc in the dentate nucleus. *Cerebellum (London, England)*, *11*(4), 845–860. https://doi.org/10.1007/s12311-012-0383-5

Koutnikova, H., Campuzano, V., Foury, F., Dolle, P., Cazzalini, O., & Koenig, M. (1997). Studies of human, mouse and yeast homologues indicate a mitochondrial function for frataxin. *Nature Genetics*, *16*(4), 345–351. https://doi.org/10.1038/ng0897-345

Ku, S., Soragni, E., Campau, E., Thomas, E. A., Altun, G., Laurent, L. C., … Gottesfeld, J. M. (2010). Friedreich's ataxia induced pluripotent stem cells model intergenerational GAATTC triplet repeat instability. *Cell Stem Cell*, *7*(5), 631–637. https://doi.org/10.1016/j.stem.2010.09.014

Labauge, P. (2002, April). Very late onset Friedreich's presenting as spastic tetraparesis without ataxia or neuropathy. *Neurology*. United States.

Labuda, M., Labuda, D., Miranda, C., Poirier, J., Soong, B. W., Barucha, N. E., & Pandolfo, M. (2000). Unique origin and specific ethnic distribution of the Friedreich ataxia GAA expansion. *Neurology*, *54*(12), 2322–2324.

Lacampagne, A., Duittoz, A., Bolanos, P., Peineau, N., & Argibay, J. A. (1995). Effect of sulfhydryl oxidation on ionic and gating currents associated with L-type calcium channels in isolated guinea-pig

ventricular myocytes. *Cardiovascular Research*, *30*(5), 799–806.
Lad, M., Parkinson, M. H., Rai, M., Pandolfo, M., Bogdanova-Mihaylova, P., Walsh, R. A., … Giunti, P. (2017). Urinary, bowel and sexual symptoms in a cohort of patients with Friedreich's ataxia. *Orphanet Journal of Rare Diseases*, *12*(1), 158. https://doi.org/10.1186/s13023-017-0709-y
Lamarche, J. B., Cote, M., & Lemieux, B. (1980). The cardiomyopathy of Friedreich's ataxia morphological observations in 3 cases. *The Canadian Journal of Neurological Sciences. Le Journal Canadien Des Sciences Neurologiques*, *7*(4), 389–396.
Lamont, P. J., Davis, M. B., & Wood, N. W. (1997). Identification and sizing of the GAA trinucleotide repeat expansion of Friedreich's ataxia in 56 patients. Clinical and genetic correlates. *Brain : A Journal of Neurology*, *120 ( Pt 4*, 673–680.
Layer, G., Ollagnier-de Choudens, S., Sanakis, Y., & Fontecave, M. (2006). Iron-sulfur cluster biosynthesis: characterization of Escherichia coli CYaY as an iron donor for the assembly of [2Fe-2S] clusters in the scaffold IscU. *The Journal of Biological Chemistry*, *281*(24), 16256–16263. https://doi.org/10.1074/jbc.M513569200
Lecocq, C., Charles, P., Azulay, J.-P., Meissner, W., Rai, M., N'Guyen, K., … Anheim, M. (2016). Delayed-onset Friedreich's ataxia revisited. *Movement Disorders : Official Journal of the Movement Disorder Society*, *31*(1), 62–69. https://doi.org/10.1002/mds.26382
Leonard, H., & Forsyth, R. (2001). Friedreich's ataxia presenting after cardiac transplantation. *Archives of Disease in Childhood*, *84*(2), 167–168.
Leone, M., Brignolio, F., Rosso, M. G., Curtoni, E. S., Moroni, A., Tribolo, A., & Schiffer, D. (1990). Friedreich's ataxia: a descriptive epidemiological study in an Italian population. *Clinical Genetics*, *38*(3), 161–169.
Lesuisse, E., Santos, R., Matzanke, B. F., Knight, S. A. B., Camadro, J.-M., & Dancis, A. (2003). Iron use for haeme synthesis is under control of the yeast frataxin homologue (Yfh1). *Human Molecular Genetics*, *12*(8), 879–889.
Lhatoo, S. D., Rao, D. G., Kane, N. M., & Ormerod, I. E. (2001). Very late onset Friedreich's presenting as spastic tetraparesis without ataxia or neuropathy. *Neurology*, *56*(12), 1776–1777.
Li, H., Gakh, O., Smith, D. Y. 4th, & Isaya, G. (2009). Oligomeric yeast frataxin drives assembly of core machinery for mitochondrial iron-sulfur cluster synthesis. *The Journal of Biological Chemistry*, *284*(33), 21971–21980. https://doi.org/10.1074/jbc.M109.011197
Libri, V., Yandim, C., Athanasopoulos, S., Loyse, N., Natisvili, T., Law, P. P., … Festenstein, R. (2014). Epigenetic and neurological effects and safety of high-dose nicotinamide in patients with Friedreich's ataxia: an exploratory, open-label, dose-escalation study. *Lancet (London, England)*, *384*(9942), 504–513. https://doi.org/10.1016/S0140-6736(14)60382-2
Lill, R. (2009). Function and biogenesis of iron-sulphur proteins. *Nature*, *460*(7257), 831–838. https://doi.org/10.1038/nature08301
Limbu, S., Hoang-Trong, T. M., Prosser, B. L., Lederer, W. J., & Jafri, M.

S. (2015). Modeling Local X-ROS and Calcium Signaling in the Heart. *Biophysical Journal*, *109*(10), 2037–2050. https://doi.org/10.1016/j.bpj.2015.09.031

Liu, J., Verma, P. J., Evans-Galea, M. V, Delatycki, M. B., Michalska, A., Leung, J., … Pebay, A. (2011). Generation of induced pluripotent stem cell lines from Friedreich ataxia patients. *Stem Cell Reviews*, *7*(3), 703–713. https://doi.org/10.1007/s12015-010-9210-x

Llorens, J. V, Navarro, J. A., Martinez-Sebastian, M. J., Baylies, M. K., Schneuwly, S., Botella, J. A., & Molto, M. D. (2007). Causative role of oxidative stress in a Drosophila model of Friedreich ataxia. *FASEB Journal : Official Publication of the Federation of American Societies for Experimental Biology*, *21*(2), 333–344. https://doi.org/10.1096/fj.05-5709com

Lobmayr, L., Brooks, D. G., & Wilson, R. B. (2005). Increased IRP1 activity in Friedreich ataxia. *Gene*, *354*, 157–161. https://doi.org/10.1016/j.gene.2005.04.040

Lodi, R., Cooper, J. M., Bradley, J. L., Manners, D., Styles, P., Taylor, D. J., & Schapira, A. H. (1999). Deficit of in vivo mitochondrial ATP production in patients with Friedreich ataxia. *Proceedings of the National Academy of Sciences of the United States of America*, *96*(20), 11492–11495.

Lodi, R., Rajagopalan, B., Blamire, A. M., Cooper, J. M., Davies, C. H., Bradley, J. L., … Schapira, A. H. (2001). Cardiac energetics are abnormal in Friedreich ataxia patients in the absence of cardiac dysfunction and hypertrophy: an in vivo 31P magnetic resonance spectroscopy study. *Cardiovascular Research*, *52*(1), 111–119.

Lodi, R., Taylor, D. J., & Schapira, A. H. (2001). Mitochondrial dysfunction in friedreich's ataxia. *Biological Signals and Receptors*, *10*(3–4), 263–270. https://doi.org/10.1159/000046891

Lu, C., Schoenfeld, R., Shan, Y., Tsai, H.-J., Hammock, B., & Cortopassi, G. (2009). Frataxin deficiency induces Schwann cell inflammation and death. *Biochimica et Biophysica Acta*, *1792*(11), 1052–1061. https://doi.org/10.1016/j.bbadis.2009.07.011

Lynch, D. R., Perlman, S. L., & Meier, T. (2010). A phase 3, double-blind, placebo-controlled trial of idebenone in friedreich ataxia. *Archives of Neurology*, *67*(8), 941–947. https://doi.org/10.1001/archneurol.2010.168

Malo, S., Latour, Y., Cote, M., Geoffroy, G., Lemieux, B., & Barbeau, A. (1976). Electrocardiographic and vectocardiographic findings in Friedreich's ataxia. *The Canadian Journal of Neurological Sciences. Le Journal Canadien Des Sciences Neurologiques*, *3*(4), 323–328.

Mariotti, C., Nachbauer, W., Panzeri, M., Poewe, W., Taroni, F., & Boesch, S. (2013). Erythropoietin in Friedreich ataxia. *Journal of Neurochemistry*, *126 Suppl*, 80–87. https://doi.org/10.1111/jnc.12301

Mariotti, C., Solari, A., Torta, D., Marano, L., Fiorentini, C., & Di Donato, S. (2003). Idebenone treatment in Friedreich patients: one-year-long randomized placebo-controlled trial. *Neurology*, *60*(10), 1676–1679.

Martelli, A., Colin, F., & Page, A. (2011). Mammalian Frataxin : An Essential Function for Cellular Viability through an Interaction with a Preformed ISCU / NFS1 / ISD11 Iron-Sulfur Assembly Complex,

*6*(1), 1–12. https://doi.org/10.1371/journal.pone.0016199
Martinez, A. R. M., Moro, A., Abrahao, A., Faber, I., Borges, C. R., Rezende, T. J. R., … Franca, M. C. J. (2017). Nonneurological Involvement in Late-Onset Friedreich Ataxia (LOFA): Exploring the Phenotypes. *Cerebellum (London, England)*, *16*(1), 253–256. https://doi.org/10.1007/s12311-015-0755-8
Marx, S. O., Reiken, S., Hisamatsu, Y., Jayaraman, T., Burkhoff, D., Rosemblit, N., & Marks, A. R. (2000). PKA phosphorylation dissociates FKBP12.6 from the calcium release channel (ryanodine receptor): defective regulation in failing hearts. *Cell*, *101*(4), 365–376.
McCabe, D. J., Ryan, F., Moore, D. P., McQuaid, S., King, M. D., Kelly, A., … Murphy, R. P. (2000). Typical Friedreich's ataxia without GAA expansions and GAA expansion without typical Friedreich's ataxia. *Journal of Neurology*, *247*(5), 346–355.
McCormack, M. L., Guttmann, R. P., Schumann, M., Farmer, J. M., Stolle, C. A., Campuzano, V., … Lynch, D. R. (2000). Frataxin point mutations in two patients with Friedreich's ataxia and unusual clinical features. *Journal of Neurology, Neurosurgery, and Psychiatry*, *68*(5), 661–664.
Meyer, C., Schmid, G., Gorlitz, S., Ernst, M., Wilkens, C., Wilhelms, I., … Schols, L. (2007). Cardiomyopathy in Friedreich's ataxia-assessment by cardiac MRI. *Movement Disorders : Official Journal of the Movement Disorder Society*, *22*(11), 1615–1622. https://doi.org/10.1002/mds.21590
Michael, S., Petrocine, S. V, Qian, J., Lamarche, J. B., Knutson, M. D., Garrick, M. D., & Koeppen, A. H. (2006). Iron and iron-responsive proteins in the cardiomyopathy of Friedreich's ataxia. *Cerebellum (London, England)*, *5*(4), 257–267. https://doi.org/10.1080/14734220600913246
Milne, S. C., Corben, L. A., Yiu, E., Delatycki, M. B., & Georgiou-Karistianis, N. (2016). Gastrocnemius and soleus spasticity and muscle length in Friedreich's ataxia. *Journal of Clinical Neuroscience : Official Journal of the Neurosurgical Society of Australasia*, *29*, 29–34. https://doi.org/10.1016/j.jocn.2016.01.011
Mincheva-Tasheva, S., Obis, E., Tamarit, J., & Ros, J. (2013). Apoptotic cell death and altered calcium homeostasis caused by frataxin depletion in dorsal root ganglia neurons can be prevented by BH4 domain of Bcl-xL protein. *Human Molecular Genetics*. https://doi.org/10.1093/hmg/ddt576
Mincheva-Tasheva, S., Obis, E., Tamarit, J., & Ros, J. (2014). Apoptotic cell death and altered calcium homeostasis caused by frataxin depletion in dorsal root ganglia neurons can be prevented by BH4 domain of Bcl-xL protein. *Human Molecular Genetics*, *23*(7), 1829–1841. https://doi.org/10.1093/hmg/ddt576
Miranda, C. J., Santos, M. M., Ohshima, K., Smith, J., Li, L., Bunting, M., … Pandolfo, M. (2002). Frataxin knockin mouse. *FEBS Letters*, *512*(1–3), 291–297.
Molla, B., Munoz-Lasso, D. C., Riveiro, F., Bolinches-Amoros, A., Pallardo, F. V, Fernandez-Vilata, A., … Gonzalez-Cabo, P. (2017).

Reversible Axonal Dystrophy by Calcium Modulation in Frataxin-Deficient Sensory Neurons of YG8R Mice. *Frontiers in Molecular Neuroscience*, *10*, 264. https://doi.org/10.3389/fnmol.2017.00264

Monros, E., Molto, M. D., Martinez, F., Canizares, J., Blanca, J., Vilchez, J. J., … Palau, F. (1997). Phenotype correlation and intergenerational dynamics of the Friedreich ataxia GAA trinucleotide repeat. *American Journal of Human Genetics*, *61*(1), 101–110.

Montermini, L., Kish, S. J., Jiralerspong, S., Lamarche, J. B., & Pandolfo, M. (1997). Somatic mosaicism for Friedreich's ataxia GAA triplet repeat expansions in the central nervous system. *Neurology*, *49*(2), 606–610.

Morral, J. A., Davis, A. N., Qian, J., Gelman, B. B., & Koeppen, A. H. (2010). Pathology and pathogenesis of sensory neuropathy in Friedreich's ataxia. *Acta Neuropathologica*, *120*(1), 97–108. https://doi.org/10.1007/s00401-010-0675-0

Muhlenhoff, U., Richhardt, N., Ristow, M., Kispal, G., & Lill, R. (2002). The yeast frataxin homolog Yfh1p plays a specific role in the maturation of cellular Fe/S proteins. *Human Molecular Genetics*, *11*(17), 2025–2036.

Muthuswamy, S., Agarwal, S., & Dalal, A. (2013). Diagnosis and Genetic Counseling for Friedreich's Ataxia: A time for consideration of TP-PCR in an Indian Setup. *Hippokratia*, *17*(1), 38–41.

Nachbauer, W., Hering, S., Seifert, M., Steinkellner, H., Sturm, B., Scheiber-Mojdehkar, B., … Boesch, S. (2011). Effects of erythropoietin on frataxin levels and mitochondrial function in Friedreich ataxia--a dose-response trial. *Cerebellum (London, England)*, *10*(4), 763–769. https://doi.org/10.1007/s12311-011-0287-9

Nair, M., Adinolfi, S., Pastore, C., Kelly, G., Temussi, P., & Pastore, A. (2004). Solution structure of the bacterial frataxin ortholog, CyaY: mapping the iron binding sites. *Structure (London, England : 1993)*, *12*(11), 2037–2048. https://doi.org/10.1016/j.str.2004.08.012

Napoli, E., Morin, D., Bernhardt, R., Buckpitt, A., & Cortopassi, G. (2007). Hemin rescues adrenodoxin, heme a and cytochrome oxidase activity in frataxin-deficient oligodendroglioma cells. *Biochimica et Biophysica Acta*, *1772*(7), 773–780. https://doi.org/10.1016/j.bbadis.2007.04.001

Navarro, J. A., Ohmann, E., Sanchez, D., Botella, J. A., Liebisch, G., Molto, M. D., … Schneuwly, S. (2010). Altered lipid metabolism in a Drosophila model of Friedreich's ataxia. *Human Molecular Genetics*, *19*(14), 2828–2840. https://doi.org/10.1093/hmg/ddq183

O'Neill, H. A., Gakh, O., Park, S., Cui, J., Mooney, S. M., Sampson, M., … Isaya, G. (2005). Assembly of human frataxin is a mechanism for detoxifying redox-active iron. *Biochemistry*, *44*(2), 537–545. https://doi.org/10.1021/bi048459j

Oda, T., Yang, Y., Uchinoumi, H., Thomas, D. D., Chen-Izu, Y., Kato, T., … Bers, D. M. (2015). Oxidation of ryanodine receptor (RyR) and calmodulin enhance Ca release and pathologically alter, RyR structure and calmodulin affinity. *Journal of Molecular and Cellular Cardiology*, *85*, 240–248. https://doi.org/10.1016/j.yjmcc.2015.06.009

Oudit, G. Y., Sun, H., Trivieri, M. G., Koch, S. E., Dawood, F., Ackerley, C., … Backx, P. H. (2003). L-type Ca 2 + channels provide a major pathway for iron entry into cardiomyocytes in iron-overload cardiomyopathy, *9*(9), 1187–1194. https://doi.org/10.1038/nm920

Oudit, G. Y., Trivieri, M. G., Khaper, N., Liu, P. P., & Backx, P. H. (2006). Role of L-type Ca2 + channels in iron transport and iron-overload cardiomyopathy, 349–364. https://doi.org/10.1007/s00109-005-0029-x

Palagi, B., Picozzi, R., Casazza, F., Possa, M., Magri, G., Zoccarato, O., … Morpurgo, M. (1988). Biventricular function in Friedreich's ataxia: a radionuclide angiographic study. *British Heart Journal*, *59*(6), 692–695.

Pandolfo, M. (1999). Friedreich's ataxia: clinical aspects and pathogenesis. *Seminars in Neurology*, *19*(3), 311–321. https://doi.org/10.1055/s-2008-1040847

Pandolfo, M. (2006). Friedreich ataxia: Detection of GAA repeat expansions and frataxin point mutations. *Methods in Molecular Medicine*, *126*, 197–216. https://doi.org/10.1385/1-59745-088-X:197

Pandolfo, M., Arpa, J., Delatycki, M. B., Le Quan Sang, K. H., Mariotti, C., Munnich, A., … Tricta, F. (2014). Deferiprone in Friedreich ataxia: a 6-month randomized controlled trial. *Annals of Neurology*, *76*(4), 509–521. https://doi.org/10.1002/ana.24248

Pandolfo, M., & Hausmann, L. (2013). Deferiprone for the treatment of Friedreich's ataxia. *Journal of Neurochemistry*, *126 Suppl*, 142–146. https://doi.org/10.1111/jnc.12300

Pandolfo, M., & Pastore, A. (2009). The pathogenesis of Friedreich ataxia and the structure and function of frataxin. *Journal of Neurology*, *256 Suppl*, 9–17. https://doi.org/10.1007/s00415-009-1003-2

Park, S., Gakh, O., O'Neill, H. A., Mangravita, A., Nichol, H., Ferreira, G. C., & Isaya, G. (2003). Yeast frataxin sequentially chaperones and stores iron by coupling protein assembly with iron oxidation. *The Journal of Biological Chemistry*, *278*(33), 31340–31351. https://doi.org/10.1074/jbc.M303158200

Parkinson, M. H., Boesch, S., Nachbauer, W., Mariotti, C., & Giunti, P. (2013). Clinical features of Friedreich's ataxia: classical and atypical phenotypes. *Journal of Neurochemistry*, *126 Suppl*, 103–117. https://doi.org/10.1111/jnc.12317

Pastore, A., & Puccio, H. (2013). Frataxin: a protein in search for a function. *Journal of Neurochemistry*, *126 Suppl*, 43–52. https://doi.org/10.1111/jnc.12220

Payne, R. M., Pride, P. M., & Babbey, C. M. (2011). Cardiomyopathy of Friedreich's ataxia: use of mouse models to understand human disease and guide therapeutic development. *Pediatric Cardiology*, *32*(3), 366–378. https://doi.org/10.1007/s00246-011-9943-6

Perdomini, M., Belbellaa, B., Monassier, L., Reutenauer, L., Messaddeq, N., Cartier, N., … Puccio, H. (2014). Prevention and reversal of severe mitochondrial cardiomyopathy by gene therapy in a mouse model of Friedreich's ataxia. *Nature Medicine*, *20*(5), 542–547. https://doi.org/10.1038/nm.3510

Perlman, S. L. (2012). A review of Friedreich ataxia clinical trial results.

*Journal of Child Neurology*, *27*(9), 1217–1222. https://doi.org/10.1177/0883073812453872

Pianese, L., Turano, M., Lo Casale, M. S., De Biase, I., Giacchetti, M., Monticelli, A., … Cocozza, S. (2004). Real time PCR quantification of frataxin mRNA in the peripheral blood leucocytes of Friedreich ataxia patients and carriers. *Journal of Neurology, Neurosurgery, and Psychiatry*, *75*(7), 1061–1063.

Pineda, M., Arpa, J., Montero, R., Aracil, A., Dominguez, F., Galvan, M., … Artuch, R. (2008). Idebenone treatment in paediatric and adult patients with Friedreich ataxia: long-term follow-up. *European Journal of Paediatric Neurology : EJPN : Official Journal of the European Paediatric Neurology Society*, *12*(6), 470–475. https://doi.org/10.1016/j.ejpn.2007.11.006

Pook, M. A., Al-Mahdawi, S., Carroll, C. J., Cossee, M., Puccio, H., Lawrence, L., … Chamberlain, S. (2001). Rescue of the Friedreich's ataxia knockout mouse by human YAC transgenesis. *Neurogenetics*, *3*(4), 185–193.

Potdar, P. D., & Raghu, A. (2013). Review on Molecular Diagnostic Techniques in Friedreich ' s Ataxia, *3*(4), 659–677.

Pousset, F., Legrand, L., Monin, M.-L., Ewenczyk, C., Charles, P., Komajda, M., … Durr, A. (2015). A 22-Year Follow-up Study of Long-term Cardiac Outcome and Predictors of Survival in Friedreich Ataxia. *JAMA Neurology*, *72*(11), 1334–1341. https://doi.org/10.1001/jamaneurol.2015.1855

Prischi, F., Konarev, P. V, Iannuzzi, C., Pastore, C., Adinolfi, S., Martin, S. R., … Pastore, A. (2010). Structural bases for the interaction of frataxin with the central components of iron-sulphur cluster assembly. *Nature Communications*, *1*, 95. https://doi.org/10.1038/ncomms1097

Puccio, H., & Koenig, M. (2000). Recent advances in the molecular pathogenesis of Friedreich ataxia. *Human Molecular Genetics*, *9*(6), 887–892.

Puccio, H., Simon, D., Cossee, M., Criqui-Filipe, P., Tiziano, F., Melki, J., … Koenig, M. (2001). Mouse models for Friedreich ataxia exhibit cardiomyopathy, sensory nerve defect and Fe-S enzyme deficiency followed by intramitochondrial iron deposits. *Nature Genetics*, *27*(2), 181–186. https://doi.org/10.1038/84818

Radisky, D. C., Babcock, M. C., & Kaplan, J. (1999). The yeast frataxin homologue mediates mitochondrial iron efflux. Evidence for a mitochondrial iron cycle. *The Journal of Biological Chemistry*, *274*(8), 4497–4499.

Ragno, M., De Michele, G., Cavalcanti, F., Pianese, L., Monticelli, A., Curatola, L., … Filla, A. (1997). Broadened Friedreich's ataxia phenotype after gene cloning. Minimal GAA expansion causes late-onset spastic ataxia. *Neurology*, *49*(6), 1617–1620.

Rajagopalan, B., Francis, J. M., Cooke, F., Korlipara, L. V. P., Blamire, A. M., Schapira, A. H. V, … Cooper, J. M. (2010). Analysis of the factors influencing the cardiac phenotype in Friedreich's ataxia. *Movement Disorders : Official Journal of the Movement Disorder Society*, *25*(7), 846–852. https://doi.org/10.1002/mds.22864

Ramay, H. R., Jafri, M. S., Lederer, W. J., & Sobie, E. A. (2010). Predicting local SR Ca(2+) dynamics during Ca(2+) wave propagation in ventricular myocytes. *Biophysical Journal*, *98*(11), 2515–2523. https://doi.org/10.1016/j.bpj.2010.02.038

Rance, G., Corben, L., Barker, E., Carew, P., Chisari, D., Rogers, M., … Delatycki, M. B. (2010). Auditory perception in individuals with Friedreich's ataxia. *Audiology & Neuro-Otology*, *15*(4), 229–240. https://doi.org/10.1159/000255341

Reetz, K., Dogan, I., Costa, A. S., Dafotakis, M., Fedosov, K., Giunti, P., … Schulz, J. B. (2015). Biological and clinical characteristics of the European Friedreich's Ataxia Consortium for Translational Studies (EFACTS) cohort: a cross-sectional analysis of baseline data. *The Lancet. Neurology*, *14*(2), 174–182. https://doi.org/10.1016/S1474-4422(14)70321-7

Reetz, K., Dogan, I., Hilgers, R.-D., Giunti, P., Mariotti, C., Durr, A., … Schulz, J. B. (2016). Progression characteristics of the European Friedreich's Ataxia Consortium for Translational Studies (EFACTS): a 2 year cohort study. *The Lancet. Neurology*, *15*(13), 1346–1354. https://doi.org/10.1016/S1474-4422(16)30287-3

Regner, S. R., Lagedrost, S. J., Plappert, T., Paulsen, E. K., Friedman, L. S., Snyder, M. L., … Lynch, D. R. (2012). Analysis of echocardiograms in a large heterogeneous cohort of patients with friedreich ataxia. *The American Journal of Cardiology*, *109*(3), 401–405. https://doi.org/10.1016/j.amjcard.2011.09.025

Rehsia, N. S., & Dhalla, N. S. (2010). Mechanisms of the beneficial effects of beta-adrenoceptor antagonists in congestive heart failure. *Experimental and Clinical Cardiology*, *15*(4), e86-95.

Richardson, D. R. (2003). Friedreich's ataxia: iron chelators that target the mitochondrion as a therapeutic strategy? *Expert Opinion on Investigational Drugs*, *12*(2), 235–245. https://doi.org/10.1517/13543784.12.2.235

Ristow, M., Mulder, H., Pomplun, D., Schulz, T. J., Muller-Schmehl, K., Krause, A., … Pfeiffer, A. F. H. (2003). Frataxin deficiency in pancreatic islets causes diabetes due to loss of beta cell mass. *The Journal of Clinical Investigation*, *112*(4), 527–534. https://doi.org/10.1172/JCI18107

Ristow, M., Pfister, M. F., Yee, A. J., Schubert, M., Michael, L., Zhang, C., … Kahn, C. R. (2000). Frataxin activates mitochondrial energy conversion and oxidative phosphorylation, *97*(22).

Rogers, T. B., Inesi, G., Wade, R., & Lederer, W. J. (1995). Use of thapsigargin to study Ca2+ homeostasis in cardiac cells. *Bioscience Reports*, *15*(5), 341–349.

Romeo, G., Menozzi, P., Ferlini, A., Fadda, S., Di Donato, S., Uziel, G., … Campanella, G. (1983). Incidence of Friedreich ataxia in Italy estimated from consanguineous marriages. *American Journal of Human Genetics*, *35*(3), 523–529.

Rotig, A., de Lonlay, P., Chretien, D., Foury, F., Koenig, M., Sidi, D., … Rustin, P. (1997). Aconitase and mitochondrial iron-sulphur protein deficiency in Friedreich ataxia. *Nature Genetics*, *17*(2), 215–217. https://doi.org/10.1038/ng1097-215

Rouault, T. A. (2012). Biogenesis of iron-sulfur clusters in mammalian cells: new insights and relevance to human disease. *Disease Models & Mechanisms*, *5*(2), 155–164. https://doi.org/10.1242/dmm.009019

Rustin, P., Rotig, A., Munnich, A., & Sidi, D. (2002). Heart hypertrophy and function are improved by idebenone in Friedreich's ataxia. *Free Radical Research*, *36*(4), 467–469.

Sacca, F., Puorro, G., Antenora, A., Marsili, A., Denaro, A., Piro, R., … Filla, A. (2011). A combined nucleic acid and protein analysis in Friedreich ataxia: implications for diagnosis, pathogenesis and clinical trial design. *PloS One*, *6*(3), e17627. https://doi.org/10.1371/journal.pone.0017627

Sakamoto, N., Chastain, P. D., Parniewski, P., Ohshima, K., Pandolfo, M., Griffith, J. D., & Wells, R. D. (1999). Sticky DNA: self-association properties of long GAA.TTC repeats in R.R.Y triplex structures from Friedreich's ataxia. *Molecular Cell*, *3*(4), 465–475.

Sanchez-Casis, G., Cote, M., & Barbeau, A. (1976). Pathology of the heart in Friedreich's ataxia: review of the literature and report of one case. *The Canadian Journal of Neurological Sciences. Le Journal Canadien Des Sciences Neurologiques*, *3*(4), 349–354.

Santoro, L., De Michele, G., Perretti, A., Crisci, C., Cocozza, S., Cavalcanti, F., … Caruso, G. (1999). Relation between trinucleotide GAA repeat length and sensory neuropathy in Friedreich's ataxia. *Journal of Neurology, Neurosurgery, and Psychiatry*, *66*(1), 93–96.

Santos, M. M., Ohshima, K., & Pandolfo, M. (2001). Frataxin deficiency enhances apoptosis in cells differentiating into neuroectoderm. *Human Molecular Genetics*, *10*(18), 1935–1944.

Schadt, K. A., Friedman, L. S., Regner, S. R., Mark, G. E., Lynch, D. R., & Lin, K. Y. (2012). Cross-sectional analysis of electrocardiograms in a large heterogeneous cohort of Friedreich ataxia subjects. *Journal of Child Neurology*, *27*(9), 1187–1192. https://doi.org/10.1177/0883073812448461

Schmucker, S., Argentini, M., Carelle-Calmels, N., Martelli, A., & Puccio, H. (2008). The in vivo mitochondrial two-step maturation of human frataxin. *Human Molecular Genetics*, *17*(22), 3521–3531. https://doi.org/10.1093/hmg/ddn244

Schmucker, S., Martelli, A., Colin, F., Page, A., Wattenhofer-Donze, M., Reutenauer, L., & Puccio, H. (2011). Mammalian frataxin: an essential function for cellular viability through an interaction with a preformed ISCU/NFS1/ISD11 iron-sulfur assembly complex. *PloS One*, *6*(1), e16199. https://doi.org/10.1371/journal.pone.0016199

Schmucker, S., & Puccio, H. (2010). Understanding the molecular mechanisms of Friedreich's ataxia to develop therapeutic approaches. *Human Molecular Genetics*, *19*(R1), R103-10. https://doi.org/10.1093/hmg/ddq165

Schols, L., Amoiridis, G., Przuntek, H., Frank, G., Epplen, J. T., & Epplen, C. (1997). Friedreich's ataxia. Revision of the phenotype according to molecular genetics. *Brain : A Journal of Neurology*, *120 ( Pt 1*, 2131–2140.

Schulz, J. B., Boesch, S., Burk, K., Durr, A., Giunti, P., Mariotti, C., … Pandolfo, M. (2009). Diagnosis and treatment of Friedreich ataxia: a

European perspective. *Nature Reviews. Neurology*, *5*(4), 222–234. https://doi.org/10.1038/nrneurol.2009.26
Schulz, J. B., Dehmer, T., Schols, L., Mende, H., Hardt, C., Vorgerd, M., … Bogdanov, M. B. (2000). Oxidative stress in patients with Friedreich ataxia. *Neurology*, *55*(11), 1719–1721.
Schulz, J. B., & Pandolfo, M. (2013, August). 150 years of Friedreich ataxia: from its discovery to therapy. *Journal of Neurochemistry*. England.
Schwartz, K. A., Li, Z., Schwartz, D. E., Cooper, T. G., & Braselton, W. E. (2002). Earliest cardiac toxicity induced by iron overload selectively inhibits electrical conduction. *Journal of Applied Physiology (Bethesda, Md. : 1985)*, *93*(2), 746–751. https://doi.org/10.1152/japplphysiol.01144.2001
Shan, Y., Napoli, E., & Cortopassi, G. (2007). Mitochondrial frataxin interacts with ISD11 of the NFS1/ISCU complex and multiple mitochondrial chaperones. *Human Molecular Genetics*, *16*(8), 929–941. https://doi.org/10.1093/hmg/ddm038
Sharma, R., Bhatti, S., Gomez, M., Clark, R. M., Murray, C., Ashizawa, T., & Bidichandani, S. I. (2002). The GAA triplet-repeat sequence in Friedreich ataxia shows a high level of somatic instability in vivo, with a significant predilection for large contractions. *Human Molecular Genetics*, *11*(18), 2175–2187.
Sharov, V. S., Dremina, E. S., Galeva, N. A., Williams, T. D., & Schoneich, C. (2006). Quantitative mapping of oxidation-sensitive cysteine residues in SERCA in vivo and in vitro by HPLC-electrospray-tandem MS: selective protein oxidation during biological aging. *The Biochemical Journal*, *394*(Pt 3), 605–615. https://doi.org/10.1042/BJ20051214
Shidara, Y., & Hollenbeck, P. J. (2010). Defects in mitochondrial axonal transport and membrane potential without increased reactive oxygen species production in a Drosophila model of Friedreich ataxia. *The Journal of Neuroscience : The Official Journal of the Society for Neuroscience*, *30*(34), 11369–11378. https://doi.org/10.1523/JNEUROSCI.0529-10.2010
Shirotani, K., Katsura, M., Higo, A., Takesue, M., Mohri, Y., Shuto, K., … Ohkuma, S. (2001). Suppression of Ca2+ influx through L-type voltage-dependent calcium channels by hydroxyl radical in mouse cerebral cortical neurons. *Brain Research. Molecular Brain Research*, *92*(1–2), 12–18.
Simon, D., Seznec, H., Gansmuller, A., Carelle, N., Weber, P., Metzger, D., … Puccio, H. (2004). Friedreich ataxia mouse models with progressive cerebellar and sensory ataxia reveal autophagic neurodegeneration in dorsal root ganglia. *The Journal of Neuroscience : The Official Journal of the Society for Neuroscience*, *24*(8), 1987–1995. https://doi.org/10.1523/JNEUROSCI.4549-03.2004
Stehling, O., Elsasser, H.-P., Bruckel, B., Muhlenhoff, U., & Lill, R. (2004). Iron-sulfur protein maturation in human cells: evidence for a function of frataxin. *Human Molecular Genetics*, *13*(23), 3007–3015. https://doi.org/10.1093/hmg/ddh324

Stemmler, T. L., Lesuisse, E., Pain, D., & Dancis, A. (2010). Frataxin and mitochondrial FeS cluster biogenesis. *The Journal of Biological Chemistry*, *285*(35), 26737–26743. https://doi.org/10.1074/jbc.R110.118679

Stephanou, A., Brar, B., Heads, R., Knight, R. D., Marber, M. S., Pennica, D., & Latchman, D. S. (1998). Cardiotrophin-1 induces heat shock protein accumulation in cultured cardiac cells and protects them from stressful stimuli. *Journal of Molecular and Cellular Cardiology*, *30*(4), 849–855. https://doi.org/10.1006/jmcc.1998.0651

Sturm, B., Bistrich, U., Schranzhofer, M., Sarsero, J. P., Rauen, U., Scheiber-Mojdehkar, B., … Petrat, F. (2005). Friedreich's ataxia, no changes in mitochondrial labile iron in human lymphoblasts and fibroblasts: a decrease in antioxidative capacity? *The Journal of Biological Chemistry*, *280*(8), 6701–6708. https://doi.org/10.1074/jbc.M408717200

Tan, G., Chen, L. S., Lonnerdal, B., Gellera, C., Taroni, F. A., & Cortopassi, G. A. (2001). Frataxin expression rescues mitochondrial dysfunctions in FRDA cells. *Human Molecular Genetics*, *10*(19), 2099–2107.

Thoren, C. (1962). Diabetes mellitus in Friedreich's ataxia. *Acta Paediatrica. Supplementum*, *135*, 239–247.

Tsai, C.-L., & Barondeau, D. P. (2010). Human frataxin is an allosteric switch that activates the Fe-S cluster biosynthetic complex. *Biochemistry*, *49*(43), 9132–9139. https://doi.org/10.1021/bi1013062

Tsai, C.-L., Bridwell-Rabb, J., & Barondeau, D. P. (2011). Friedreich's ataxia variants I154F and W155R diminish frataxin-based activation of the iron-sulfur cluster assembly complex. *Biochemistry*, *50*(29), 6478–6487. https://doi.org/10.1021/bi200666h

Tsirikos, A. I., & Smith, G. (2012). Scoliosis in patients with Friedreich's ataxia. *The Journal of Bone and Joint Surgery. British Volume*, *94*(5), 684–689. https://doi.org/10.1302/0301-620X.94B5.28391

Tsou, A. Y., Paulsen, E. K., Lagedrost, S. J., Perlman, S. L., Mathews, K. D., Wilmot, G. R., … Lynch, D. R. (2011). Mortality in Friedreich ataxia. *Journal of the Neurological Sciences*, *307*(1–2), 46–49. https://doi.org/10.1016/j.jns.2011.05.023

van den Ouweland, A. M. W., van Minkelen, R., Bolman, G. M., Wouters, C. H., Becht-Noordermeer, C., Deelen, W. H., … Halley, D. J. J. (2012). Complete FXN deletion in a patient with Friedreich's ataxia. *Genetic Testing and Molecular Biomarkers*, *16*(9), 1015–1018. https://doi.org/10.1089/gtmb.2012.0012

Vankan, P. (2013). Prevalence gradients of Friedreich's Ataxia and R1b haplotype in Europe co-localize, suggesting a common Palaeolithic origin in the Franco- Cantabrian ice age refuge, *126*, 11–20. https://doi.org/10.1111/jnc.12215

Vazquez-Manrique, R. P., Gonzalez-Cabo, P., Ros, S., Aziz, H., Baylis, H. A., & Palau, F. (2006). Reduction of Caenorhabditis elegans frataxin increases sensitivity to oxidative stress, reduces lifespan, and causes lethality in a mitochondrial complex II mutant. *FASEB Journal : Official Publication of the Federation of American Societies for Experimental Biology*, *20*(1), 172–174.

https://doi.org/10.1096/fj.05-4212fje
Velasco-Sanchez, D., Aracil, A., Montero, R., Mas, A., Jimenez, L., O'Callaghan, M., … Pineda, M. (2011). Combined therapy with idebenone and deferiprone in patients with Friedreich's ataxia. *Cerebellum (London, England)*, *10*(1), 1–8. https://doi.org/10.1007/s12311-010-0212-7
Ventura, N., Rea, S. L., Handerson, S. T., Condo, I., Testi, R., & Johnson, T. E. (2006, May). C. elegans as a model for Friedreich Ataxia. *FASEB Journal : Official Publication of the Federation of American Societies for Experimental Biology*. United States. https://doi.org/10.1096/fj.06-0505ufm
Verma, R., & Gupta, M. (2012). Freidreich's ataxia with retained reflexes: a phenotype and genotype correlation. *BMJ Case Reports*, *2012*. https://doi.org/10.1136/bcr-2012-007496
Warner, J. P., Barron, L. H., Goudie, D., Kelly, K., Dow, D., Fitzpatrick, D. R., & Brock, D. J. (1996). A general method for the detection of large CAG repeat expansions by fluorescent PCR. *Journal of Medical Genetics*, *33*(12), 1022–1026.
Wedding, I. M., Kroken, M., Henriksen, S. P., Selmer, K. K., Fiskerstrand, T., Knappskog, P. M., … Tallaksen, C. M. E. (2015). Friedreich ataxia in Norway - an epidemiological, molecular and clinical study. *Orphanet Journal of Rare Diseases*, *10*, 108. https://doi.org/10.1186/s13023-015-0328-4
Weidemann, F., Rummey, C., Bijnens, B., Stork, S., Jasaityte, R., Dhooge, J., … Meier, T. (2012). The heart in Friedreich ataxia: definition of cardiomyopathy, disease severity, and correlation with neurological symptoms. *Circulation*, *125*(13), 1626–1634. https://doi.org/10.1161/CIRCULATIONAHA.111.059477
Willis, J. H., Isaya, G., Gakh, O., Capaldi, R. A., & Marusich, M. F. (2008). Lateral-flow immunoassay for the frataxin protein in Friedreich's ataxia patients and carriers. *Molecular Genetics and Metabolism*, *94*(4), 491–497. https://doi.org/10.1016/j.ymgme.2008.03.019
Wilson, R. B. (2012). Therapeutic developments in Friedreich ataxia. *Journal of Child Neurology*, *27*(9), 1212–1216. https://doi.org/10.1177/0883073812449691
Wong, A., Yang, J., Cavadini, P., Gellera, C., Lonnerdal, B., Taroni, F., & Cortopassi, G. (1999). The Friedreich ' s ataxia mutation confers cellular sensitivity to oxidant stress which is rescued by chelators of iron and calcium and inhibitors of apoptosis, *8*(3), 425–430.
Wu, S. M., & Hochedlinger, K. (2011). Harnessing the potential of induced pluripotent stem cells for regenerative medicine. *Nature Cell Biology*, *13*(5), 497–505. https://doi.org/10.1038/ncb0511-497
Xu, K. Y., Zweier, J. L., & Becker, L. C. (1997). Hydroxyl radical inhibits sarcoplasmic reticulum Ca(2+)-ATPase function by direct attack on the ATP binding site. *Circulation Research*, *80*(1), 76–81.
Yan, Y., Liu, J., Wei, C., Li, K., Xie, W., Wang, Y., & Cheng, H. (2008). Bidirectional regulation of Ca2+ sparks by mitochondria-derived reactive oxygen species in cardiac myocytes. *Cardiovascular Research*, *77*(2), 432–441. https://doi.org/10.1093/cvr/cvm047
Yandim, C., Natisvili, T., & Festenstein, R. (2013). Gene regulation and

epigenetics in Friedreich's ataxia. *Journal of Neurochemistry*, *126 Suppl*, 21–42. https://doi.org/10.1111/jnc.12254

Ying, J., Sharov, V., Xu, S., Jiang, B., Gerrity, R., Schoneich, C., & Cohen, R. A. (2008). Cysteine-674 oxidation and degradation of sarcoplasmic reticulum Ca(2+) ATPase in diabetic pig aorta. *Free Radical Biology & Medicine*, *45*(6), 756–762. https://doi.org/10.1016/j.freeradbiomed.2008.05.029

Yoon, H., Golla, R., Lesuisse, E., Pain, J., Donald, J. E., Lyver, E. R., … Dancis, A. (2012). Mutation in the Fe-S scaffold protein Isu bypasses frataxin deletion. *The Biochemical Journal*, *441*(1), 473–480. https://doi.org/10.1042/BJ20111637

Yoon, T., & Cowan, J. A. (2003). Iron-sulfur cluster biosynthesis. Characterization of frataxin as an iron donor for assembly of [2Fe-2S] clusters in ISU-type proteins. *Journal of the American Chemical Society*, *125*(20), 6078–6084. https://doi.org/10.1021/ja027967i

Yoon, T., & Cowan, J. A. (2004). Frataxin-mediated iron delivery to ferrochelatase in the final step of heme biosynthesis. *The Journal of Biological Chemistry*, *279*(25), 25943–25946. https://doi.org/10.1074/jbc.C400107200

Zanella, I., Derosas, M., Corrado, M., Cocco, E., Cavadini, P., Biasiotto, G., … Arosio, P. (2008). The effects of frataxin silencing in HeLa cells are rescued by the expression of human mitochondrial ferritin. *Biochimica et Biophysica Acta*, *1782*(2), 90–98. https://doi.org/10.1016/j.bbadis.2007.11.006

Zarse, K., Schulz, T. J., Birringer, M., & Ristow, M. (2007). Impaired respiration is positively correlated with decreased life span in Caenorhabditis elegans models of Friedreich Ataxia. *FASEB Journal : Official Publication of the Federation of American Societies for Experimental Biology*, *21*(4), 1271–1275. https://doi.org/10.1096/fj.06-6994com

Zima, A. V, & Mazurek, S. R. (2016). Functional Impact of Ryanodine Receptor Oxidation on Intracellular Calcium Regulation in the Heart. *Reviews of Physiology, Biochemistry and Pharmacology*, *171*, 39–62. https://doi.org/10.1007/112_2016_2

Zuhlke, C. H., Dalski, A., Habeck, M., Straube, K., Hedrich, K., Hoeltzenbein, M., … Schwinger, E. (2004). Extension of the mutation spectrum in Friedreich's ataxia: detection of an exon deletion and novel missense mutations. *European Journal of Human Genetics : EJHG*, *12*(11), 979–982. https://doi.org/10.1038/sj.ejhg.5201257

*E quindi uscimmo a riveder le stelle.*